EUROPEAN COMMISSION

European Research Area

Fire resistance of long span cellular beam made of rolled profiles (FICEB)

Research Fund for Coal & Steel

Interested in European research?

RTD info is our quarterly magazine keeping you in touch with main developments (results, programmes, events, etc.). It is available in English, French and German. A free sample copy or free subscription can be obtained from:

Directorate-General for Research and Innovation
Information and Communication Unit
European Commission
1049 Bruxelles/Brussel
BELGIQUE/BELGIË
Fax +32 229-58220
E-mail: research@ec.europa.eu
Internet: http://ec.europa.eu/research/rtdinfo.html

EUROPEAN COMMISSION
Directorate-General for Research and Innovation
Research Fund for Coal and Steel Unit

Contact: RFCS publications
Address: European Commission, CDMA 0/178, 1049 Bruxelles/Brussel, BELGIQUE/BELGIË

Fax +32 229-65987; e-mail: rtd-steel-coal@ec.europa.eu

European Commission

Research Fund for Coal and Steel

Fire resistance of long span cellular beam made of rolled profiles (FICEB)

O. Vassart
ArcelorMittal Belval & Differdange S.A.
66 rue de Luxembourg, 4009 Esch-sur-Alzette, LUXEMBOURG

M. Hawes
ASD Westok Ltd
Horbury Junction Industrial Estate, Wakefield, WF4 5ER, UNITED KINGDOM

I. Simms
Steel Construction Institute
Unit D, Silwood Park, Ascot, SL5 7QN, UNITED KINGDOM

B. Zhao
CTICM
Espace technologique, L'orme des merisiers, Immeuble Apollo, 91193 Saint-Aubin, FRANCE

J.-M. Franssen
Université de Liège
7 Place du XX Août, 4000 Liège, BELGIUM

A. Nadjai
Ulster University
Shore Road, Belfast, BT37 0QB, UNITED KINGDOM

Contract No RFSR-CT-2007-00042
1 July 2007 to 30 June 2010

Final report

Directorate-General for Research and innovation

2012 EUR 25112 EN

Cataloguing data can be found at the end of this publication.

Luxembourg: Publications Office of the European Union, 2012

ISBN 978-92-79-22428-7

doi:10.2777/38158

ISSN 1831-9424

Printed in Luxembourg

PRINTED ON WHITE CHLORINE-FREE PAPER

TABLE OF CONTENT

FINAL SUMMARY

The first par of the project was devoted to the creation of a database with all the results of the available tests on cellular beams. This database was used to define the tests that will be performed.

The next part was devoted to the realisation of four loaded fire tests in the fire laboratory of CTICM.

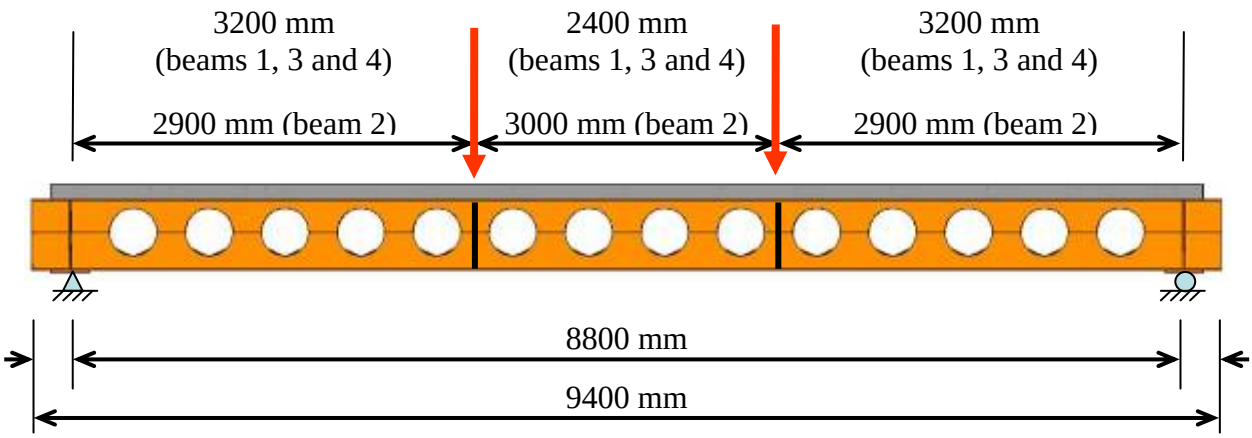

Figure 0–1 : Elevation view of the composite beams

All the beams were tested without fire protection but 3 of the beams were tested with the ISO fire curve in the durance and the beam n°2 was tested with a reduced fire curve in order to simulate the behaviour of protection material (Figure 0–2).

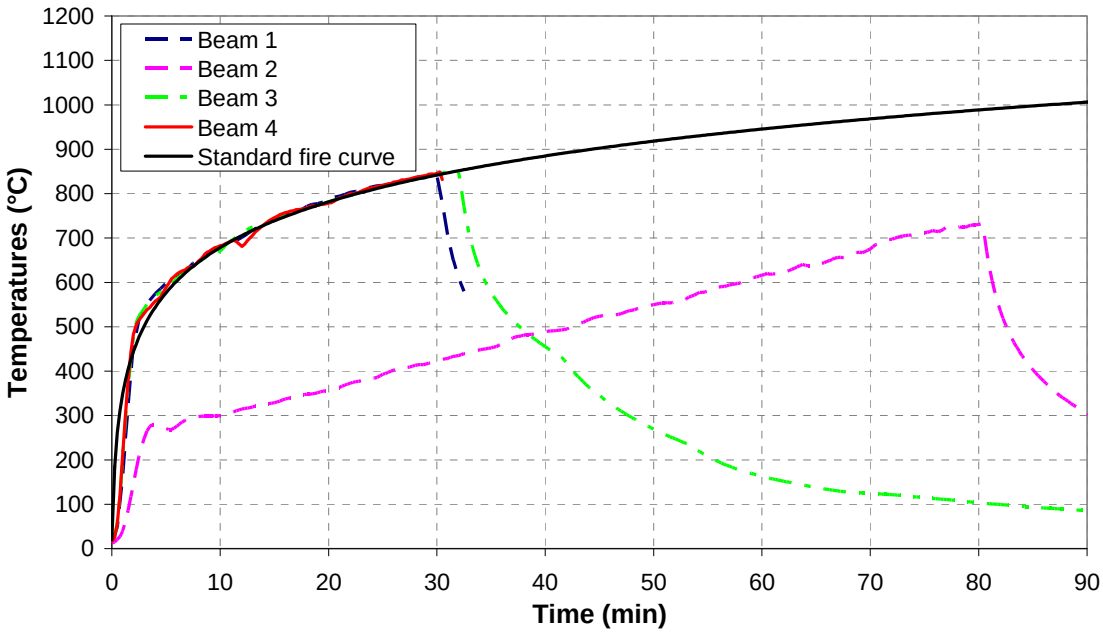

Figure 0–2 : Furnace average temperature vs. time

The temperatures and the displacements of the beams were recorded for the entire durations of the tests. The next Figure 0–3 show the shape of the beams after the fire test.

Beam 1 Beam 2

Beam 3 Beam 4

Figure 0–3 : Deformed beams in their RHS zone

The data available in the database and the different tests results were used to implement and calibrate finite element models in the Software SAFIR, ANSYS and CAST3M. The next Figures (Figure 0–4 to Figure 0–7) show the different FEM modelling:

SAFIR Model

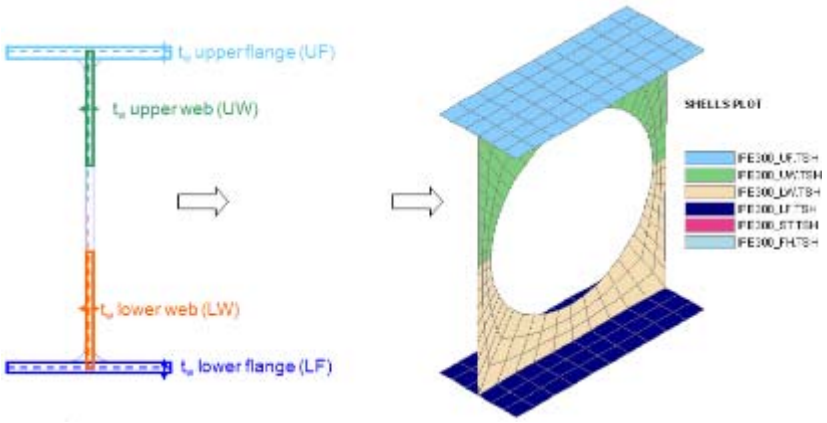

Figure 0–4 : Mechanical model

The beam was simply supported. Symmetry was used at the mid-span and the lateral displacement of the upper flange was restrained to avoid any lateral torsional buckling (Figure 0–5).

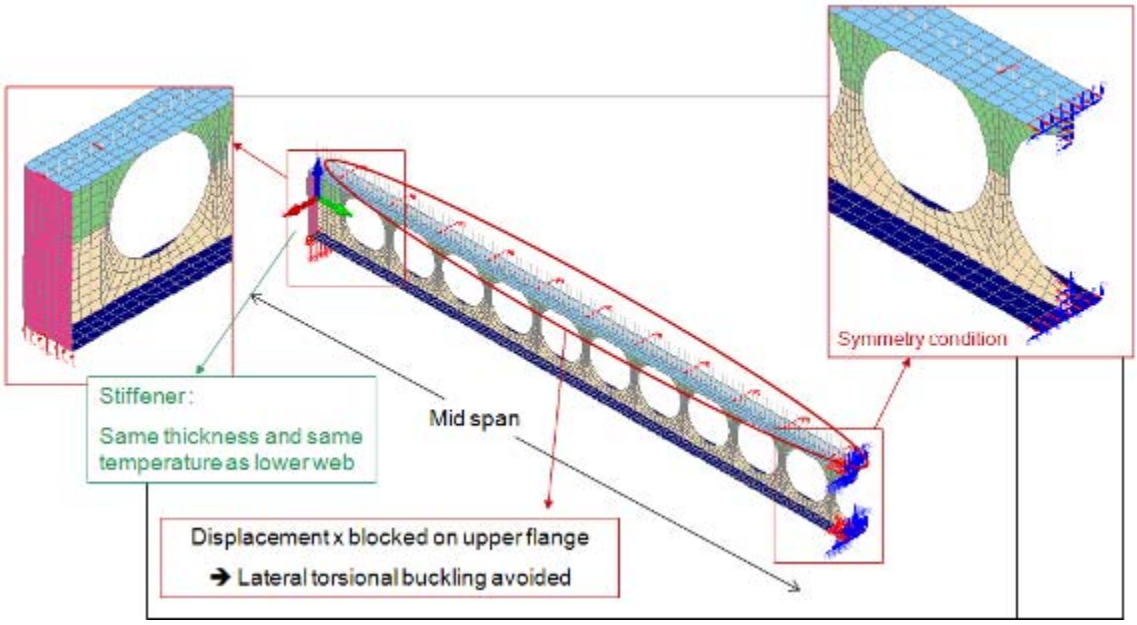

Figure 0–5 : Boundary conditions for modelled beam

ANSYS Model:

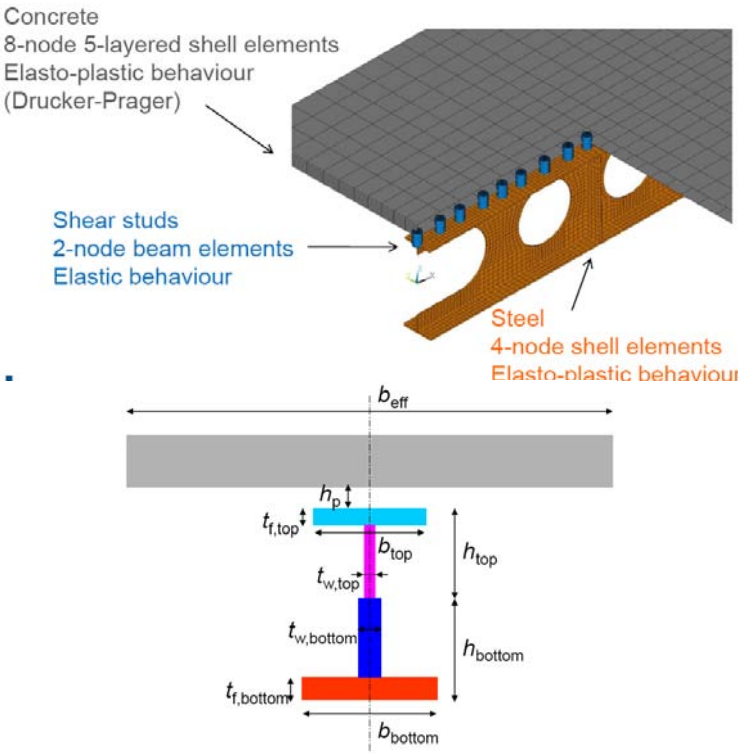

Figure 0–6 : a) Mechanical analysis model and b) Mechanical analysis cross-section

CAST3M Thermal Model

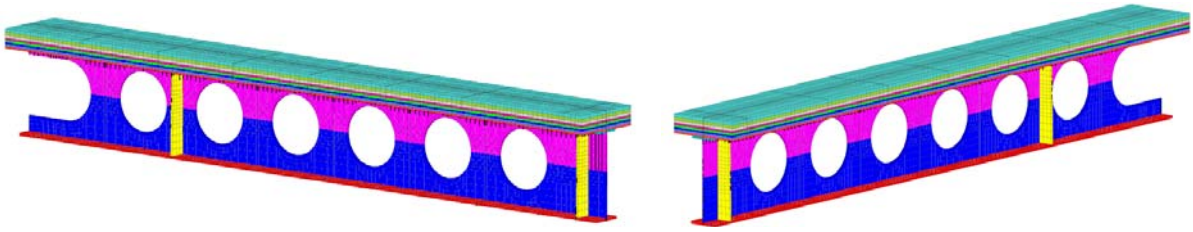

(c) 3D view 1 *(d)* 3D view 2

Figure 0–7 : Beam 1 mesh

A good agreement between the tests and both FEM models is observed, in terms of failure modes and critical temperatures (SAFIR and ANSYS). Thus, theses models can accurately predict the mechanical behaviour of a simply-supported composite cellular beam at elevated temperatures, and can be used for the parametric study which aims to check the relevance of the simplified design method.

The CAST 3M Model was able to reproduce with an acceptable level of accuracy the thermal behaviour of composite cellular beams.

The next step was de development a analytical methods to assess the fire resistance of unprotected cellular beams. Two models were analysed:

- ArcelorMittal model based on Eurocodes principle
- The Existing Engineering model coming from SCI

The results given by theses models were compared to the results provided by the different Finite Element models in the scope of a large parametrical study.

Figure 0–8 shows the comparison of the results between FEM and analytical model based on Eurocode principles

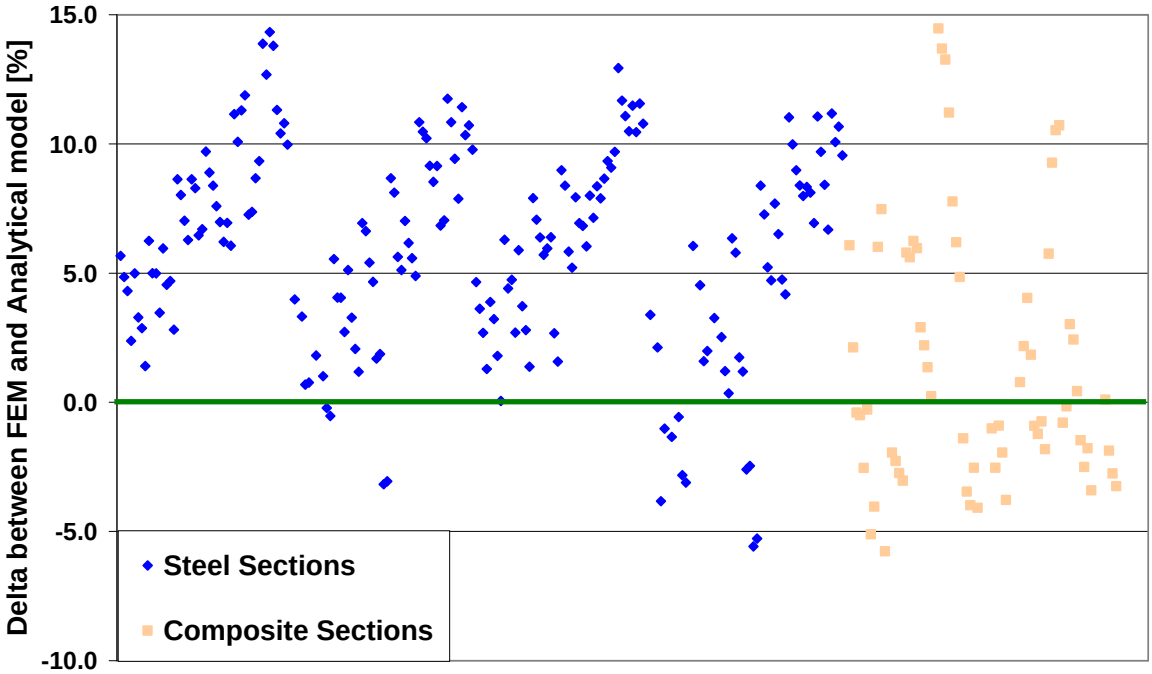

Figure 0–8 : Time-Analytical model Vs FEM Modelling

Analysing Figure 0–8, it can be pointed out that the analytical models can predict the critical temperature of steel cellular beams. The analytical model, based on Eurocodes principles, provides safe sided results with acceptable level of accuracy.

It can also be pointed out that the analytical models can also predict the critical temperature of composite cellular beams.

Figure 0–9 shows the comparison of the results between FEM and analytical model of SCI introduced in the Cellbeam Software.

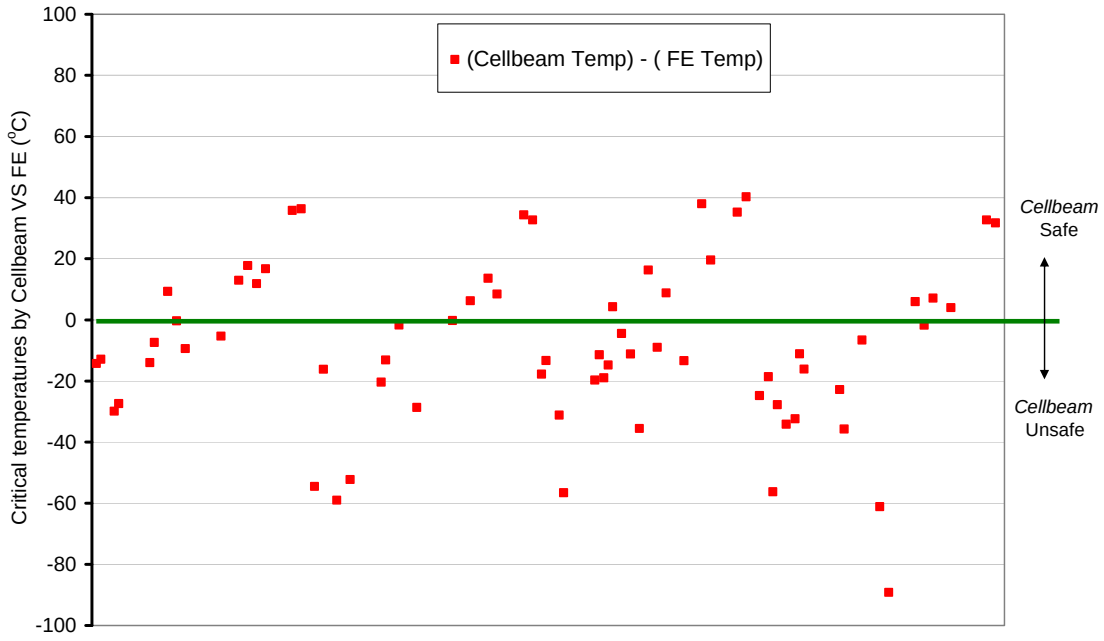

Figure 0–9 : *Cellbeam* results for critical temperatures versus the analytical model (temperature)

The amount of point is reduced compared to the study with the Eurocode model due to a different scope of application of the methodology.

Conclusions on the analytical model and parametric study

Eurocode based Model

The Eurocode based analytical model was again validated by this parametrical study and can be used for the prediction of the critical temperature of cellular beam in case of fire. This model takes into account the complex behaviour of cellular beams in fire conditions and is based on the Eurocodes principles taking into account the loss of material properties and stiffness required in the Eurocodes. This model was implemented in a design software called ACB^{+} and can be downloaded for free on www.arcelormittal.com/sections .

SCI Engineering Model

Comparison between the *Cellbeam* and FE models of the 15 case studies on cellular composite floors carried out by SCI showed that *Cellbeam* results were slightly non-conservative in some cases. In particular, cellbeam results were unconservative by a maximum of 12% (in UDL) and 10% (in critical temperature), for design of cellular beams at room and elevated temperatures. Unconservative results were not limited to only one failure mode.

Cellbeam results were also compared against the results of the FE analyses carried out on bare cellular steel section in the scope of the parametrical study, by other project partners. These comparisons show that Cellbeam results for bare steel sections tend to be generally slightly unconservative.

The Eurocode base Model will be introduce in the design guide including a hand design example.

The WP 5 was devoted to the extension of the Bailey's method to long span Cellular beam. The Figure 0–10 explains the basis of the Model equilibrium and the complete method is described further in the documents. This method has been implemented in an Excel spreadsheet which simplifies a lot the use of the methodology by the practitioners.

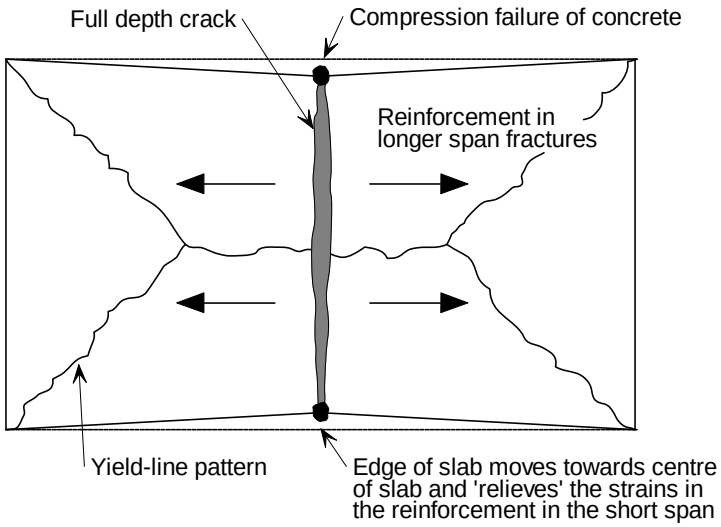

(a) Tensile failure of mesh reinforcement

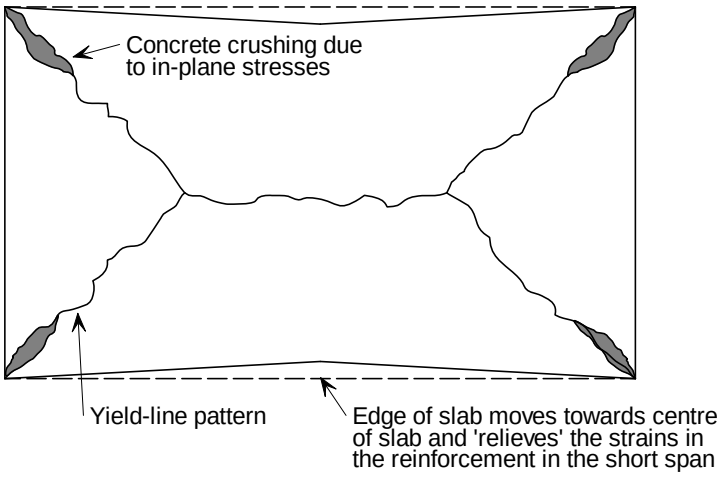

(b) compressive failure of concrete

Figure 0–10 : Assumed failure mode for composite floor

The experimental test programme at Ulster is the essential core of this project and has the aim to investigate the behaviour of the composite cellular beams under accurately simulated applied static loads in a realistic compartment fire (Figure 0–11). The fire load will be provided by 40kg/m^2 (720MJ/m^2) of floor area in the form of wooden cribs (average moisture content < 14%) placed in a uniform manner within the test area representing typical office fire loading to the EN 1991-1-2. Openings for ventilation will be used in the longest wall side of the fire compartment. The fire compartment walls (block work lined with plasterboard) will be sealed to the soffit of the floor level with a ceramic fire blanket.

Figure 0–11 : Compartment in fire test.

The imposed load was simulated using sandbags each weight 10kN applied over an area of 15m by 9m. The ventilation area will consist of a single opening of 3.0m in length with 1.5m high situated at 0.6m from the level floor. The fire design parameters are calculated according to the EN 1991-1-2.

The two central secondary beams were unprotected. This test provided unique experimental data on the performance of the cellular beams acting in membrane action. The information recorded during the test was used to validate the natural fire safety concept and provide design rules and guidance for protected and unprotected cellular beams.

Complete tests results are available on a DVD (pictures, movies, data) and reported in a paragraph hereafter.

To design the building tested and after to perform a finial validation, FEM models were built in SAFIR and ANSYS:

ANSYS Model

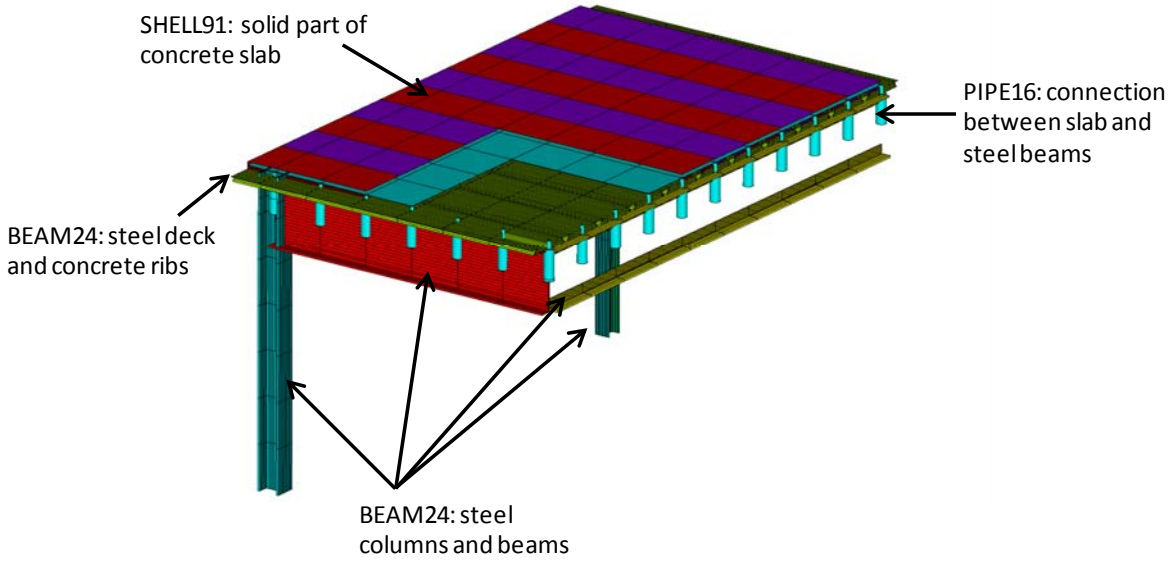

Figure 0–12 : Floor finite element model under ANSYS

SAFIR Model

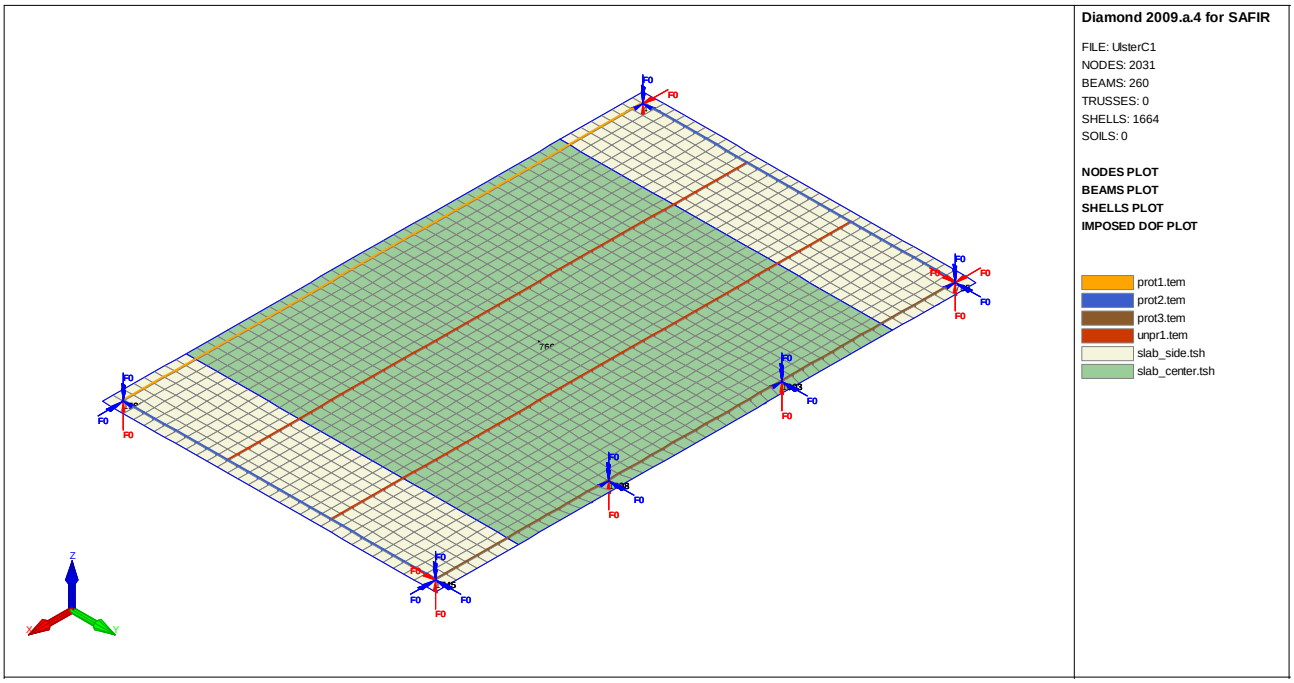

Figure 0–13 : Structural analysis model

The last part of the project was devoted to the redaction of a design guide.

The first part of the design guide will be devoted to the description of the simplified calculation method developed in WP4 to assess the resistance of cellular beams in fire conditions.This method has been implemented in the Software ACB^{+} [22] available for free on *www.arcelormittal.com/sections*.

The second part of the design guide will be devoted to the improvement of the Bailey's method to long span cellular beams.

SCIENTIFIC AND TECHNICAL PROGRESS

1. BACKGROUND

As spans become longer, steel framed buildings become more competitive compared with reinforced concrete framed buildings. For maximum economy, steel beams should be designed to act compositely with the floor slab. The increased use of long span composite beams leads to large open offices with minimal columns. However, as the span increases, the beam depth will also increase which, in turn, can lead to increased storey heights. The use of cellular beams (CB) largely overcomes this problem because ducts, pipes and other services can pass through the openings in the web. Also, as CB is constructed from rolled sections, the increased section depth results in added strength without additional material and thus tends to reduce the total weight of steelwork.

Efficient assessment of structures in fire conditions is becoming more and more relevant and is covered by the use of numerical models. However, numerical models are based on small scale tests and experience. To date, no rigorous research into the performance of CB in fire has taken place. The design assumptions are still largely based on the performance of solid web beams in fire standard tests.

The fire resistance of CB has been very controversial in recent years, with most of the debate being concerned with their requirements for intumescent protection. There is a clear need for improved understanding of the performance in fire of the CB itself in order to provide clear design guidance and promote cost effective design.

2. WP1 : DEFINITION OF THE LONG SPAN BEAM FIRE TESTS

A database was created with all the results of the available tests on cellular beams.

This database was used to define the tests that will be performed in the fire laboratory of CTICM

Annex II, attached to this report, outlines the full list of reports covering Cellular Beams in Fire. Many of these are confidential reports, and are referenced only. The reports, which are available for publication are:

- Indicative fire test on a cellular and solid web steel beam
  Professor Colin Bailey

- Performance of Cellular Composite Floor Beams at Elevated Temperatures
  Ali Nadjai, Olivier Vassart, Faris Ali, Didier Talamona, Ahmed Allam, Mike Hawes

3. WP2 : FURNACE FIRE TESTS OF CELLULAR BEAMS

3.1. Experimental set-up

3.1.1. Beam geometric and material properties

An overall view of the four beams is shown in Figure 3–1. As parts of composite floors, beams 1, 3 and 4 were considered to be secondary beams, and beam 2 was considered as a primary beam. They were fire designed according to [18].

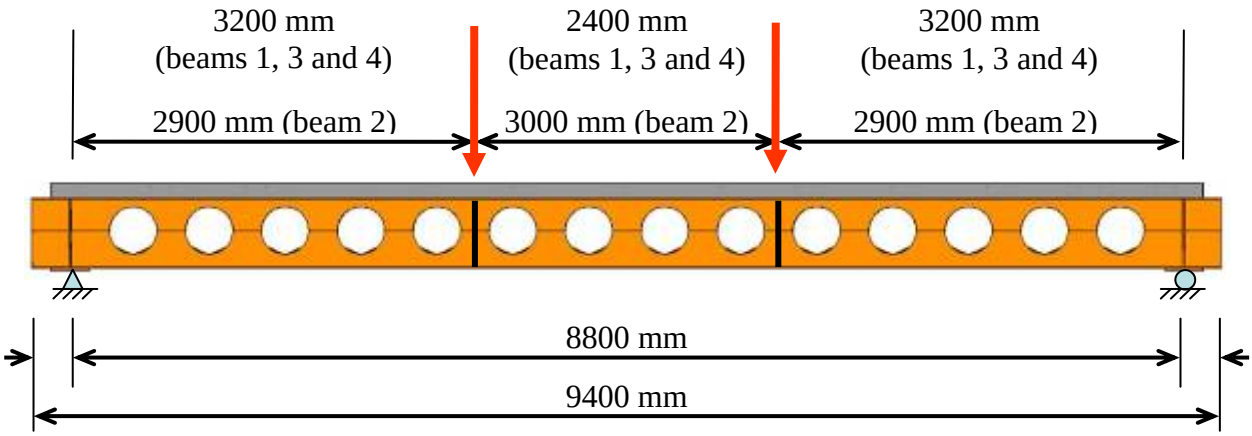

Figure 3–1 : Elevation view of the composite beams

The main geometric and material properties of the beams are shown in Table 3-1 [20 and 21]. In addition to the web stiffeners at load points and at its end supports, for beam 4, there was a one-side stiffener at each web-post. The upper steel flange was fully connected to the 120 mm deep composite slab, which comprised a COFRASTRA 40 ® re-entrant deck perpendicular to the span direction of the beam, via Nelson headed studs. The slab width was 2.20 m, which equals to the effective width beff according to [21], i.e. $2 \times L/8$. As for the reinforcement steel, a mesh of 252 mm²/m was used.

Table 3-1 : Geometric and material properties of the fire-tested beams

	Beam 1	Beam 2	Beam 3	Beam 4
Top tee section	IPE 360	IPE 450	IPE 360	IPE 360
Top tee depth h_{top} (mm)	255	275	255	255
Bottom tee section	IPE 450	IPE 450	HEB 450	IPE 450
Bottom tee depth h_{bot} (mm)	300	275	300	300
Stiffener thickness (mm)	20	20	20	20 / 15*
Span : L (mm)	8,800			
Overall slab length: L_t (mm)	9,100			
Slab width : b_{eff} (mm)	2,200			
Number of openings	13	13	13	14
Number of circular openings	12	11	12	14
Number of elongated openings	1	2	1	0
Number of semi-infilled openings	0	2	0	0
Cell diameter (mm)	375	335	375	375
Reinforcement mesh	A252			
Number of shear studs	59			
Shear stud diameter (mm)	19			
Shear stud length (mm)	100			
Shear stud spacing (mm)	150			
Mechanical load (kN)	140	160	160	140
Steel grade	S355			
NWC compressive strength (MPa)	31.0	33.0	33.5	29.5

*Two-side stiffeners: 20 mm thick; one-side stiffeners: 15 mm thick

3.1.2. Mechanical load

A mechanical load was applied through a hydraulic pump, and then distributed via a steel beam to 2 horizontal steel cylinders, providing two loading lines corresponding to the stiffeners' location (see Figure 3–2). The hydraulic jack had a 400 mm stroke.

3.1.3. Thermal load

The thermal load was applied from beneath: hence, the steel profile was fire-exposed on 3 sides, while only the lower side of the slab was fire-exposed (see Figure 3–2).

None of the four beams was fire-protected. For beams 1, 3 and 4, a 30-min exposure to the standard fire was assumed, whereas a specific bi-linear fire curve was used for beam 2, in order to simulate the heating regime of a fire protected beam.

For beams tested under ISO fire condition, despite their failure occurred prior to 30 minutes, the thermal load was maintained until 30 minutes (see Table 3-2) in order to investigating the heating of the beams to the lowest standard fire rating commonly defined by the fire regulations.

The average furnace temperatures are given in Figure 3–3.

Table 3-2 : Test duration

	Beam 1	Beam 2	Beam 3	Beam 4
Heating phase (min)	30	80	30	30
Collapse time (min)	~18	~73	~26	~19

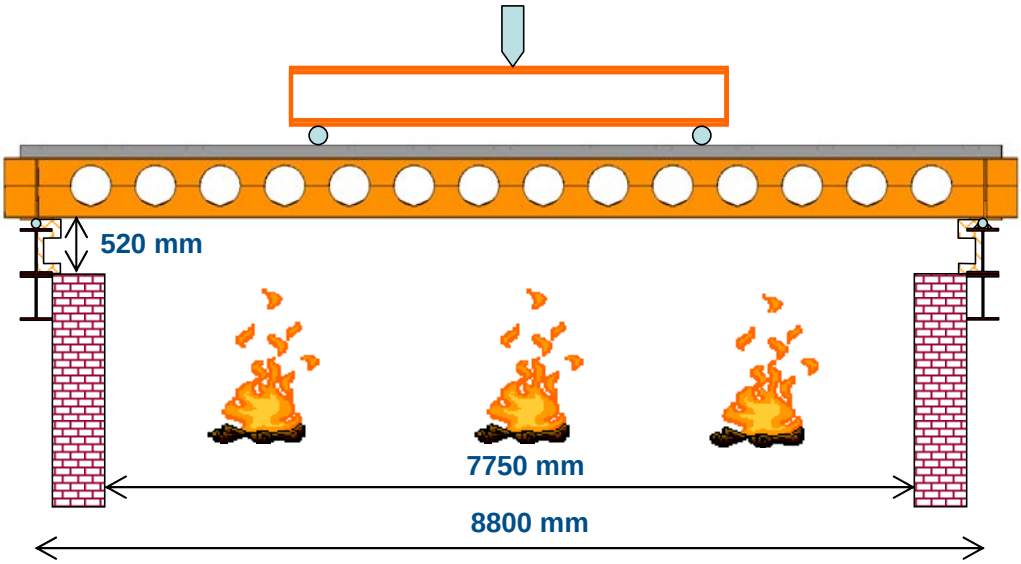

Figure 3–2 : Schematic view of the furnace

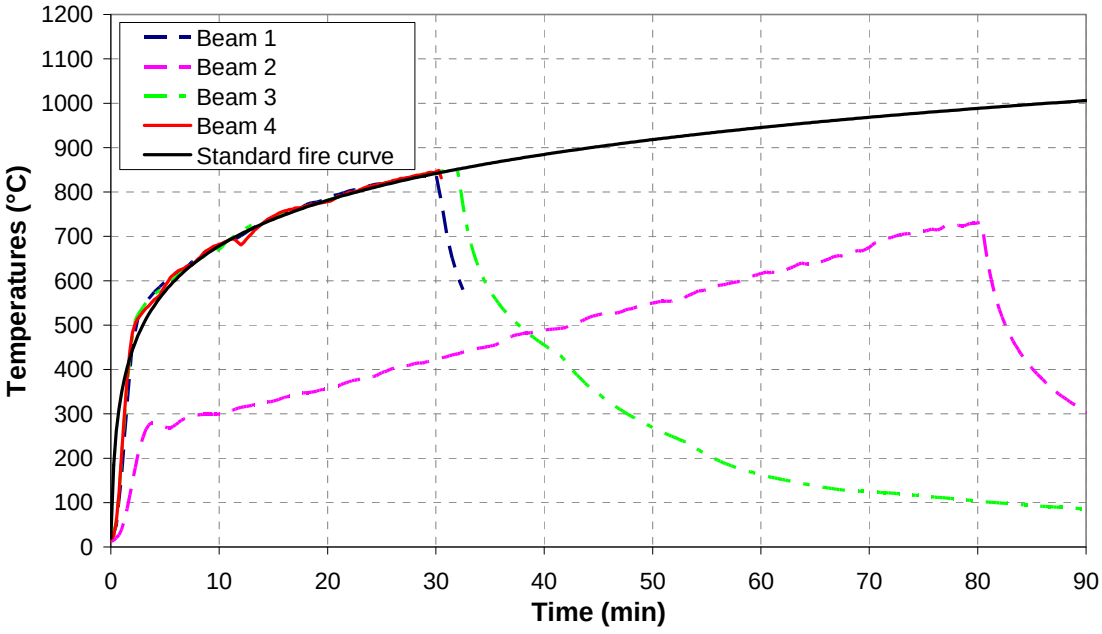

Figure 3–3 : Furnace average temperature vs. time

3.1.4. Measurement of experimental results

For each test, about 100 thermocouples were disposed in the furnace and at various locations along the beams in both the steel profile and the composite slabs, though most of them were located in the steel profile (see Table 3-3). Sensors were also used to check the rotations near the supports, the bond-slip between the steel profile and the slabs, and the vertical displacements in the central part of the slab.

Table 3-3 : Distribution of the thermocouples in the tested composite beams

	Beam 1	Beam 2	Beam 3	Beam 4
Top flange	18	22	18	18
Top web	25	21	25	18
Bottom flange	18	22	18	18
Bottom web	25	21	25	18
Tee junction	0	2	0	0
Stiffeners	0	0	0	3
Shear studs	2	2	2	2
Composite slab	14	22	14	14
Overall number	102	112	102	91

3.2. Test results

3.2.1. Temperatures

In the following graphs, the red dotted line refers to the time when the beam failed, according to 3.2.2. The other curves correspond to thermocouples that worked properly and gave reliable results.

3.2.1.1. Beam 1

Figure 3–4 to Figure 3–7 give the temperatures recorded at different steel sections.

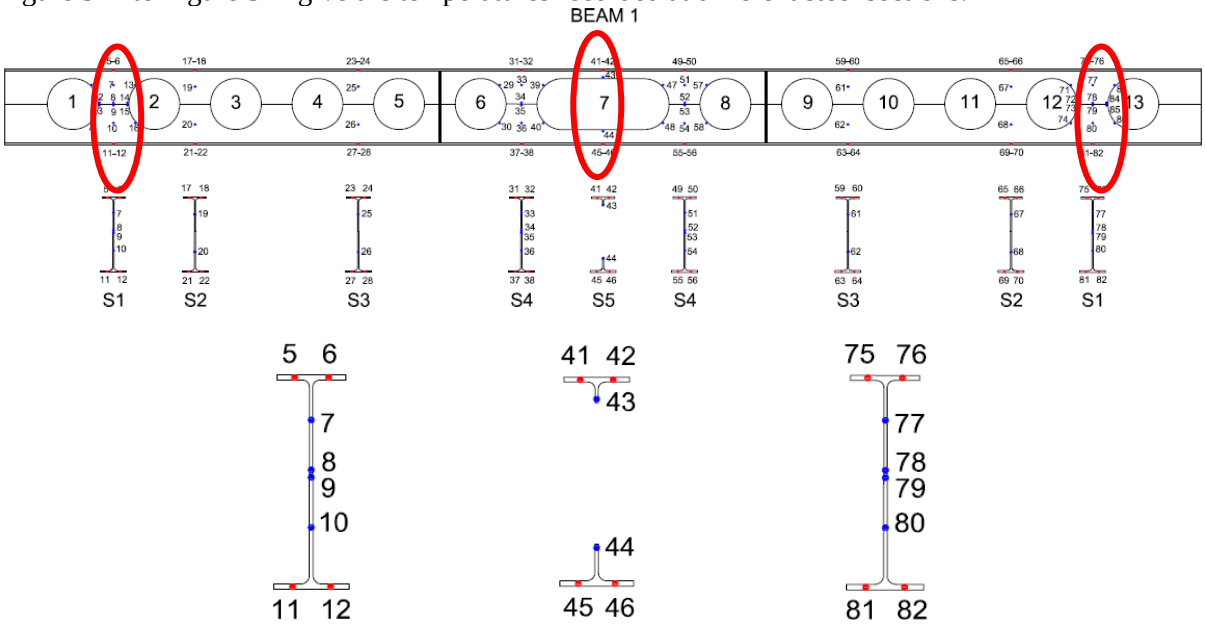

Figure 3–4 : Beam 1 – selected steel sections: both ends and mid-span

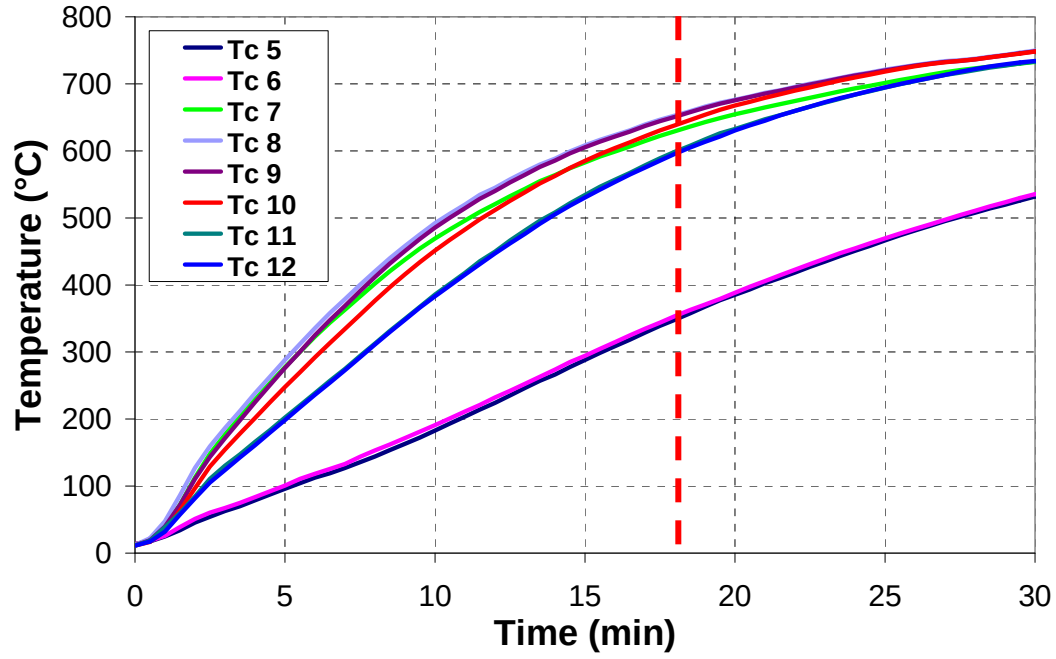

Figure 3–5 : Beam 1 – steel LHS end temperatures

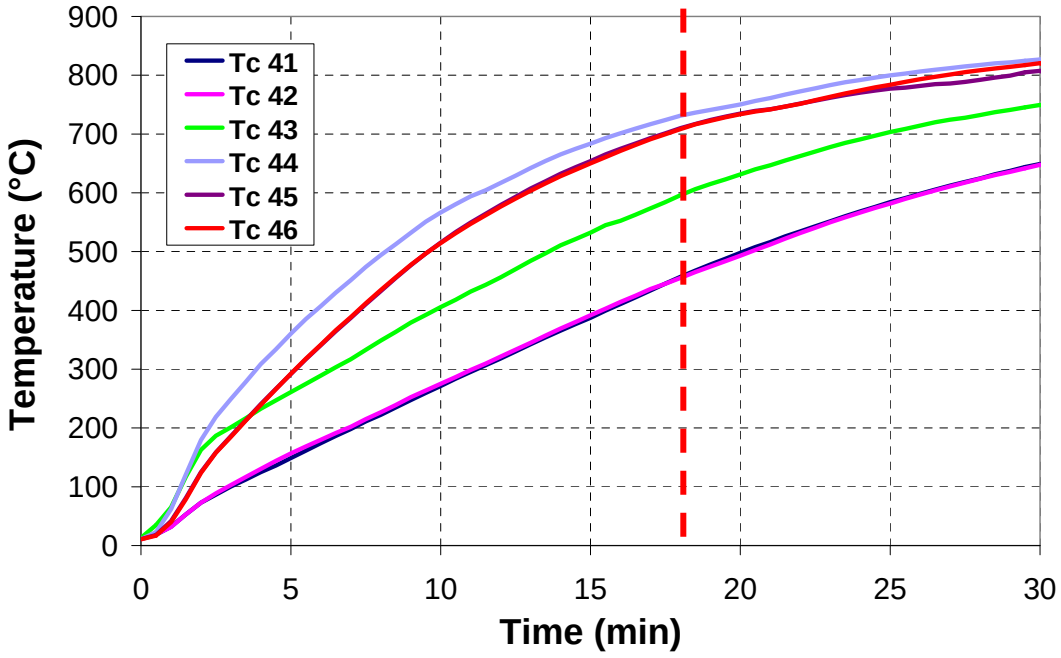

Figure 3–6 : Beam 1 – steel mid-span temperatures

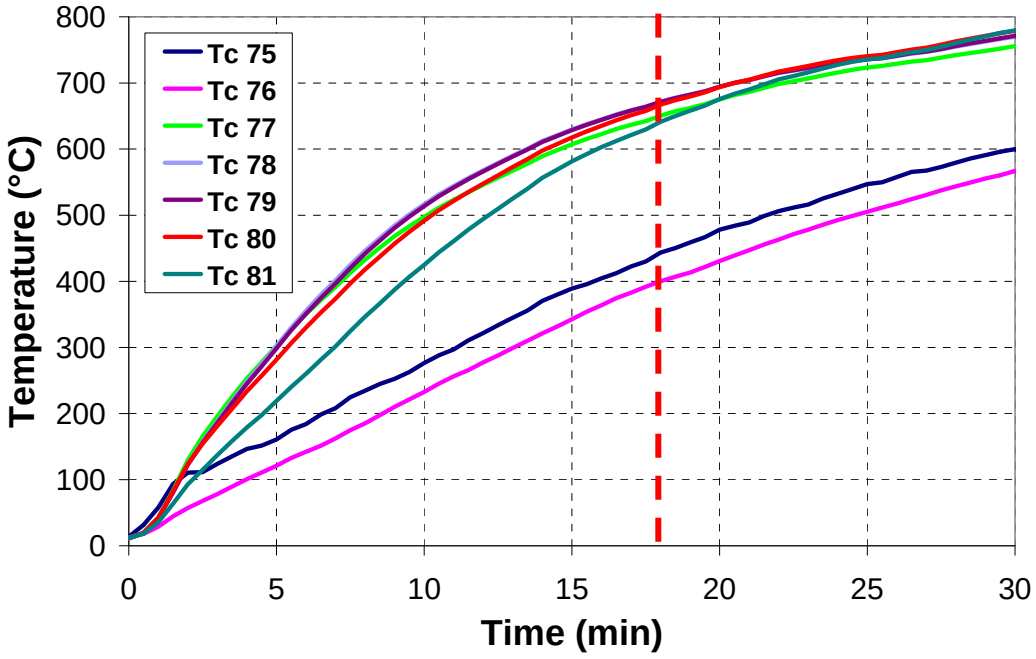

Figure 3–7 : Beam 1 – steel RHS end temperatures

Because the front of the furnace was hotter than its back, the temperatures at the right-hand-side end of the beam were greater than the temperatures at its left-hand-side end.

Regardless of the section, the highest temperatures were recorded in the web. Hence, at failure time, the maximum temperature, at mid-span and in the bottom web, was equal to ~720 °C. At this temperature, steel yield strength had already lost more than 50 % of its value at 20 °C.

On the other hand, at that particular moment, the top flange was heated up to ~450 °C, and the bottom flange up to ~710 °C.

3.2.1.2. Beam 2

Figure 3–8 to Figure 3–14 give the temperatures recorded at different steel sections.

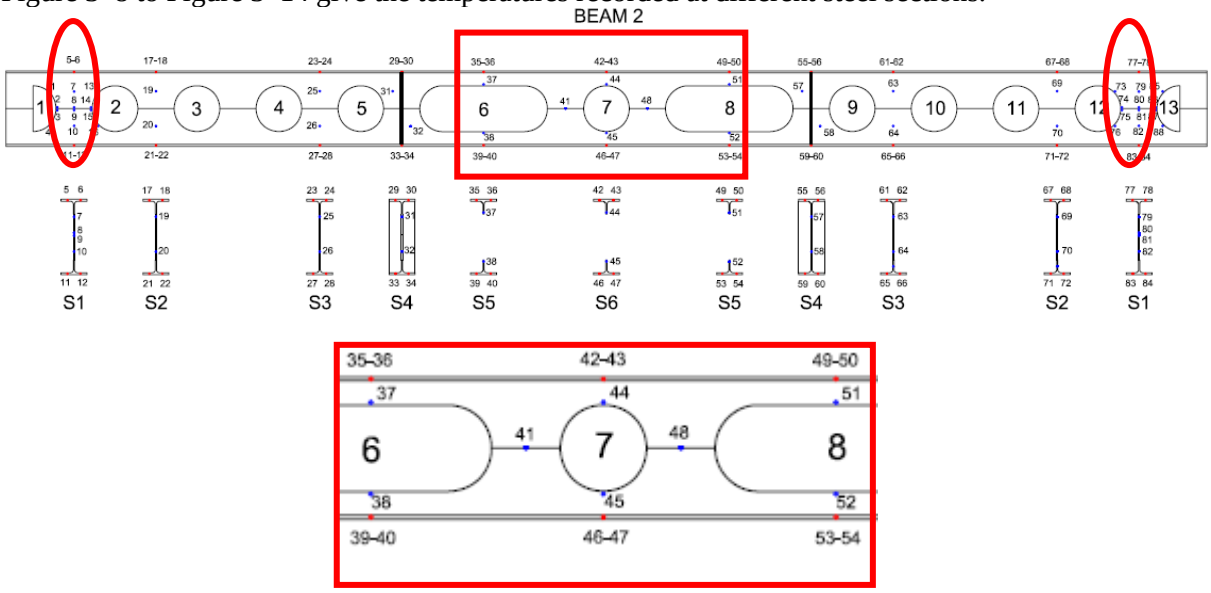

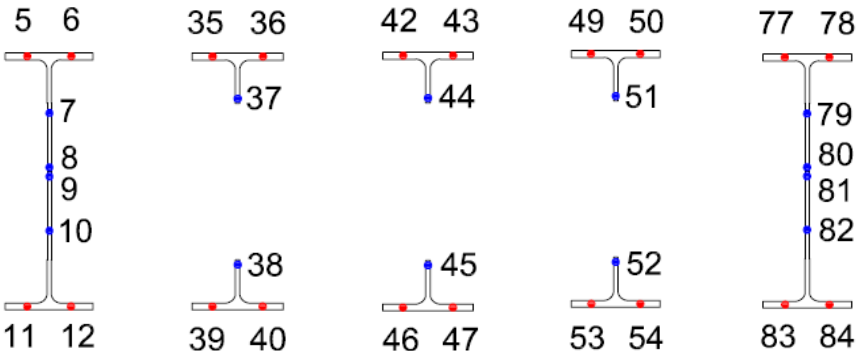

Figure 3–8 : Beam 2 – selected steel sections: both ends and central zone

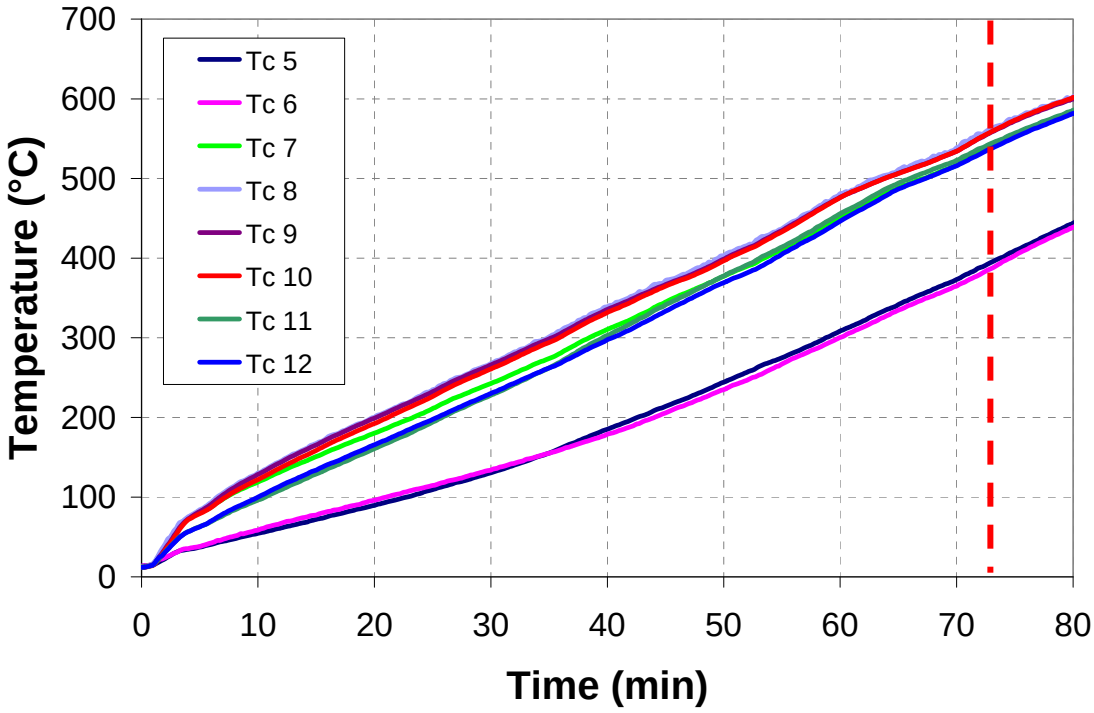

Figure 3–9 : Beam 2 - steel LHS end temperatures

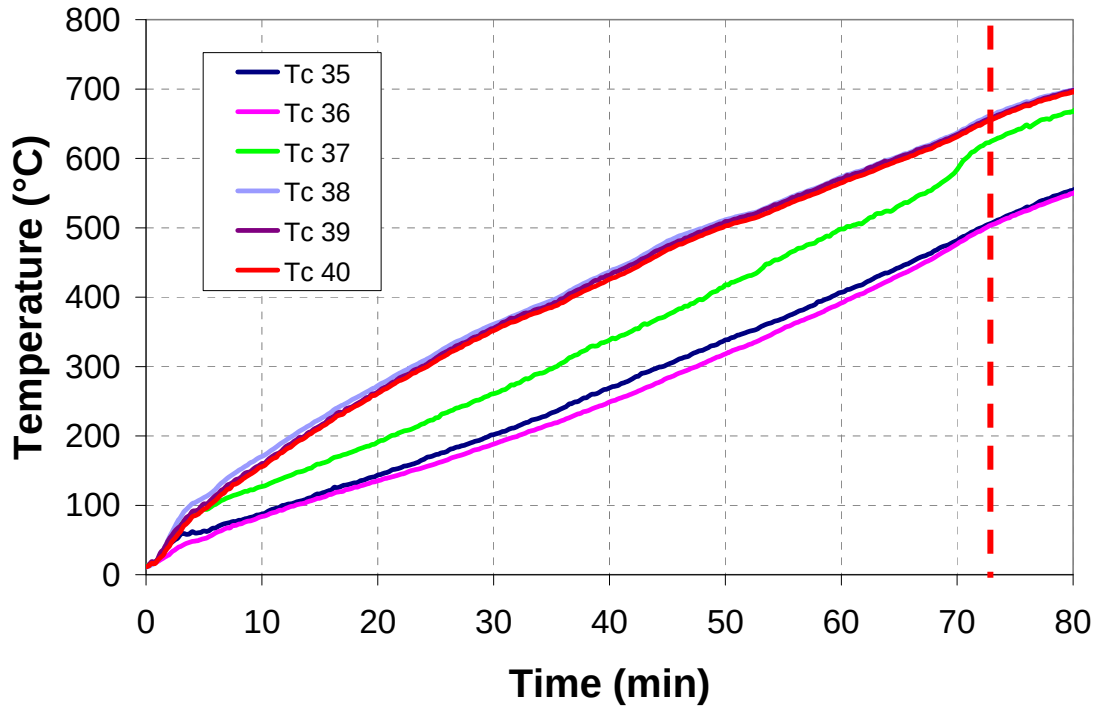

Figure 3–10 : Beam 2 - steel central temperatures (LHS)

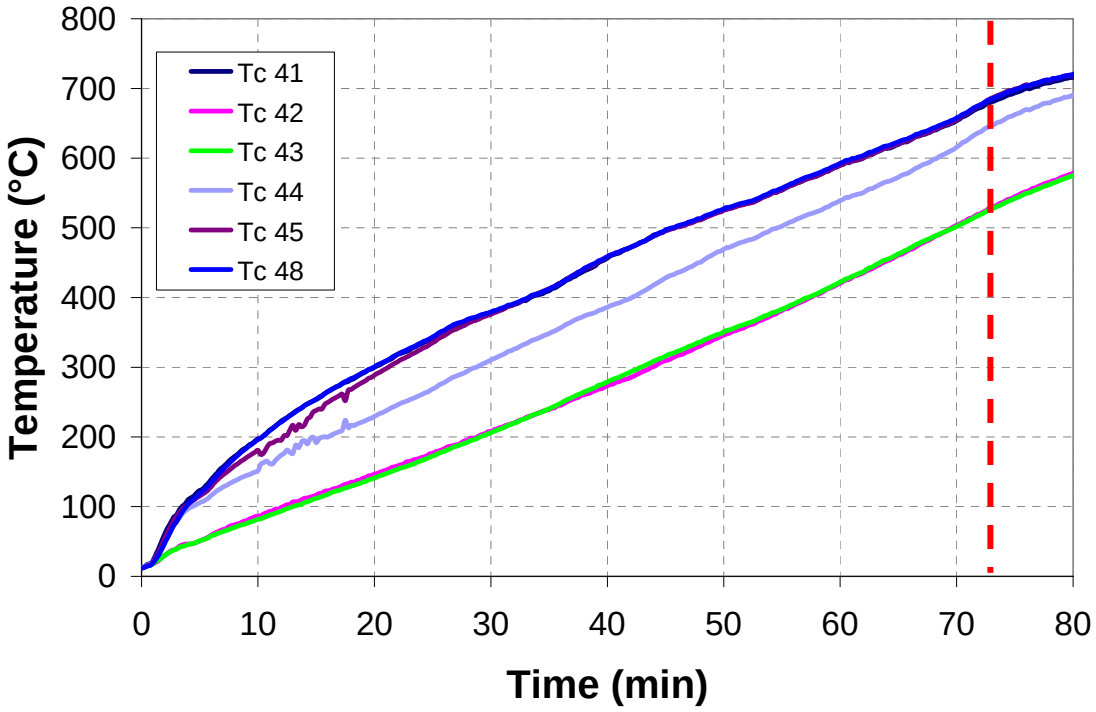

Figure 3–11 : Beam 2 - steel mid-span temperatures

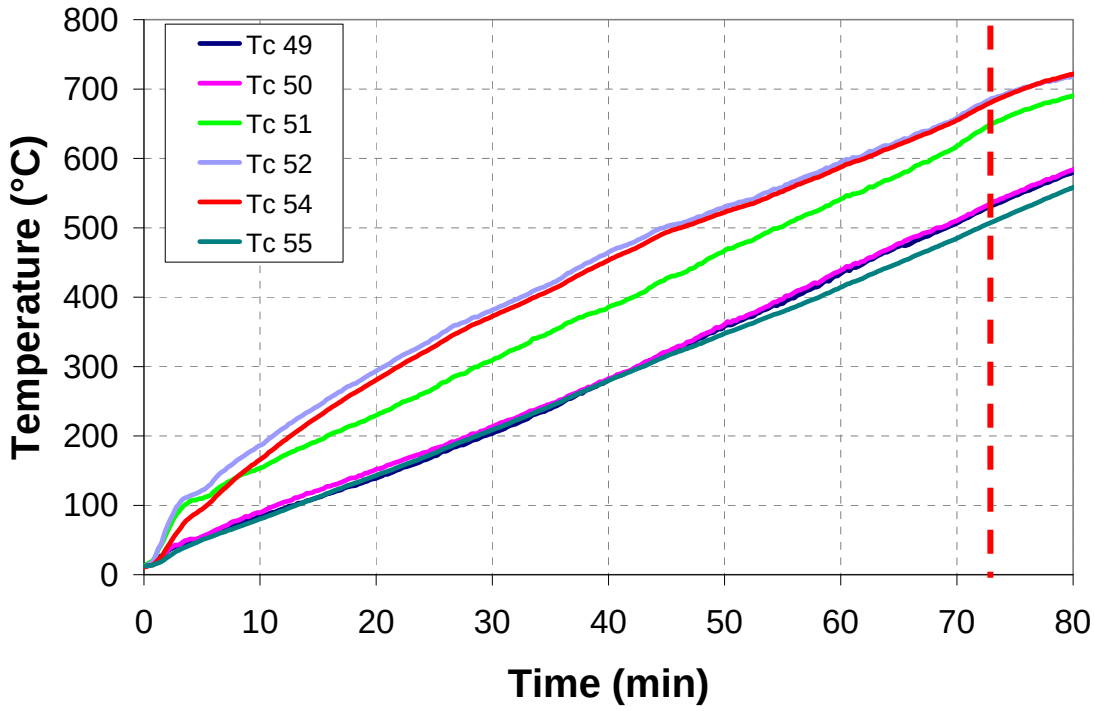

Figure 3–12 : Beam 2 - steel central temperatures (RHS)

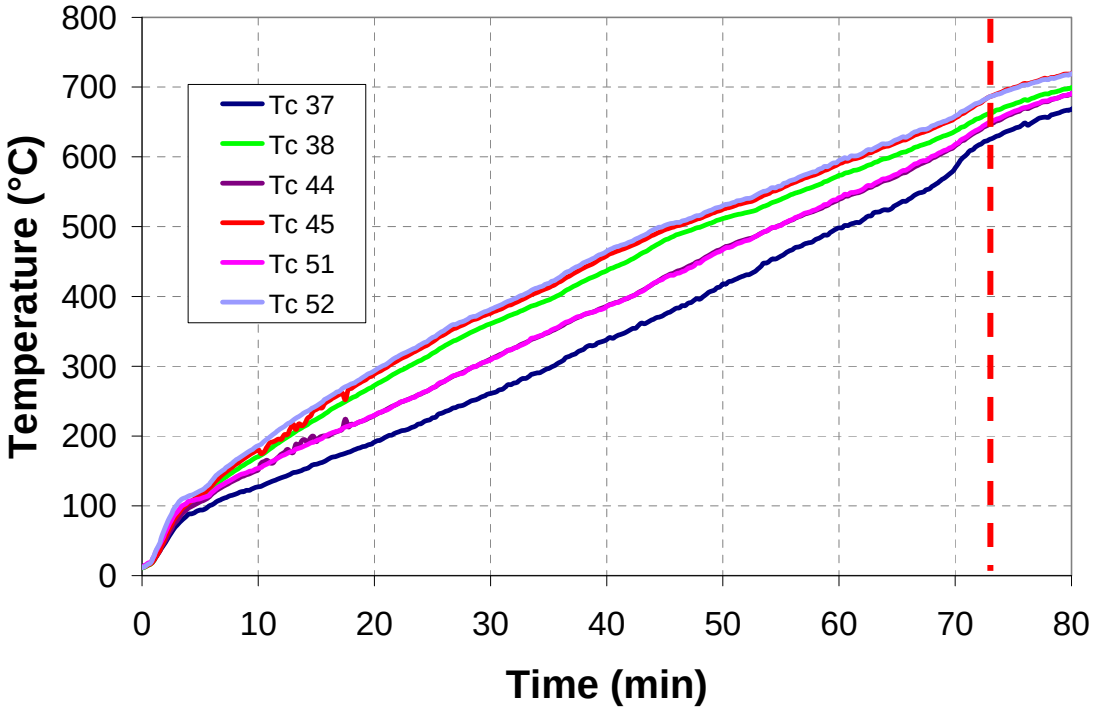

Figure 3–13 : Beam 2 – temperatures on central cell edges

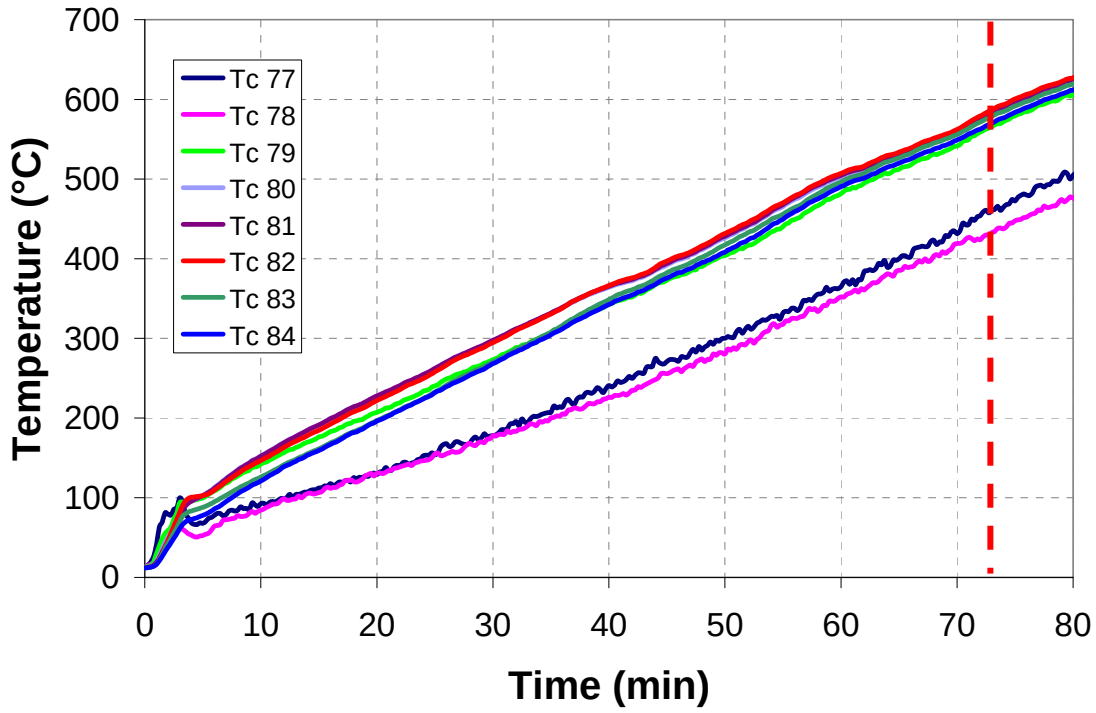

Figure 3–14 : Beam 2 - steel RHS end temperatures

For the same reason as above, the right-hand-side end of the beam was hotter than its left-hand-side end.

Again, the maximum temperatures were recorded in the bottom web at mid-span, reaching ~670 °C when the beam failed. Despite a slower temperature increase, as compared to beam 1, beam 2 failed faster (see also Figure 3–26). It must be kept in mind that both beams had the same top tee section, and that beam 2, which was a primary beam, had the same bottom tee section as its top tee section; its bottom tee section was hence less thick than beam 1 bottom tee section.

Also, the shape of the cells, whether they were elongated or circular, did not have any impact on the temperature distribution (see Figure 3–10 to Figure 3–13). The discrepancy that was observed (see Figure 3–13) was rather caused by the front of the furnace being hotter than its back.

3.2.1.3. Beam 3

Figure 3–15 to Figure 3–18 give the temperatures recorded at different steel sections.

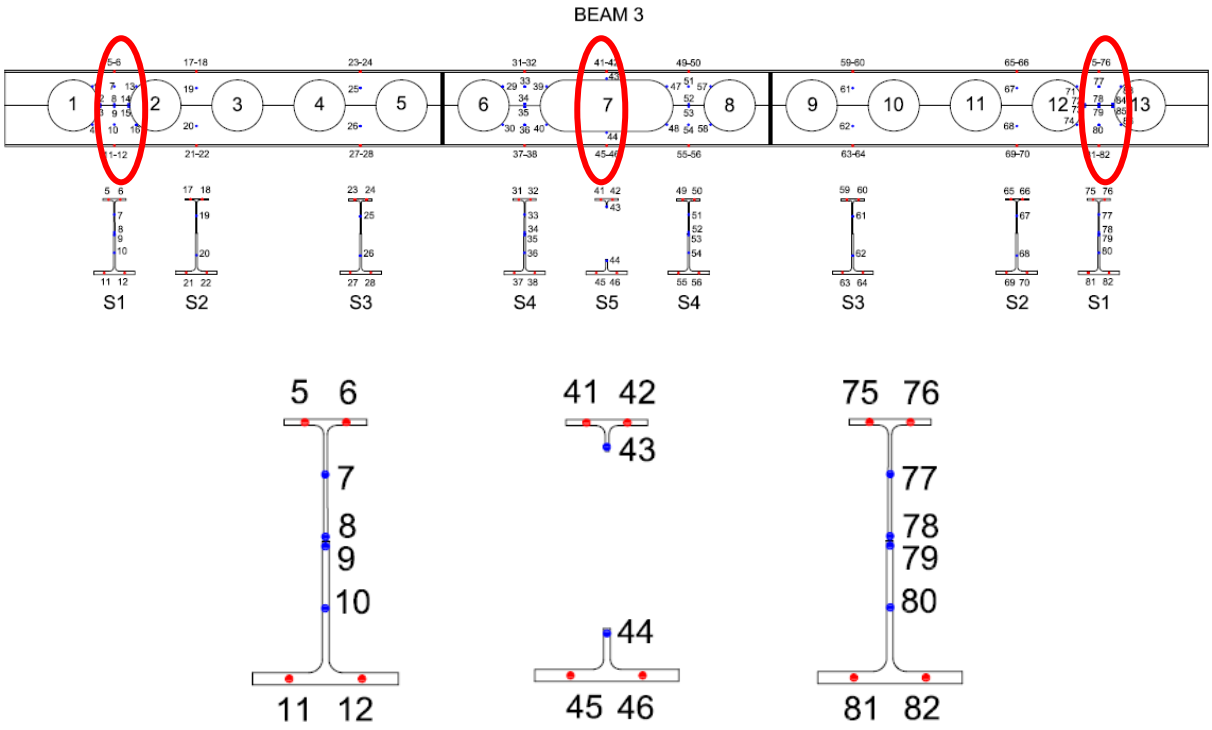

Figure 3–15 : Beam 3 – selected steel sections

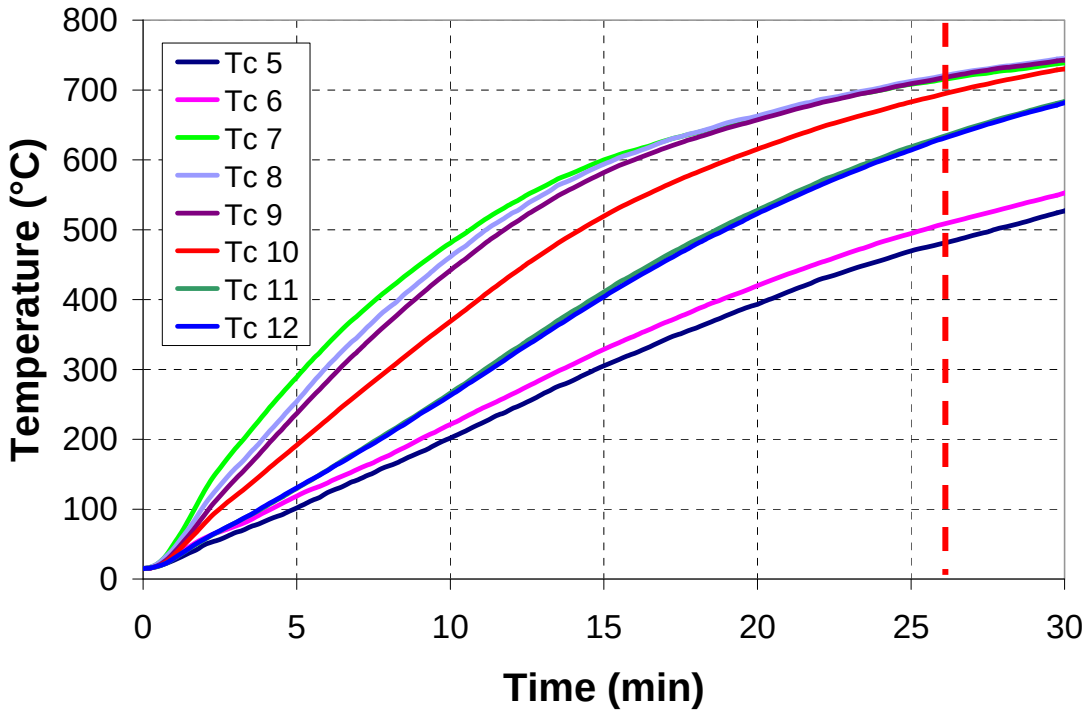

Figure 3–16 : Beam 3 – steel LHS end temperatures

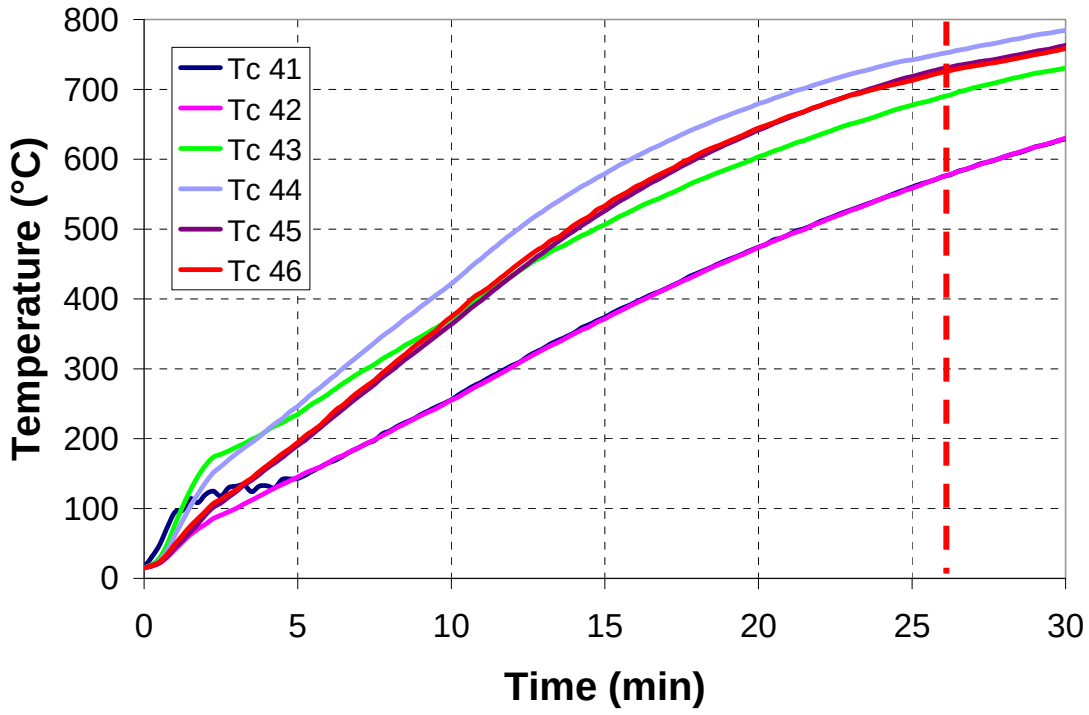

Figure 3–17 : Beam 3 – steel mid-span temperatures

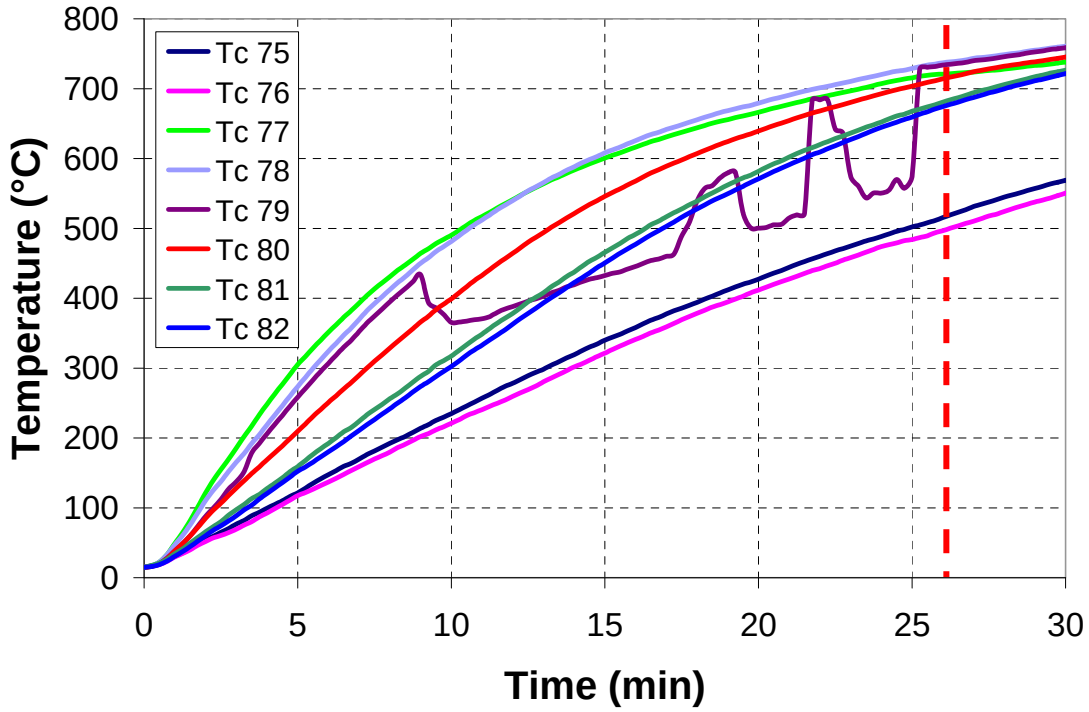

Figure 3–18 : Beam 3 – steel RHS end temperatures

Again, the right-hand-side end of the beam was hotter than its left-hand-side, and the highest temperature value at failure time was recorded in the bottom web at mid-span, reaching ~750°C.

As compared to beam 1, which had the same top tee section, beam 3 was heated up more slowly, probably because of a thicker bottom tee section. This might also explains why it failed more slowly than beam 1.

3.2.1.4. Beam 4

Figure 3–19 to Figure 3–22 give the temperatures recorded at different steel sections.

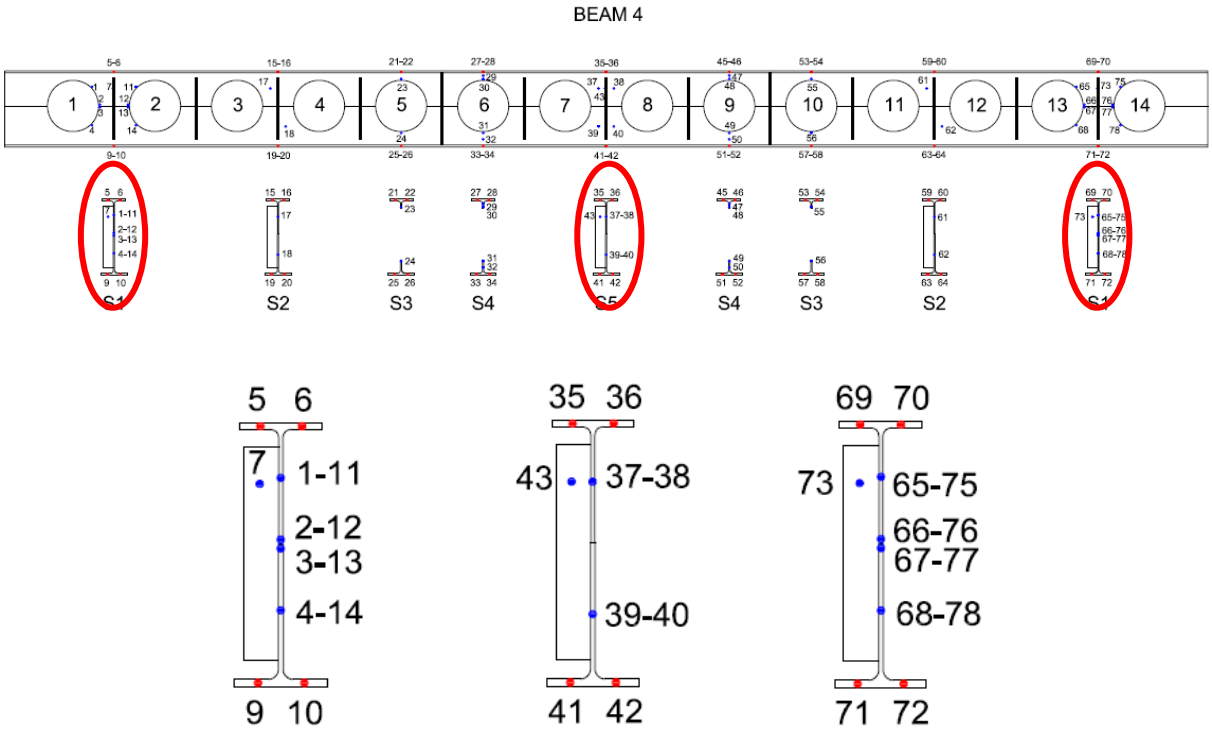

Figure 3–19 : Beam 4 – selected steel sections

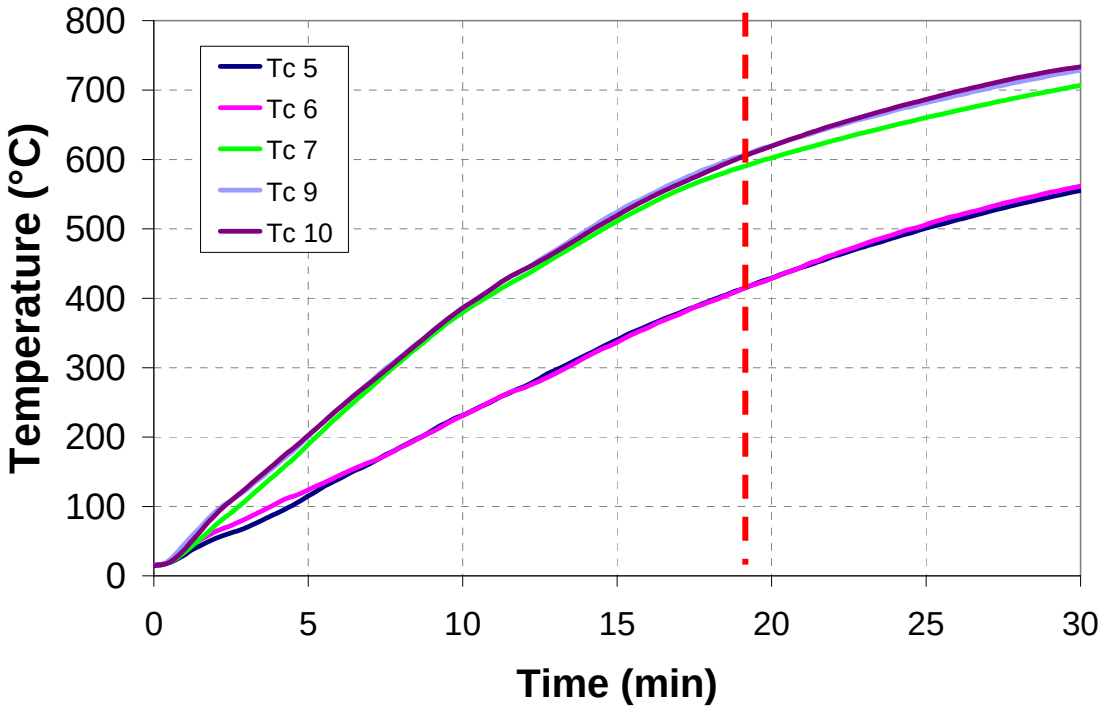

Figure 3–20 : Beam 4 – steel LHS end temperatures

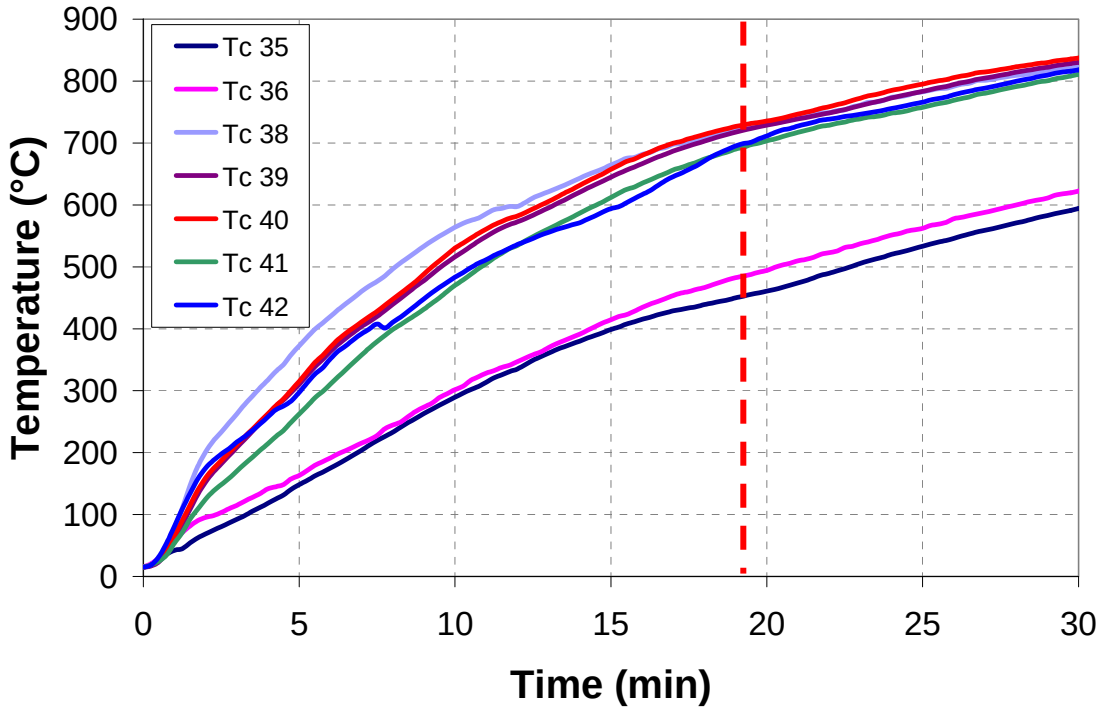

Figure 3–21 : Beam 4 – steel mid-span temperatures

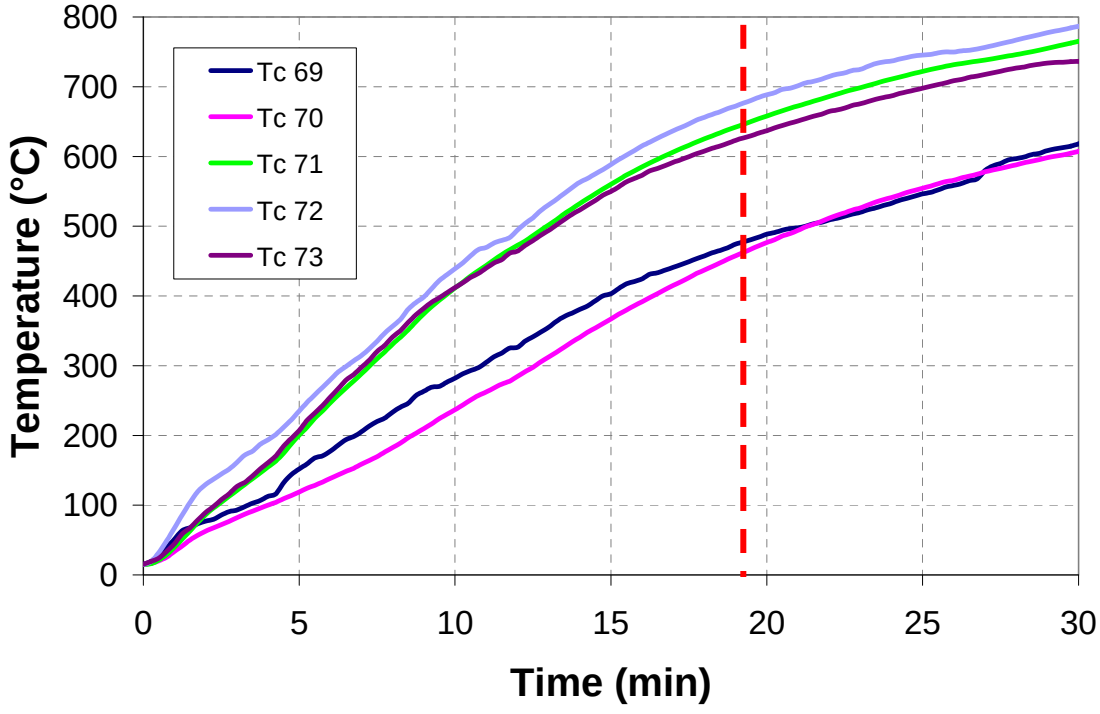

Figure 3–22 : Beam 4 – steel RHS end temperatures

For the same reason as above, the right-end-side end of the beam was hotter than its left-hand-side end.

At failure time, the greatest temperature recorded in the bottom web at mid-span reached a value of ~720°C, which was quite the same for beam 1. Also, the temperature distribution was the same in both beams. It must be reminded that these two beams had the exact same section, though beam 1 had one

central elongated opening beam 4 had one-side stiffener at each web-post in addition to the stiffeners located at load points. This explains why beam 4 failed ~1 min later than beam 1.

3.2.2. Deflections

The test deflections recorded at a L/4 distance from the supports and at mi-span are shown in Figure 3–23 to Figure 3–27 [19].

As long as a mechanical load was applied, the beams underwent vertical displacements increasing progressively and linearly until a heating around 550 °C. Afterwards, their deflections increased very quickly with the temperature rising until the collapse.

A slight deflection decrease was observed once the hydraulic jack reached its stroke limit and was taken away. However, after this decrease, some beams continue bending downwards under their self-weight without any additional mechanical load until maximum thermal load.

It must be reminded that all the beams exposed to ISO fire had the same top tee section, and in particular, beam 1 and beam 4 had exactly the same cross-section. Nevertheless, in spite of its one-side additional stiffeners, beam 4 underwent approximately the same deflections as beam 1. In fact, the behaviour of these two beams is very close if it is related to their heating instead of the time. Besides, beam 3 behaved stiffer than both beam 1 and beam 4, as its bottom tee section was more resistant.

Also, in all the tests, the temperature distribution in the furnace was not homogenous, since one side was always hotter than the other. Thus, the beams always underwent more important displacements in the "hotter" zone than in the "cooler" zone.

Besides, Figure 3–27 confirms that beam 2 failed faster than the other beams, in spite of a lower heating rate.

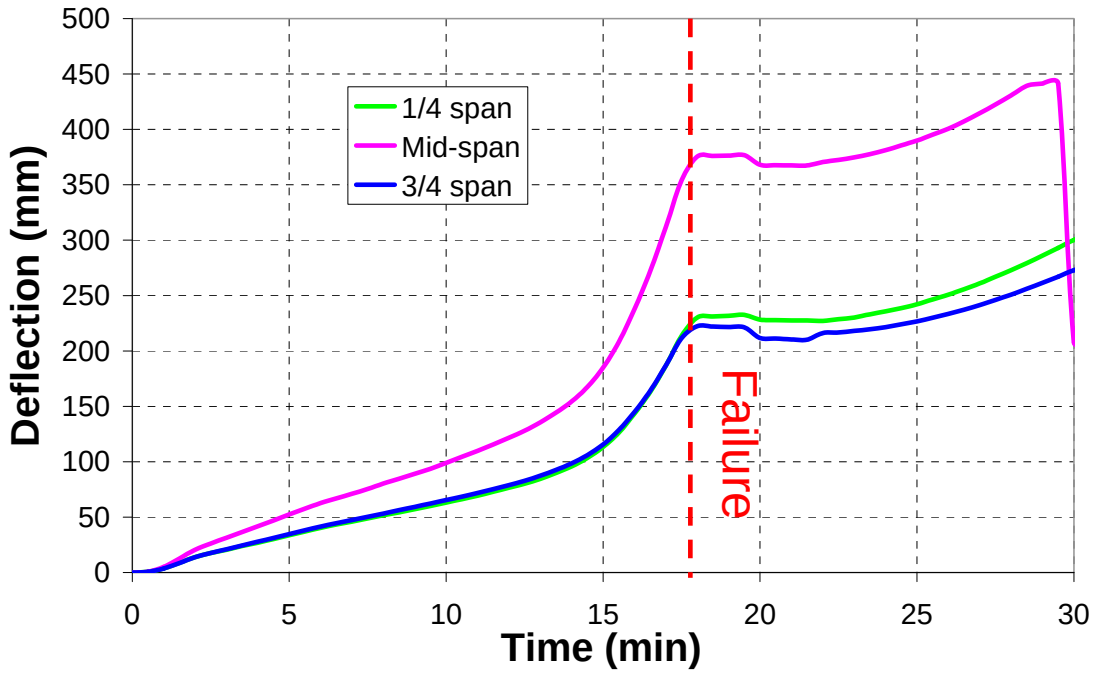

Figure 3–23 : Beam 1 – deflection vs. time

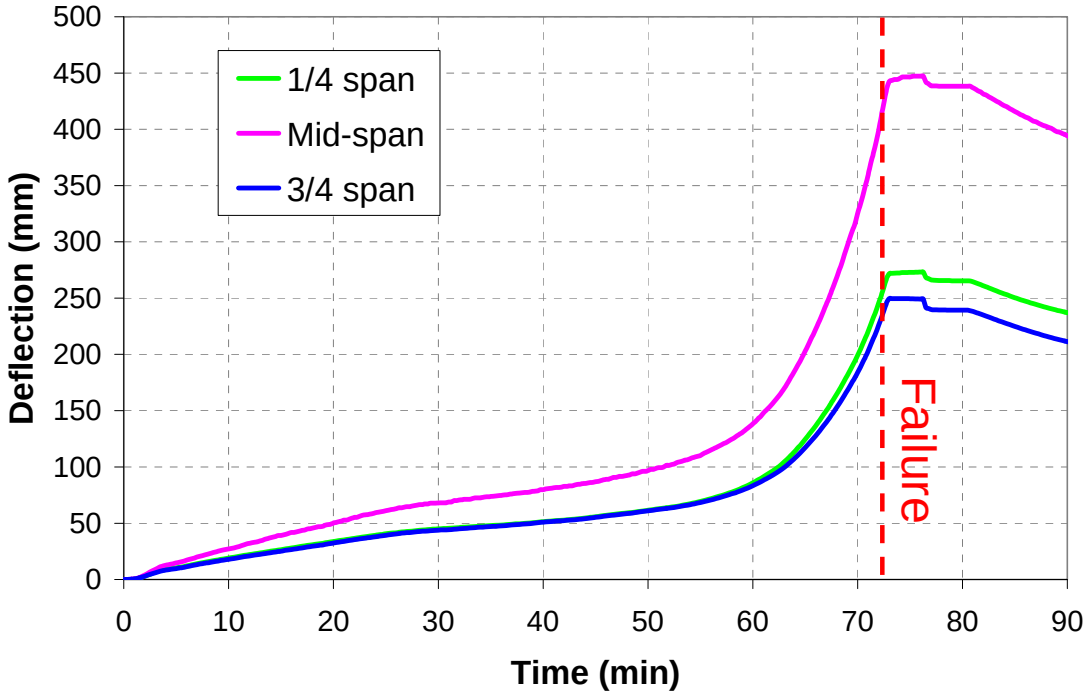

Figure 3–24 : Beam 2 – deflection vs. time

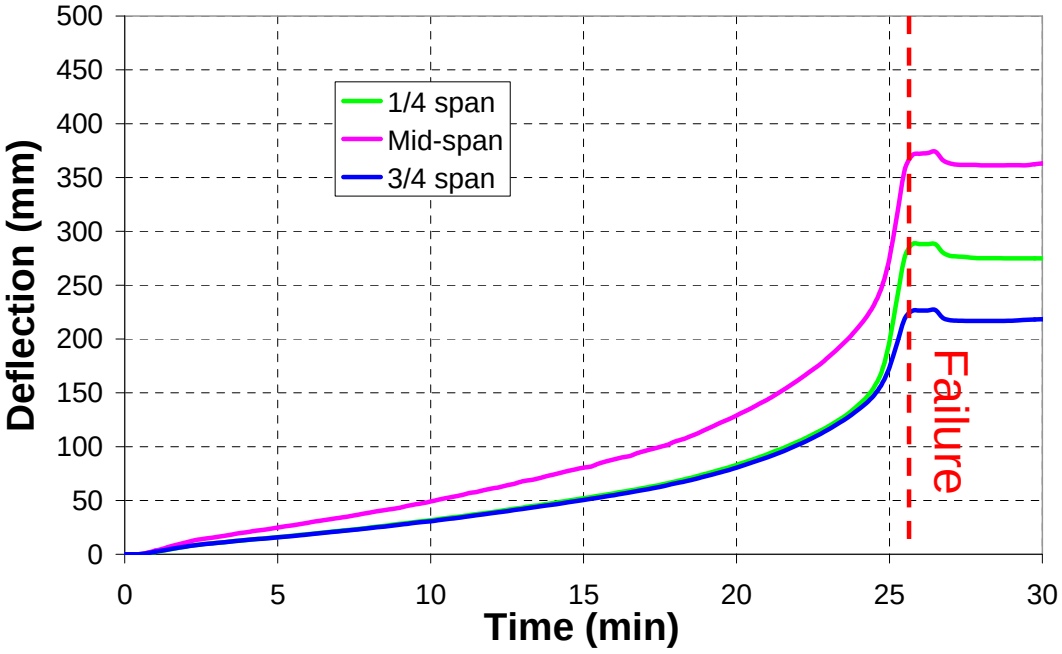

Figure 3–25 : Beam 3 – deflection vs. time

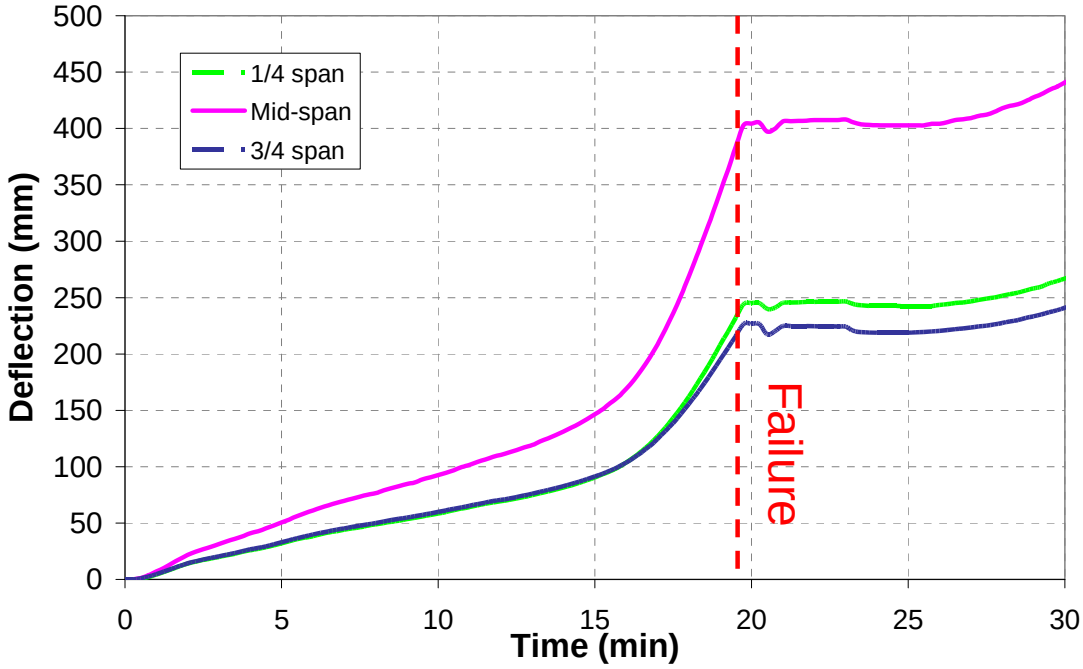

Figure 3–26 : Beam 4 - deflection vs. time

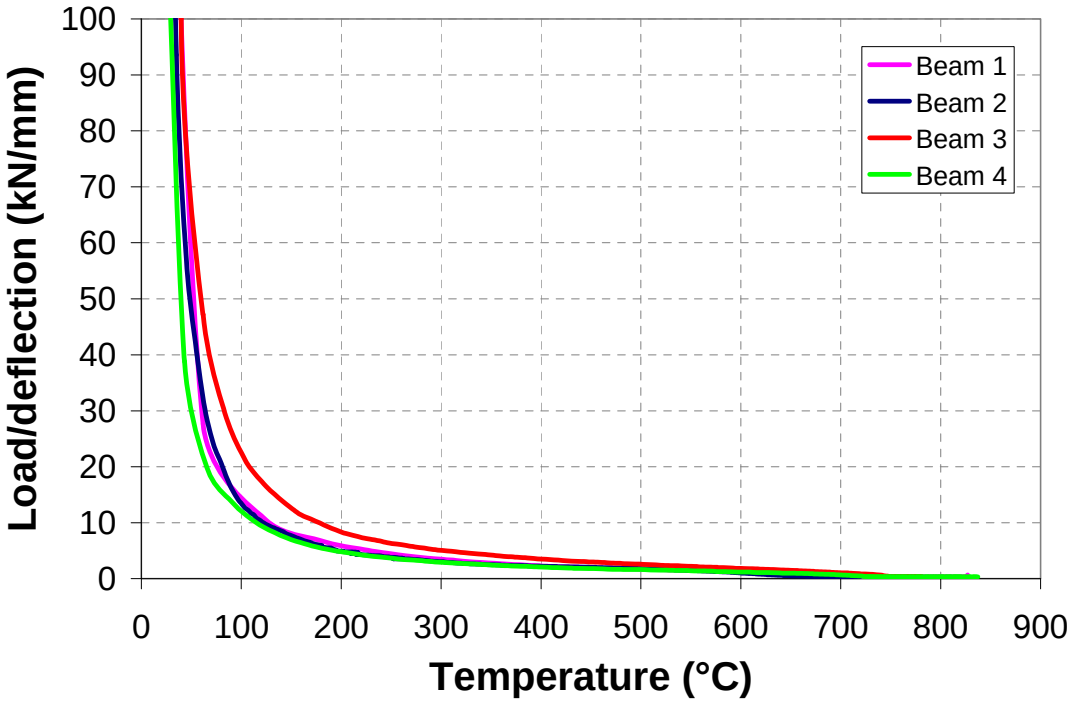

Figure 3–27 : Load/deflection vs. temperature

3.2.3. Failure mode

For both beam 1 and beam 3, the failure was due to web-post buckling near the beam supports (see Figure 3–28 and Figure 3–29), which is one of the usual modes of failure observed for such beams in fire situation. This web-post buckling could even generate a tee welding breakage.

Besides, because of its web-post stiffeners, beam 4 had a flexural bending failure, as it behaved like an “ordinary” beam. Hence, as beam 1 and beam 4 had the same cross-section, and as their deflection vs.

time graphs are very close, beam 1's collapse might have been caused by combined web-post buckling and flexural bending.

As for the primary beam, i.e. beam 2, no web-post buckling was observed, which leads to the conclusion that this beam also failed by flexural bending.

Beam 1

Beam 2: Cell 5 to 7

Beam 2 : cell 7 to 9

Beam 3

Beam 4

Figure 3–28 : Deformed beams in their central part

Beam 1

Beam 2

Beam 3

Beam 4

Figure 3–29 : Deformed beams in their RHS zone

4. WP3 : F.E. SIMULATIONS OF FURNACE TESTS AND PARAMETRIC STUDY

The parametric study was run conducted using SAFIR (version 2007a), CAST 3M and Ansys.

4.1. SAFIR Mechanical model

For the mechanical model of the steel profile, 4-node shell finite elements were used, as shown in Figure 4–1.

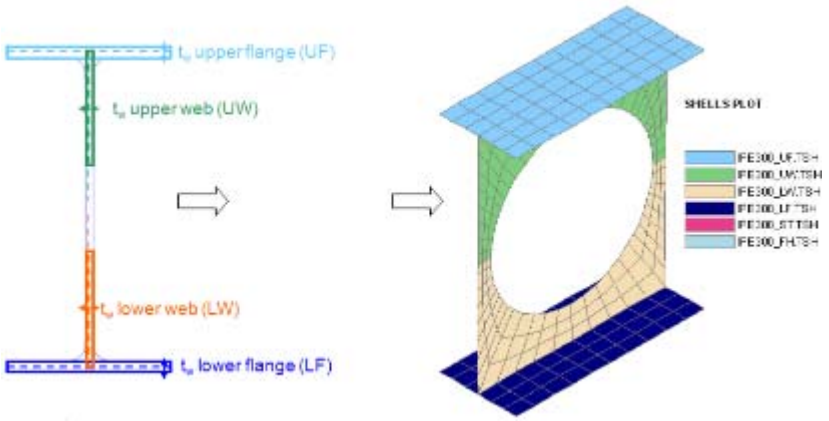

Figure 4–1 : Mechanical model

The beam was simply supported. Symmetry was used at the mid-span and the lateral displacement of the upper flange was restrained to avoid any lateral torsional buckling (Figure 4–2).

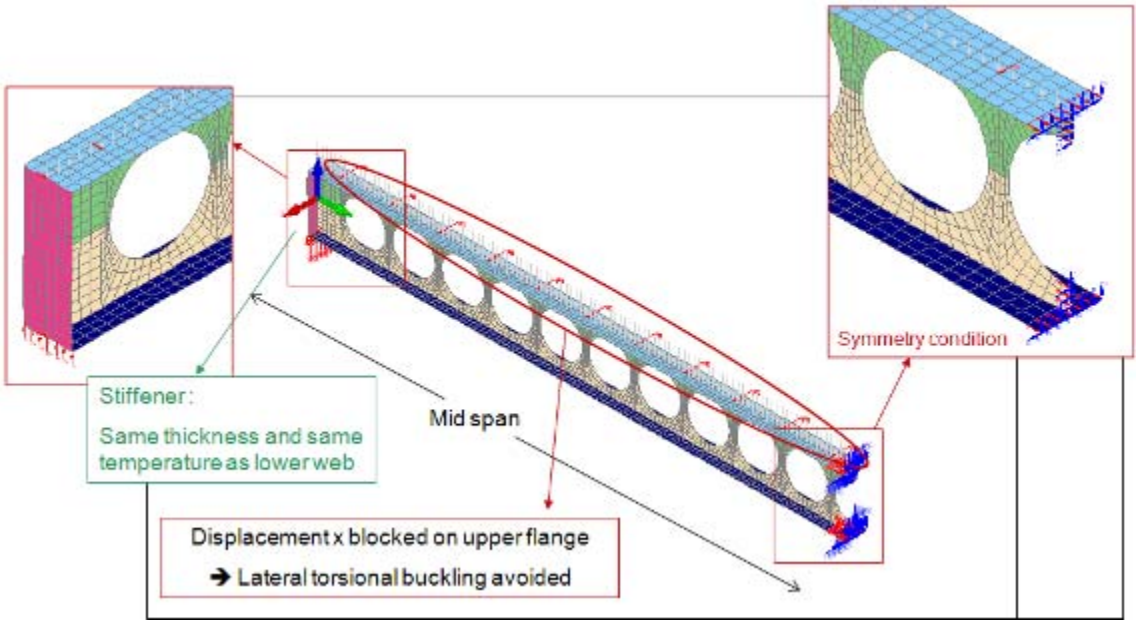

Figure 4–2 : Boundary conditions for modelled beam

An initial deformation was given to the beam (Figure 4–3a). This deformation results from the product of a sine curve on the height of the profile (Figure 4–3b) and of a cosine curve on the length of the beam. The maximum amplitude was 2 mm.

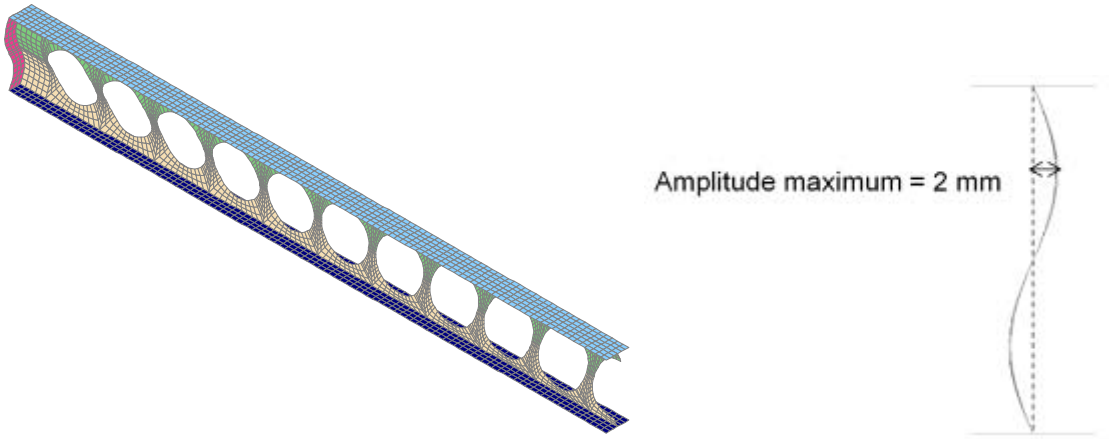

Figure 4–3
a) CB with amplified initial deformation (x 15) and b) initial deformation of the web-post

The assumed material properties of the steel were taken according to Eurocode EN1993-1-2 [20], with the variation of different parameters with temperature taken from Eurocode EN1993-1-2.

The Figure 4–4 shows the comparison between FEM model and the fire test beam 2.

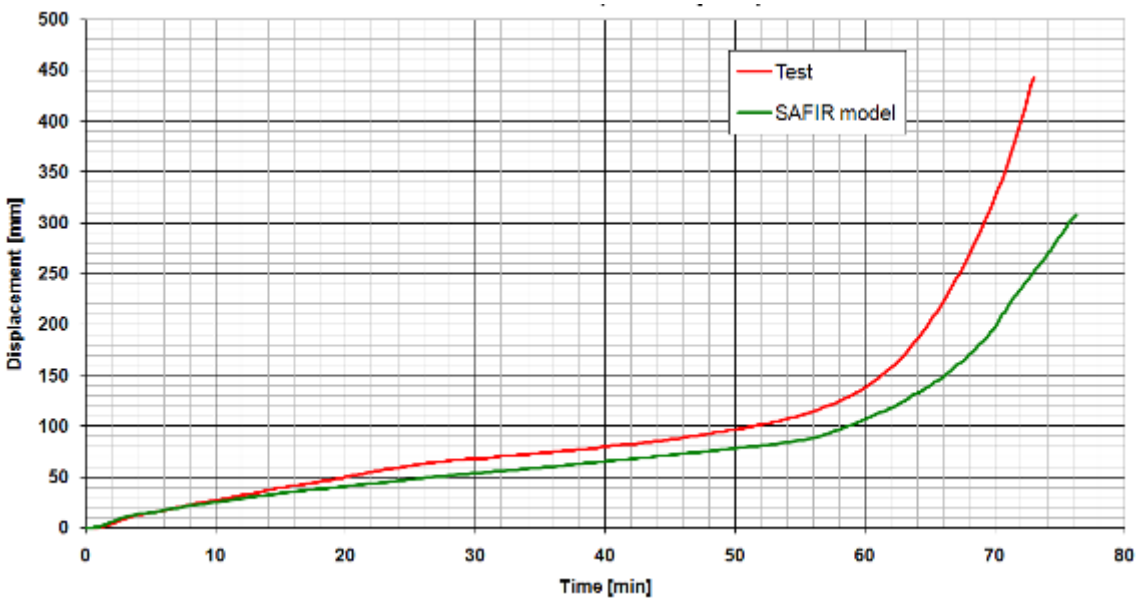

Figure 4–4 : Time–Displacement diagram of the beam 2 at mid-span

4.2. Ansys Numerical Model

The Ansys model was based on a 3D mesh made of shell and beam elements (Figure 4–5a). As the ribs were neglected in the model, only the concrete part above the steel deck was modelled (Figure 4–5b). The experimental measured yield strengths were used.

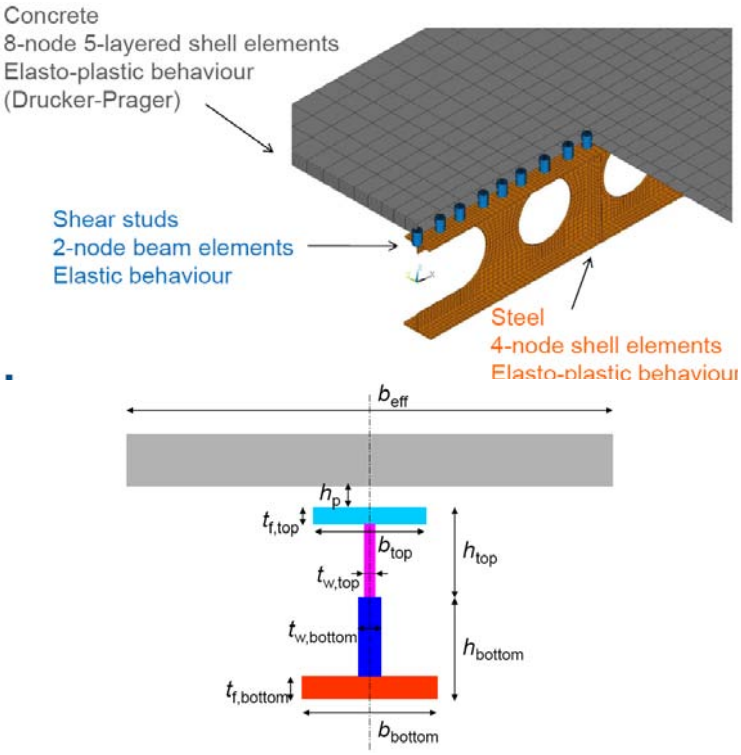

Figure 4–5 : a)Mechanical analysis model and b)Mechanical analysis cross-section

Due to mid-span symmetry, axial restraints and rotational restraints about the two axes of mid-span cross-section were applied. Support conditions were modelled by restraining vertical displacements. Also, so as to prevent lateral torsional buckling, flange-web junctions in both tees were laterally restrained. The mechanical load was applied to the top steel flange, including self-weight. The analysis was run until numerical failure. Figure 4–6 shows the comparison between the FEM model and the fire test beam 2.

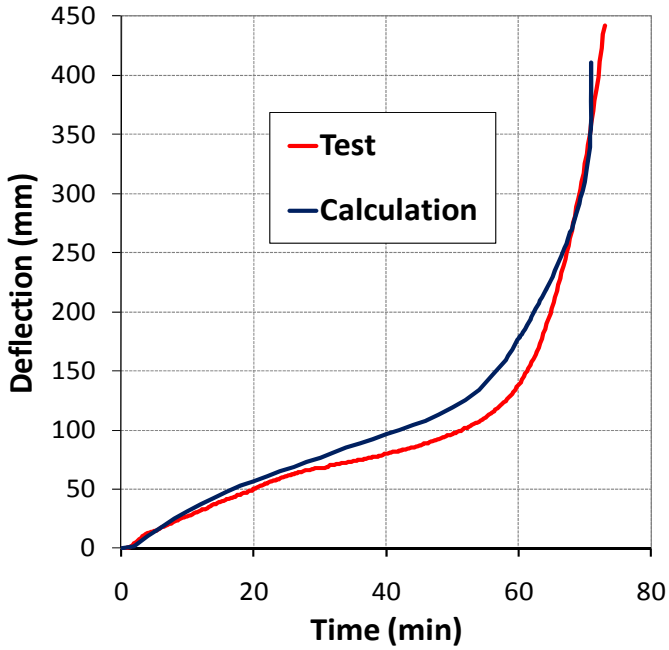

Figure 4–6 : Time-Displacement diagram of the beam 2 at mid-span CTICM numerical model

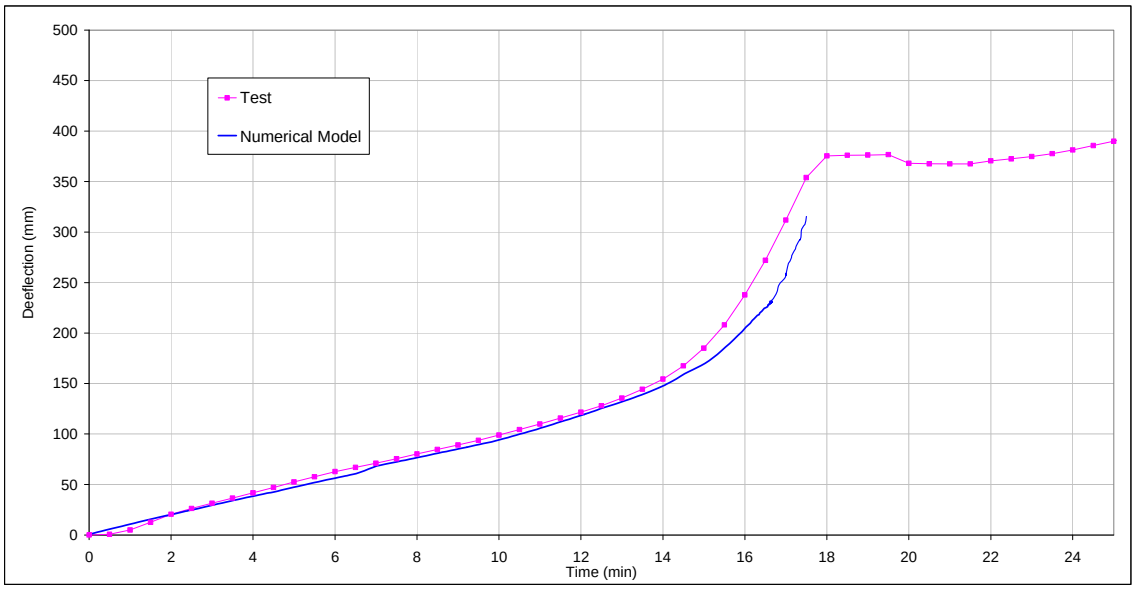

Figure 4–7 : Time-Displacement diagram of the beam 1 at mid-span SCI numerical model

4.3. Cast3M F.E. model" Heat Transfer modelling

The fire tests were simulated under Cast3M, a finite element code developed by CEA (Commissariat à l'Energie Atomique). The heat transfer model takes into account conduction, convection and radiation.

4.3.1. Mesh

As shell element non-linear radiation has not been implemented in Cast3M yet, 8-node solid elements were used. The calculation results were then projected on the shell element model, and considered as thermal load.

This implies common nodes between the solid element mesh and the shell element mesh. Thus, 2 elements were used through the thickness of the different steel parts, i.e. both flanges, both tee webs and stiffeners.

The actual bottom tee web thickness was used for both tees in the model, regardless of the possible difference between the tee sections (beam 1, 3 and 4).

As for the slab, a 10-layered 120 mm deep concrete slab without any rib was modelled. In order to avoid time consuming calculation, a ~500 mm width was considered, instead of the 2,200 mm actual width. The temperatures in the non-modelled slab part were then assumed to be equal to the temperatures on the edges of the modelled slab. Besides, due to the symmetry of the four beams at mid-span, only one half of the composite beams was modelled, as shown in Figure 4–8.

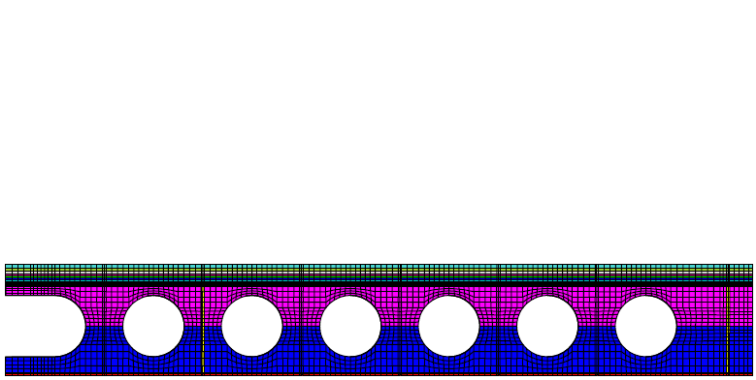

(a) Elevation view 1

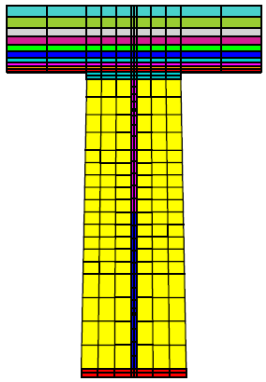

(b) Elevation view 2

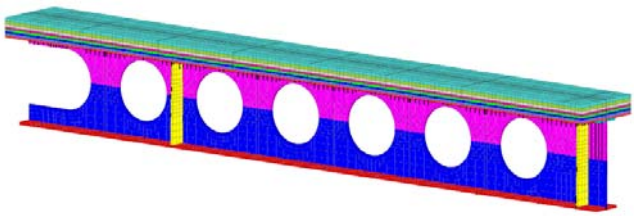

(c) 3D view 1

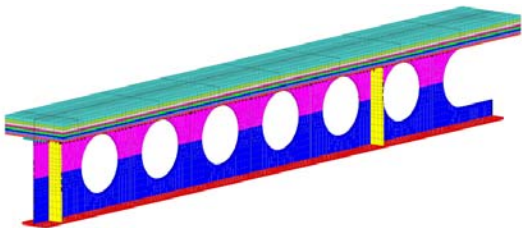

(d) 3D view 2

Figure 4–8 : Beam 1 mesh

4.3.2. Boundary conditions and thermal load

As the beams were heated up from beneath, the steel beam contour and the bottom concrete side were fire-exposed. However, no heat transfer was assumed in the adjacent parts of the steel mesh and the concrete mesh.

Moreover, as the ends of the tested beams were located outside the furnace, the end stiffeners and all the elements beyond these stiffeners were not fire-exposed in the model. The top side of the slab was not fire-exposed either.

A 25 $W.m^{-2}.K^{-1}$ convection exchange coefficient was used on the exposed sides, whereas a value of 4 $W.m^{-2}.K^{-1}$ was used on the unexposed sides.

Different emissivity values were considered, as shown in Figure 4–9. Near the beam end, i.e. in the vicinity of the end cell, the emissivity of the exposed top flange was taken as half the emissivity of the rest of the exposed top flange, to include the shadow effect.

Under each beam, room temperature was assumed to increase according to the average test values given in Figure 3–3. Beams 1, 3 and 4 had a 30-min fire exposure, whereas beam 2 had an 80-min fire exposure.

(a) In the central zone *(b)* Around end cell

Figure 4–9 : Emissivity on the exposed sides of the composite beams

4.3.3. FEA results

In the following graphs, dotted lines refer to test results in the hotter half of each beam, while continuous lines refer to numerical modelling results. Moreover, for each beam, the FEA curves in the top flange and in the bottom flange respectively, lie on top of each other, because of the assumed geometric and thermal load symmetry.

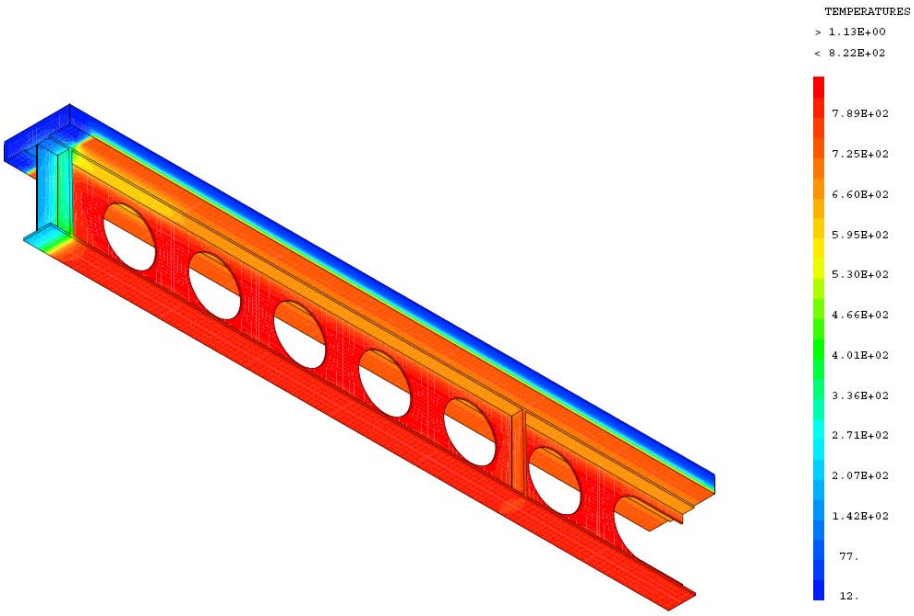

Figure 4–10 : Beam 1 – temperatures after 30-min fire exposure

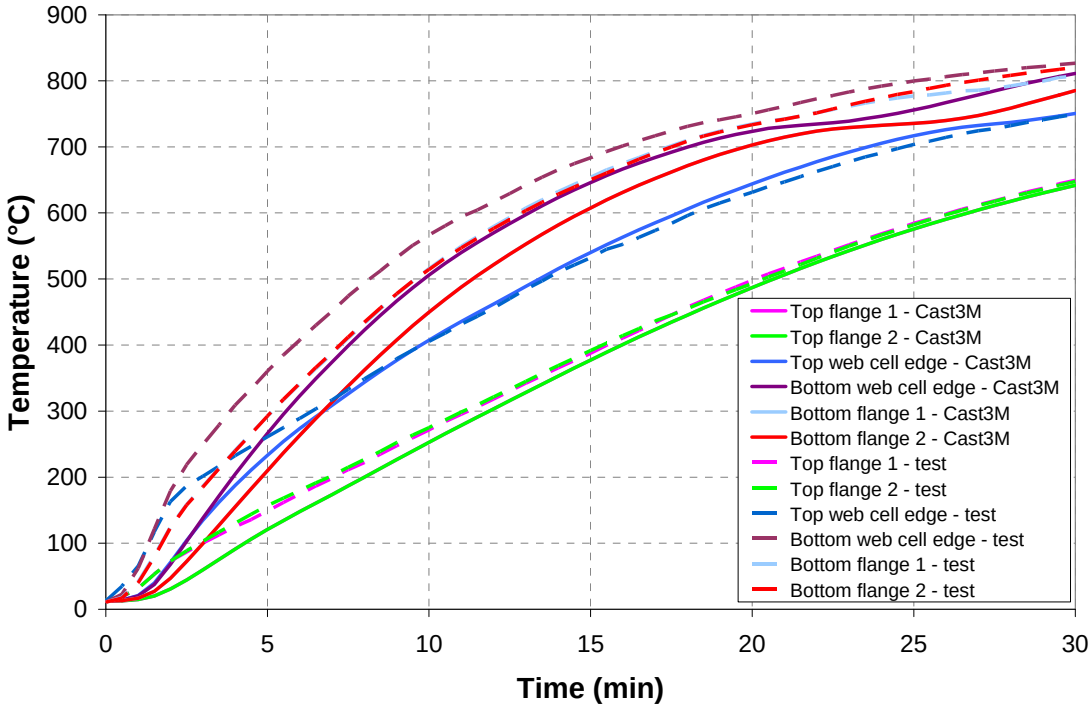

Figure 4–11 : Beam 1 - steel mid-span temperatures

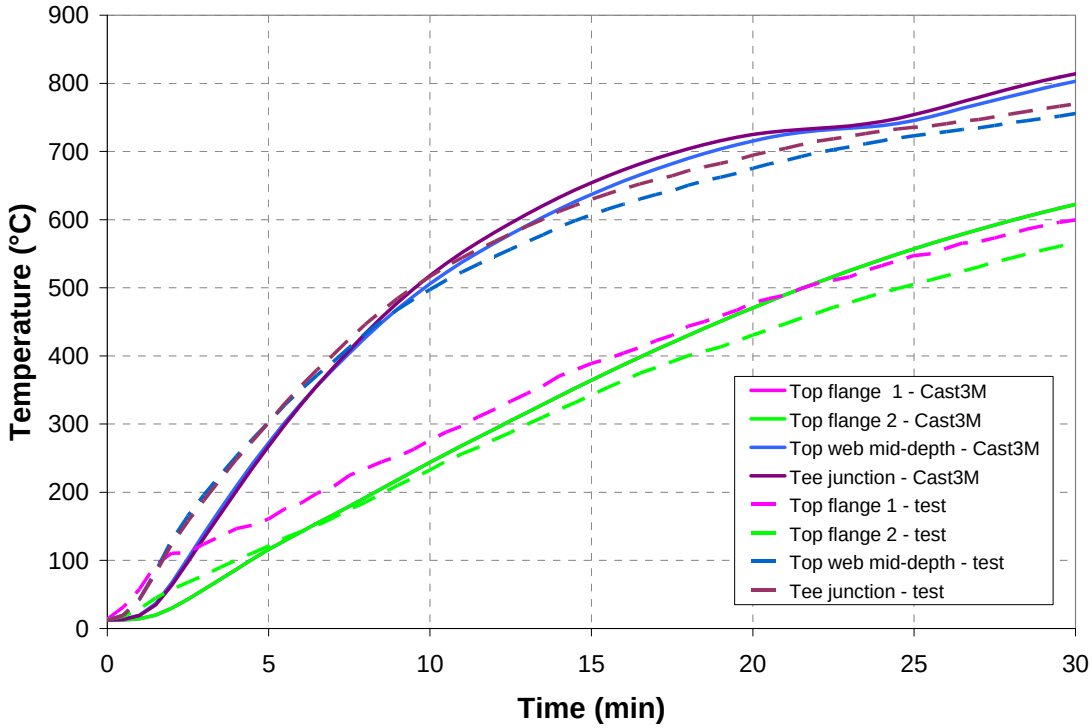

Figure 4–12 : Beam 1 - top tee temperatures near end cell

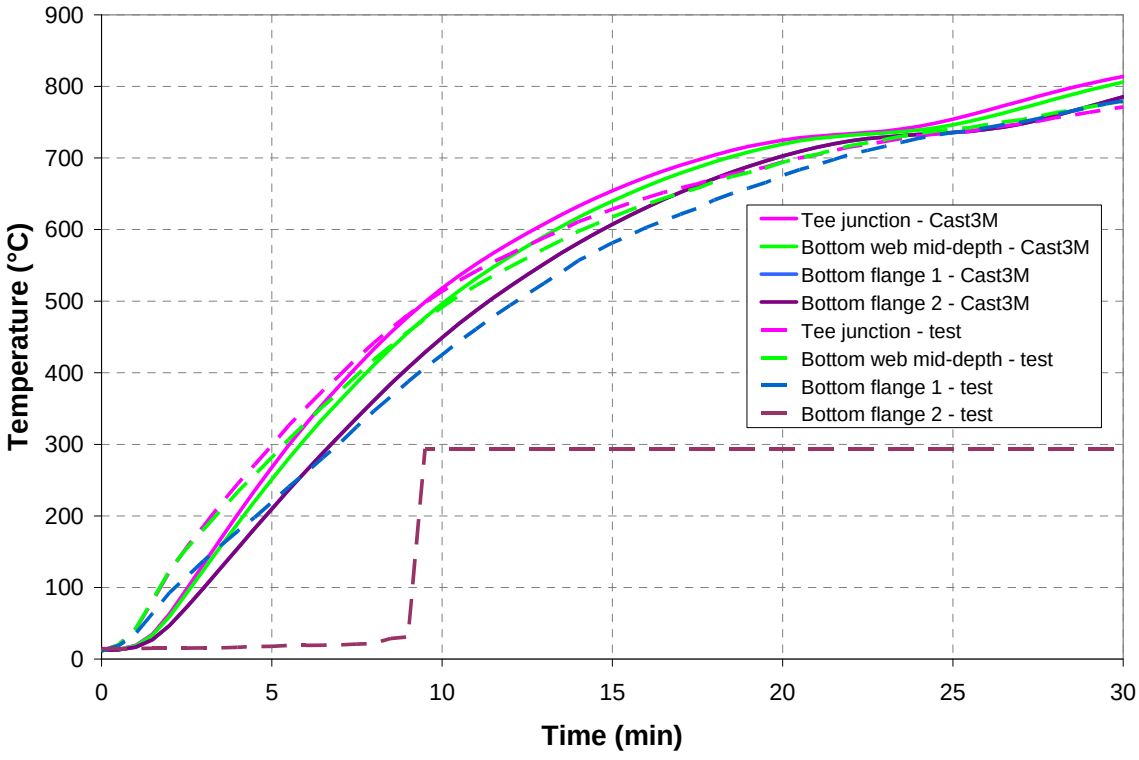

Figure 4–13 : Beam 1 - bottom tee temperatures near end cell

A good correlation between the test and the numerical simulation can be noticed, though the test temperatures rose faster at the beginning of the fire exposure.

4.4. Conclusion on FEM Modelling

A good agreement between the tests and both FEM models is observed, in terms of failure modes and critical temperatures (SAFIR and ANSYS). Thus, theses models can accurately predict the mechanical behaviour of a simply-supported composite cellular beam at elevated temperatures, and can be used for the parametric study which aims to check the relevance of the simplified design method.

The CAST 3M Model was able to reproduce with an acceptable level of accuracy the thermal behaviour of composite cellular beams.

4.5. Parametrical study

This parametrical study was made varying the following parameters:

- steel profile
- geometry of the web-post
- steel strength limit
- loading type
- slab type

Table 4-1 is summarising the different calculated cases.

Table 4-1 : Parametrical study cases

	Parameter		minimum value	maximum value	step	number of different beams	
						PS (Pure steel)	CB (Composite Beam)
general properties	span	L	8 m	20 m	4 m	4	4
	Pure Steel beam or Composite Beam	PS - CB				1	1
	fire curve		ISO fire curve			1	1
	loading	G - Q	PS : 2 concentrated loads - distributed load (load ratio = 0.5) CB : distributed load (load ratio = 0.5)			2	1
steel profile	steel profile	IPE .... - HE ...	PS : IPE300 - HEA400 - HEM900 CB : IPE300 - HEA400 - IPE300/HEA400			3	3
	steel grade of the profile	f_y	IPE300 : S275 - S355 HEA400 et HEM900 : S355 - S460 IPE300/HEA400 : 355/355 - 355/460			2	2
	total height of the profile	H_t	depending of the steel profile, a_0 and w			1	1
	height lower profile	H_{LP}	depending of the steel profile			1	1
	upper flange thickness	t_{UF}	depending of the steel profile			1	1
	upper web thickness	t_{UW}	depending of the steel profile			1	1
	lower web thickness	t_{LW}	depending of the steel profile			1	1
	lower flange thickness	t_{LF}	depending of the steel profile			1	1
	diameter of openings	a_0	a_0 "normal"	$a_0$max	-	2	2
	position of the first opening	w_0	-	-	-	1	1
	web post width	w	for a_0 "normal" : w_{max} and w_{min} (>50) for $a_0$max : $w_{optimum}$ and $w_{small value}$"		-	2	2
	protection	no protection				1	1
concrete slab	concrete slab thickness	h_c	hp = 59mm hc = 61mm	hp = 0mm hc = 120mm	60		2
	overall depth of the profiled steel sheeting	h_p					
	concrete effective width	b_{eff}	min (2 m ; L/4)		-		1
	concrete grade	f_{ck}	C25/30 if S275 and S355 - C30/37 if S460				1
	concrete slab reinforcement	A_s	0.00%				1
	reinforcement grade	f_{sk}	S500				1
	degree of shear connection	h	100%		-		1
						192	192
						= total number of simulations for steel CB	= total number of simulations for composite CB

Sum-total, 192 simulations are foreseen for pure steel beams and 192 simulations for composite beams.

4.6. Results of the parametrical study

The critical temperature and the failure modes were assessed using finite element models and compared with analytical model using the following formula:

$$\frac{\left(\text{Crit}\_\text{Temp}_{\text{FEM}} - \text{Crit}\_\text{Temp}_{\text{Analytical}}\right)}{\text{Crit}\_\text{Temp}_{\text{FEM}}} \times 100 = \Delta$$

This means that when the points are positive, the analytical model predicts a lower critical temperature than the finite element model and so is considered conservative (i.e safe sided).

Two different analytical models were used for the comparison:

- the model developed by O.Vassart [23] based on Eurocode principles and presented hereafter in point 5.1. This model has been introduced in the ArcelorMittal Cellular Beam Software.
- The Existing Engineering Model coming from SCI which was introduced in the Westok Cellbeam Software.

Figure 4–14 shows the comparison of the results between FEM and analytical model based on Eurocode principles

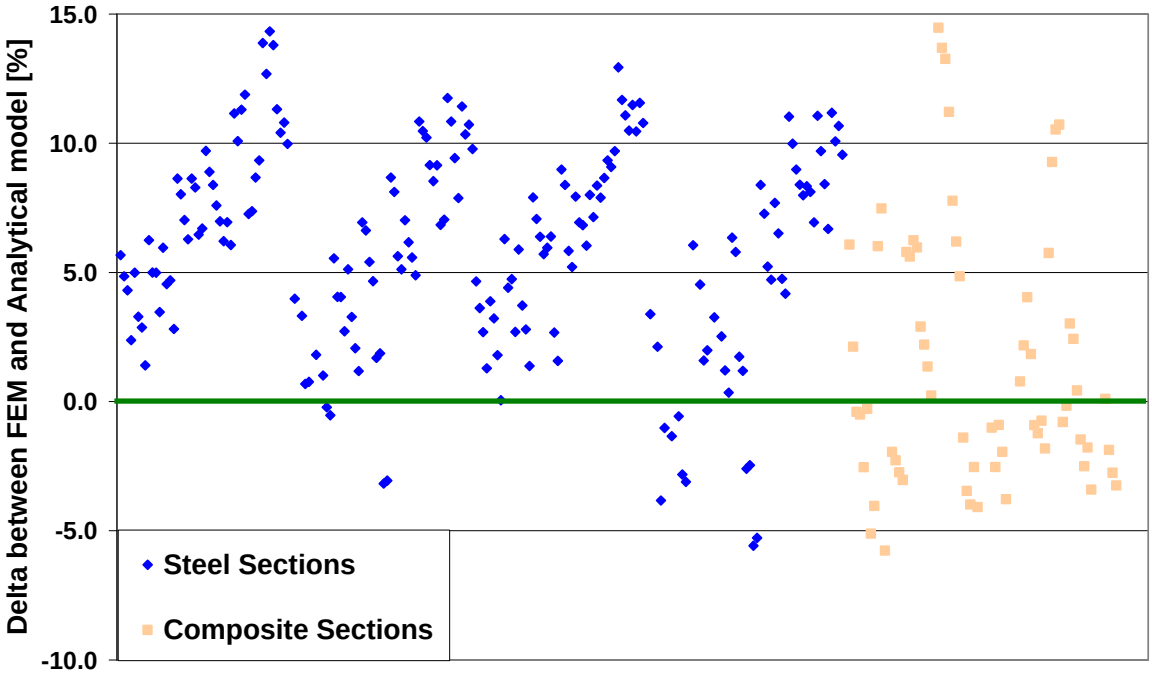

Figure 4–14 : Time-Analytical model Vs FEM Modelling

Analysing Figure 4–14, it can be pointed out that the analytical models can predict the critical temperature of steel cellular beams. The analytical model, based on Eurocodes principles, provides safe sided results with acceptable level of accuracy.

It can also be pointed out that the analytical models can also predict the critical temperature of composite cellular beams.

Figure 4–15 shows the comparison of the results between FEM and analytical model of SCI introduced in the Cellbeam Software.

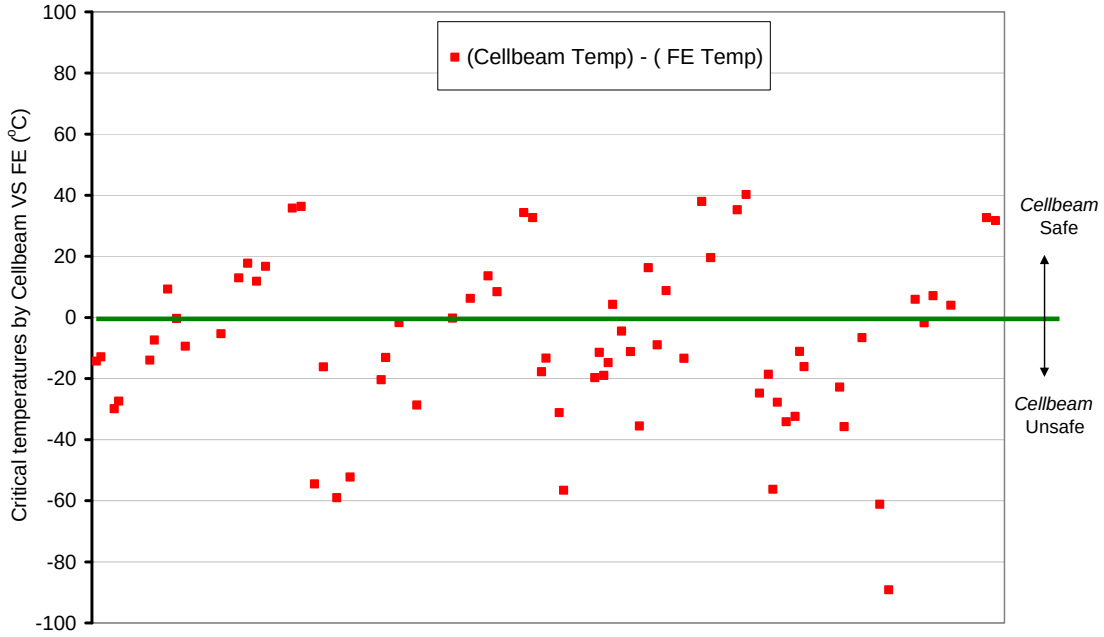

Figure 4–15 : *Cellbeam* results for critical temperatures versus the analytical model (temperature)

The amount of point is reduced compared to the study with the Eurocode model due to a different scope of application of the methodology.

From the Figure 4–14, it can be pointed out that Cellbeam tends to be slightly unconservative at prediction the buckling load. This suggests that the current effective length considered for the compression strut needs to increase slightly to give more conservative results for the web post buckling.

In order to understand what happens, SCI has launched another study:

The aim of these case studies was to evaluate the reasonability of *Cellbeam* software for long-span composite beams. A total of 18 cases were studied at this case study.

Table 4-2 includes the geometric details of the 18 cases (all spanning 15000 mm) investigated in ANSYS and compared against *Cellbeam*.

Table 4-2 : List of the symmetric and asymmetric composite cellular beams investigated at ambient and elevated temperature using *ANSYS*

Section Type	Case No.	Top Tee	Bottom Tee	d_o (mm)	h (mm)	t_{top} (mm)	t_{bot} (mm)	d (m)	L (mm)	S (mm)	w (mm)
Symmetric Sections	Case 1	605x305x179UB	605x305x179UB	500	750	14.1	14.1	669.8	15	600	100
	Case 2	605x305x179UB	605x305x179UB	500	750	14.1	14.1	669.8	15	700	200
	Case 3	605x305x179UB	605x305x179UB	500	750	14.1	14.1	669.8	15	800	300
	Case 4	605x305x179UB	605x305x179UB	500	750	14.1	14.1	669.8	15	900	400
	Case 5	605x305x179UB	605x305x179UB	600	750	14.1	14.1	669.8	15	850	250
	Case 6	605x305x179UB	605x305x179UB	400	750	14.1	14.1	669.8	15	650	250
	Case 7	605x305x179UB	605x305x179UB	550	750	14.1	14.1	669.8	15	800	250
	Case 8	605x305x179UB	605x305x179UB	450	750	14.1	14.1	669.8	15	600	150
	Case 9	605x305x179UB	605x305x179UB	400	750	14.1	14.1	669.8	15	600	200
	Case 10	605x305x179UB	605x305x179UB	600	750	14.1	14.1	669.8	15	900	300
	Case 11	605x305x149UB	605x305x149UB	400	750	11.8	11.8	677.6	15	600	200
	Case 12	605x305x149UB	605x305x149UB	600	750	11.8	11.8	677.6	15	900	300
Asymmetric Sections	Case 13	533x210x82UB	610x229x140UB	500	750	9.6	13.1	689.3	15	750	250
	Case 14	533x210x82UB	610x229x140UB	600	750	9.6	13.1	689.3	15	850	250
	Case 15	533x210x82UB	610x229x140UB	500	750	9.6	13.1	689.3	15	650	150

A first set of simulations was launched at room temperature.

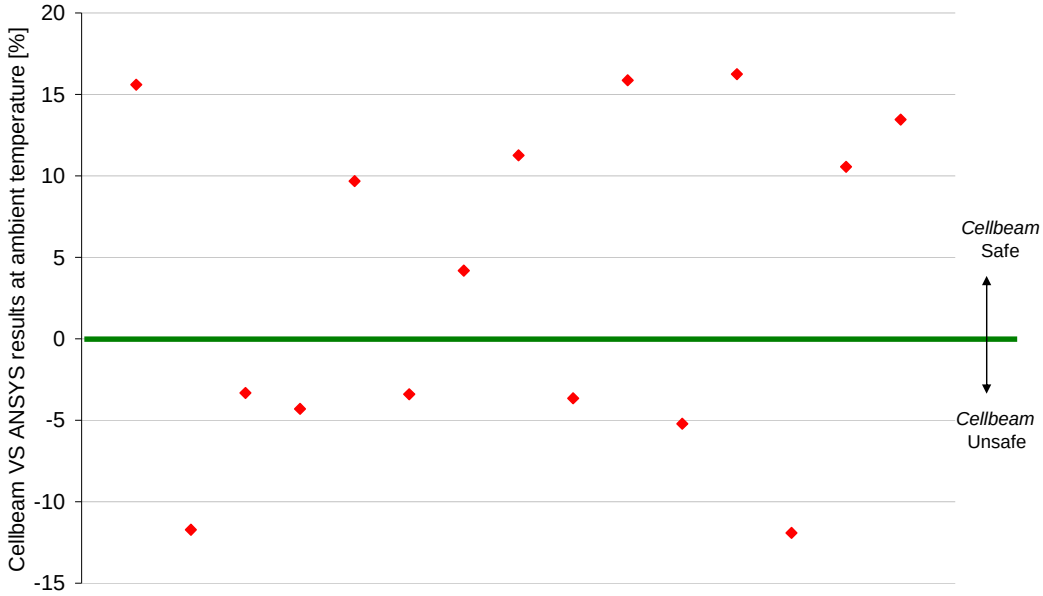

Figure 4–16 : ANSYS against *Cellbeam* results at room temperature design

According to these charts, Cellbeam results were mostly conservative in predicting the failure loads at room temperature. However, cellbeam results have also been unconservative compared to ANSYS results in some cases. As shown by Figure 4–14, Cellbeam results appear to be unconservative in 7 of the 15 cases considered at room temperature. All but one of these cases failure occurred by global bending and the conservatism is due to strain hardening of the steel being omitted from the ANSYS model. In one case the failure is due to web post buckling.

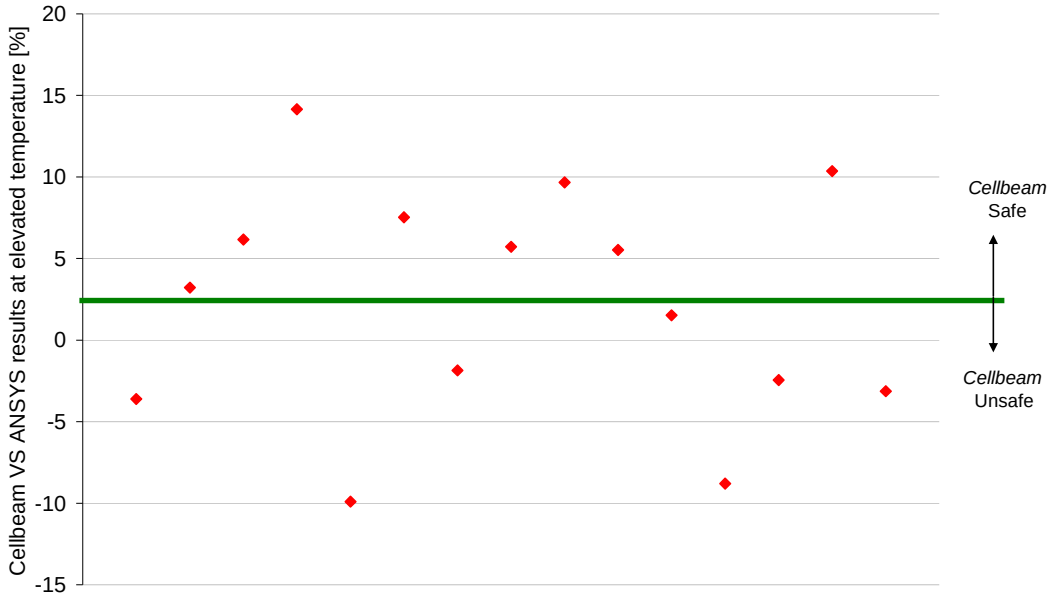

Figure 4–17 : ANSYS against *Cellbeam* results at elevated temperature (%)

In brief, the comparisons at ambient and elevated temperature suggest that the Cellbeam results are most of the time conservative but not always. Cellbeam results were within 15% of the ANSYS results in all the cases studied. They were either conservative or non-conservative depending on the geometry of the beam.

4.7. Conclusions

The different FEM models were able to reproduce with an acceptable level of accuracy the complex behaviour of cellular beams in fire conditions.

On the basis of theses different FEM models, a parametric study was made to validate the developed analytical model.

Eurocode based Model

The Eurocode based analytical model was again validated by this parametrical study and can be used for the prediction of the critical temperature of cellular beam in case of fire. This model takes into account the complex behaviour of cellular beams in fire conditions and is based on the Eurocodes principles taking into account the loss of material properties and stiffness required in the Eurocodes. This model was implemented in a design software called ACB^{+} and can be downloaded for free on www.arcelormittal.com/sections .

SCI Engineering Model

Comparison between the *Cellbeam* and FE models of the 15 case studies on cellular composite floors carried out by SCI showed that *Cellbeam* results were slightly non-conservative in some cases. In particular, cellbeam results were unconservative by a maximum of 12% (in UDL) and 10% (in critical temperature), for design of cellular beams at room and elevated temperatures. Unconservative results were not limited to only one failure mode.

Cellbeam results were also compared against the results of the FE analyses carried out on bare cellular steel section in the scope of the parametrical study, by other project partners. These comparisons show that Cellbeam results for bare steel sections tend to be generally slightly unconservative.

5. WP4 : SIMPLE DESIGN RULES FOR CELLULAR BEAMS SUBJECTED TO FIRE

5.1. Simple design rules for cellular beams subjected to fire Eurocode based Model coming from ArcelorMittal

The analytical method for the web post buckling in cold Condition has been developed by CTICM on behalf of ArcelorMittal, as part of the ACB Design Optimisation study. It is described in many references [1, 8-10].

This method was adapted for the cellular beam calculation in fire conditions [23]. It is presented hereafter.

Following the observations and the analyse of all the tests performed on cellular beam in cold and in fire situation, it was chosen that the analytical model must be based on the principal stress resistance at the border of the opening (see Figure 5–1).

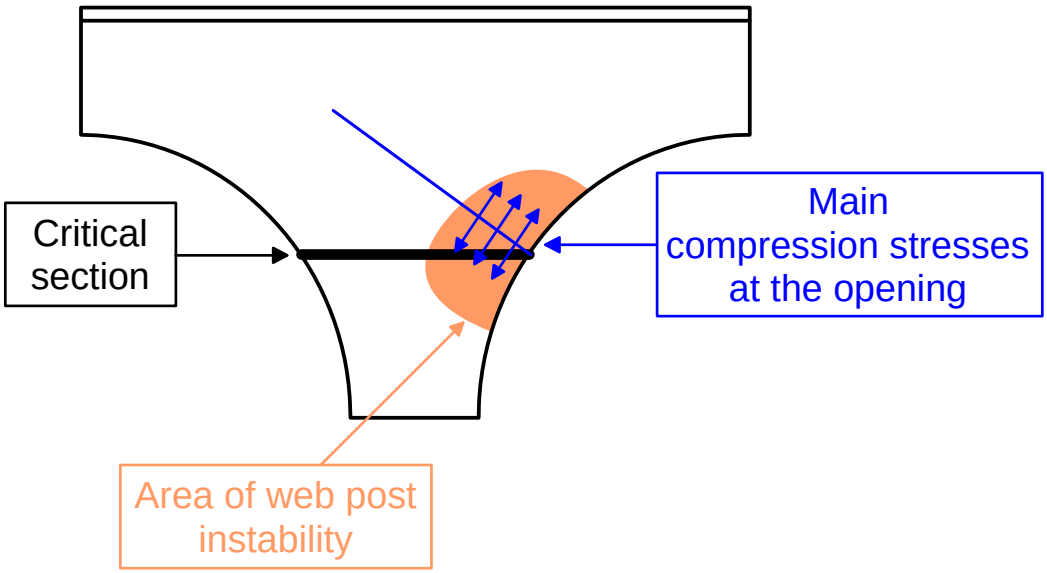

Figure 5–1 : Principle of the check of the web post stability

The criterion for resistance to buckling of an intermediate web post at elevated temperature is given by equation 1. It is based on the calculation of $\sigma_{wfi.Rd}$, the principal stress resistance in fire situation for the half post being studied and $\sigma_{wfi.Ed}$, the principal compressive stress in fire situation in the half post being studied ($\sigma_{wfi.Ed.up}$ for the upper half post and $\sigma_{wfi.Ed.low}$ for the lower half post). These stresses are calculated for the critical section of the member being verified, adjacent to the opening where compression is at a maximum (see Figure 5–2) :

$$\Gamma_b = \frac{|\sigma_{w.fi.Ed}|}{\kappa \sigma_{w.fi.Rd}}$$

where κ is the factor for post critical reserve of strength, taking into account failure by a mechanism that occurs after the appearance of local buckling of the web post (given by Chapter 5.1.8).

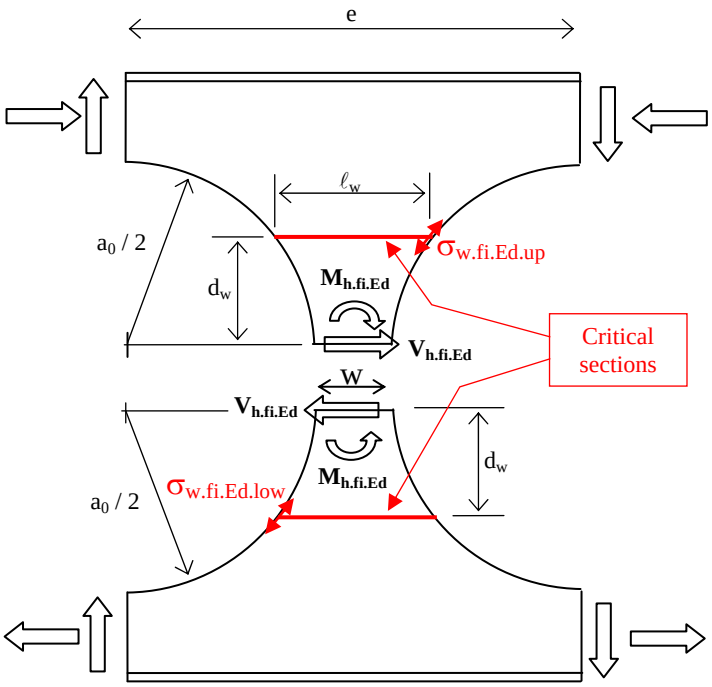

Figure 5–2 : definition of critical section for stability of an intermediate web post

This approach based on the principal stresses came from the analyse of the multiples laboratory tests realised by ArcelorMittal and on the localisation of the compression stresses in the cellular beam web post using finite element modelling (see Figure 5–3).

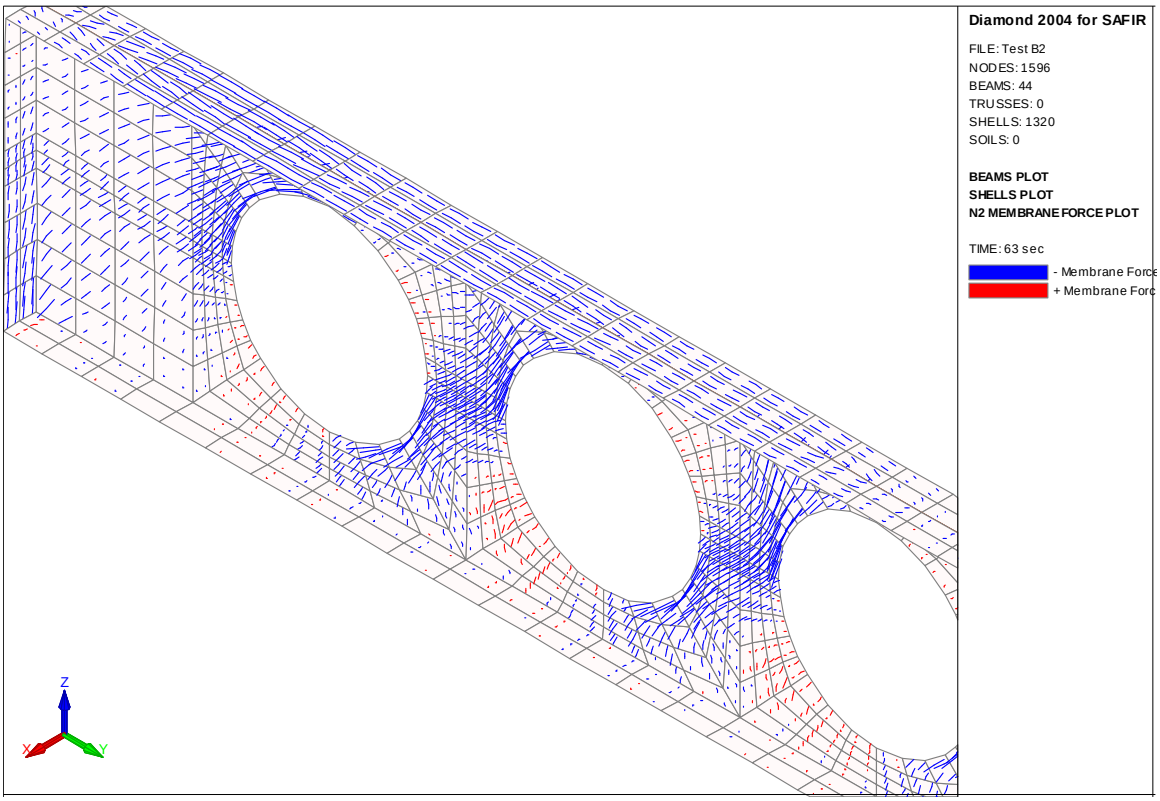

Figure 5–3 : Finite Element Modelling

Throughout the following parts of this thesis, the parameter α defines the width of the web post in terms of the following relationship:

$\alpha = 1 + w / a_0$

5.1.1. Position of the critical section in the web post

The critical section of a half post is the section where the horizontal shear $V_{h.fi.Ed}$ gives the maximum bending stress in the plane of the web. This section is defined in terms of its distance d_w from the joint between the two half posts, given by the following relationship based on geometrical considerations:

$$d_w = \frac{a_0}{2}\sqrt{\frac{\sqrt{\alpha^4 + 8\alpha^2} - 2 - \alpha^2}{2}}$$

The width ℓ_w of the critical section is obtained by considering the following relationship:

$$\ell_w = a_0\left(\alpha - \sqrt{1 - \left(\frac{2\,d_w}{a_0}\right)^2}\right)$$

5.1.2. Principal compressive stress

The principal compressive stress in case of fire at the critical section due to local bending moment (Figure 5–4) is given by :

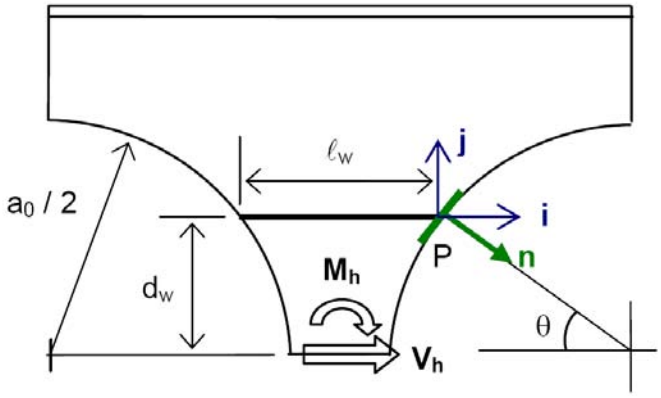

Figure 5–4 : Orientation of the face tengent to the border of the opening

The stress distribution in the point P of the critical section due to the horizontal shear $V_{h.fi.Ed}$ and bending Moment $M_{h.fi.Ed}$ can be expressed by the following relationship on the axes system (i, j) (see Figure 5–4)

$$\begin{bmatrix} -\sigma_x & \tau_v \\ \tau_v & -\sigma_f \end{bmatrix}$$

$\sigma_{w.fi.Ed}$ is the principal stress in the plane of the web and can be expressed by the following relation:

$$\sigma_f = \frac{6\,M_c}{\ell_w^2\ t_w}$$

For the face tangent to the opening, the Normal n can be expressed in the axes system (i, j) taking into account the angle θ:

$\sigma_{i\theta} = -\sigma_{x}\cos\theta - \tau_{v}\sin\theta$
$\sigma_{j\theta} = \tau_{v}\cos\theta + \sigma_{f}\sin\theta$

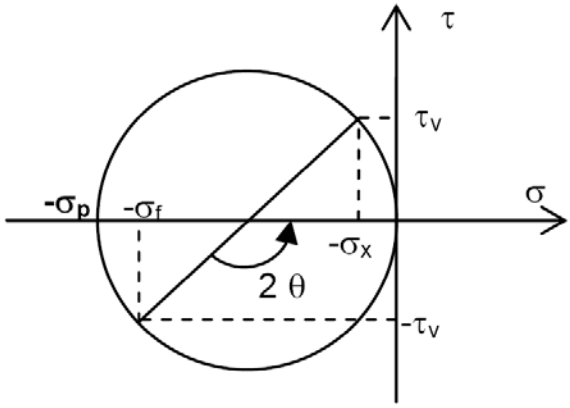

Figure 5–5 : Stresses at point P (Mohr circle)

The boundary conditions impose $\sigma_{i\theta} = \sigma_{j\theta} = 0$, and we found the following expression for the is the principal stress $\sigma_{w.fi.Ed} = \sigma_{x} + \sigma_{f}$:

$$\sigma_{w.fi.Ed} = \frac{6\, M_{c.fi.Ed}}{\ell_{w}^{2}\, t_{w}\left(1-4\left(d_{w}/a_{0}\right)^{2}\right)}$$

With $M_{c.fi.Ed}$ is the bending moment in the critical section in fire situation.

Upper member : $M_{c.fi.Ed.up} = V_{h.fi.Ed}\, dw - M_{h.fi.Ed}$
Lower member : $M_{c.fi.Ed.low} = V_{h.fi.Ed}\, dw + M_{h.fi.Ed}$

5.1.3. Forces acting on Ts in a pure steel section

The forces acting on the Ts at the location of an opening are obtained using the following relationships. They are a function of the global forces M_{Ed} and V_{Ed} calculated at the openings to the left (subscript i) and right (subscript i+1) of the web post :

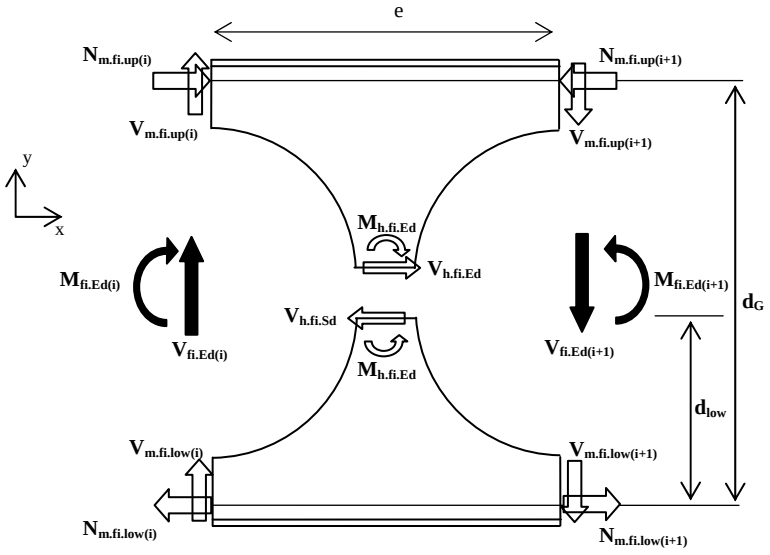

If the hypothesis of an inflection point (point where the bending moment is null) in the Te sections at maximum opening, hypothesis validated by numerical simulations [8], the global bending moment can be expressed by two axial forces in each Te member:

$N_{m.fi.low(i)} = N_{m.fi.up(i)} = M_{fi.Ed(i)} / d_G$
$N_{m.fi.low(i+1)} = N_{m.fi.up(i+1)} = M_{fi.Ed(i+1)} / d_G$

The shear force in each Te member are determined on the basis on the global shear values $V_{fi.Ed(i)}$ and $V_{fi.Ed(i+1)}$.

The repartition of the shear force was studied by Daniel Bitar [10] and is summarised in the next paragraph.

The forces in the web post are given by :

$$V_{hm.fi} = N_{m.fi.up(i+1)} - N_{m.fi.up(i)} = N_{m.fi.low(i+1)} - N_{m.fi.low(i)}$$

$$M_{hm.fi} = \left(V_{m.fi.low(i+1)} + V_{m.fi.low(i)}\right) \cdot \frac{e}{2} - V_{hm.fi} \cdot d_{low}$$

Rem: for a symmetrical profile, $M_{hm.fi} = 0$

With d_{low} is the distance between the centre of gravity of the lower T (at the opening centre line) and the line of the joint between the half posts (see Figure 5–6).

5.1.4. Repartition of the shear between the Te members

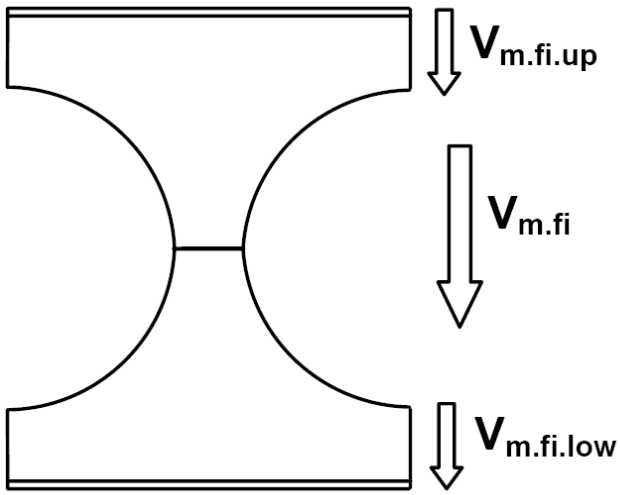

Figure 5–6 : Shear forces repartition

$V_{m.fi}$: Global Shear force in the steel beam at the maximum opening position
$V_{m.fi.low}$: Shear force in the lower Te section
$V_{m.fi.up}$: Shear force in the upper Te section
$A_{v.0.up}$: Shear area of the upper T
$A_{v.0.low}$: Shear area of the lower T

The shear forces are linked by the following equation :

$V_{m.fi} = V_{m.fi.low} + V_{m.fi.up}$

A first approach consisted in the reparation of the global shear force in function of the shear area.

After the analysis of the different tests results and the numerical simulation [10], it was pointed out that this hypothesis was not perfectly correct for asymmetric sections. A new model was propsed by Bitar in order to better reflect the reality. On the Figure 5–7, you can find a comparison between the old method, the new method and the test results.

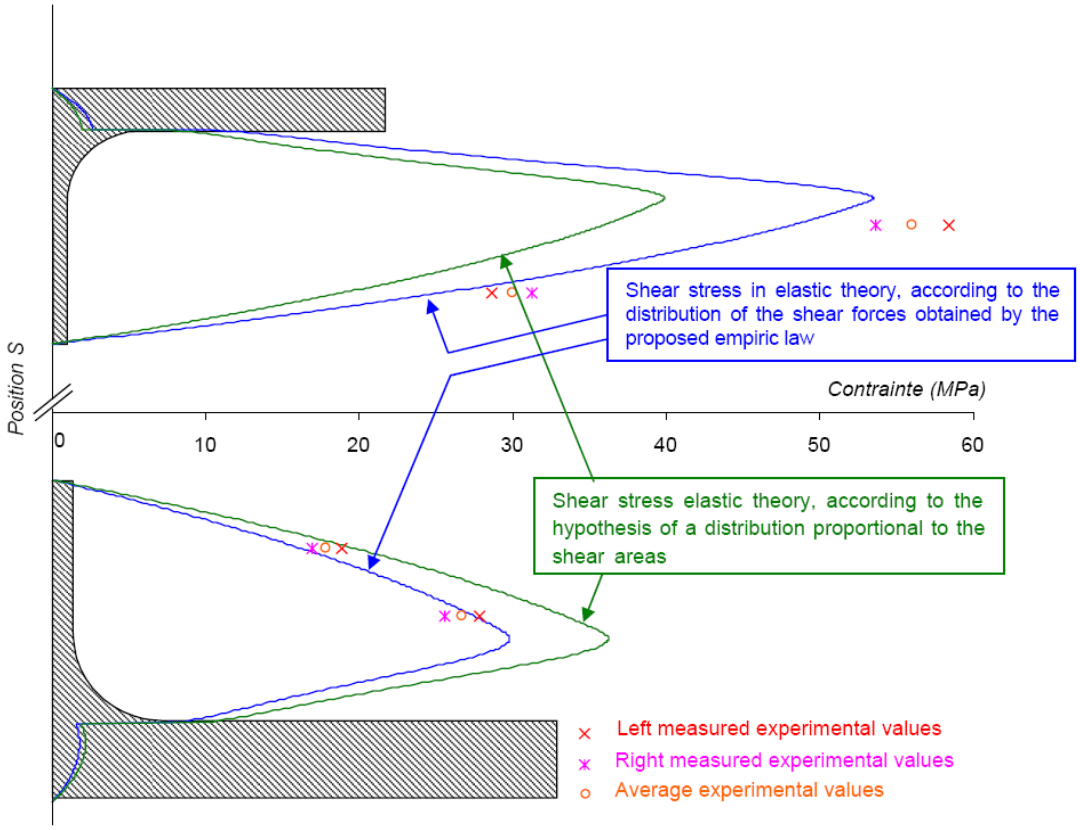

Figure 5–7 : Steel beam test 3a - Shear stresses comparison

This new empirical model can be expressed by the following relationship :

$V_{m.fi.low(i)} = (1 - k_{Av})\, V_{fi.Ed(i)}$ $\qquad$ $V_{m.fi..up(i)} = k_{Av}\, V_{fi.Ed(i)}$

$V_{m.fi.low(i+1)} = (1 - k_{Av})\, V_{fi.Ed(i+1)}$ $\qquad$ $V_{m.fi.up(i+1)} = k_{Av}\, V_{fi.Ed(i+1)}$

With : k_{Av} is the coefficient for distribution of the shear force, given by :

$$k_{Av} = \frac{A_{v.0.low}^{\eta}}{A_{v.0.up}^{\eta} + A_{v.0.low}^{\eta}}$$

η : Empirical coefficient calibrated using numerical simulations given by :

$$\eta = \frac{1}{9{,}48 - 4{,}84\,\alpha}$$

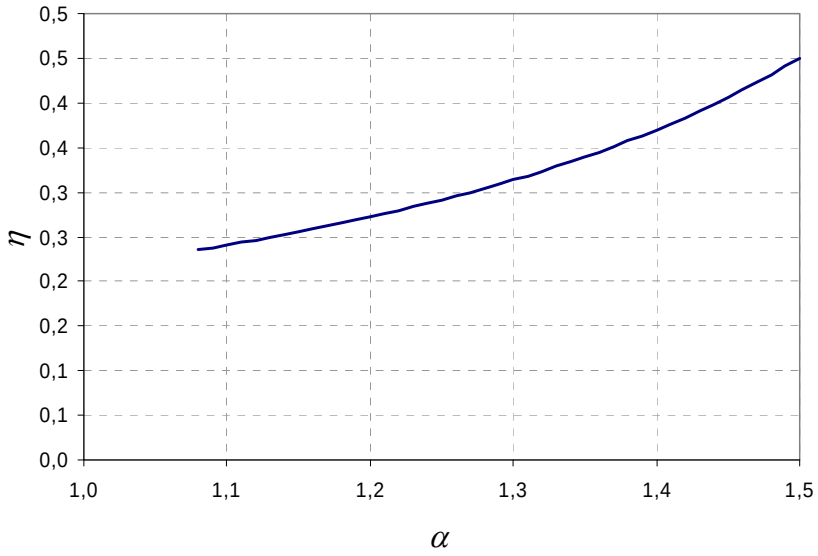

Figure 5–8 : Form of the variable η as a function of α

The shear area of a T is given by :

$$A_{v.0} = \left(h_m - \frac{a_0}{2} - \frac{t_f}{2} \right) t_w + r_c t_f + \frac{4-\pi}{2} r_c^2$$

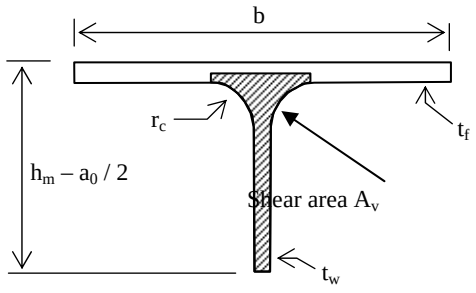

Figure 5–9 : shear area of a T at the location of an opening

5.1.5. Forces acting on Ts in a composite section

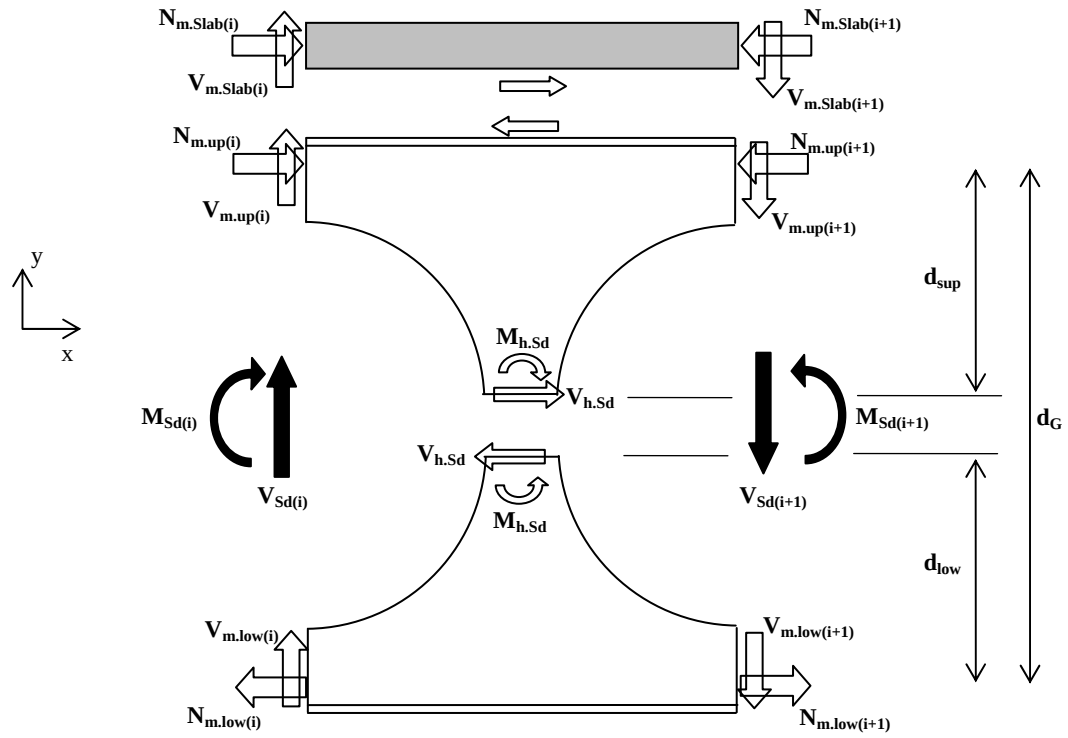

Figure 5–10 : Forces in the steel Ts and the slab

At an opening the axial forces applied at the centres of gravity of the T shaped steel members and the slab are taken as being equal to the forces deduced from the diagram of stresses at the ULS of plastic resistance of the section, reduced in proportion to the ratio $M_{fi.Ed} / M_{fi.Rd}$. This leads to the following relationships:

$$N_{m.fi.up} = N_{m.ULS.up} \frac{M_{fi.Ed}}{M_{fi.Rd}}$$

$$N_{m.fi.low} = N_{m.ULS.low} \frac{M_{fi.Ed}}{M_{fi.Rd}}$$

$$N_{m.fi.slab} = N_{m.ULS.slab} \frac{M_{fi.Ed}}{M_{fi.Rd}}$$

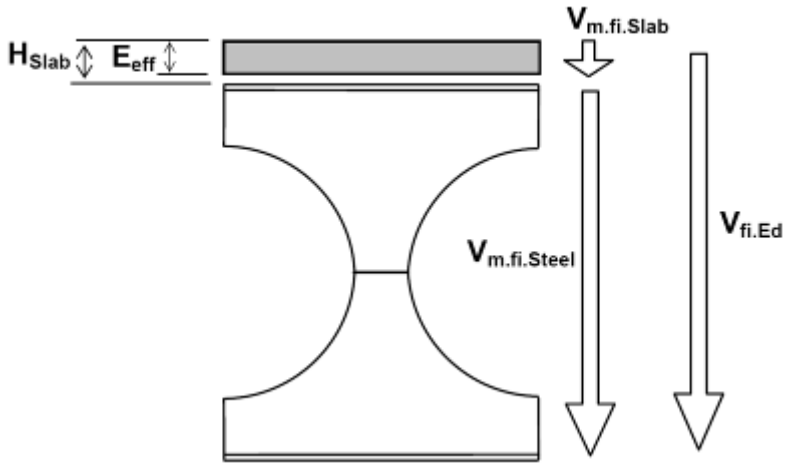

Figure 5–11 : Shear force distribution between concrete slab and steel beam

At an opening the global shear force $V_{fi.Ed}$ is divided by the shear force in the slab and the shear force in the steel beam (see Figure 5–11). The shear forces applied at the centres of gravity of the Ts and the slab are determined using the following relationships :

$V_{m.fi.Slab} = k_{Slab}\ V_{fi.Ed}$
$V_{m.fi.Steel} = (1 - k_{Slab})\ V_{fi.Ed}$

$V_{m.fi.up} = k_{Av}\ V_{m.fi.Steel}$
$V_{m.fi.low} = (1 - k_{Av})\ V_{m.fi.Steel}$

With :

$$k_{Slab} = \min\left(\frac{A_{v.Slab}}{A_{v.Slab} + A_{v.up} + A_{v.low}}; \frac{V_{fi.Rd.Slab}}{V_{fi.Ed}}\right)$$

$$k_{Av} = \frac{A_{v.0.up}^{\eta}}{A_{v.0.up}^{\eta} + A_{v.0.low}^{\eta}} \text{ and } \eta = \frac{1}{9{,}48 - 4{,}84\,\alpha}$$

$A_{v.0.up}$: Shear area of upper T

$A_{v.0.low}$: Shear area of lower T

$A_{v.slab}$: Homogenised shear area of the slab. The value of this shear area has been determined by experience in the scope of Soo Ho Cho's thesis. It can be calculated using the following expression:

$$A_{v.slab} = \frac{L_{Slab}\ E_{eff}}{m}$$

E_{eff} : Effective thickness of the slab adjacent to the opening (see Figure 5–11)

L_{Slab} : Effective width of the slab adjacent to the opening being considered. The value of this length has been determined by experience in the scope of Soo Ho Cho's thesis. It can be calculated using the following expression:

$L_{Slab} = \text{Min}\ (1.5\ E_{eff}\ ;\ L_{disp,l}) + \text{Min}\ (1.5\ E_{eff}\ ;\ L_{disp,r})$

$L_{disp,r}$ and $L_{disp,l}$: Available length of slab (right and left)

m : Coefficient of equivalence steel/concrete for short term loading.

$V_{Rd.Slab}$: Shear resistance of the concrete slab, calculated according to :

$V_{Rd.Slab} = 3.6\ \tau_{Rd.Slab}\ E_{eff}\ L_{Slab}$

$\tau_{Rd.Slab}$: Design shear resistance of the slab

$$\tau_{Rd.Slab} = 0.25 \cdot 0.7 \cdot \frac{f_{ctm}}{\gamma_c}$$

f_{ctm} : Average tension resistance of the concrete forming the slab

$$f_{ctm} = 0.3 \cdot (f_{ck})^{2/3}$$

f_{ck} : Characteristic compressive resistance of the concrete after 28 days.

5.1.6. Principal stress resistance

The principal stress resistance is calculated using the following formula based on EN 1993-1-2:

$$\sigma_{w.fi.Rd} = \frac{\chi_{fi} \cdot \xi \cdot k_{y,\theta} \cdot f_y}{\gamma_{M1}}$$

With:

χ_{fi} : Reduction factor for out-of-plane buckling of the web post adapted for Fire situation following EN 1993-1-2, and calculated using the following formulae :

$$\chi_{fi} = \frac{1}{\phi_\theta + \left(\phi_\theta^2 - \bar{\lambda}_\theta^2\right)^{0,5}} \text{ and } \chi_{fi} \leq 1,0$$

$$\phi_\theta = 0,5[1 + \alpha\ \bar{\lambda}_\theta + \bar{\lambda}_\theta^2]$$

$$\alpha = 0,65\sqrt{\frac{235}{f_y}}$$

ξ : Shape factor for the critical section was calibrated using the finite element modelling and is given by :

$$\xi = 1,5 + \frac{2 \cdot 10^{-5}}{(1-\alpha)^4}$$

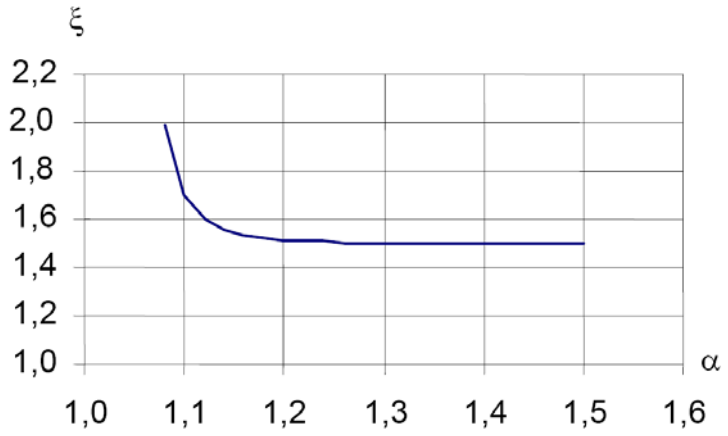

Figure 5–12 : curve ξ in function of α

For the large web posts, the shape factor ξ is equal to 1.5. It is equal to the ratio between the plastic and the elastic modulus of a rectangle section. It reflect the fact that the failure mode due to the shear V_h ,without taking into account the instability, is obtained by a plastic hinge in the critical section.

For smaller web posts, the shape factor ξ varies from 1.5 to 2. It reflects the ability of the web post to work as a connecting rod in tension after the yielding of the critical section.

The reduced slenderness $\bar{\lambda}_\theta$ of the web post being considered in case of fire is given by :

$$\bar{\lambda}_\theta = \bar{\lambda}\sqrt{\frac{k_{y,\theta}}{k_{E,\theta}}} = \sqrt{\frac{\xi f_{yw}}{\sigma_{w.fi.cr}}}\sqrt{\frac{k_{y,\theta}}{k_{E,\theta}}}$$

$k_{y,\theta}$ and $k_{E,\theta}$ are the reduction factors for steel strength limit and young modulus, respectively, at elevated temperature.

5.1.7. Principal stress resistance for instability

The critical principal stress for instability $\sigma_{w.fi.cr}$ is determined taking into account the two possible instabilities :

- The buckling of the web caused by the shear force V_h (left part of Figure 5–13)
- The buckling of the web caused by the axial force in the Tees (right part of Figure 5–13)

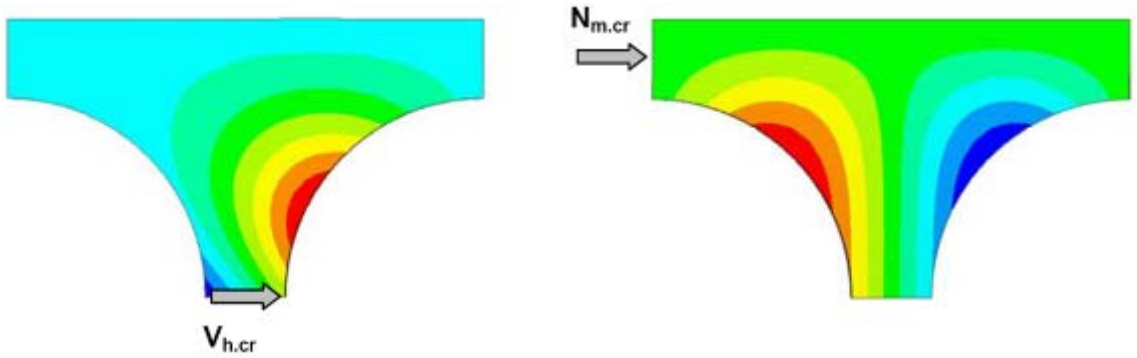

Figure 5–13 : Instability mode of the Tees

The critical principal stress for instability $\sigma_{w.fi.cr}$ in fire condition is given by :

Upper half post : $\sigma_{w.fi.cr.up} = \alpha_{cr.fi.up}\,\sigma_{w.fi.up}$
Lower half post : $\sigma_{w.fi.cr.low} = \alpha_{cr.fi.low}\,\sigma_{w.fi.low}$

$\sigma_{w.fi.up}$, $\sigma_{w.fi.low}$ are the principal stresses in fire situation in the upper and lower half posts respectively, due to the shear force $V_{h.m.fi}$ alone and calculated using the formula in the equation 5 of this chapter.

$\alpha_{cr.fi.up}$, $\alpha_{cr.fi.low}$: Critical coefficients for the upper and lower half posts respectively, taking into account interaction between the two members and given by :

$$\alpha_{cr.fi.up} = \max\left(\beta_{cr.fi.up}\,;\frac{2\,\beta_{cr.fi.up}\,\beta_{cr.fi.low}}{\beta_{cr.fi.up}+\beta_{cr.fi.low}}\right)$$

$$\alpha_{cr.fi.low} = \max\left(\beta_{cr.fi.low}\,;\frac{2\,\beta_{cr.fi.up}\,\beta_{cr.fi.low}}{\beta_{cr.fi.up}+\beta_{cr.fi.low}}\right)$$

$\beta_{cr.fi.up}$, $\beta_{cr.fi.low}$: Critical coefficients for the upper and lower half posts respectively, taking into account only compression in the member and shear in the web post.

It must be noticed that the buckling of the web due to the shear force V_h is the dominating failure mode. The influence of the axial force in the Tees is taken into account by the linear interaction of Dunkerly. The two type of action were separated, the unfavourable action of the compression member and the favourable action of the tensile member. The stabilisation of the web post by the member in

tension is less important than the instability effect of the compression. So a factor of ½ was taken into account in the interaction for the member in tension.

$$\beta_{cr.fi.up} = \frac{1}{\frac{V_{h.fi.Sd}}{V_{h.cr.fi.up}} + \frac{N_{m.fi.up}}{N_{m.cr.fi.up}}}$$

$$\beta_{cr.fi.low} = \frac{1}{\frac{V_{h.fi.Sd}}{V_{h.cr.fi.low}} - \frac{1}{2}\frac{N_{m.fi.low}}{N_{m.cr.fi.low}}}$$

It is important to note that these coefficients are calculated assuming that the lower member is in tension and the upper member is in compression.

$V_{h.cr.fi.up}$, $V_{h.cr.fi.low}$: Critical shear forces in fire condition for out-of-plane buckling of the upper and lower half posts respectively (see definition herafter)

$N_{m.cr.fi.up}$, $N_{m.cr.fi.low}$: Critical axial forces in fire condition for local buckling of the web of the upper and lower members respectively (see definition herafter).

$N_{m.fi.up}$, $N_{m.fi.low}$: Axial forces in fire condition in the webs of the upper and lower members respectively, given by :

$$N_{m.fi.up} = \frac{A_{w.up}}{A_{0.up}} \min\left(N_{m.fi.up(i)} ; N_{m.fi.up(i+1)}\right)$$

$$N_{m.fi.low} = \frac{A_{w.low}}{A_{0.low}} \min\left(N_{m.fi.low(i)} ; N_{m.fi.low(i+1)}\right)$$

$A_{0.up}$, $A_{0.low}$: Areas of the upper and lower Te sections respectively, at the location of the openings.

$A_{w.up}$, $A_{w.low}$: Areas of the webs of the upper and lower Te sections respectively, at the location of the openings, given by :
$A_{w.up} = A_{0.up} - b_{up}\, t_{f.up}$
$A_{w.low} = A_{0.low} - b_{low}\, t_{f.low}$

This equation consists in the repartition of the global axial force in function of the shear area of the members. A similar approach than the repartition of the shear force between the members could be used. This approach has not yet been validated for the cold situation and will not be used in the scope of this report.

CTICM performed more than 600 numerical simulations [8] in order to determine the critical forces, $V_{h.cr.fi}$ for shear in the web post and $N_{m.cr.fi}$ for compression in a member. Theses simulations covered all the value of α between 1.08 and 1.5 and all the values of δ $\left(\delta = \frac{h_w}{a_0}\right)$ from 0.6 and 2. (see Figure 5–14)

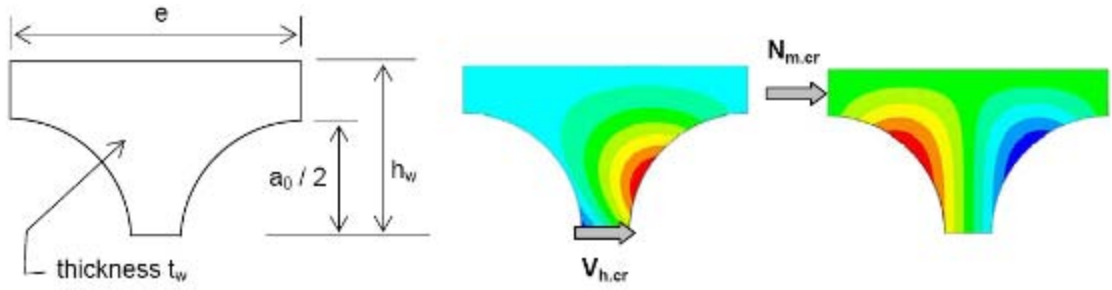

Figure 5–14 : Critical forces for a membre

The web of the Tee member was considered fully encased in the flange. This assumption is fully correct for hot rolled profiles but is really complex to ensure in case of welded sections.

So this calibration is only valid for hot rolled section and must be completely recalibrated in case of welded sections.

After analysing the results of the 600 numerical simulations, the following relations were established:

$V_{h.cr.fi} = P_E (C_0 + C_1 t_w)$
$N_{m.cr.fi} = P_E (D_0 + D_1 t_w)$

P_E is the Reference Euler buckling load.

Euler has demonstrated that this buckling load can be mathematically expressed by the following equation:

$P_E = EI\frac{\pi^2}{4\ell^4}$ for a beam encased on one support and hinged on the other support.

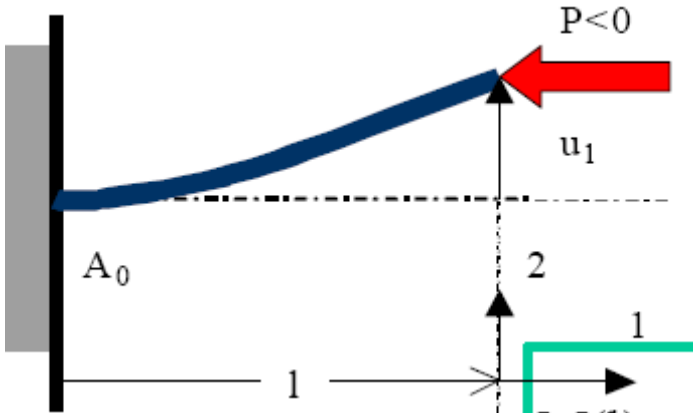

Figure 5–15 : Euler buckling forces

Following the assumption that we are only taking into account the rectangular part of the web post (see Figure 5–16), the Reference Euler buckling load can be expressed by the following equation :

$$P_E = \frac{\pi^2 E_a}{a_0^2} w t_w^3$$

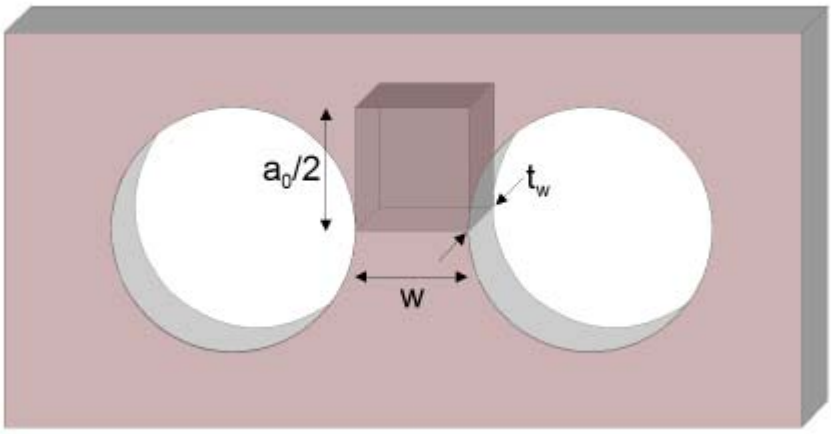

Figure 5–16 : Rectangular part of the web post

Expressions for the coefficients C_0, C_1, D_0 and D_1, based on experimental and numerical calibration, are expressed in function of the following non-dimensional parameters and can be found in reference [8].

$$\delta = \frac{h_w}{a_0} \qquad \zeta = \frac{1}{\sqrt{\delta - 0.5}} \qquad \mu = \frac{1}{\sqrt{\alpha - 1}}$$

5.1.8. Post critical reserve of strength

During the laboratory tests in cold conditions and numerical simulations in cold conditions, it was pointed out that the web-post buckling of the first web post can be a local failure without causing the global failure of the beam. The beam will act like a beam with elongated opening

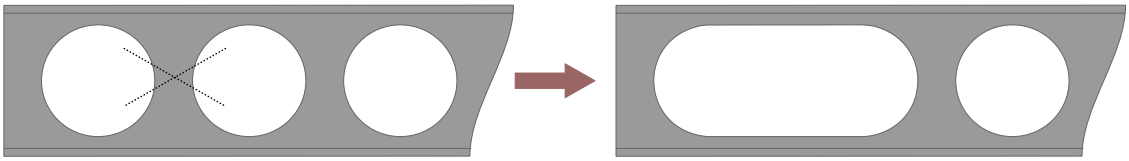

Figure 5–17 : Elongated opening

The factor for post critical reserve of strength κ has been determined on the basis of the numerical simulations and is given by :

$\kappa = 1 + 0{,}625\ (\psi - 0{,}3)$

But $\quad 1 < \kappa < 1.25$

ψ is a Non-dimensional factor given by :

Upper T : $\quad \psi = \dfrac{M_{pl.Rd.up}}{e \cdot V_{fi.up}}$ $\qquad$ Lower T : $\quad \psi = \dfrac{M_{pl.Rd.low}}{e \cdot V_{fi.low}}$

where

$M_{pl.Rd.up}$, $M_{pl.Rd.low}$ are the plastic moment resistances of the upper and lower T, respectively, at the location of an opening.

$V_{fi.up}$, $V_{fi.low}$ are the shear forces in the upper and lower members respectively. The lower of the values for ψ obtained to the right and left of the web post is used.

e is the length of none panel (See Figure 5–18)

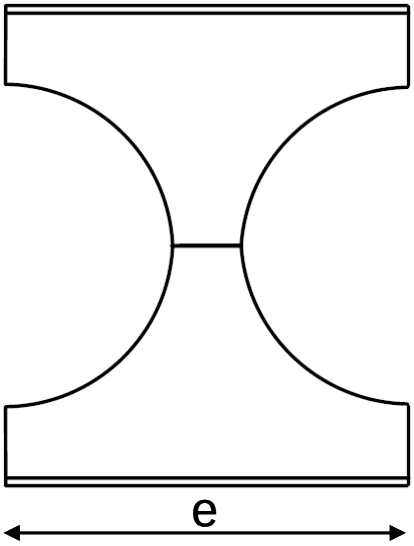

Figure 5–18 : Standard panel

5.2. Existing Engineering Model coming from SCI

SCI's contribution to WP 4 centres around the improvement and further validation of an existing engineering model for Cellbeams in fire conditions. The objective will be to develop a consistent set of engineering checks which will be capable of dealing with room temperature and fire design checks. The main output from the fire design module will be a critical temperature for the beam based on the geometry of the section and the magnitude of the applied loading.

The structure of the fire design process to be adopted is shown in Figure 5–19. The first step in the procedure is to set the temperature of elements in the cross section as appropriate for the type of cross section (see Section 5.2.1). Using this temperature distribution, the appropriate value of design strength and elastic modulus is assigned according to the temperature of the element. The fire module will then call the existing sub routine for calculating the applied loads on the beam followed by the existing subroutines for each of the normal stage design checks. The only exception is that for these checks, the new web post buckling and lateral torsional buckling models are substituted for the existing Cellbeam model.

The value of maximum unity factor (UF) obtained from all the checks is returned to the fire module and checked against the exit criteria. If a solution has not been found the temperature is increased or decreased and a further iteration is completed. The iterative process is controlled using a binary search process that halves the temperature increment each time the error in the unity factor changes sign.

The exit criteria are as follows

- Temperature $\theta = 1200^{o}C$ as material property data is not available at higher temperatures. This temperature could only be reached if the beam is lightly loaded.
- Temperature increment $<=1^{o}C$
  (This value may be adjusted depending on the time taken to find a solution)

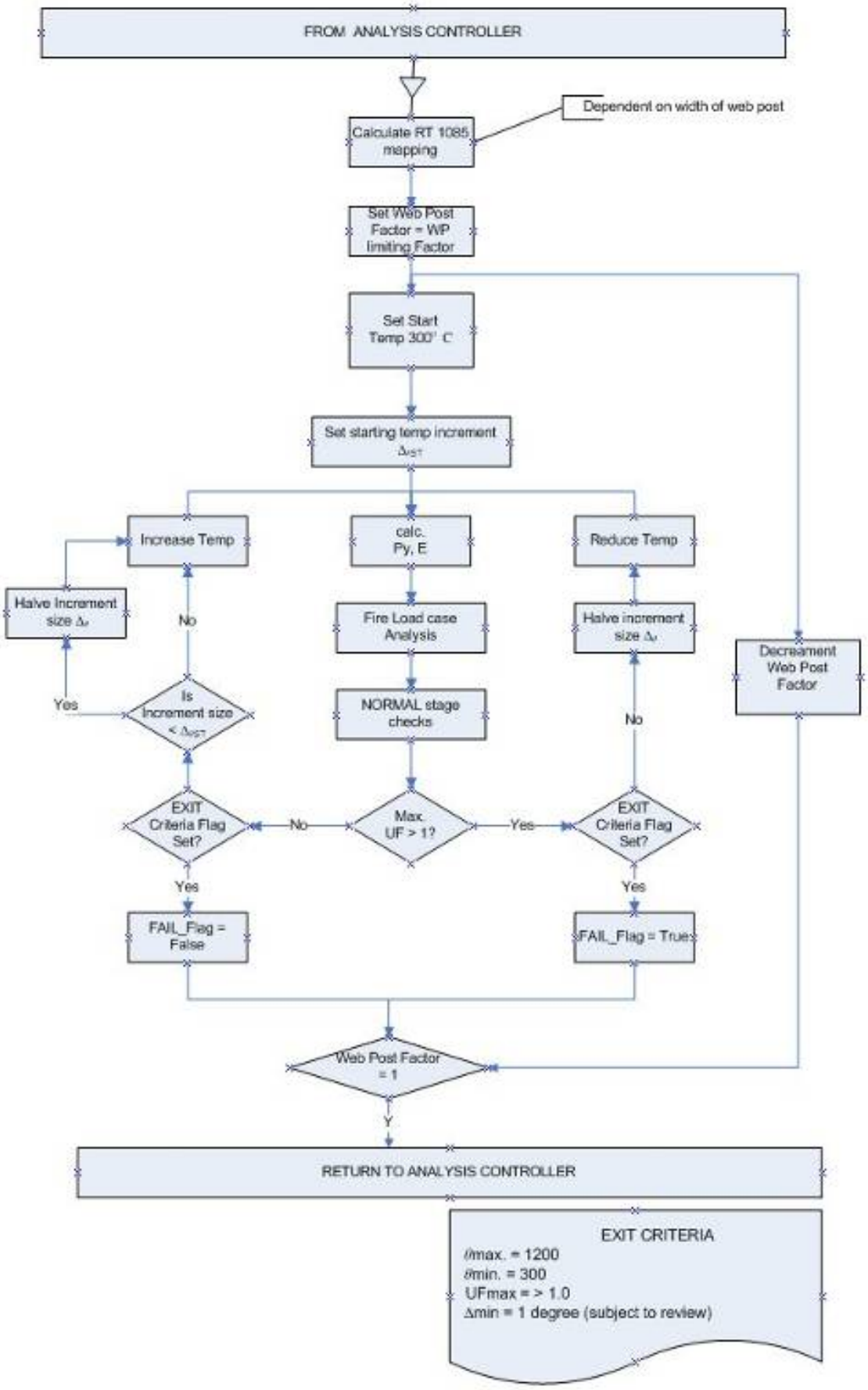

Figure 5–19 : Structure of Fire module

5.2.1. Temperature Distribution

For symmetric sections, the fire module will assume a uniform distribution of temperature across the section. However, as this may produce conservative results the capability to assign a lower temperature to the top flange will also be included in the software.

Figure 5–20 shows how the cellular beam will be modelled as a series of elements. Temperatures can be assigned separately to each of these elements as required. The temperature distribution used by the fire module will be predefined based on temperature mapping functions for each of the 14 elements in the cross section. The choice of temperature distribution will be determine from the observations of the temperature distributions in the fire test.

Previous testing work has shown that the relationship between web post temperature and bottom flange temperature is dependent on protection material. It is undesirable to include such a relationship in this model, instead the bottom flange and web post will always be assigned a uniform temperature for general solutions.

SCI proposes that for symmetric sections the top flange is assumed to be cooler than the rest of the section, in order to avoid excessive conservatism. It is well known from numerous fire resistance tests on protected and unprotected symmetric beams that if the top flange is in contact with a concrete or composite slab then its temperature will be between 60% and 80% of the bottom flange.

The top flange temperature will also have to be increased, for beams supporting trapezoidal decks that span perpendicular to the beam, to allow for leaving the voids unfilled. The magnitude of this temperature increase depends on the period of fire resistance. However, as the fire resistance period is not defined in the software a value of 900°C will be used in the fire module, appropriate to 90 minutes fire resistance. For re-entrant deck types or solid slabs, no increase in top flange temperature is required. The design model will be able to design beams with filled voids or unfilled voids.

Following the temperature distribution for composite beams proposed in EC4-1-2 the temperature of the shear connectors will be taken as 80% of the top flange temperature and the concrete slab will be assumed to have a uniform temperature equal to 40% of the top flange temperature

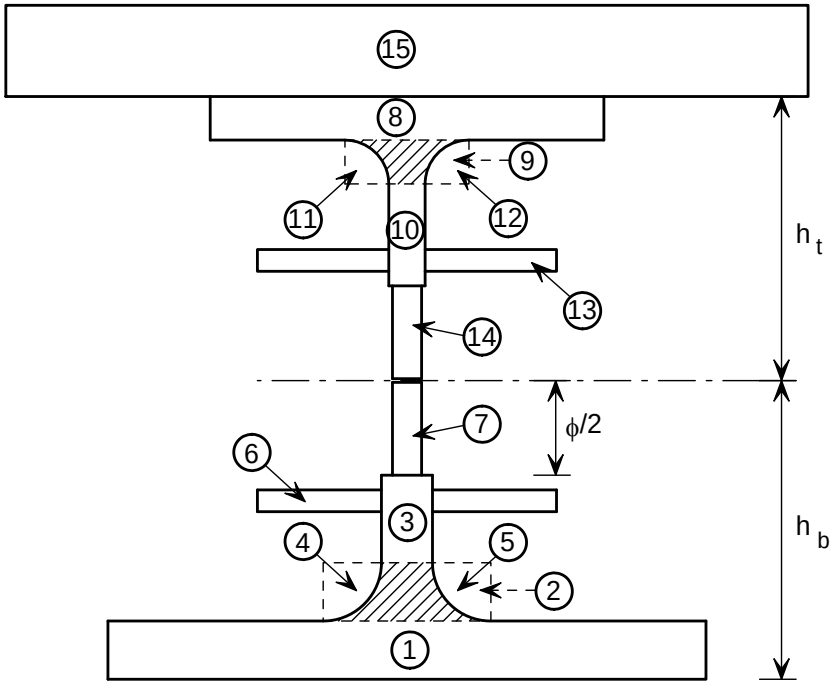

Figure 5–20 : Elements in *Cellbeam* Cross Section

5.2.2. Material Properties

The appropriate strength reduction factors will be applied to the strength of the steel and concrete based on the guidance given in EC4-1-2. The recommendations of EC4-1-2 will also be adopted with respect to the capacity of the shear connectors at elevated temperature.

The design strength of the steel shall be determined in accordance with the thickness of each element using the existing methods within Cellbeam.

5.2.3. Geometrical Limits of Fire Design Model

The fire module will only operate when the geometry of the beam is within the following limits.

- d/t <= 100
- The asymmetry ratio should not be greater than 4:1

These limits are consistent with the range of fire test data available for cellular beams.

5.2.4. Engineering Model

The fire design model will utilise the core engineering models used for design at room temperature. These models will be modified for fire conditions using material modification factors appropriate to the temperature of each element of the cross section.

5.2.4.1. Calculation of Section Properties

Existing procedures **Plaspro** and **Elaspro** divide the section into several calculation elements, as shown in Figure 5–21, and provide for the assignment of different E and P_y to each element.

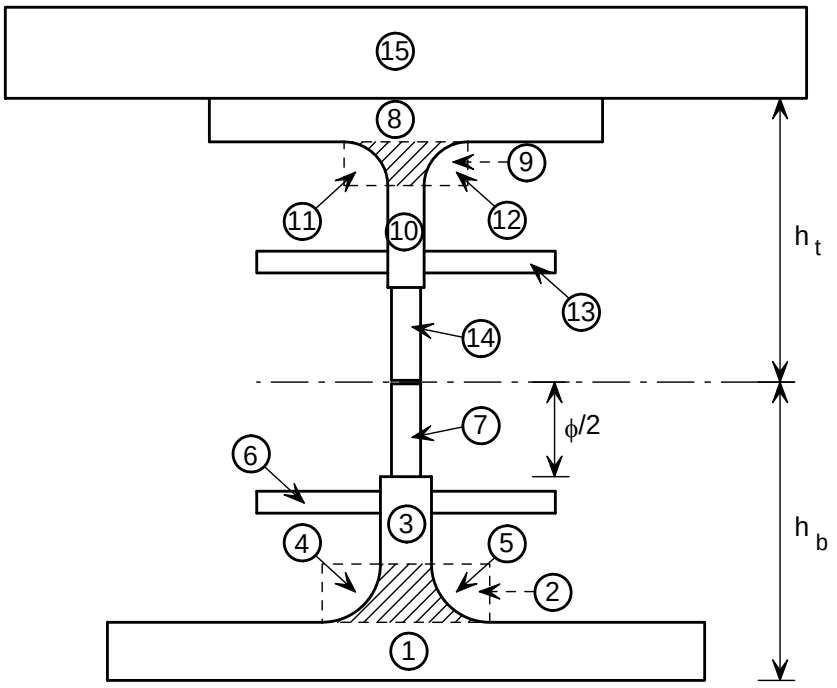

Figure 5–21 : *Cellbeam* Elements in Cross Section

5.2.4.2. Vertical Shear

The model of the cross section used for vertical shear at an opening is shown in Figure 5–22. For symmetric sections the top and bottom web elements have the same temperature, but for an asymmetric section the temperature will be assigned in accordance with the section factors for the top and bottom tees respectively, as described in Section 5.2.1.

For this check, the shear resistance of the concrete slab is ignored.

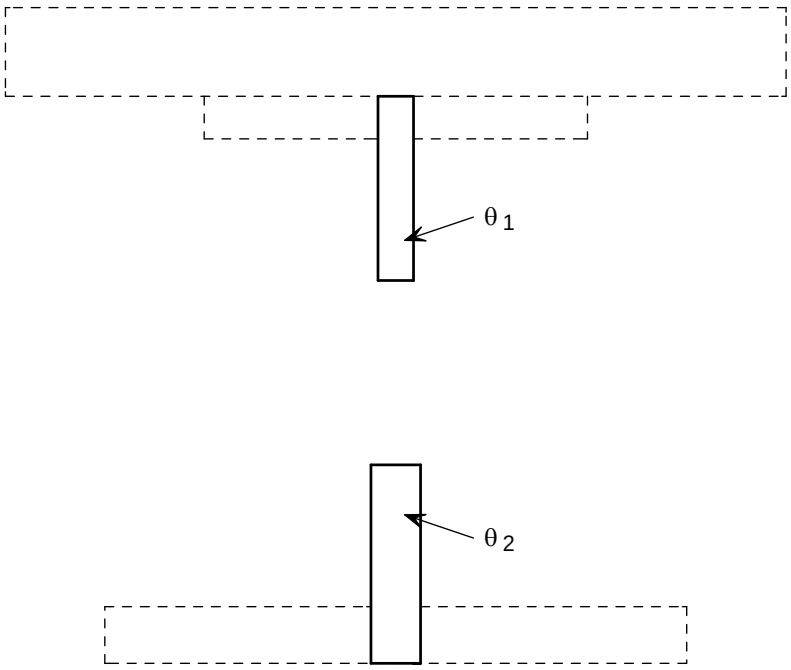

Figure 5–22 : Model of cross section for vertical shear

5.2.4.3. Global Bending

The interaction of global bending and vertical shear will be performed at the centre of each opening using the existing (cold) model. Shear is first divided between the top tee and the bottom tee in such a ratio as to minimise the web post moment (see below). The effect of vertical shear on the bending capacity is accounted for by reducing the web thickness.

For this check, the shear resistance of the concrete slab is taken into account.

The strength of the shear connectors at elevated temperatures will be based on the resistance given in EN1994-1-2. The model consists of a stud and concrete capacity term. The stud resistance is taken as the lesser of these two terms.

Stud Resistance Term

$$P_{Rd} = 0.8\, k_{u,\theta}\, k_{\ell} \left(0.8 f_u \frac{\pi d^2}{4} \right) \frac{1}{\gamma_{M,fi,v}}$$

Concrete Resistance Term

$$P_{Rd} = \frac{k_{c,\theta}\, k_{\ell} \left(0.29 \alpha\, d^2 \sqrt{(f_{ck}\, E_{cm})} \right)}{\gamma_{M,fi,v}}$$

Where

- d is the diameter of the shank of the stud
- f_u is the specified ultimate tensile strength of the stud material

f_{ck} is the characteristic cylinder strength of the concrete
E_{cm} is the mean value of the secant modulus of the concrete
$\alpha = 0.2[(h/d)+1]$ for $3 \le (h/d) \le 4$
$\alpha = 1$ for $(h/d) > 4$
h is the overall height of the stud.
$k_{u,\theta}$ is the strength reduction factor for the stud material
$k_{c,\theta}$ is the strength reduction factor for concrete
k_{ℓ} is the reduction factor for profiled decks
$\gamma_{M,fi,v}$ is the partial safety factor in the fire design case.

Cellbeam ultimate limit state design is based on stud resistances calculated using BS5950. A calibration process will therefore be required to ensure the stud resistances calculated for the fire limit state are compatible with the ULS design values.

5.2.4.4. Lateral Torsional Buckling Check

The fire model will include a separate lateral torsional buckling check, based on the design rules for lateral torsional buckling given in EN 1993-1-2 which includes an appropriate buckling curve for fire conditions. For this design check the temperature θ is taken as the temperature of the compression flange.

Classification of cross sections

$$\varepsilon = 0.85\left(\frac{235}{p_y}\right)^{0.5}$$

The 0.85 factor in the above equation considers the influence of increasing temperature. The section classification should be checked against the limits given in EN1993-1-1.

Class 1 or Class 2 cross-sections

The design buckling moment resistance $M_{b,fi,t,Rd}$ shall be determined as follows:

$$M_{b,fi,t,Rd} = \frac{\chi_{LT,fi}\, W_{pl,y}\, k_{y,\theta}\, p_y}{\gamma_{M,fi}}$$

Where
$\chi_{LT,fi}$ is the reduction factor for lateral torsional buckling in the fire design situation
$k_{y,\theta}$ is the reduction factor for yield strength of steel at maximum temperature in the compression flange.
$W_{pl,y}$ is the plastic modulus about the major axis

Class 3 cross-sections

The design buckling moment resistance $M_{b,fi,t,Rd}$ shall be determined as follows:

$$M_{b,fi,t,Rd} = \frac{\chi_{LT,fi}\, W_{el,y}\, k_{y,\theta}\, p_y}{\gamma_{M,fi}}$$

Where
$W_{el,y}$ is the elastic modulus about the major axis

Reduction Factor for Lateral Torsional Buckling

$$\chi_{LT,fi} = \frac{1}{\phi_{LT,\theta} + \sqrt{\left[\phi_{LT,\theta}\right]^2 - \left[\bar{\lambda}_{LT,\theta}\right]^2}}$$

Where

$$\phi_{LT,\theta} = \frac{1}{2}\left[1 + \alpha\bar{\lambda}_{LT,\theta} + \left(\bar{\lambda}_{LT,\theta}\right)^2\right]$$

$$\alpha = 0.65\sqrt{235/p_y}$$

$$\bar{\lambda}_{LT,\theta} = \bar{\lambda}_{LT}\left[k_{y,\theta}/k_{E,\theta}\right]^{0.5}$$

5.2.4.5. Vierendeel bending

The resistance of the beam to vierendeel forces will be checked at the centre of each opening using the updated model for ULS design which will include composite action. This is based on the Sahmel method where potential failure planes are considered at 2.5 degrees intervals around the opening. If the temperature of the top flange is set lower than the rest of the section, the top tee will consist of elements of differing properties. The analysis must be modified to account for this case.

Advantage will be taken of redistribution of shear where there is a reserve of capacity in one of the tees (usually the top tee) whilst the capacity of the other tee is exceeded. In this case, the web post will be checked for the additional web post moments induced in the web in order to maintain equilibrium.

5.2.4.6. Web Post Bending and horizontal shear

The web post will be checked for co-existent bending moment and horizontal shear using the existing rules, modified for the design strength of the web at elevated temperature. The bending capacity of the web post is limited to its elastic value. A shape factor of 0.9 is used to reduce the horizontal shear capacity of the webs.

5.2.4.7. Web Post Buckling Capacity

For each web post, the capacity of the web post will be based on the following web post buckling check.

Calculation of web post capacity

The buckling capacity of the web post at temperature θ, expressed in terms of horizontal shear on the web post, is given by:

$$V_{h,buck,\theta} = \frac{\chi p_{y,\theta}(S - d_o)t_w}{\gamma_{M,fi}}$$

In which

$$\chi = \frac{1}{\left(\phi + \sqrt{\phi^2 - \lambda_\theta{}^2}\right)}$$

$$\phi = 0.5\left(1 + \alpha(\lambda_\theta - 0.2) + \lambda_\theta{}^2\right)$$

$$\lambda_\theta = \sqrt{\frac{p_{y,\theta}}{k\, p_{E,\theta}}}$$

where

S	is the pitch of the openings
d_o	is the opening diameter
k	is a coefficient to account for varying web thickness and strength)
t_w	is the thickness of the web
$p_{y,\theta}$	is the design yield strength at temperature θ
$p_{E,\theta}$	is the elastic buckling stress at temperature θ

The value of $p_{E,\theta}$ is determined on the basis of an effective length of an equivalent strut. The properties of this equivalent strut were determined from finite element modelling.

The effect of ring stiffeners and infill stiffeners on the buckling capacity of the web posts will be taken into account by modifying the effective length and effective width used in the calculation of the elastic buckling stress, $p_{E,\theta}$.

For asymmetric sections where there is a variation in web thickness or steel grade the calculation of web post capacity will be based on the squash capacity of the effective strut and a modified Euler buckling capacity.

The squash capacity will be calculated for the top and bottom parts of the web post and the lesser value will be used to compute the web post buckling capacity. The modified Euler capacity will be obtained using the coefficients given by Roark and will vary depending on the proportion of the overall height of the web post formed by the heavier section and the ratio of the thickness of the web of the top and bottom sections cubed.

Table 5-1 : Euler Buckling Coefficient from Roark.

$(t_{wb}/t_{wt})^3$	Height of thicker web as a proportion of overall height		
	0.33	**0.5**	**0.67**
1.0	1.00	1.00	1.00
1.5	1.11	1.18	1.34
2.0	1.21	1.31	1.62

6. WP 5 : ADDITIONAL FIRE RESISTANCE THROUGH 3D MEMBRANE EFFECT

6.1. Simple design method

Since Johansen's pioneering work on yield line analysis [33] researchers have observed the beneficial effects of membrane forces in improving the load bearing capacity of concrete slabs, compared to estimates of capacity based only on flexural behaviour [34].

A number of experimental and theoretical investigations have been carried out to investigate the beneficial effects of in-plane forces at room temperature, leading to a good theoretical understanding of the behaviour. Following the experimental work carried out at Cardington, this theory has been extended to fire design scenarios, as discussed below.

The experimental work at Cardington and evidence from other real fires in building structures had served to illustrate that there are significant reserves of strength in composite steel concrete buildings, which means that the performance of the structure in fire exceeds the expectations created by standard fire tests on individual structural elements. Cardington demonstrated that it was possible to leave the composite steel beams that supported the concrete floor slab unprotected; work commenced to investigate suitable design models to allow structural engineers to justify the fire design of a floor slab supported by unprotected steel beams.

Researchers at the Building Research Establishment (BRE), with funding from the Steel Construction Institute, developed a simple design method for composite steel concrete floor slabs following the experimental work at Cardington [35-36]. The BRE model has been validated against the Cardington large scale fire test results and previous experimental work conducted at room temperature. The use of this method must now be validated for floor plates with incorporate long span cellular beams.

The simple design method differs from the simple design procedures provided in design codes [55-56], as it considers the behaviour of an assembly of structural members acting together, rather than individual elements. While it would also be technically possible to use non-linear finite elements to determine the load bearing capacity in fire, that is a more expensive solution requiring a significant amount of expertise and prior knowledge. The method presented in this document is more accessible to structural engineers with only a basic appreciation of fire engineering.

6.1.1. Introduction to yield line theory and membrane action

The yield line theory pioneered by Johansson is an ultimate load theory based on assumed collapse mechanisms and plastic properties of under-reinforced concrete slabs. The collapse mechanism is defined by a pattern of yield lines along which the reinforcement yields and the slab undergoes plastic deformations. The areas bounded by the yield lines are assumed to remain rigid with all rotation taking place at the yield line.

For yield line theory to be valid, shear failures, bond failures and compression failures must be prevented. The moment-curvature response of the slab must be sufficiently ductile to allow a mechanism to form; in practice this is not a problem as slabs are always under-reinforced, leading to ductile yielding of the reinforcement before more brittle modes of failure such as compressive failure in the concrete.

For square and rectangular slabs that are simply supported along their free edges, the patterns of yield lines shown in Figure 6–1 are expected to occur. These are the yield line patterns which are assumed in the following theoretical development. In reality, for a steel framed building, the slab is supported on steel beams which will have a finite stiffness between column positions. This will be discussed in Section 6.2.4.

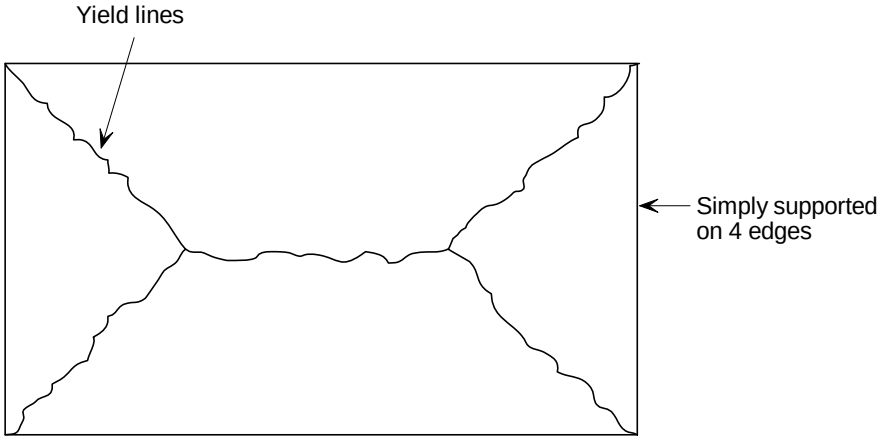

Figure 6–1 : A typical yield line pattern for a rectangular slab simply supported on four sides

An upper bound solution may be obtained for an assumed yield line pattern. The solution is based on energy theory, with the external work done by the applied load due to a unit displacement of the rigid regions being equated to the internal work done by the rotation of the yield lines. The load which corresponds to any assumed failure mechanism will be greater than or equal to the true collapse load of the structure, thus giving an upper bound solution.

However, due to membrane action in the slab and strain hardening of the reinforcement after yielding, this theoretical upper bound solution from the yield line analysis tends to be significantly lower than the actual failure load of the slab observed during experiments.

Membrane action in slabs creates in-plane forces that are governed by the in-plane boundary conditions of the slab. Two extreme cases, of full restraint and no restraint, are considered below.

Slab with full in-plane restraint

With full in-plane restraint to the slab boundaries, the initial small bending deflections of a slab result in compressive membrane action[37-38]. This mechanism is illustrated in Figure 6–2, for a one way spanning element. A compressive action along a path from the bottom surface at the boundary to the top surface at mid-span develops, inducing a compressive arching action in the slab, which results in an enhanced resistance as shown in Figure 6–3. However, this arching action becomes unstable once the magnitude of the vertical deflection exceeds a value equal to approximately half the slab thickness, resulting in the rapid decrease of resistance. The slab can then go on to develop tensile membrane action at larger displacements.

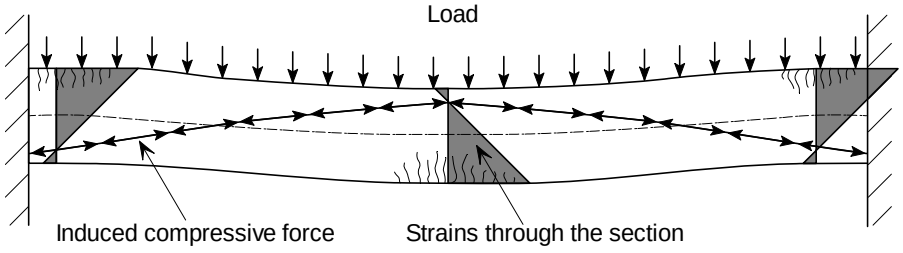

Figure 6–2 : Compressive membrane action in a restrained slab

Park [37] illustrated the effect of compressive membrane action on a restrained slab using a figure similar to Figure 6–3. The initial peak load shown in this figure at displacements less than the slab thickness is due to compressive membrane action. When compression failure occurs in the concrete a sudden drop in capacity is observed, accompanied by an increase in displacement. The load capacity then increases with increasing deflection until fracture of the reinforcement occurs.

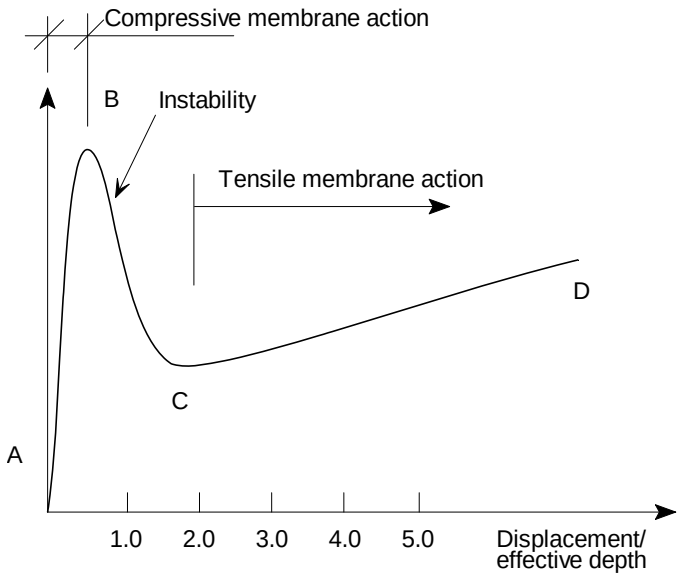

Figure 6–3 : Membrane action in a slab with restrained in-plane boundaries

Slab with no in-plane restraint

Where the boundary of the slab is unrestrained, the slab behaviour is different. Compressive membrane action cannot occur and the post-yielding behaviour is characterised by tensile membrane action. For a one-way spanning element, large vertical displacements will cause end shortening of the member. If this end shortening is prevented then tensile forces will develop. For a one-way spanning member, these restraint forces would have to be developed externally at the supports. However, for a two way spanning slab, i.e. a slab with simple supports on four edges, external horizontal restraints are not required as the slab can develop an internal system of in-plane forces which has the same effect.

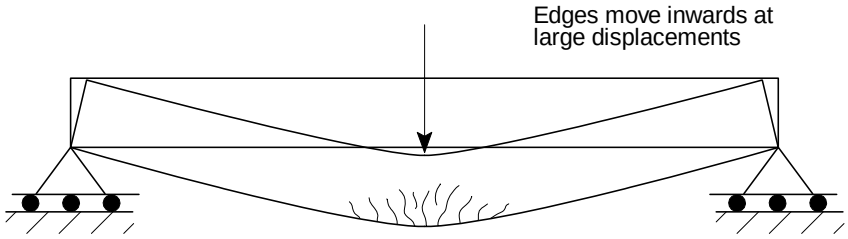

Figure 6–4 : One way spanning structural members

Considering the case of a two-way spanning slab, as shown in Figure 6–5. This slab has vertical supports around its perimeter but no in-plane horizontal restraints. The strip at the centre of the slab denoted X-X will tend to have end shortening behaviour similar to the one-way spanning element shown in Figure 6–4. However, the strips denoted Y-Y on a supported edge do not have the same vertical displacement and will therefore not have significant end shortening. In-plane forces will therefore occur at the interface of these strips of slab in order to maintain equilibrium, thus inducing tensile stresses in strips such as X-X and compressive stresses in strips such as Y-Y. As this behaviour occurs in two directions the result is an area of tensile stress in the centre of the slab denoted by the shaded area in Figure 6–5 and a compressive ring around the perimeter.

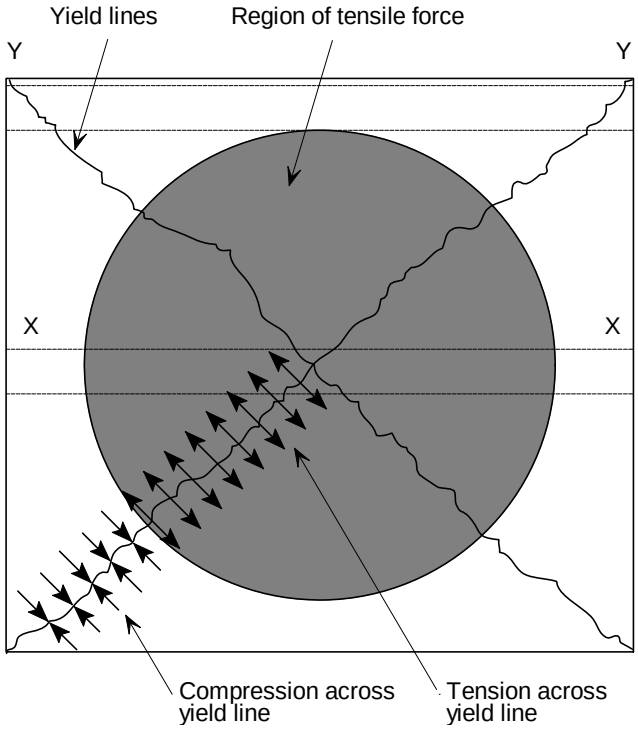

Figure 6–5 : Development of in-plane membrane forces

Effect of membrane stresses on yield lines

The development of tensile and compressive in-plane forces will influence the yield line moments developed in the slab, with reductions in bending resistance occurring in the tensile zone and enhancement of the bending resistance of the yield lines in the compression zone. In addition to this influence on bending resistance, there is also the additional load bearing capacity due to tensile membrane action.

Following the work of Johansson on yield line analysis, tests to destruction of a complete building were reported by Ockleston [34]. These test revealed that the loads that could be sustained by the floor slabs were considerably greater than those predicted by yield line theory. This generated considerable interest in research into membrane effects and a number of researchers investigated these effects both experimentally and analytically in subsequent years.

Observations from tests on unrestrained slabs show that the pattern of yield lines is unchanged at large displacements. The ultimate mode of failure has also been shown to be the development of large cracks across the shorter span of the slab and fracture of the reinforcement, as reported by Wood [38].

Methods of analysis taking account of membrane action have been developed for unrestrained slabs by Wood [38], Kemp [40], Taylor [39], Sawczuk [41], Hayes [42] and Bailey and Moore [35-36].

Wood developed a solution for a circular slab with simply supported boundaries subject to distributed loading. A similar solution was developed for square slabs by Kemp. Kemp's method involved a rigorous rigid-plastic solution, in which the load bearing capacity is determined from consideration of the equilibrium of the rigid regions of the slab. This enables the magnitude of the membrane forces and yield line moments to be determined as a function of the slab deflection. Kemp's theory demonstrates that the capacity of the slab is a function of the slab deflection. He notes that in practice a collapse load would be reached when fracture of the reinforcement occurs or when the concrete in the outer region crushes, although his model does not attempt to define this end point on the load deflection response.

In the approach used by Sawczuk, the formation of the crack across the short span was included. Sawczuk identified that the rigid triangular elements of the slab are subject to in-plane moments due to the variation of membrane forces along the yield lines. By estimating the bending resistance of the rigid regions, Sawczuk predicted the development of bending hinges along the centre line of the slab and cracking across the short span. This cracking is not allowed for by the methods developed by Taylor and Kemp. Sawczuk's energy based method, considered two possible crack formations, as shown in Figure 6–6. The conclusion was that the critical mode of failure was caused by cracks forming across the shorter span, at the intersection of the yield lines, as shown in Figure 6–6(a).

a- Crack forming at the intersection of the yield lines

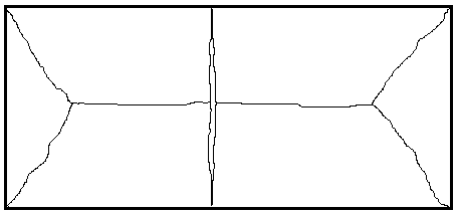

b- Crack forming at the centre of the slab

Figure 6–6: Failure modes identified by Sawczuk

Hayes noted that the Sawczuk's analysis implied that boundary forces were present, when in reality these forces could not exist at an unrestrained simply supported edge. Hayes also observed that no increase in the load bearing capacity was apparent when moment equilibrium of the rigid regions was considered. Hayes went on to develop a solution for orthotropically reinforced rectangular slabs which addressed his criticisms of Sawczuk method and which was in good agreement with Kemp's solution for square slabs. In his method, Hayes also assumed that the cracks across the short span occur at the intersection of the yield lines. Comparing his method with Sawczuk's, Hayes concluded that the differences were not significant. Importantly, Hayes also noted that the enhancement due to membrane effects decreases with increase in the aspect ratio of the slab or the orthotropy of the reinforcement.

Sawczuk's assumption, which was also adopted by Hayes, that the failure mode includes two cracks across the short span of the slab at the intersection of the yield lines contradicts a large portion of the test results, including a test conducted by Building Research Establishment in 2000 [43]. Therefore, Bailey and Moore [35-36] modified the method developed by Hayes's approach and based their equilibrium method on the formation of a single crack in the centre of the slab, the mode of failure commonly observed in the tests conducted at ambient and elevated temperatures, Figure 6–7(b). The derivation used by Bailey and Moore is described in Section 6.1.2. Initially this was developed for isotropic reinforcement, but has been updated to include the effects of the orthotropic reinforcement and the catenary action of the steel beams [44].

6.1.2. Calculation of resistance of composite floors in accordance with the simple design method

This Section describes the development of a simple design method that can be used to calculate the resistance of rectangular composite floor plates. The method has developed over a number of years. The initial development [35-36] of the method for use with isotropic reinforcement only considered one failure mode, due to fracture of the mesh across the short span, as shown by Figure 6–7(a). Later developments [44-48] included a more general derivation allowing the use of orthotropic reinforcement, and also the inclusion of compression failure of the concrete at the slab corners (see Figure 6–7(b)).

6.1.2.1. Calculation of resistance

The load bearing capacity of a two-way spanning simply supported slab, with no in-plane horizontal restraint at its edges, is greater than that calculated using the normal yield line theory. The enhancement of the resistance is as a result of tensile membrane action developing in the slab at large displacement and also due to the increase of the yield moment in the outer regions of the slab, where compressive stresses occur across the yield lines (see Figure 6–8).

The enhancement of the resistance determined as a lower bound solution for yield line failure is based on the assumption that at ultimate conditions the yield line pattern will be as shown in Figure 6–7(a) and that failure will occur due to fracture of the mesh across the short span at the centre of the slab. A second mode of failure might, in some cases, occur due to crushing of the concrete in the corners of the slab where high compressive in-plane forces occur as shown by Figure 6–7(b). This mode of failure is discussed in Section 6.1.3.

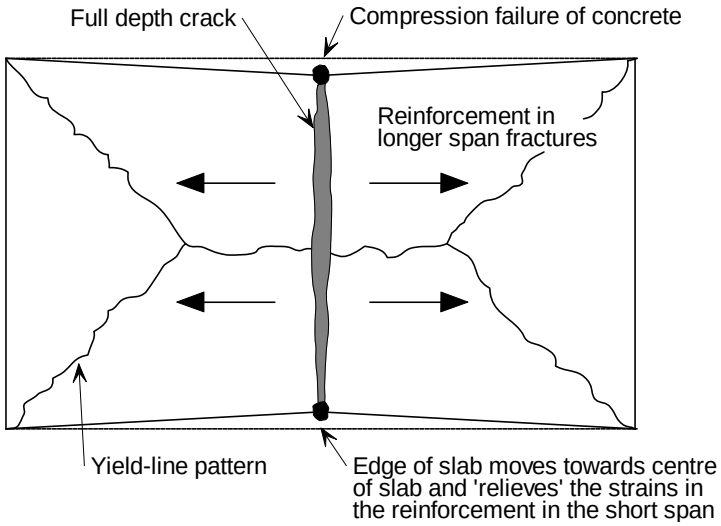

(a) Tensile failure of mesh reinforcement

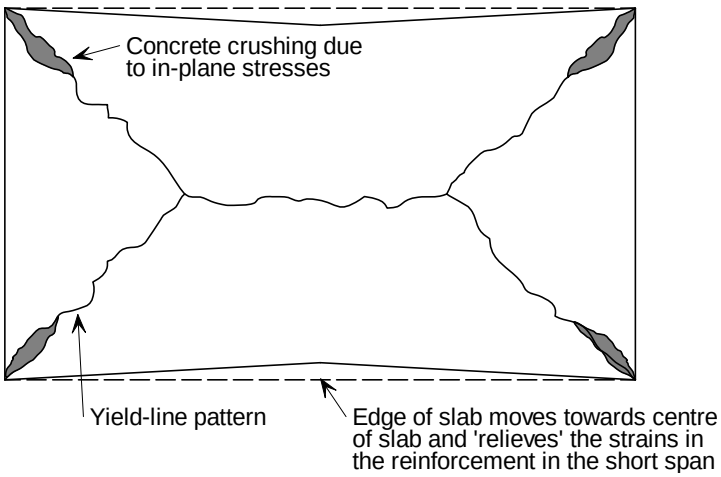

(b) compressive failure of concrete

Figure 6–7 : Assumed failure mode for composite floor

The first failure mode will occur when the compressive strength of the concrete exceeds the ultimate strength of the mesh in tension, leading to fracture of the mesh. The second failure mode will occur in cases were the ultimate strength of the mesh exceeds the compressive strength of the concrete, resulting in compression failure of the concrete at the corners of the slab.

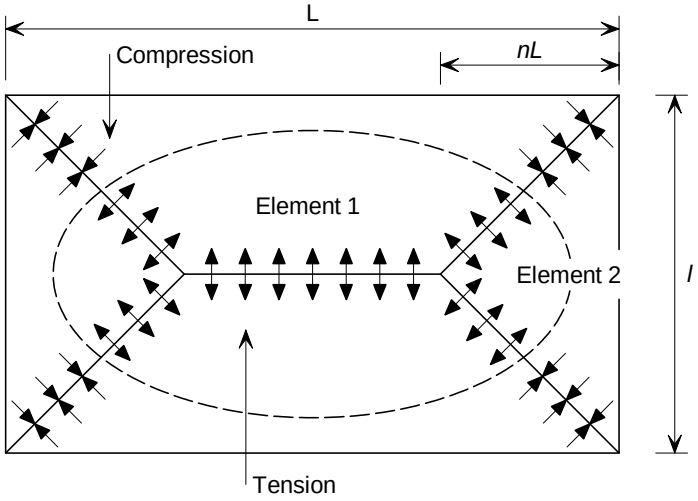

Figure 6–8 : Rectangular slab simply supported on four edges showing in-plane forces across the yield lines due to tensile membrane action.

Figure 6–8 shows a rectangular slab simply supported on its perimeter and the expected lower bound yield line pattern that would develop due to uniformly distributed loading. The intersection of the yield lines is defined by the parameter n calculated using the general yield line theory and given by:

$$n = \frac{1}{2\sqrt{\mu}a^2}\left(\sqrt{3\mu a^2 + 1} - 1\right)$$

where

a is the aspect ratio of the slab (L/l)

μ is the ratio of the yield moment capacity of the slab in orthogonal directions (should always be less than or equal to 1.0)

The shorter span should be defined by the span with the lower moment capacity resulting in coefficient of orthography (μ) being always less than, or equal to one. Therefore n would be limited to maximum of 0.5 resulting in a valid yield line pattern.

The resistance of the mechanism which occurs due to the formation of these yield lines is given by the following equation:

$$P = \frac{24\mu M}{l^2}\left[\sqrt{3 + \frac{1}{(a')^2}} - \frac{1}{a'}\right]^{-2}$$

where

a' $= \sqrt{\mu a}$

Hayes [42] noted that assuming rigid-plastic behaviour, only rigid body translations and rotations are allowed. Further assumptions that the neutral axes along the yield lines are straight lines and that the concrete stress-block is rectangular, means that the variations in membrane forces along the yield lines become linear, as shown in Figure 6–9. These assumptions and the resulting distribution of membrane forces were also adopted by Bailey [35-49].

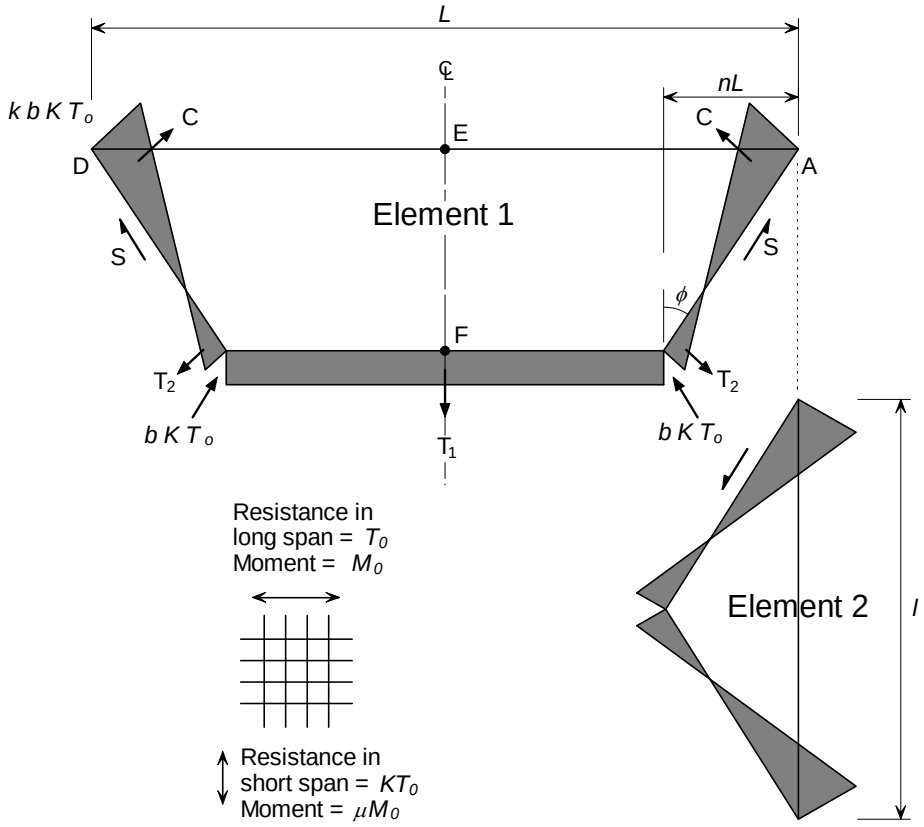

Figure 6–9 : In-plane stress distribution for the elements 1 and 2

Derivation of an expression for parameter k

Considering the equilibrium of the in-plane forces T_1, T_2 and C acting on Element 1 allows the following relationships to be derived:

$$S\sin\phi = (C - T_2)\cos\phi$$

and

$$-S\cos\phi = (C - T_2)\sin\phi - \frac{T_1}{2}$$

Therefore,

$$\frac{T_1}{2}\sin\phi = (C - T_2)$$

where

ϕ is the angle defining the yield line pattern.

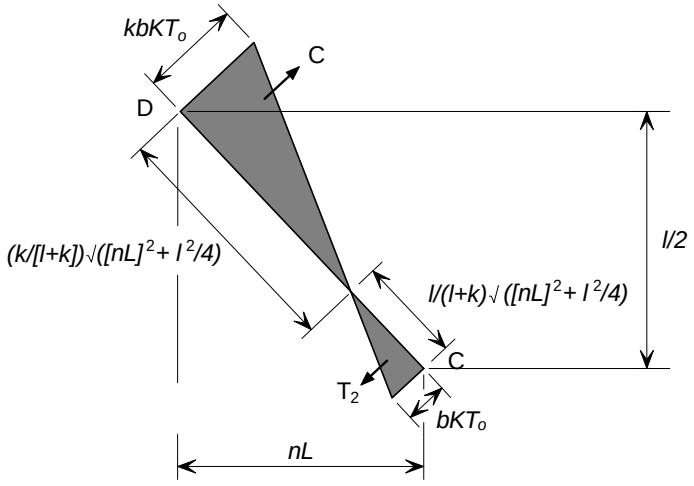

Figure 6–10 : In-plane stress distribution along yield line CD

Figure 6–10 shows the geometry of the stress distribution along yield line CD. Considering Figure 6–9 and Figure 6–10,

$$T_1 = bKT_0(L - 2nL)$$

$$T_2 = \frac{bKT_0}{2}\left(\frac{1}{1+k}\right)\sqrt{(nL)^2 + \frac{l^2}{4}}$$

$$C = \frac{kbKT_0}{2}\left(\frac{k}{1+k}\right)\sqrt{(nL)^2 + \frac{l^2}{4}}$$

$$\sin\phi = \frac{nL}{\sqrt{(nL)^2 + \frac{l^2}{4}}}$$

where

b, k are parameters defining the magnitude of the membrane force,

KT_0 is the resistance of the steel reinforcing mesh per unit width,

n is a parameter defining the yield line pattern

Substituting the above values into Equation (1) gives,

$$\frac{bKT_0(L-2nL)}{2}\frac{nL}{\sqrt{(nL)^2+\frac{l^2}{4}}} = \frac{kbKT_0}{2}\left(\frac{k}{1+k}\right)\sqrt{(nL)^2+\frac{l^2}{4}} - \frac{bKT_0}{2}\left(\frac{1}{1+k}\right)\sqrt{(nL)^2+\frac{l^2}{4}}$$

This expression can then be rearranged to give an expression for parameter *k*.

$$k = \frac{4na^2(1-2n)}{4n^2a^2+1} + 1$$

Derivation of an expression for parameter b

Considering the fracture of the reinforcement across the short span of the slab, an expression for the parameter *b* can be developed. The line EF shown in Figure 6–11 represents the location of the mesh fracture, which will result in a full depth crack across the slab. An upper bound solution for the in-plane moment of resistance along the line EF can be obtained by assuming that all the reinforcement

along the section is at ultimate stress (f_u) and the centroid of the compressive stress block is at location E in Figure 6–11.

It is assumed that,

$f_u = 1.1 f_y$

where

f_y is the yield stress.

Taking moment about E in Figure 6–11,

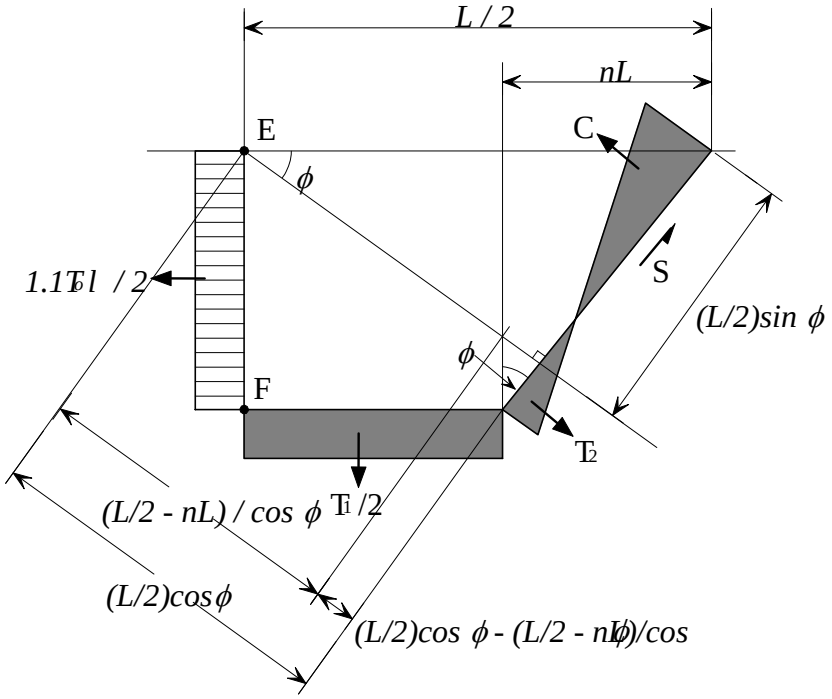

Figure 6–11 : In-plane stress distribution along fracture line EF

$$T_2\left[\left(\frac{L}{2}\cos\phi - \frac{\left(\frac{L}{2} - nL\right)}{\cos\phi}\right)\frac{1}{\tan\phi} - \frac{1}{3}\left(\frac{1}{1+k}\right)\sqrt{(nL)^2 + \frac{l^2}{4}}\right]$$

$$+ C\left[\frac{L}{2}\sin\phi - \frac{l}{3}\left(\frac{k}{k+1}\right)\sqrt{(nL)^2 + \frac{l^2}{4}}\right]$$

$$+ S\frac{L}{2}\cos\phi - \frac{T_1}{2}\left[\frac{1}{2}\left(\frac{L}{2} - nL\right)\right] = \frac{1.1T_o l^2}{8}$$

where

$$\frac{T_1}{2} = bKT_o\left(\frac{L}{2} - nL\right)$$

$$T_2 = \frac{bKT_o}{2}\left(\frac{1}{1+k}\right)\sqrt{(nL)^2 + \frac{l^2}{4}}$$

$$C = \frac{kbKT_o}{2}\left(\frac{k}{k+1}\right)\sqrt{(nL)^2 + \frac{l^2}{4}}$$

$$S = \frac{bKT_o l}{4nL}(k-1)\sqrt{(nL)^2 + \frac{l^2}{4}}$$

$$\cos\phi = \frac{(l/2)}{\sqrt{(nL)^2 + \frac{l^2}{4}}}$$

$$\sin\phi = \frac{nL}{\sqrt{(nL)^2 + \frac{l^2}{4}}}$$

$$\tan\phi = \frac{nL}{(l/2)}$$

Substituting these expressions into equation above leads to,

$$\frac{bKT_o}{2}\left(\frac{1}{1+k}\right)\sqrt{(nL)^2 + \frac{l^2}{4}}\left[\left(\frac{\left(\frac{l}{2}\right)}{\sqrt{(nL)^2 + \frac{l^2}{4}}}\frac{L}{2} - \frac{\left(\frac{L}{2} - nL\right)}{\left(\frac{l}{2}\right)}\sqrt{(nL)^2 + \frac{l^2}{4}}\right)\frac{\left(\frac{l}{2}\right)}{nL}\right]$$
$$-\frac{1}{3}\left(\frac{1}{1+k}\right)\sqrt{(nL)^2 + \frac{l^2}{4}}$$

$$+\frac{kbKT_o}{2}\left(\frac{k}{k+1}\right)\sqrt{(nL)^2 + \frac{l^2}{4}}\left[\frac{nL}{\sqrt{(nL)^2 + \frac{l^2}{4}}}\frac{L}{2} - \frac{1}{3}\left(\frac{k}{1+k}\right)\sqrt{(nL)^2 + \frac{l^2}{4}}\right]$$

$$+\frac{bKT_o l}{4nL}(k-l)\sqrt{(nL)^2 + \frac{l^2}{4}}\frac{\left(\frac{l}{2}\right)}{\sqrt{(nL)^2 + \frac{l^2}{4}}}\left(\frac{L}{2}\right) - bKT_o\left(\frac{L}{2} - nL\right)\left[\frac{l}{2}\left(\frac{L}{2} - nL\right)\right] = \frac{1.1T_o l^2}{8}$$

which can be rearranged to give,

$$\frac{b}{2}\left(\frac{1}{1+k}\right)\left[\left(\frac{l^2}{8n} - \frac{\left(\frac{L}{2} - nL\right)}{nL}\left((nL)^2 + \frac{l^2}{4}\right) - \frac{1}{3}\left(\frac{1}{1+k}\right)\left((nL)^2 + \frac{l^2}{4}\right)\right)\right]$$

$$+\frac{b}{2}\left(\frac{k^2}{1+k}\right)\left[\frac{nL^2}{2} - \frac{k}{3(1+k)}\left((nL)^2 + \frac{l^2}{4}\right)\right]$$

$$+\frac{bl^2}{16n}(k-1) - b\left(\frac{L}{2} - nL\right)\left(\frac{L}{4} - \frac{nL}{2}\right) = \frac{1.1l^2}{8K}$$

This equation can be rewritten as,

$$Ab + Bb + Cb - Db = \frac{1.1l^2}{8K}$$

Whence:

$$b = \frac{1.1l^2}{8K(A + B + C - D)}$$

where

$$A = \frac{1}{2}\left(\frac{1}{1+k}\right)\left[\frac{l^2}{8n} - \frac{\left(\frac{L}{2} - nL\right)}{nL}\left((nL)^2 + \frac{l^2}{4}\right) - \frac{1}{3}\left(\frac{1}{1+k}\right)\left((nL)^2 + \frac{l^2}{4}\right)\right]$$

$$B = \frac{1}{2}\left(\frac{k^2}{1+k}\right)\left[\frac{nL^2}{2} - \frac{k}{3(1+k)}\left((nL)^2 + \frac{l^2}{4}\right)\right]$$

$$C = \frac{l^2}{16n}(k-1)$$

$$D = \left(\frac{L}{2} - nL\right)\left(\frac{L}{4} - \frac{nL}{2}\right)$$

The parameters k and b, which define the in-plane forces, can be calculated using these equations.

Membrane forces

The load bearing capacity for Elements 1 and 2 of the slab can be determined by considering the contribution of the membrane forces to the resistance and the increase in bending resistance across the yield lines separately as shown below. These effects are expressed in terms of an enhancement factor, to be applied to the lower bound yield line resistance. Initially, the effects of the in-plane shear S (Figure 6–9) or any vertical shear on the yield line was ignored, resulting in two unequal loads being calculated for Elements 1 and 2 respectively. An averaged value was then calculated, considering contribution of the shear forces.

Contribution of membrane forces to load bearing capacity.
a) Element 1

According to Figure 6–12, the moment about the support due to membrane force is given by:

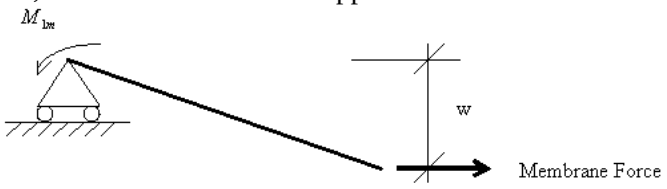

Figure 6–12 : Calculating the moment caused by the membrane force

$$M_{1m} = bKT_0(L - 2nL)w + bKT_0nLw\left(\frac{3k+2}{3(1+k)^2}\right) - bKT_0nLw\left(\frac{k^3}{3(1+k)^2}\right)$$

where

M_{1m} is the moment about the support due to membrane forces for element 1.

The expression reduces to:

$$M_{1m} = KT_0Lbw\left((1-2n) + \frac{n(3k+2) - nk^3}{3(1+k)^2}\right).$$

The above formulation defines the contribution from the membrane forces to the load bearing capacity that needs to be added to the contribution due to the enhanced bending capacity in the areas where the slab is experiencing compression forces. For simplicity, the contribution from the membrane forces

and enhanced bending action is related to the normal yield line load. This allows an enhancement factor to be calculated for both the membrane force and also the enhanced bending moments. These enhancement factors can finally be added to give the overall enhancement of the slab due to membrane action.

Dividing M_{1m} by $\mu M_0 L$, the moment of resistance of the slab, when no axial force is present, allows the effect of tensile membrane action to be expressed as an enhancement of yield line resistance (Figure 6–13).

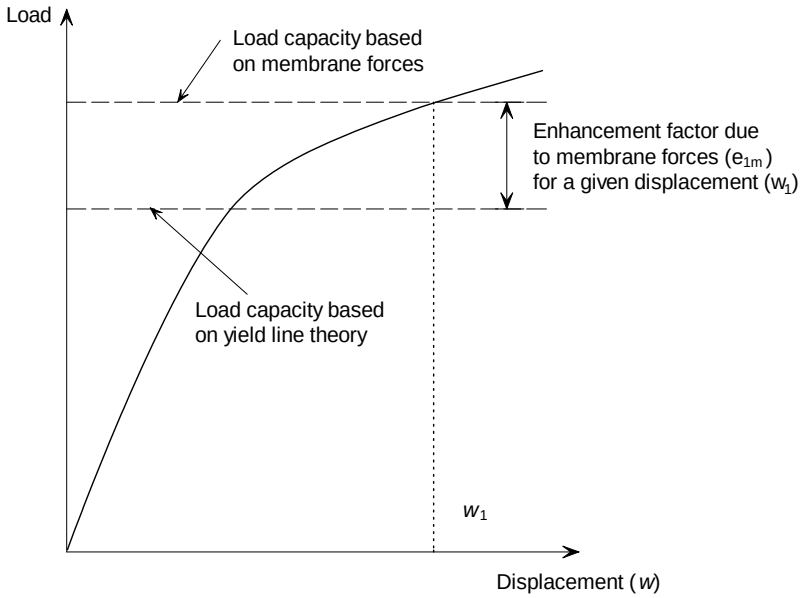

Figure 6–13 : Enhancement factor due to membrane force

The value of μM_o is obtained by considering Figure 6–14.

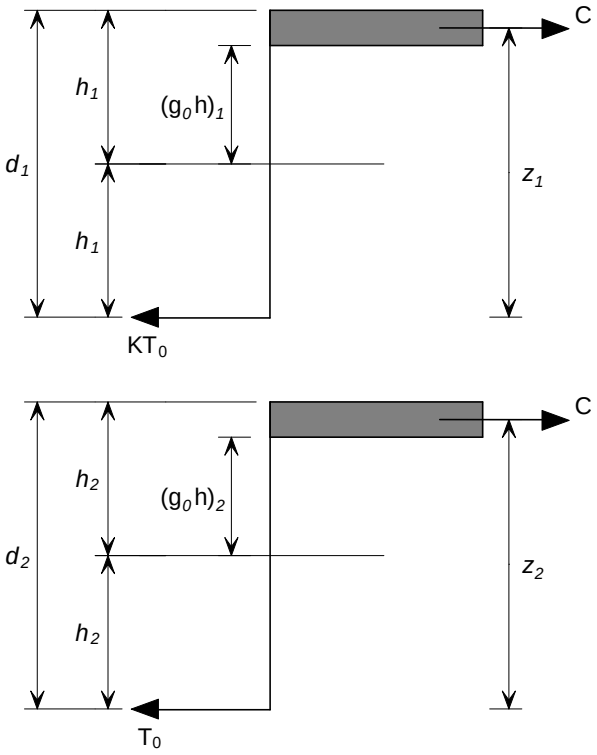

Figure 6–14 : Calculation of the moment resistance

The bending moments μM_o and M_o per unit width of slab in each orthogonal direction are given by:

$$\mu M_0 = KT_0 d_1\left(\frac{3+(g_0)_1}{4}\right)$$

$$M_0 = T_0 d_2\left(\frac{3+(g_0)_2}{4}\right)$$

where

$(g_0)_1, (g_0)_2$ are parameters which define the flexural stress block in the two orthogonal directions

d_1, d_2 are the effective depths of the reinforcement in each direction

The enhancement factor, e_{1m}, is given by:

$$e_{1m} = \frac{M_{1m}}{\mu M_0 L} = \frac{4b}{3+(g_0)_1}\left(\frac{w}{d_1}\right)\left((1-2n)+\frac{n(3k+2)-nk^3}{3(1+k)^2}\right)$$

b) Element 2

The moment about the support due to the membrane forces is given by:

$$M_{2m} = KT_0 lbw\left(\frac{2+3k-k^3}{6(1+k)^2}\right)$$

where

M_{2m} is the moment about support due to membrane force for element 2.

The effect of tensile membrane action can be expressed as an enhancement of yield line resistance by dividing the moment about the support due to membrane action, M_{2m} by the moment resistance in the longitudinal direction, when no axial force is present, $M_0 l$, which results in,

$$e_{2m} = \frac{M_{2m}}{M_0 l} = \frac{4bK}{3+(g_0)_2}\left(\frac{w}{d_2}\right)\left(\frac{2+3k-k^3}{6(1+k)^2}\right)$$

The effect of the membrane forces on the bending resistance along the yield lines is evaluated by considering the yield criterion when axial load is also present, as given by Wood [38]. In the case of the short span the bending moment in the presence of an axial force is given by

$$\frac{M_N}{\mu M_0} = 1+\alpha_1\left(\frac{N}{KT_0}\right)-\beta_1\left(\frac{N}{KT_0}\right)^2$$

where

$$\alpha_1 = \frac{2(g_0)_1}{3+(g_0)_1}$$

and

$$\beta_1 = \frac{1-(g_0)_1}{3+(g_0)_1}$$

Similarly for the long span,

$$\frac{M_N}{\mu M_0} = 1+\alpha_2\left(\frac{N}{T_0}\right)-\beta_2\left(\frac{N}{T_0}\right)^2$$

where

$$\alpha_2 = \frac{2(g_0)_2}{3+(g_0)_2}$$

and

$$\beta_2 = \frac{1-(g_0)_2}{3+(g_0)_2}$$

Effect of membrane forces on bending resistance
a) Element 1

The effect of the membrane forces on the bending resistance is considered separately for the each yield line,

For the yield line BC, the membrane force is constant and equals $-bKT_0$ and therefore:

$$\left(\frac{M_N}{M_0}\right)_{BC} = 1-\alpha_1 b-\beta_1 b^2$$

For the yield line AB (Figure 6–15),

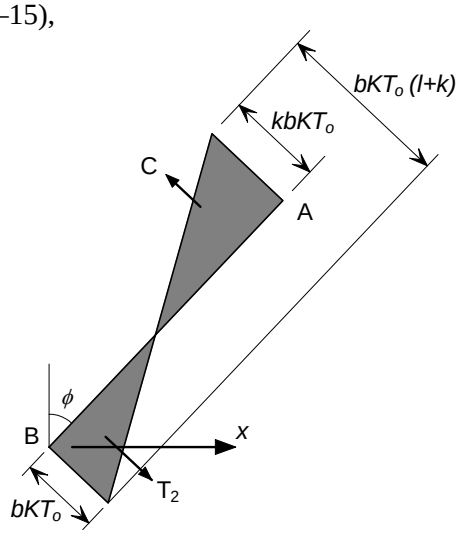

Figure 6–15 : Forces applied to element 1, yield line CD

The membrane force across the yield line, at a distance of x from B is given by:

$$N_x = -bKT_0 + \frac{x}{nL}(K+1)bKT_0$$

$$N_x = bKT_0\left(\frac{x(k+1)}{nL}-1\right)$$

Substitution into previous equation gives, for yield lines AB and CD:

$$2\int_0^{nL}\frac{M}{M_0}dx = 2\int_0^{nL}\left[1+\alpha_1 b\left(\frac{x(k+1)}{nL}-1\right)-\beta_1 b^2\left(\frac{x(k+1)}{nL}-1\right)^2\right]dx$$

This results in:

$$2\int_0^{nL}\frac{M}{M_0}dx = 2nL\left[1+\frac{\alpha_1 b}{2}(k-1)-\frac{\beta_1 b^2}{3}\left(k^2-k+1\right)\right]$$

The enhancement of bending resistance due to membrane forces on Element 1 is given by:

$$e_{1b} = \frac{M}{\mu M_0 L} = 2n\left[1+\frac{\alpha_1 b}{2}(k-1)-\frac{\beta_1 b^2}{3}\left(k^2-k+1\right)\right]+(1-2n)\left(1-\alpha_1 b-\beta_1 b^2\right)$$

b) Element 2

Referring to the previous case for element 2, the force at a distance *y* from B can be expressed as:

$$N_y = -bKT_0 + \frac{y}{l/2}(k+1)bKT_0$$

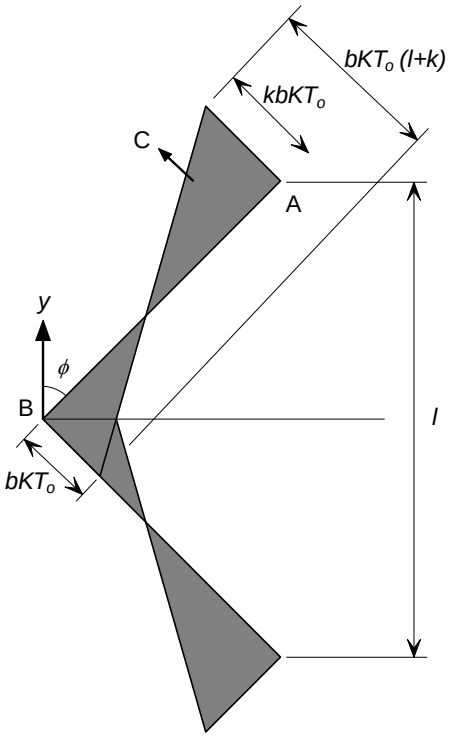

Figure 6–16 : Forces applied to element 2

By rearranging

$$N_y = bKT_0\left(\frac{2y(k+1)}{l}-1\right)$$

Substitution into equation here above gives:

$$\int_0^{1/2}\frac{M}{M_0}dy = 2\int_0^{1/2}\left[1+\alpha_2 bK\left(\frac{2y(k+1)}{l}-1\right)-\beta_2 b^2 K\left(\frac{2y(k+1)}{l}-1\right)^2\right]dy$$

Resulting in,

$$2\int_0^{1/2}\frac{M}{M_0}dx = l\left[1+\frac{\alpha_2 b}{2}(k-1)-\frac{\beta_2 b^2}{3}(k^2-k+1)\right]$$

Which gives the enhancement factor due to the effect of the membrane forces on the bending resistance according to the following formulation,

$$e_{2b}=\frac{M}{M_0 l}=1+\frac{a_2 bK}{2}(k-1)-\frac{\beta_2 b^2 K}{3}(k^2-k+1)$$

These equations provide the contribution to the load bearing capacity due to the membrane forces and the effect of the membrane forces on the bending resistance of the slab.

Consequently, the combined enhancement factor is obtained for each element as follows

$e_1 = e_{1m} + e_{1b}$

$e_2 = e_{2m} + e_{2b}$

As stated earlier, the values e_1 and e_2 calculated based on the equilibrium of elements 1 and 2 will not be the same and Hayes suggests that these differences can be explained by the effect of the vertical or in-plane shear and that the overall enhancement is given by.

$$e = e_1 - \frac{e_1 - e_2}{1+2\mu a^2}$$

6.1.3. Compressive failure of concrete

The enhancement factor in Section 6.1.2.1 was derived by considering tensile failure of the mesh reinforcement. However, compressive failure of the concrete in the proximity of the slab corners must also be considered as a possible mode of failure, which in some cases may precede mesh fracture. This was achieved by limiting the value of the parameter '*b*', which represents the magnitude of the in-plane stresses.

According to Figure 6–9, the maximum in-plane compressive force at the corners of the slab is given by $kbKT_0$. The compressive force due to the bending should also be considered. By assuming that the maximum stress-block depth is limited to 0.45d, and adopting an average effective depth to the reinforcement in both orthogonal directions results in:

$$kbKT_0 + \left(\frac{KT_0 + T_0}{2}\right) = 0.85 f_{ck} \times 0.45\left(\frac{d_1 + d_2}{2}\right)$$

Where, f_{ck} is the concrete cylinder strength.

Solving for the constant *b* gives:

$$b = \frac{1}{kKT_o}\left(0.85 f_{ck} \times 0.45\left(\frac{d_1 + d_2}{2}\right) - T_0\left(\frac{K+1}{2}\right)\right)$$

The constant *b* is then taken as the minimum value given by the two equations.

6.2. Development of design guidance

Previous tests at normal temperature, reviewed in Section 6.1, have shown that the load bearing capacity of concrete slabs will be enhanced by membrane forces provide that vertical support is maintained along the slab boundaries. Flat slabs, which only have vertical supports at their corners, do not develop significant tensile membrane forces and therefore benefit little from enhancement due to membrane action.

Therefore, for a composite slab supported on a grillage of steel beams in fire conditions, it is important to divide the slab into rectangular areas, referred to as floor design zones, where vertical support can be maintained on the perimeter of each area. These lines of vertical support are achieved by ensuring that the perimeter beams frame into column positions and are fire protected.

At ambient temperature, the floor is continuous over the boundary of each floor design zone. However, in fire conditions it is likely that cracks will form over the perimeter beams, due to the large thermal curvatures experienced by the slab. This may lead to fracture of the reinforcement, either due to the curvature or due to the combination of bending and membrane stresses. The fracture of the reinforcement in these hogging regions will occur before fracture of the reinforcement in the centre of the floor design zone. Therefore, the floor design zones are considered to have no rotational or transverse restraint along the boundary of the slab.

6.2.1. Design assumptions

For a composite floor slab, the yield line pattern will depend on the behaviour of the unprotected composite beams, which are continually losing strength as the temperature increases. Unlike ambient conditions the load carrying mechanism of the floor changes with increasing temperature. Initially, the composite slab acts as a one-way spanning element supported on the secondary beams. As these beams lose strength with increasing temperature and the behaviour of the slab tends to the behaviour of a simple supported two-way spanning element, resulting in the formation of the yield line pattern shown in Figure 6–17. By assuming that this ultimate failure condition will occur when the beam strength is low relative to the slab, a conservative estimate of capacity can be obtained relatively simply.

The load bearing capacity of the slab is calculated on the assumption that the composite beams have no strength and is based on the yield line pattern which is compatible with the boundary conditions and which provides the lowest load bearing capacity. This resistance is then enhanced by taking account of the tensile membrane effects based on the estimated deflection of the slab and the modes of failure described in Section 6.1 . The bending resistance of the composite beams are added to this enhanced slab resistance in order to give the total load bearing capacity of the system.

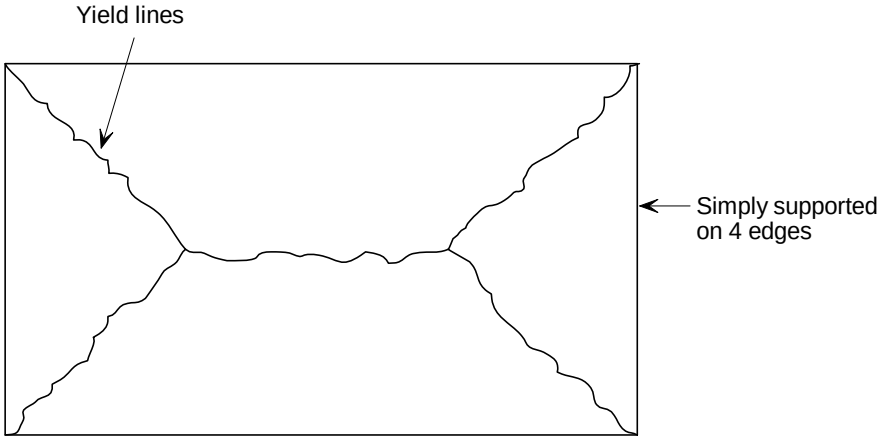

Figure 6–17 : Typical yield line pattern for a rectangular slab simply supported along four edges

6.2.2. Failure criterion

Two modes of failure have been witnessed in room temperature and elevated temperature tests, depending on the reinforcement ratio, slab aspect ratio and the reinforcement ductility. Fracture of the reinforcement across the shorter span dominates the failure mode in most of the lightly reinforced slabs, whilst the heavily reinforced slabs and slabs with highly ductile reinforcement may experience compressive failure at the corners of the slab. Both modes of failure are considered by the simple design method as described in Section 6.1.2

Most tests conducted at elevated temperatures on simply supported concrete slabs have failed due to full depth crack forming across the shorter span (*l*), as shown in Figure 6–18. This was also the mode of failure witnessed in the large scale test with cellular beams carried out as part of this project. The design method presented in Section 6.1.2 predicts the load bearing capacity for a given deflection. Section 6.2.2.1 describes the development of an expression for estimating slab deflection just prior to slab failure which is required to calculate the effect of membrane action.

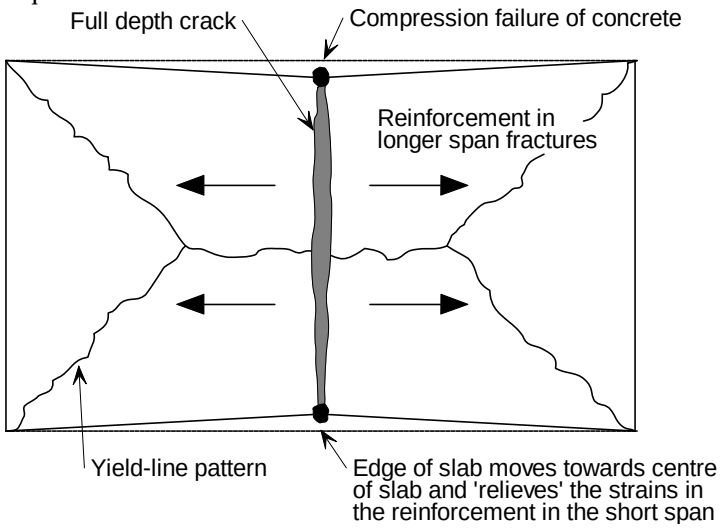

Figure 6–18 : Tensile failure of the slab due to fracture of the reinforcement

6.2.2.1. Slab deflection

As the simple design method is based on plastic theory, deflection cannot be calculated using the method. However, in order to calculate the membrane forces a value of deflection for the slab just prior to failure must be estimated. This estimate of slab deflection will include thermal strains due to the slabs temperature gradient as well as the mechanical strains in the reinforcement. The following method of estimating floor deflection may be used for solid web beams or cellular beams. The recent large scale test on a 15m by 9m floor plate constructed with cellular beams has shown that the estimated deflections using this method are conservative when compared to measured deflections.

6.2.2.2. Thermal effects

Based on the previous investigations, when the maximum deflection of the slab is greater than almost 0.5 times its depth and tensile forces start to build up at the slab centre, any in-plane restraint to the thermal expansion would increase the vertical displacements (i.e. the slab is in the post-buckling phase) and therefore the tensile membrane action. Conservatively, and in order to allow this approach to be used also for the edge slabs, this beneficial effect is ignored and slab is assumed to be unrestrained.

The composite slab in the fire conditions would experience thermal curvature, which, for an unrestrained slab, increases the vertical displacement without inducing any mechanical strains into the mesh reinforcement. If the temperature distribution through the slab is assumed to be linear then the displacements caused by the thermal deflection is calculated as:

$$\frac{d^2w}{dx^2} = \frac{\alpha(T_2 - T_1)}{h}$$

where

w = Vertical displacement

α = Coefficient of thermal expansion

T_2 = Bottom temperature

T_1 = Top temperature

h = Depth of slab

The vertical displacement of the slab due to thermal curvature can be obtained by integrating the above Equation, which gives:

$$w_\theta = \frac{\alpha(T_2 - T_1)l^2}{8h}$$

where

l is the length of the shorter span of the slab

This formulation is based on a constant atmospheric temperature throughout the fire compartment. To the estimated displacement, allowing for real fire conditions where uniform heating is less likely, a reduction factor of 2.0 is applied to the above expression. This results in the design value of vertical displacement due to the thermal curvature given by:

$$w_\theta = \frac{\alpha(T_2 - T_1)l^2}{16h}$$

6.2.2.3. Mechanical strains in the reinforcement

Assuming that the deflected shape of the slab due to transverse loading is parabolic, the length of the deflected slab is given by the following formulation in which the longer span is (L).

$$L_c = L\left(1 + \frac{8w^2}{3L^2} - \frac{32w^4}{5L^4} + ...\right)$$

where

L_c is the length of the curve,

L is the length of longer span of slab at zero displacement,

w is the vertical displacement of the curve.

For flat curves,

$$L_c = L\left(1 + \frac{8w^2}{3L^2}\right)$$

Hence, the strain in the mesh can be calculated by:

$$\varepsilon = \frac{8w^2}{3L^2}$$

This equation assumes the strain is the same value along the length of the slab. In reality, the slab will experience tension stiffening with strains being concentrated where cracks have occurred. The reinforcement across a crack will also experience a significant increase in the strain, resulting in the eventual fracture of the reinforcement. Therefore, to allow for tension stiffening the component of displacement due to strain in the reinforcement w_ε is based on a conservative value of average strain calculated at a stress equal to half the yield stress at room temperature. The displacement is then given by:

$$w_\varepsilon = \sqrt{\left(\frac{0.5f_{sy}}{E_s}\right) \quad \frac{3L^2}{8}}$$

where

E_s is the room temperature elastic modulus of the reinforcement

f_{sy} is the room temperature yield strength of the reinforcement

The displacements due to strain in the reinforcement calculated using equation hereabove have been compared to maximum deflections measured in tests at room temperature. In all the cases considered, the displacement predicted by equation hereabove was lower than the maximum displacement recorded in the test, as shown in Table 6-1.

Table 6-1 : Comparison of allowable deflection from the equation and maximum deflections measured in room temperature tests.

Test	Slab size (m)	Effective Depth (mm)	Reinforcement Diameter (mm)	Bar Spacing (mm)	Steel yield strength (N/mm^2)	Max. test deflection (mm)	Allowable deflection (mm)
BRE	9.56x6.46	66.0	6.0	200	580	223	216
Sawczuk & Winnicki	1.6x1.1	26.0	3.0	30.0	263	127*	25
	2.0x1.0	26.0	3.0	60.0	263	76*	31
Hayes & Taylor	0.914x0.914	15.9	9.5	-†	505	50.8*	19.4
	0.914x1.372	15.9	9.5	-†	505	50.8*	29.1
	0.914x1.829	15.9	9.5	-†	505	50.8*	38.8
Taylor, Maher & Hayes	1.829x1.829	43.6	4.8	76.2	376	81	33.5
	1.829x1.829	37.3	4.8	63.5	376	98	33.5
	1.829x1.829	69.0	4.8	122	376	84	33.5
Brothie & Holley	0.381x0.381	14.2	2.3	-†	414	11.6	7.32
	0.381x0.381	31.0	3.4	-†	379	7.45	7.0

*test terminated before fracture of the reinforcement

† Data not reported

6.2.2.4. Calculation of slab deflection to allow the calculation of membrane forces

The tensile membrane action of the slab is then calculated based on a slab displacement estimated by combining the components due to thermal curvature and strain in the reinforcement, resulting in:

$$w_m = \frac{\alpha(T_2 - T_1)l^2}{16h} + \sqrt{\left(\frac{0.5f_{sy}}{E_s}\right) \quad \frac{3L^2}{8}}$$

This equation results in a conservative estimate of load bearing capacity since:

- the estimated vertical displacements due to thermal curvature are divided by two.
- the thermal curvature is calculated based on the shorter span of the slab
- any additional vertical displacements induced by the restrained thermal expansion when the slab is in a post buckled state are ignored
- any contribution from the steel decking is ignored
- the increase of the mesh ductility with the temperature increase is ignored.

6.2.2.5. Calibration against Cardington fire tests

Bailey & Moore [35] demonstrated that the design method in Section 6.1.2 provided a reasonable prediction of floor slab capacity when compared to the Cardington Fire Tests. As part on this project a further furnace based fire test has been conducted as described in Work Package 7.

The above expression for slab deflection was compared to the maximum deflections recorded during the Cardington fire tests. The object was to ensure that the deflections estimated would be conservative when compared to actual slab behaviour just prior to failure. The drawback in using these tests for this purpose was that failure was not reached by the slabs tested therefore the maximum measured deflections do not correspond to failure of the slab. However, it is known that the results of the comparison will be conservative but the degree of conservatism can not be quantified.

Table 6-2 shows the comparison between the limiting deflection given by the equation w_m and the maximum measured deflection from each of the Cardington tests. This comparison includes both thermal and mechanical strains, which are impossible to distinguish in test data.

In all cases, calculation method gives deflections which are greater than the measured deflections. In order to ensure that the deflection limit is conservative Bailey and Moore [35] limited the deflection to those recorded in the tests.

Table 6-2 : Comparison of the displacement given by the equation against the maximum displacements recorded in the six Cardington fire tests.

Test	L (m)	l (m)	Deflection due to thermal curvature (mm)	Deflection due to mechanical strain (mm)	Deflection limit (mm)	Maximum deflection recorded in test (mm)	Deflection Limit/test deflection
BRE Corner Test	9.0	6.0	135	208	343	269	1.28
British Steel Restrained Beam	9.0	6.0	135	208	343	232	1.50
British Steel 2-D test	14.0	9.0	0*	324	324	293	1.11
BS Corner Test	10.223	7.875	231	237	468	428	1.09
BRE Large Compartment Test	21.0	9.0	303	486	789	557	1.42
BS Office Demo Test	14.6	10.0	373	338	711	641	1.11

*Due to the small area of slab heated in this test the displacement due to thermal curvature was taken as zero.

For mechanical strains, Bailey and Moore introduced an additional limit as shown below.

$$w_\varepsilon = \sqrt{\left(\frac{0.5f_y}{E}\right)_{reinf} \frac{3L^2}{8}} \quad \text{but} \quad w_\varepsilon \le \frac{l}{30}$$

For thermal deflection they also increased the 'factor of safety' from 2 to 2.4 giving the following conservative expressions for estimating slab deflections:

$$w_m = \frac{\alpha(T_2 - T_1)l^2}{19.2h} + \sqrt{\left(\frac{0.5f_{sy}}{E_s}\right) \frac{3L^2}{8}}$$

but not more than $\frac{\alpha(T_2 - T_1)l^2}{19.2h} + \frac{l}{30}$

Table 6-3 shows the comparison between the limiting deflection given by equation hereabove. Given that failure did not occur in any of the tests it was felt that it would be overly conservative to reduce the deflection limit to a point where the ratio of deflection limit to measured deflection was one for all tests. For the large compartment tests this limit appears to be reasonable.

Table 6-3 : Comparison of the displacement given by the equation against the maximum displacements recorded in the six Cardington fire tests.

Test	L (m)	l (m)	Deflection due to thermal curvature (mm)	Deflection due to mechanical strain (mm)	Deflection limit (mm)	Maximum deflection recorded in test (mm)	Deflection Limit/test deflection
BRE Corner Test	9.0	6.0	112	200	312	269	1.16
British Steel Restrained Beam	9.0	6.0	112	200	312	232	1.34
British Steel 2-D test	14.0	9.0	0*	300	300	293	1.02
BS Corner Test	10.223	7.875	193	237	430	428	1.00
BRE Large Compartment Test	21.0	9.0	252	300	552	557	0.99
BS Office Demo Test	14.6	10.0	311	333	644	641	1.00

*Due to the small area of slab heated in this test the displacement due to thermal curvature was taken as zero.

6.2.3. Design methodology

The design methodology advocated in this document is based on two key principles.

- The risk to life safety of the building occupants, fire fighters and others in the vicinity of the building in the event of a fire should not increase relative to current practice as a result of using the method.
- The fire should be contained within its compartment of origin and the application of the design method should not lead to failure of the compartmentation of the building

The design method is intended to apply to composite steel-concrete floor plates supported on composite or non-composite columns. The structural frame should be braced (non-sway), the connections should be simple nominally pinned connections and the concrete floor slab should be constructed using steel decking not exceeding 80 mm in depth and supported on the top flange of the steel section. The steel beams should be designed to act compositely with the floor slab in accordance with the recommendations of EN 1994-1-1. Excluded from the scope of application are slabs with an exposed concrete soffit including precast concrete slabs and beams with multiple web openings.

In order to apply the simple design method described in Section 6.1 to a design scenario, the floor plate being considered must be divided into a number of ‘floor design zones’. These floor design zones are bounded on their perimeters by beams (normally fire protected) which satisfy the fire resistance requirements specified for the floor plate. Each floor design zone may include a number of internal secondary beams without fire protection which have a much lower fire resistance. The provision of protected beams on the perimeter of the floor slab is intended to result in slab behaviour in keeping with the assumption that the perimeter of the floor design zone is simply supported.

For periods of fire resistance of 60 minutes or above the perimeter of the floor design zones should correspond to the column gridlines and the perimeter beams should be connected to the columns at either end.

The composite slab may be designed in accordance with EN 1994-1-1 and should also satisfy the minimum insulation thickness recommended by EN 1994-1-2 in fire conditions. Reinforcement of the

composite slab should be achieved using a steel mesh. Reinforcement in the ribs of the slab is not considered in the design method. The inclusion of such reinforcement can have a negative as well as a positive effect on the slab performance in fire conditions, as compressive failure in the concrete may result if the slab is over reinforced.

6.2.3.1. Calculation of load bearing capacity for the slab

The calculation of the yield line capacity of the composite slab and the associated enhancement of this resistance due to large slab deflections is described in detail in Section 6.1 .

6.2.3.2. Calculation of load bearing capacity for unprotected beams

In fire conditions, the unprotected cellular beams within each floor design zone provide additional tensile resistance via catenary action. Currently, the design method conservatively assumes that only the bending resistance of these unprotected members contribute to the total slab capacity. For unprotected cellular beams allowance must also be made for the possibility of buckling failure preventing the whole section for contributing to the bending resistance. Therefore as a conservative approach only the bending resistance of the top tee of the cellular section is included when calculating the total resistance of the floor plate.

The temperature of the bottom flange of the unprotected beams is calculated using the method given in EN 1994-1-2, 4.3.4.2. The bottom flange, top flange and web of the section are assumed to be at uniform temperature for the calculation of moment resistance.

The calculation of the plastic moment resistance of the beam at elevated temperature follows the principles of EN 1994-1-2, 4.3 taking account of the degree of shear connection between the steel section and the concrete.

6.2.4. Design of fire resisting perimeter beams

The perimeter beams which bound each floor design zone must be designed to achieve the period of fire resistance required by the floor slab. This will ensure that the pattern of yield lines and the associated enhancement due to tensile membrane action which are assumed to occur in the design methodology actually occur in practice. The required moment resistance of the edge beams is calculated by considering alternative yield line patterns that would allow the slab to fold along an axis of symmetry without developing tensile membrane action, as shown by 0 and 0.

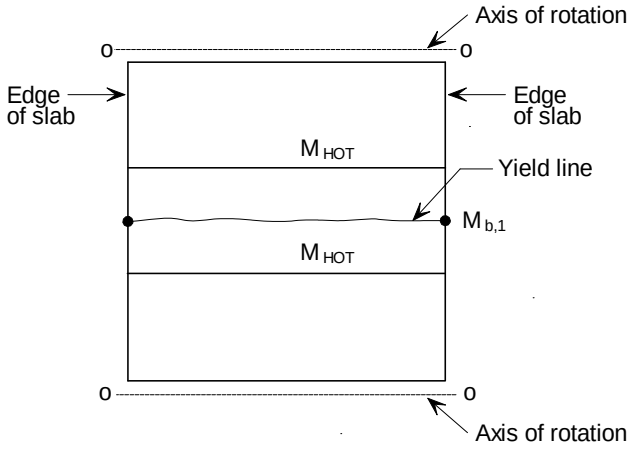

Figure 6–19 : Alternative yield line patterns involving the formation of plastic hinges in the perimeter beams

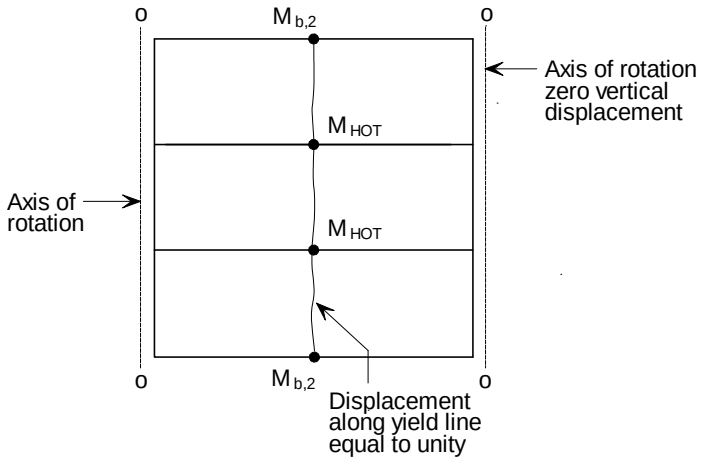

Figure 6–20 : Alternative yield line patterns involving the formation of plastic hinges in the perimeter beams

Having calculated the required moment capacity of these beams to ensure that they provide sufficient support to allow development of the tensile membrane enhancement of the slab load bearing resistance, a critical temperature for the beams can be calculated and appropriate levels of fire protection can be applied to ensure that this critical temperature is not exceeded during the required fire resistance period.

The design method described in Section 6.1 assumes that an envelope pattern of yield lines will form in the slab at the ultimate limit state. In order for this to occur, the beams on the perimeter of the floor design zone must have sufficient moment resistance to prevent a beam and slab mechanism occurring at a lower load level.

For a typical floor design zone, as shown in Figure 6–21, two yield line patterns have been considered which include the formation of a plastic hinge in the perimeter beams. The yield lines may occur across the centre of the slab, either parallel to the unprotected beams in the Span 1 direction with plastic hinges forming in the perimeter beams on Sides A and C or perpendicular to the unprotected beams in the Span 2 direction with plastic hinges forming in the perimeter beams on Side B and D and in the unprotected beams.

Using this pattern of yield lines and equating the internal and external work for the mechanism, the moment resistance of the perimeter beams required to achieve a load bearing capacity equal to that for the floor slab may be determined. The derivation of appropriate design equations is given below.

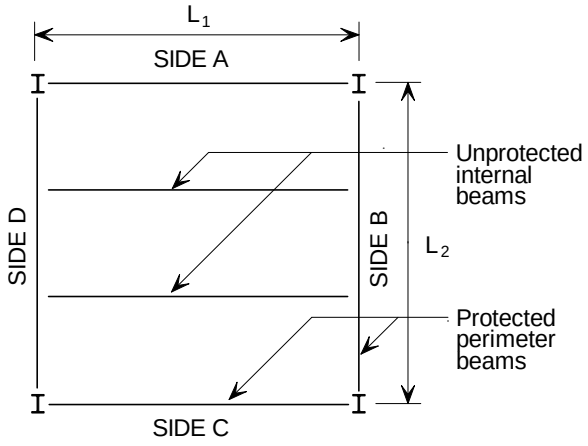

Figure 6–21 : Typical floor design zone

6.2.4.1. Unprotected beams with edge beams on both sides

Yield line parallel to unprotected beams

This case considers the required moment resistance of the perimeter beams on Sides B and D of the floor design zone. These beams are also assumed to be at the edge of the slab. A single yield line is assumed to form across the centre of the floor design zone in the Span 1 direction, as shown in Figure 6–22. In keeping with the assumptions of the design method the perimeter of the floor design zone is assumed to be simply supported.

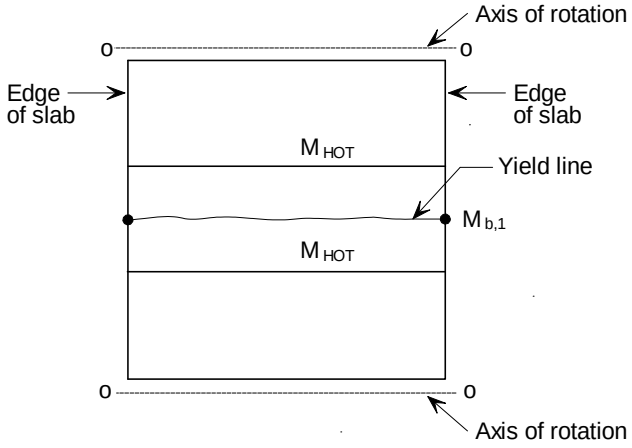

Figure 6–22 : Yield line in parallel to the unprotected beams edge condition on Sides B and D

Considering a unit displacement along the yield line, the rotation of the yield line can be calculated as follows:

$$\text{Yield line rotation} = 2\frac{1}{L_2/2} = \frac{4}{L_2}$$

The internal work done due to the rotation of the yield line is given by:

$$\text{Internal Work} = \left(ML_{1,\text{eff}} + 2M_{b,1}\right)\frac{4}{L_2} = \frac{4ML_{1,\text{eff}}}{L_2} + \frac{8M_{b,1}}{L_2}$$

where

$L_{1,\text{eff}}$ is the effective length of the yield line discounting the effective width of slab assumed to act with the perimeter beams where these are design as composite members.

M is the moment resistance of the slab per unit length of yield line

For a uniform load on the slab, *p*, the external work due to the displacement is given by:

$$\text{External Work} = \frac{1}{2}pL_1L_2$$

Equating internal and external work gives:

$$pL_1L_2 = \frac{8ML_{1,\text{eff}}}{L_2} + \frac{16M_{b,1}}{L_2}$$

If the load on the slab is the load bearing capacity determined in accordance with Section 6.1, the required minimum values of moment resistance for the perimeter beams on Side B and D is given by:

$$M_{b,1} = \frac{pL_1 L_2{}^2 - 8ML_{1,eff}}{16}$$

where

p is the uniformly distributed load to be supported by the floor design zone in fire conditions.

Yield line perpendicular to unprotected beams

This case considers the required moment resistance of the perimeter beams on Sides A and C of the floor design zone. A single yield line is assumed to form across the centre of the floor design zone in the Span 2 direction, as shown in Figure 6–23. In keeping with the assumptions of the design method the perimeter of the floor design zone is assumed to be simply supported.

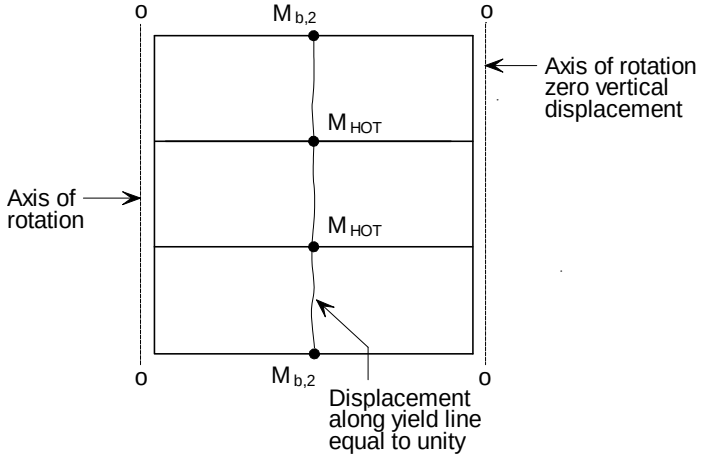

Figure 6–23 : Yield line perpendicular to the unprotected beams edge condition on Sides A and C

Considering a unity displacement along the yield line the rotation of the yield line can be calculated as follows:

$$\text{Yield line rotation} = 2\frac{1}{L_1/2} = \frac{4}{L_1}$$

The internal work done due to the rotation of the yield line is given by:

$$\text{Internal Work} = \left(ML_{2,eff} + 2M_{b,2} + nM_{HOT}\right)\frac{4}{L_1}$$

$$= \frac{4ML_{2,eff}}{L_1} + \frac{8M_{b,2}}{L_1} + \frac{4nM_{HOT}}{L_1}$$

where

$L_{2,eff}$ is the effective length of the yield line discounting the effective width of slab assumed to act with the perimeter beams where these are designed as composite members and the composite unprotected internal beams.

M is the moment resistance of the slab per unit length of yield line

The external work due to the slab displacement is given by:

$$\text{External Work} = \frac{1}{2}pL_1L_2$$

Equating internal and external work gives:

$$pL_1L_2 = \frac{8ML_{2,eff}}{L_1} + \frac{16M_{b,2}}{L_1} + \frac{8nM_{HOT}}{L_1}$$

If the load on the slab is the load bearing capacity determined in accordance with Section 6.1, the required minimum values of moment resistance for the perimeter beams on Side A and C is given by:

$$M_{b,2} = \frac{pL_1^{\,2}L_2 - 8ML_{2,eff} - 8nM_{HOT}}{16}$$

where

p is the uniformly distributed load to be supported by the floor design zone in fire conditions.

6.2.4.2. Unprotected beams with an edge beam on one side

Yield line parallel to unprotected beams

This case considers the required moment resistance of the perimeter beams on Sides B and D of the floor design zone. In this case the beam on side B is an internal perimeter beam. As the software only deals with an isolated floor plate the calculation of resistance for an internal perimeter beam must assume that the floor design zone is adjacent to an identical area of slab sides where internal beams have been specified. A single yield line is assumed to form across the centre of the floor design zone in the Span 1 direction, as shown in Figure 6–24.

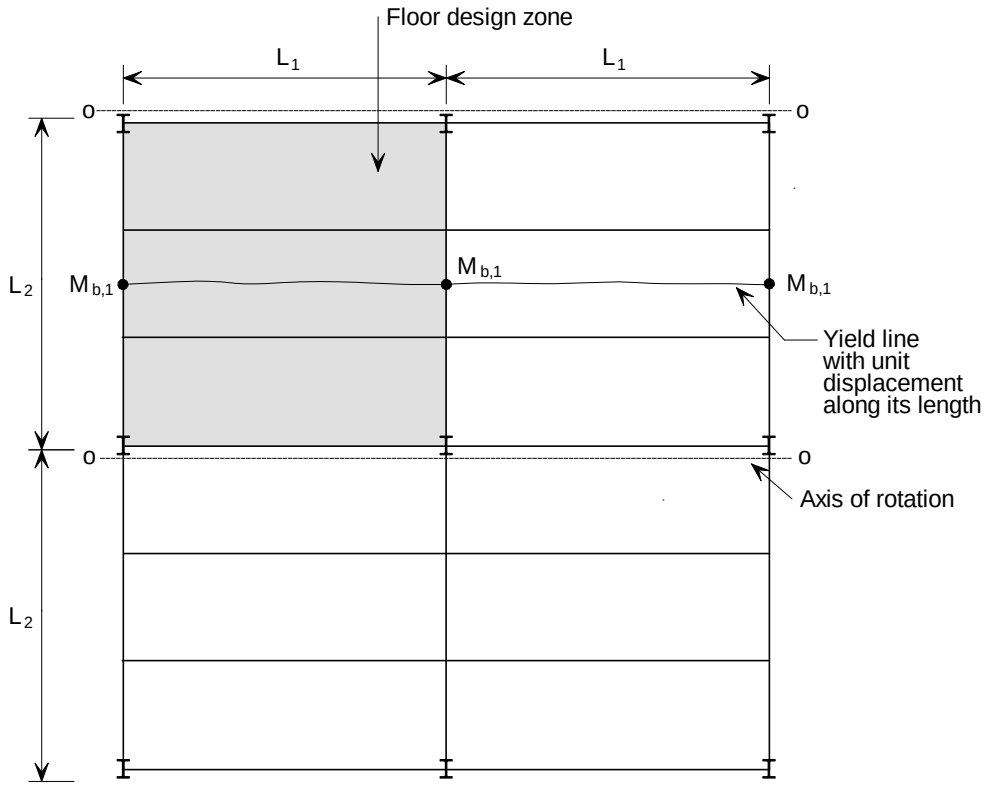

Figure 6–24 : Yield line parallel to the unprotected beams edge condition on Side D

Considering a unit displacement along the yield line the rotation of the yield line can be calculated as follows:

$$\text{Yield line rotation} = 2\frac{1}{L_2/2} = \frac{4}{L_2}$$

The internal work done due to the rotation of the yield line is given by:

$$\text{Internal Work} = \left(2ML_{1,eff} + 3M_{b,1}\right)\frac{4}{L_2} = \frac{8ML_{1,eff}}{L_2} + \frac{12M_{b,1}}{L_2}$$

The external work due to the slab displacement is given by:

External Work = $\frac{1}{2}p2L_1L_2$

Equating internal and external work gives:

$$pL_1L_2 = \frac{8ML_{1,eff}}{L_2} + \frac{12M_{b,1}}{L_2}$$

If the load on the slab is the load bearing capacity determined in accordance with Section 6.1, the required minimum values of moment resistance for the perimeter beams on Side B and D is given by:

$$M_{b,1} = \frac{pL_1L_2{}^2 - 8ML_{1,eff}}{12}$$

where

$\underline{L}_{1,eff}$ is the effective length of the yield line discounting the effective width of slab assumed to act with the perimeter beams where these are design as composite members.

M is the moment resistance of the slab per unit length of yield line

p is the uniformly distributed load to be supported by the floor design zone in fire conditions.

Yield line perpendicular to unprotected beams

A single yield line is assumed to form across the centre of the floor design zone in the Span 2 direction, as shown in Figure 6–25.

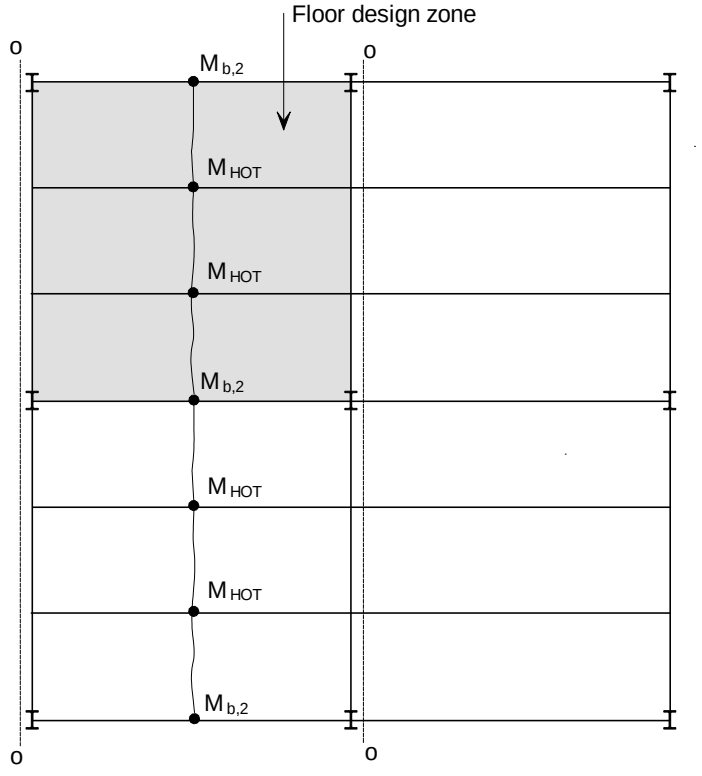

Figure 6–25 : Yield line perpendicular to the unprotected beams edge condition on Side A

Considering a unity displacement along the yield line the rotation of the yield line can be calculated as follows:

Yield line rotation = $2\frac{1}{L_1/2} = \frac{4}{L_1}$

The internal work done due to the rotation of the yield line is given by:

$$\text{Internal Work} = \left(2ML_{2,eff} + 3M_{b,2} + 2nM_{HOT}\right)\frac{4}{L_1} = \frac{8ML_{2,eff}}{L_1} + \frac{12M_{b,2}}{L_1} + \frac{8nM_{HOT}}{L_1}$$

The external work due to the slab displacement is given by:

$$\text{External Work} = \frac{1}{2}pL_1 2L_2$$

Equating internal and external work gives:

$$pL_1L_2 = \frac{8ML_{2,eff}}{L_1} + \frac{12M_{b,2}}{L_1} + \frac{8nM_{HOT}}{L_1}$$

If the load on the slab is the load bearing capacity determined in accordance with Section 6.1, the required minimum values of moment resistance for the perimeter beams on Side A and C is given by:

$$M_{b,2} = \frac{pL_1^2 L_2 - 8ML_{2,eff} - 8nM_{HOT}}{12}$$

where

$L_{2,eff}$ is the effective length of the yield line discounting the effective width of slab assumed to act with the perimeter beams where these are design as composite members and the composite unprotected internal beams.

M is the moment resistance of the slab per unit length of yield line

p is the uniformly distributed load to be supported by the floor design zone in fire conditions.

6.2.4.3. Floor zone without edge beams

For zones where none of the perimeter beams are edge beams, it is conservative to use the values determined by the expressions in 6.2.4.2.

6.2.4.4. Design of edge beams

It is common practice for beams at the edge of floor slabs to be designed as non composite. This is because the costs of meeting the requirements for transverse shear reinforcement are more than the costs of installing a slightly heavier non composite beam. However, for fire design, it is important that the floor slab is adequately anchored to the edge beams, as these beams will be at the edge of floor design zones. For this purpose, if edge beams are designed as non composite, they must have shear connectors at not more than 300 mm centres and U-bars should be provided to tie the edge beam to the composite slab.

6.2.5. Thermal Analysis

The FiCEB spreadsheet uses a 2D finite difference heat transfer method to predict the temperature distribution within the composite slab. This method has been used for many years by SCI to predict the temperature distributions in steel and steel-concrete composite cross sections and has been shown to be able to reasonably predict the behaviour of sections in fire resistance tests.

The object to be analysed must defined on a rectangular grid of cells. The method can also analyse the sloping sides of trapezoidal or re-entrant composite slabs by using configuration factors given below.
The thermal properties of steel and concrete used by the FiCEB spreadsheet are based on the values given by EN1994-1-2.
The thermal actions are calculated on the basis of the net heat flux, $\dot{h}_{net}$ to which the surface of the member is exposed. The net heat flux is determined considering the heat transfer by convection and radiation.

$$\dot{h}_{net} = \dot{h}_{net,c} + \dot{h}_{net,r}$$

The net convective heat flux component is determined as follows:

$$\dot{h}_{net,c} = \alpha_c \left(\theta_g - \theta_m\right)$$

Where

α_c is the coefficient of heat transfer by convection

θ_g is the gas temperature

θ_m is the surface temperature of the member

When carrying out a thermal analysis for a member exposed to the standard temperature –time curve the coefficient of heat transfer by convection on the exposed face is taken as α_C = 25 W/m^{2}K.

For natural fire models the coefficient of heat transfer by convection is increased to α_C = 35 W/m^{2}K.

On the unexposed side of the slab the net heat flux is based on heat transfer by convection , but the coefficient of heat transfer by convection is taken as α_C = 9 W/m^{2}K, to allow for the effects of heat transfer by radiation which are not considered explicitly in the model.

The net radiative heat flux is determined from the following formula

$$h_{net,r} = \Phi\, \varepsilon_m\, \varepsilon_f\, \sigma\left[\left(\theta_r + 273\right)^4 - \left(\theta_m + 273\right)^4\right]$$

Where

Φ is the configuration factor

ε_m is the surface emissivity of the member

ε_f is the emissivity of the fire

σ is the Stephan Boltzmann constant (5,67 x 10^{-8} W/m^{2}K^4)

θ_r is the effective radiation temperature of the fire

θ_m is the surface temperature of the member

The emissivity of the fire is taken as $\varepsilon_f = 1.0$ in accordance with the recommended value in EN1994-1-2.

6.2.5.1. Configuration Factors

For steel decking profiles the following configuration factors are used to modify the net heat flux incident on each surface. The locations in which the following factors are applied are shown in Figure 6–26 for trapezoidal deck profiles and in Figure 6–27 for re-entrant deck profiles.

Trapezoidal Profiles

The bottom flange of the trapezoidal profile is assumed to have a configuration factor of 1.0. For the top flange the configuration factor, Φ_{TOP} , is calculated as follows.

$$\Phi_{TOP} = \frac{2\tan^{-1}\left(\dfrac{h}{2\left(p - b_1\right)}\right)}{3.14}$$

Similarily for the sloping web of the trapezoidal profile, the configuration factor, Φ_{SIDE} , is calculated as follows,

$$\Phi_{SIDE} = 0.5\frac{L}{x + y}$$

Re-entrant Deck

The bottom flange of re-entrant steel profiles is assumed to have a configuration factor of 1.0. The configuration factor for the surfaces of the re-entrant dovetail is calculated as follows,

$$\Phi_{INT} = 0.3\frac{L}{x+y}$$

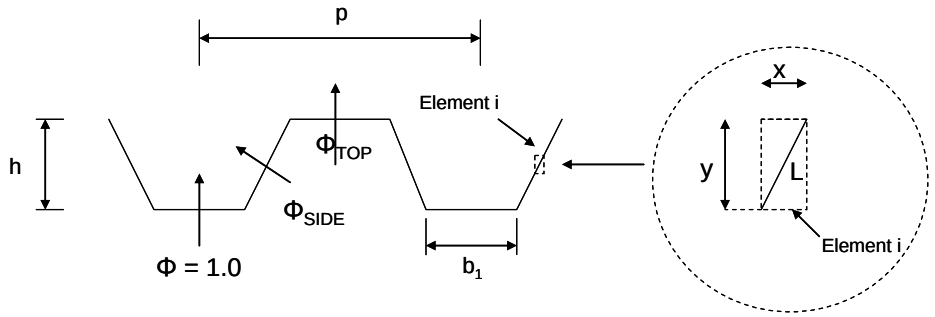

Figure 6–26 : Configuration Factors for trapezoidal decks

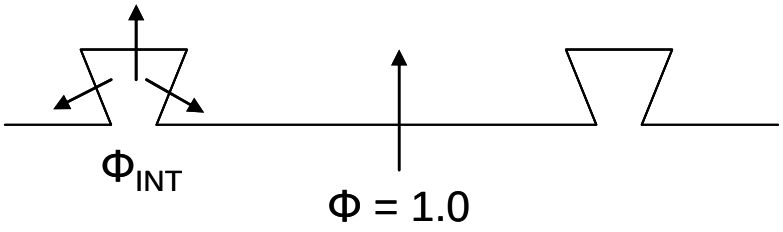

Figure 6–27 : Configuration Factors for re-entrant decks

6.2.5.2. Material Properties

The following material properties are used for steel and concrete. These values are based on the recommendations of EN1994-1-2. Table 6-4 shows the values of surface emissivity, density and moisture content used for steel, normal weight concrete and light weight concrete.

Table 6-4 : Material properties for steel and concrete

	Steel	NWC	LWC
Emissivity, ε_m	0.7	0.7	0.7
Density, ρ	7850	2300	1850
% moisture by mass	0	4	4

The specific heat capacity of steel, C_a, for all structural and reinforcing steel is given by the following temperature dependant formulae:

$$C_a = 425 + 0.773\theta - 0.00169\theta^2 + 0.00000222\theta^3 \quad \text{(J/kg K)} \quad \text{for } 20°C \le \theta \le 600°C$$

$$C_a = 666 - \frac{13002}{(\theta - 738)} \quad \text{(J/kg K)} \quad \text{for } 600°C \le \theta \le 735°C$$

$$C_a = 545 - \frac{17820}{(\theta - 731)} \quad \text{(J/kg K)} \quad \text{for } 735°C \le \theta \le 900°C$$

$$C_a = 650 \quad \text{(J/kg K)} \quad \text{for } 900°C \le \theta \le 1200°C$$

The following temperature dependant values of specific heat capacity, C_c, are used for normal weight dry concrete with siliceous of calcareous aggregates.

$C_c = 900$	(J/kg K)	for $20°C \le \theta \le 100°C$
$C_c = 900 + (\theta - 100)$	(J/kg K)	for $100°C \le \theta \le 200°C$
$C_c = 1000 + (\theta - 200)/2$	(J/kg K)	for $200°C \le \theta \le 400°C$
$C_c = 1100$	(J/kg K)	for $400°C \le \theta \le 1200°C$

As recommended by EN1994-1-2 the following temperature independent value of specific heat capacity is assumed for lightweight concrete.

$C_c = 840$ (J/kg K) for all temperatures

The thermal conductivity of steel is defined using the following temperature dependent relationship.

$$\lambda_a = 54 - 0.033(\theta - 20) \quad \text{but not less than 27.3} \quad \text{(W/mK)}$$

For normal weight concrete the upper limit of thermal conductivity as defined by EN1994-1-2 has been used. The thermal conductivity for normal weight concrete is determined from the following temperature dependent relationship.

$$\lambda_C = 2 - 0.2451(\theta/100) + 0.0107(\theta/100)^2 \quad \text{(W/mK)}$$

The thermal conductivity of lightweight concrete is also temperature dependent and is given by the following formula.

$$\lambda_C = 1 - (\theta/1600) \quad \text{but not less than 0.5} \quad \text{(W/mK)}$$

6.2.5.3. Internal heat transfer by conduction

The thermal analysis computes the conducted heat transfer between a cell and the four cells above, below and to the sides (Figure 6–28). No other cells are involved.

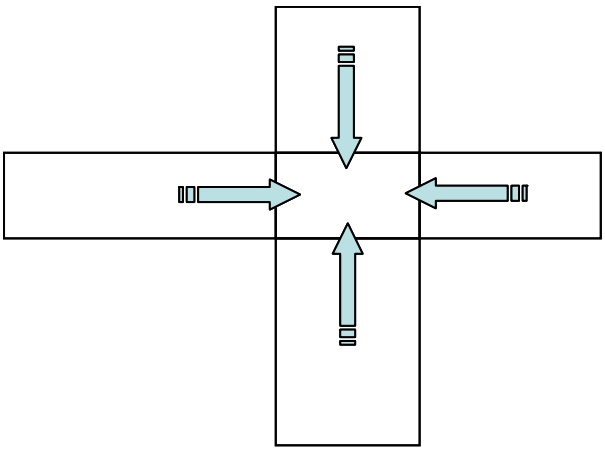

Figure 6–28 : Basis of conductive heat transfer

The heat transferred per unit time depends on the sizes of the cells, the temperature of each cells and the thermal conductivity of each cell. Each pair of cells are considered in turn and the net heat transferred into or out of a cell is computed. The basic conduction model is illustrated in Figure 6–29.

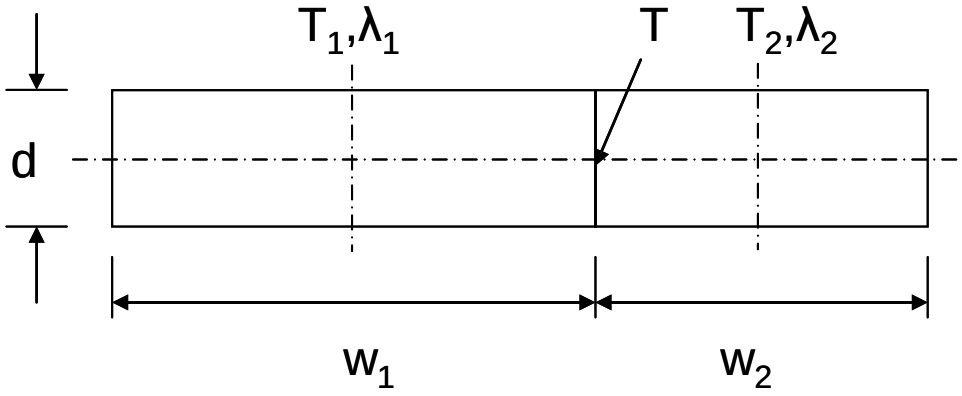

Figure 6–29 : Basic conduction model

The temperature of each cell is defined at its centre (T_1, T_2). The temperature of the interface between the cells is T. The heat transfer from cell 1 to the interface is the same as the heat transfer from the interface to cell 2. The thermal conductivities of each cell are λ_1 and λ_2.

The heat transfer per unit time from the centre of cell 1 to the interface is:

$$h = \frac{2D\lambda_1}{w_1}(T - T_1)$$

This is equal to the heat transfer per unit time from the interface to the centre of cell 2:

$$h = \frac{2D\lambda_2}{w_2}(T_2 - T)$$

Thus, by eliminating the interface temperature, T:

$$h = \frac{(T_2 - T_1)}{\left(\frac{w_1}{2D\lambda_1} + \frac{w_2}{2D\lambda_2}\right)} \text{ per unit time}$$

This equation is used to compute the heat transfer between all cells. For each cell, the value of:

$$\frac{w}{2D}$$

is precalculated. The value of thermal conductivity will often vary with temperature and is calculated at preset intervals (normally 30 seconds) to speed up computation.

6.2.5.4. Design temperatures for unprotected steel beams

The design temperature of the unprotected steel beams are calculated based on the simple method given in EN1994-1-2 Section 4.3.4.2.2. The increase in steel temperature during a small time interval is calculated using the following equation.

$$\Delta\theta_{a,t} = k_{shadow}\left(\frac{1}{c_a \rho_a}\right)\left(\frac{A_i}{V_i}\right)\dot{h}_{net}\,\Delta t$$

Where

k_{shadow} is the correction factor for shadow effect

ρ_a is the density of the steel

Δt is the time interval

A_i / V_i is the section factor for part i of the cross section

The FiCEB spreadsheet calculates the steel temperature for the bottom flange of the section for time increments of 2.5 seconds. The correction factor for the shadow effect is taken as 1.0.

The section factor for the bottom flange is expressed as a function of flange thickness, e_1, as follows

$$A_i / V_i = \frac{2000}{e_1}$$

The material properties are given in Section 6.2.5.2.

The net heat flux is calculated as shown in Equation 12, with the convective and radiative components calculated as shown by Equations 13 and 14 respectively. When calculating the radiative heat flux using Equation 14 the configuration factor should be taken as 1.0.

7. WP6 : ADDITIONAL FIRE RESISTANCE THROUGH 3D MEMBRANE EFFECT - NUMERICAL SIMULATIONS AND DEFINITION OF THE 3D FIRE TEST

7.1. Introduction

The aim of this paragraph is to present the results of the F.E. simulations performed for the Ulster test. All theses simulations were performed before the fire test in order to design the tested structure.

First, the model is described and the data for the reference case are given. Then, a parametric study is performed in order to consider a possible variation of the values of some parameters by comparison to the predicted values. The numerical simulations are performed with the SAFIR 2007a software.

7.2. Data

7.2.1. General data

The internal dimensions of the compartment are 15.0 m length, 9.0 m width and 3.0 m height. There are three openings in the façade, each one of 4.5 m² as described in Figure 7–1.

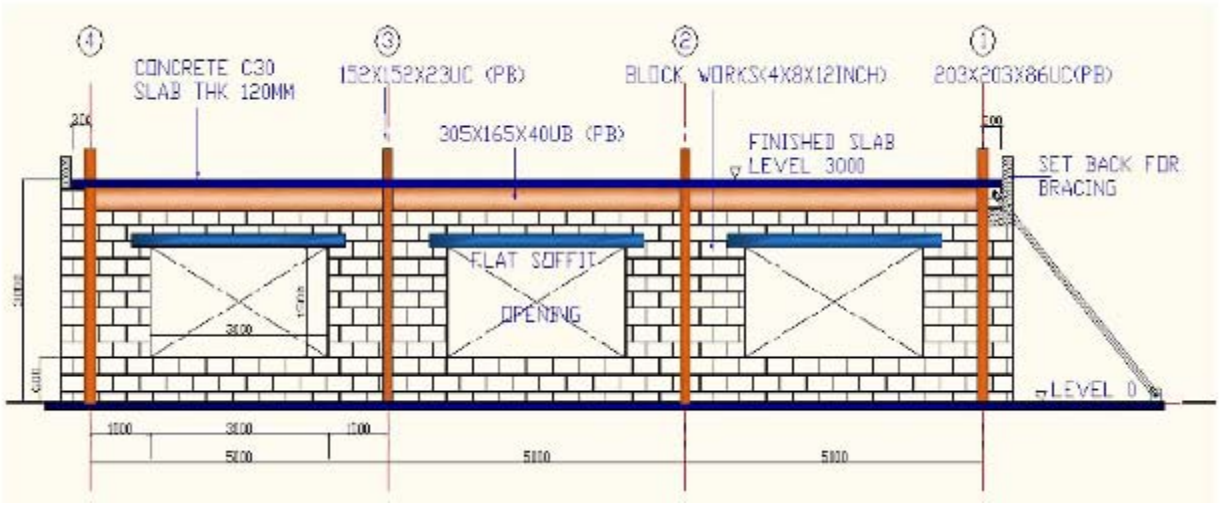

Figure 7–1 : Elevation view of the compartment façade

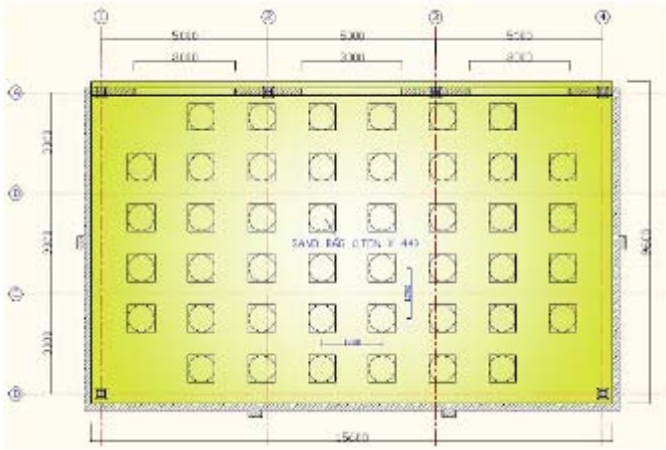

Figure 7–2 : Plan view of the compartment

The applied load is 3.25 kN/m² and the self-weight of the slab is 2.83 kN/m² so that the total load is 6.08 kN/m².

The steel beams are made of S355 steel while the rebars are S500. The concrete strength at 20°C is 30MPa.

7.2.2. Fire

The fire load density is taken equal to 570 MJ/m². The fire considered as reference fire in this report (Figure 7–3) is the fire given by OZone when considering the following parameters:

- Fire growth: medium
- Combustion model: extended fire duration
- Fuel height: 0.5 m
- RHRf: 1250 kW/m²
- Combustion heat of fuel: 17.5 MJ/kg
- Combustion efficiency: 0.8

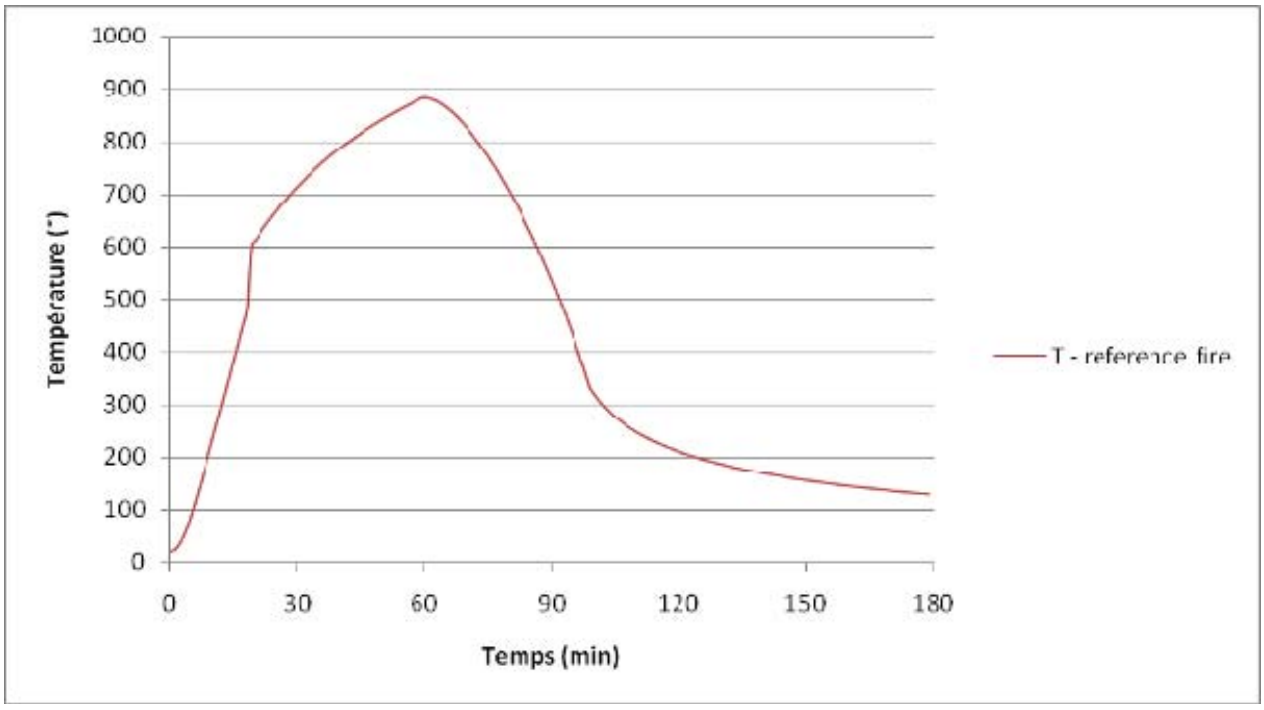

Figure 7–3 : Reference fire (OZone)

The maximum temperature is 884°C after 60 minutes. The flash-over occurs after 18' and the temperature remains higher than 500°C until the 91th minute.

7.2.3. Steel profiles

The sections of the profiles are given in the following pictures (Figure 7–4). The edge beams are protected so the beam profiles (2) and (3) are all protected. The edge beam profile (1) is also protected but the central secondary beams (1) are unprotected (see Figure 7–4).

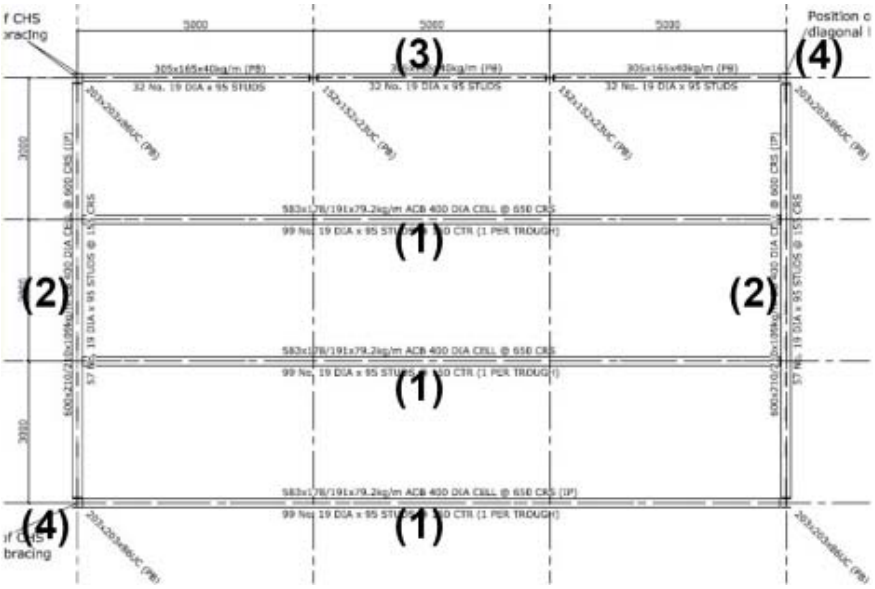

Beam (1) - UB 406x178x60

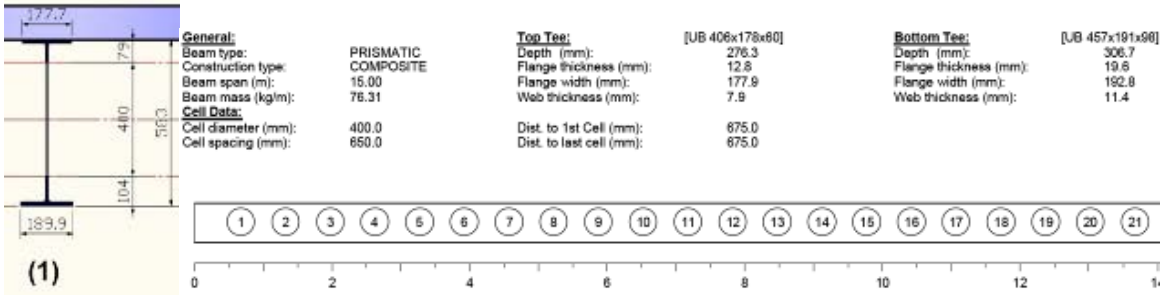

Beam (2) - UB 533x210x109

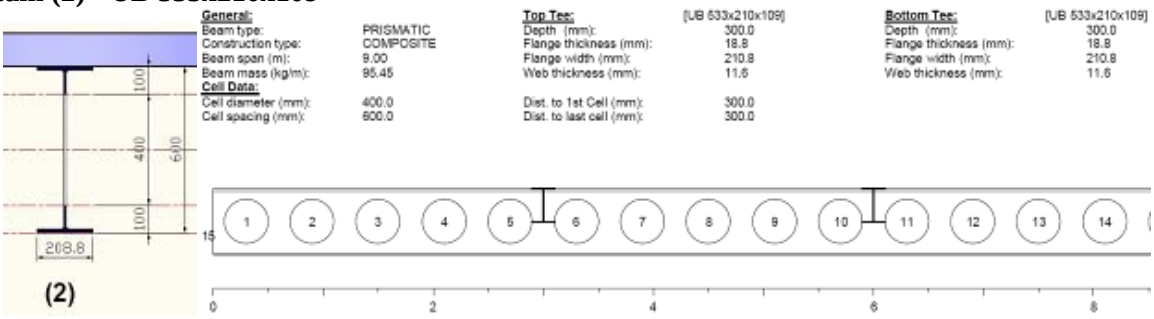

Beam (3) - UB 305x165x40

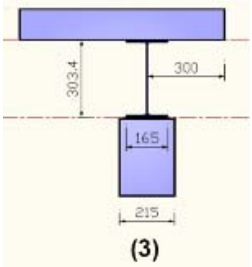

Figure 7–4 : Steel profiles

7.2.4. Slab

The total height of the slab is 120 mm. The steel deck is a COMFLOR 51 which characteristics are as follow (see Figure 7–5):

- Depth h_2 : 51 mm
- Trough width l_2: 136 mm
- Pitch of deck ribs: 150 mm
- Crest width l_3: 38 mm

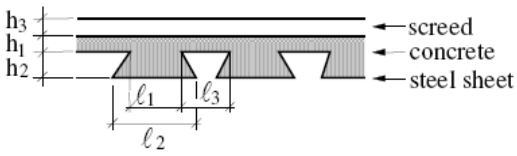

Figure 7–5 : Steel deck

In its central part, the slab has a reinforcement mesh of 393 mm²/m in both directions. On a 2.4m wide section on each side, the slab has a reinforcement mesh of 786 mm²/m in both directions. The T10 additional bars @200 on 2.4m wide section each end of slab (Figure 7–7) are centrally placed in the same layer with the mesh (blue lines in Figure 7–6).

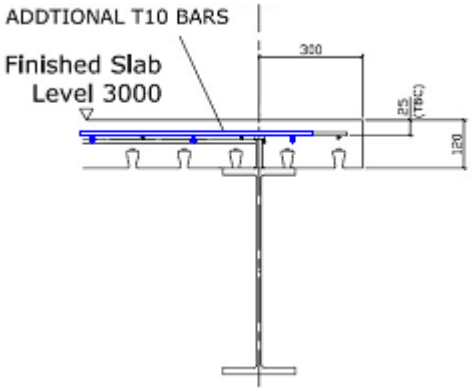

Figure 7–6 : Reinforcement mesh of the slab

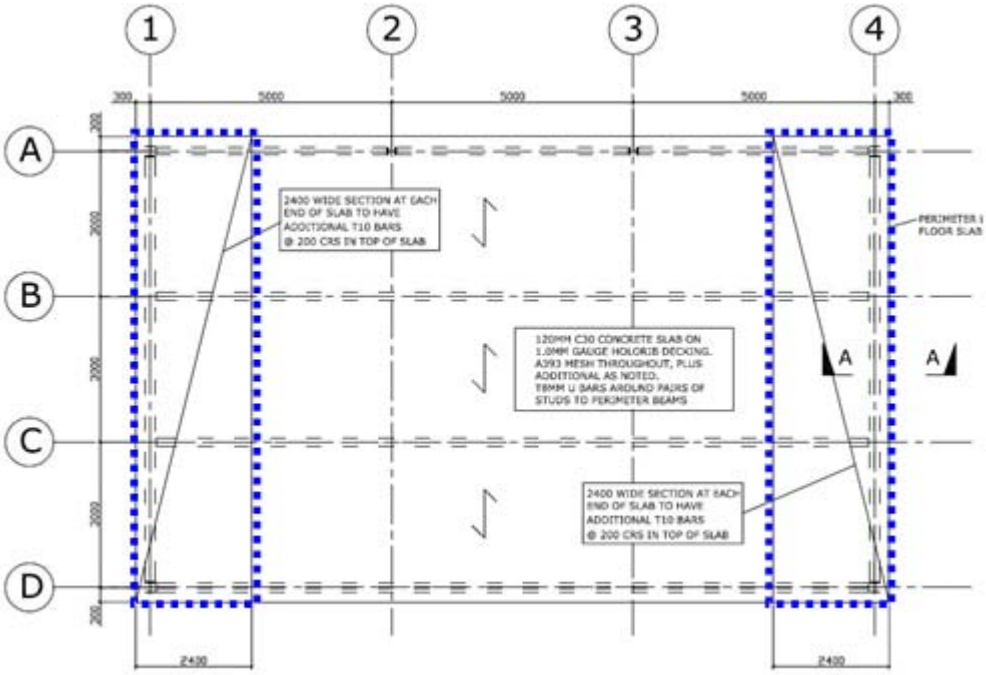

Figure 7–7 : Reinforcement mesh of the slab: view on top of slab

7.3. ULg SAFIR Model

7.3.1. Fire

The fire is given by an OZone analysis as explained before. The maximum temperature is 884°C after 60'.

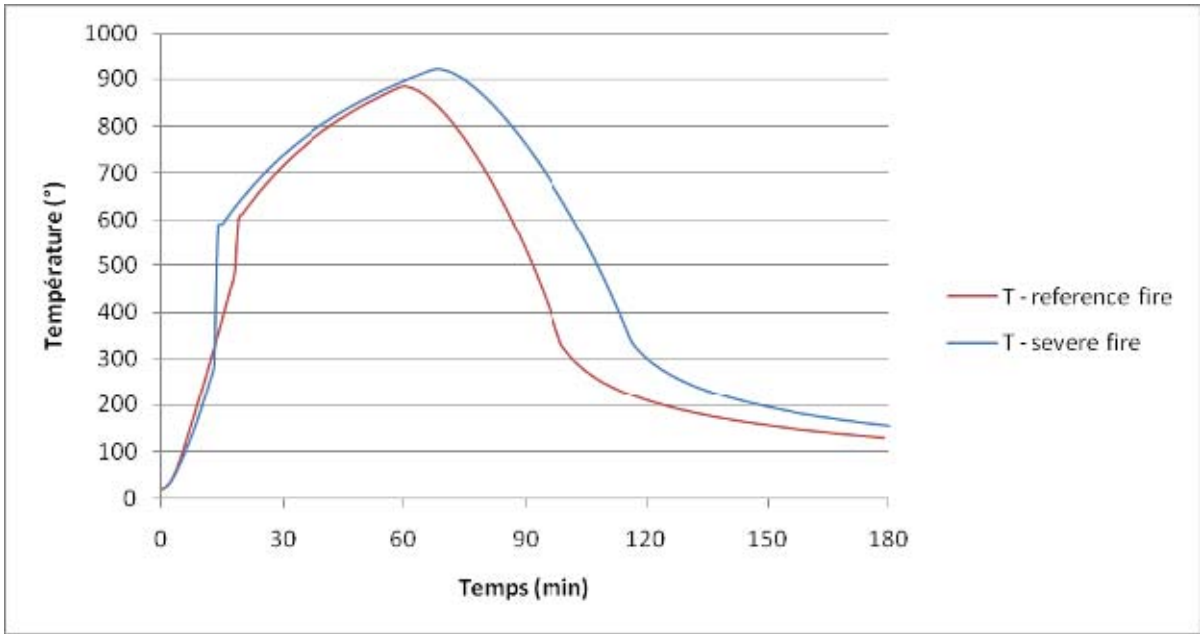

Figure 7–8 : Reference fire and severe fire considered for the numerical analysis of the Ulster test

For the parametric study, a more severe fire is also considered. The aim is to ensure that the test could be successful even if the fire has a longer duration and a higher temperature peak. This critical fire is obtained by an OZone analysis considering that the RHRf is 250 kW/m² and the fire load is 700 MJ/m². In this case, the temperature peak is 921°C after 68' and the flash-over occurs after 14'. The temperature remains higher than 500°C until the 108th minute, so during 94' instead of during 73'.

7.3.2. Thermal analysis of the steel profiles

Reference case

For the thermal model of the steel profile, solid finite elements are used. The material used is steel according to EN1993-1-2 in which :

- convection coefficient on hot surfaces : 35.0 [W/m²K]
- convection coefficient on cold surfaces : 4.0 [W/m²K]
- relative emissivity : 0.7 [-]

For the unprotected section, a k_{shadow} k_{shadow} must be taken into account. Its value is: k_{shadow} = 0,716. As a result, the following values are obtained for the unprotected section:

- convection coefficient on hot surfaces : 25.1 [W/m²K]
- convection coefficient on cold surfaces : 4.0 [W/m²K]
- relative emissivity : 0.5 [-]

The concrete slab is modeled in order to take into account its capacity of absorbing heat. The material used for the concrete slab is siliceous concrete according to EN1992-1-2 in which :

- specific mass : 2400 [kg/m³]
- moisture content : 72 [kg/m³]
- convection coefficient on hot surfaces : 35 [W/m²K]
- convection coefficient on cold surfaces : 4 [W/m²K]
- relative emissivity : 0.8 [-]
- parameter for thermal conductivity : 0.5

The concrete above the upper flange of the steel profile is only considered for thermal analysis. The thermal concrete has no mechanical resistance.

Figure 7–9 gives the temperature in the unprotected section (central beam profiles (1)) after 60 minutes, considering the reference fire.

As the section that is here analyzed thermally will be used as the section of a beam finite element in the subsequent structural analyses, a section passing through the center of a circular opening is considered. Indeed, the longitudinal stresses of a beam model cannot “enter” in the web posts that separate two openings.

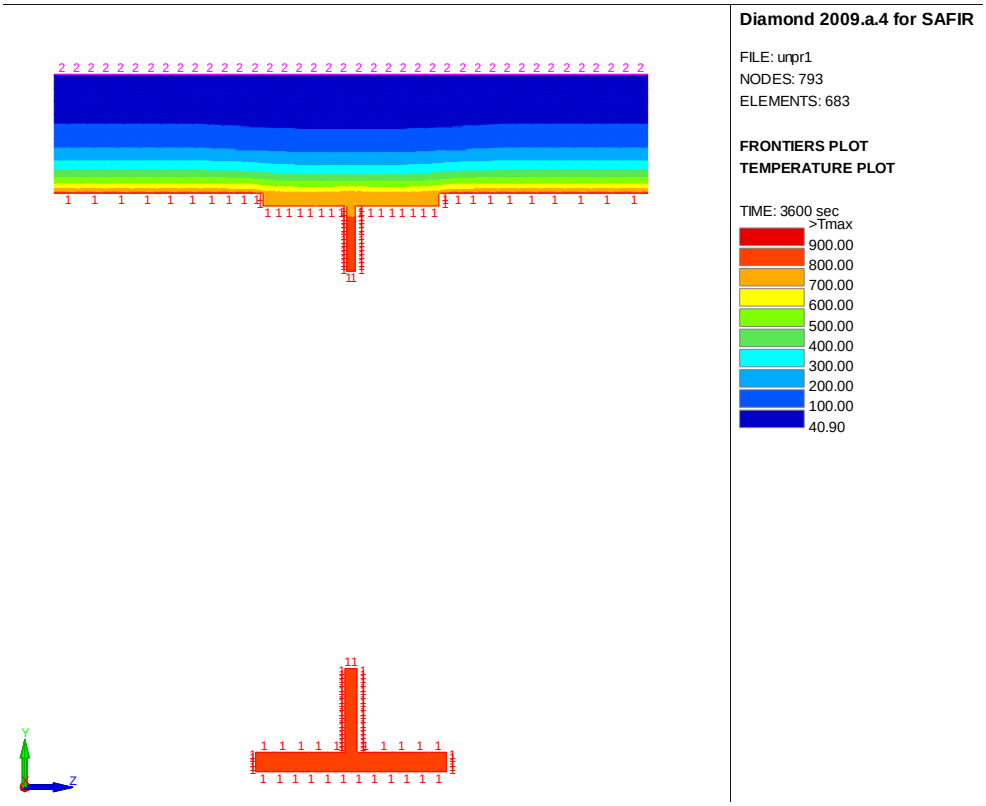

Figure 7–9 : T in the unprotected section after 60 min

The temperatures reached in the unprotected section are much higher than the critical temperature for such cellular beams. Indeed, when performing a structural analysis of such beams using shell elements, web post buckling can be observed for temperatures around 600°C. So, the structural model of the unprotected sections should take into account the fact that their behavior is affected by web post buckling. A simple way to take this phenomenon into account is to model only the upper tee of the section. Obviously, the deflection at room temperature will be much higher than the real one; but at high temperature, the behavior should be more accurate with this model. That’s why the simulations are performed twice for each parametric case: once with the whole section as shown in Figure 7–9 and once with only the upper tee (Figure 7–10), to represent the section after web post buckling.

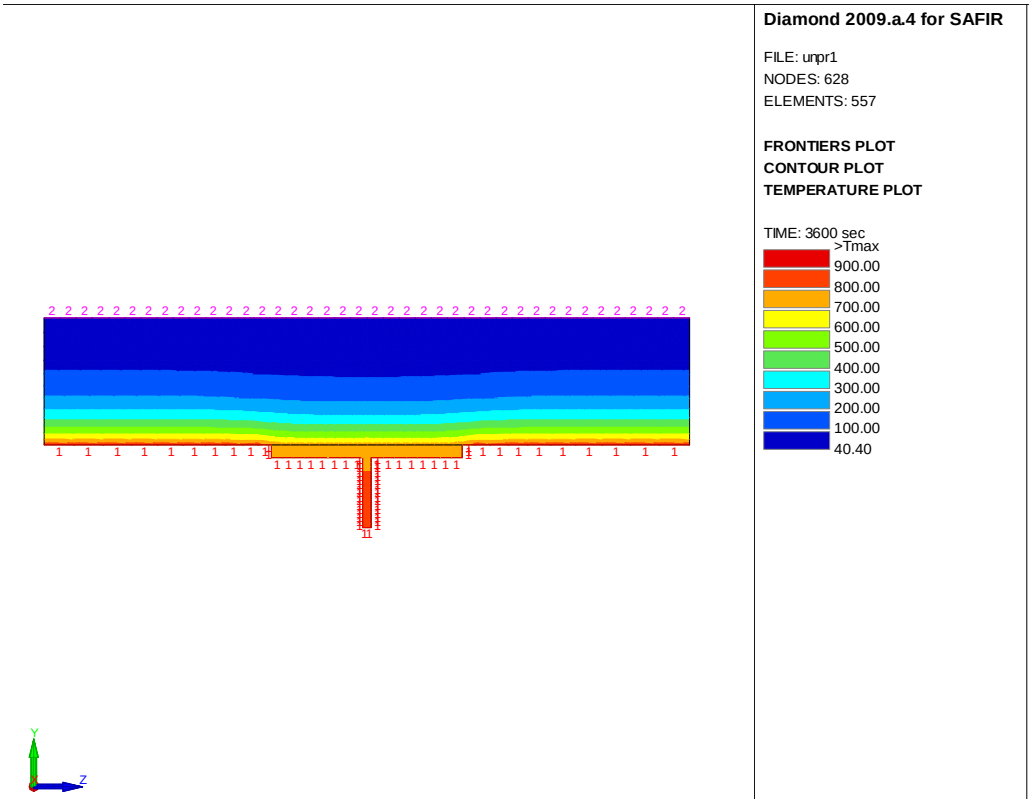

Figure 7–10 : T in the unprotected section after 60 min - model post web post buckling

For the protected sections, the insulation material is modeled. A 20mm spray vermiculit-cement is used for the sections (1) and (2) while a 20mm board siliceous fiber is used for the section (3). The materials have constant thermal properties, which are for the vermiculit:

- thermal conductivity : 0.12 [W/mK]
- specific heat : 1100 [J/kgK]
- specific mass : 550[kg/m³]
- moisture content : 16.5 [kg/m³]
- convection coefficient on hot surfaces : 35 [W/m²K]
- convection coefficient on cold surfaces : 4 [W/m²K]
- relative emissivity : 0.8 [-]

The thermal properties of the board siliceous fiber are:

- thermal conductivity : 0.15 [W/mK]
- specific heat : 1200 [J/kgK]
- specific mass : 600[kg/m³]
- moisture content : 18 [kg/m³]
- convection coefficient on hot surfaces : 35 [W/m²K]
- convection coefficient on cold surfaces : 4 [W/m²K]
- relative emissivity : 0.8 [-]

Solid finite elements are used for the insulation material, which is only considered for thermal analysis. The insulation material has no mechanical resistance. For the board siliceous fiber, the radiation between the board and the steel profile is taken into account. The steel sections are affected by the fire on one side and on the bottom flange, while the other side is supposed to be an adiabatic boundary. Figure 7–11 and Figure 7–12 give the temperature in the steel profiles after 60 minutes, considering the reference fire.

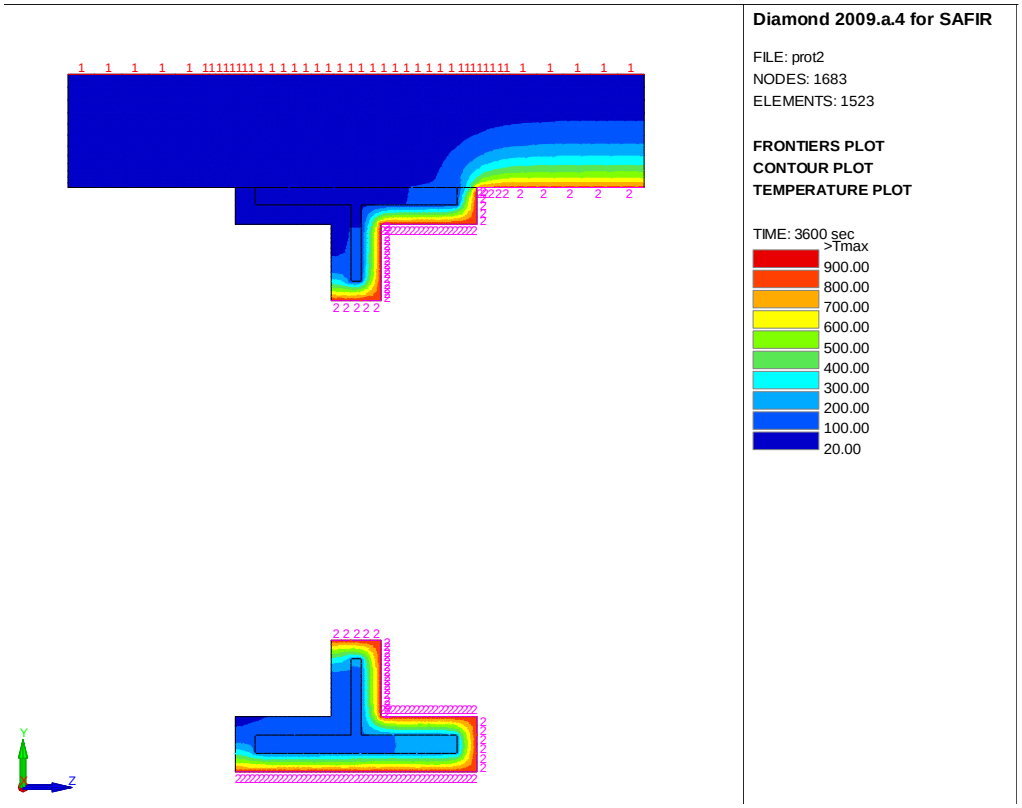

Figure 7–11 : T in the protected section 2 after 60 min

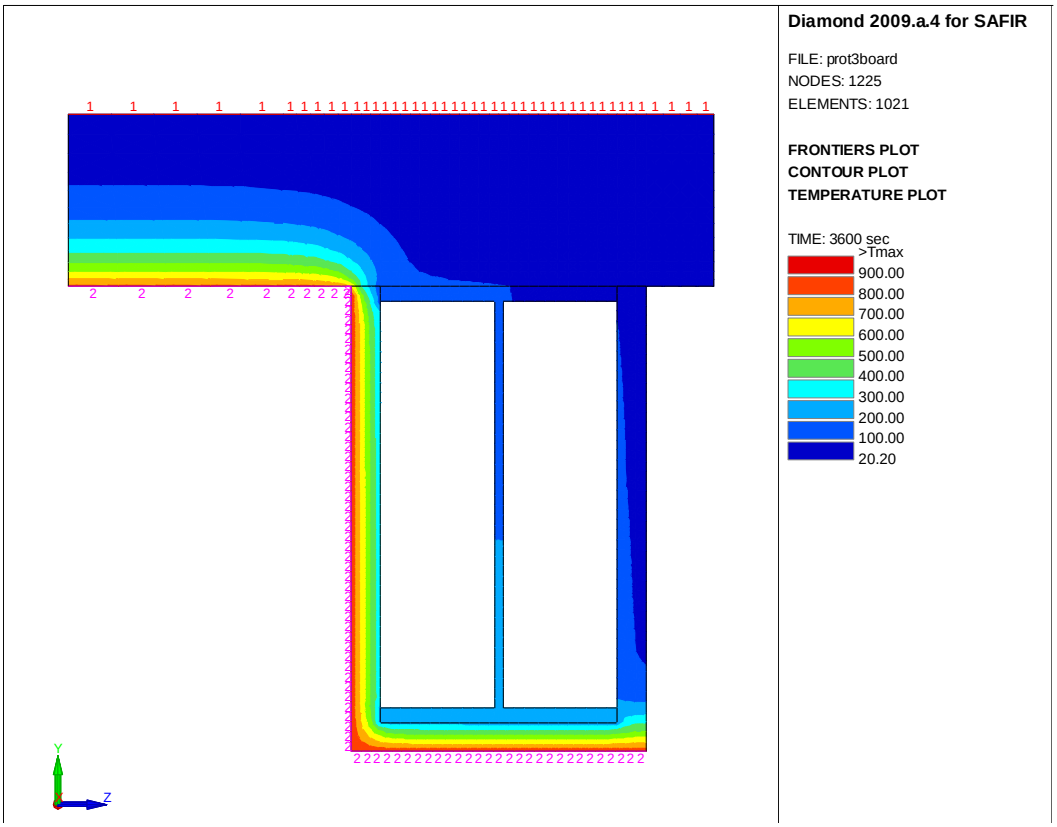

Figure 7–12 : T in the protected section 3 after 60 min

The temperatures in the protected sections are below the critical temperature for these cellular beams so that the model with only the upper tee must not be considered for the protected sections.

7.3.3. Parametric study

For the parametric study, the following cases are considered:

- Temperature in the protected steel profiles if the conductivity of the insulation materials is multiplied by 3 (0.36 W/mK and 0.45 W/mK instead of 0.12 W/mK and 0.15 W/mK)
- Temperature in the steel profiles with the severe fire (fire with higher fire load)

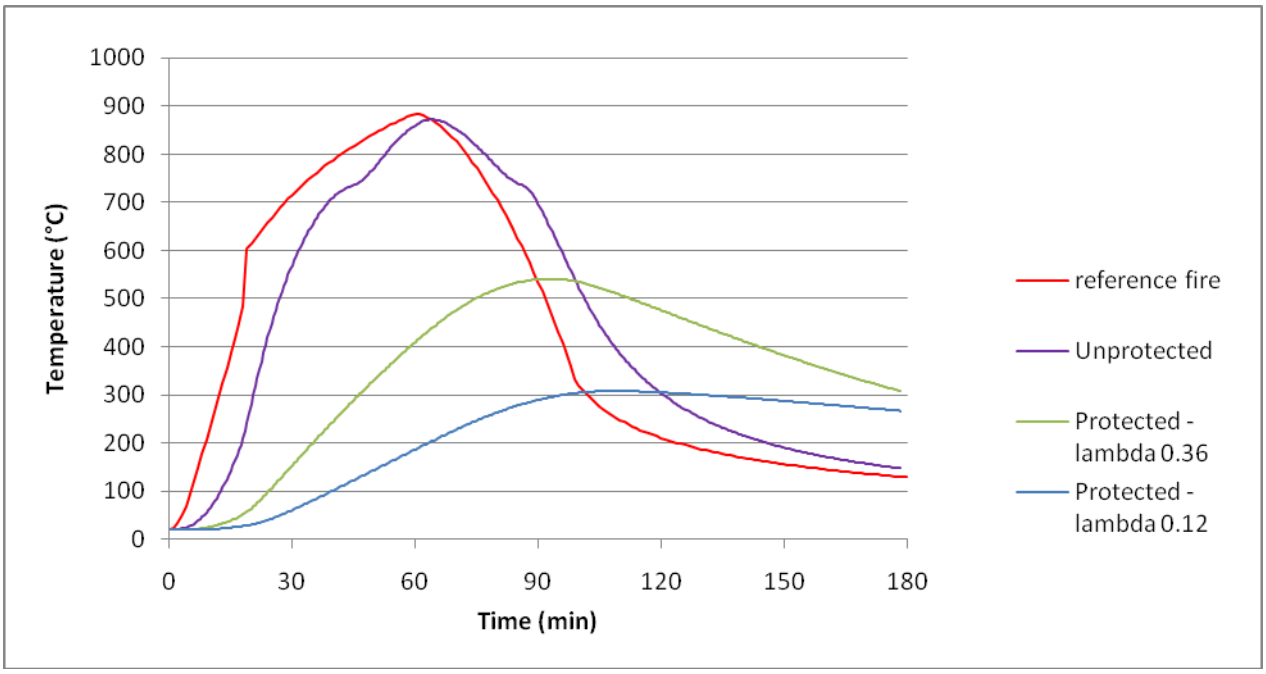

Figure 7–13 : T in the bottom tee of the beam profile 1, with the reference fire

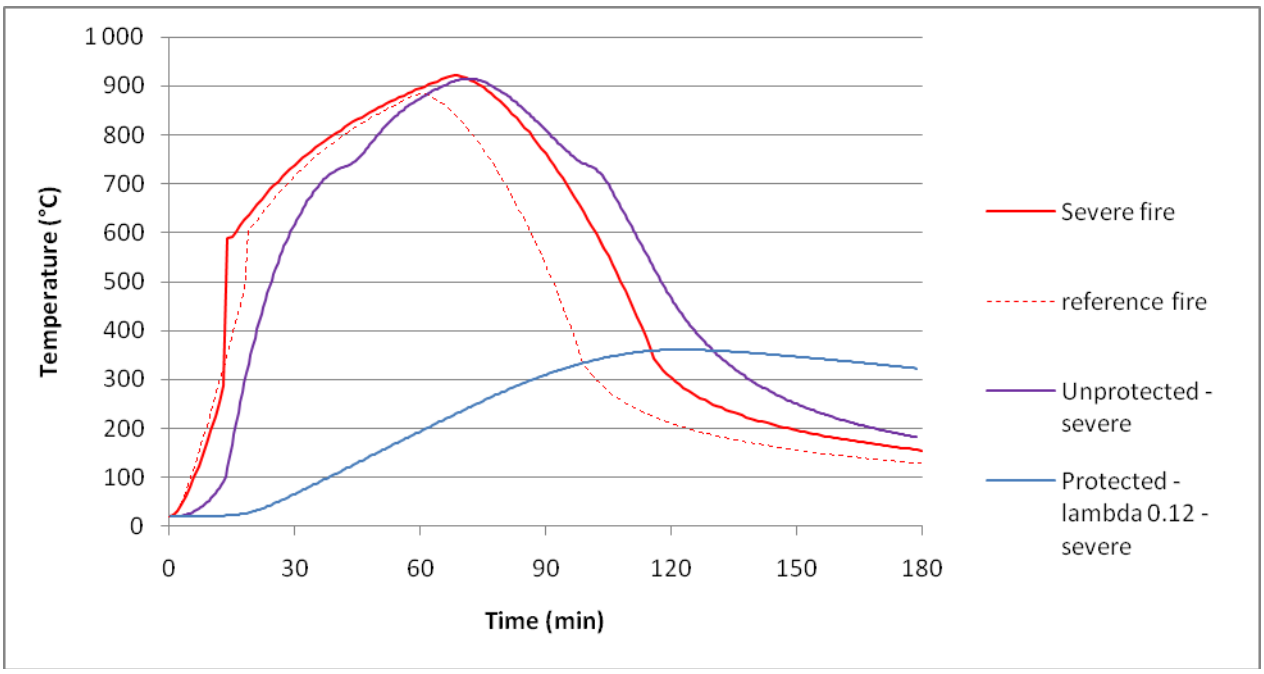

Figure 7–14 : T in the bottom tee of the beam profile 1, with the severe fire

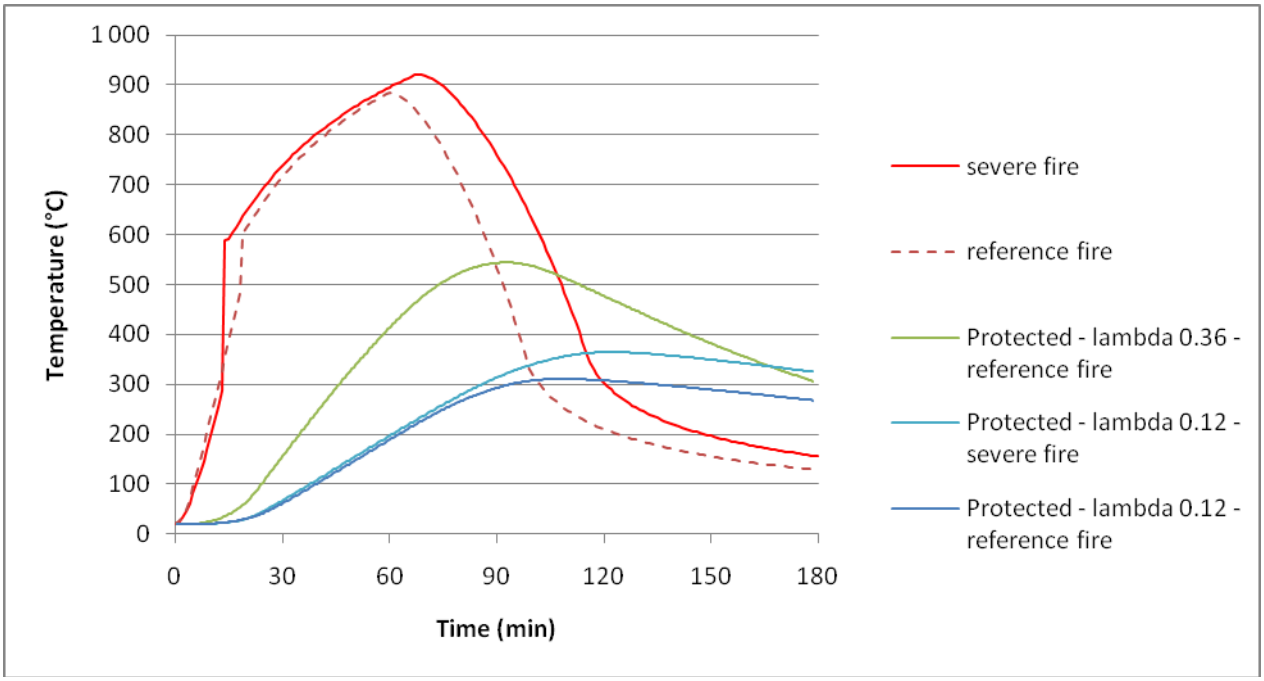

Figure 7–15 : T in the bottom tee of the beam profile 2

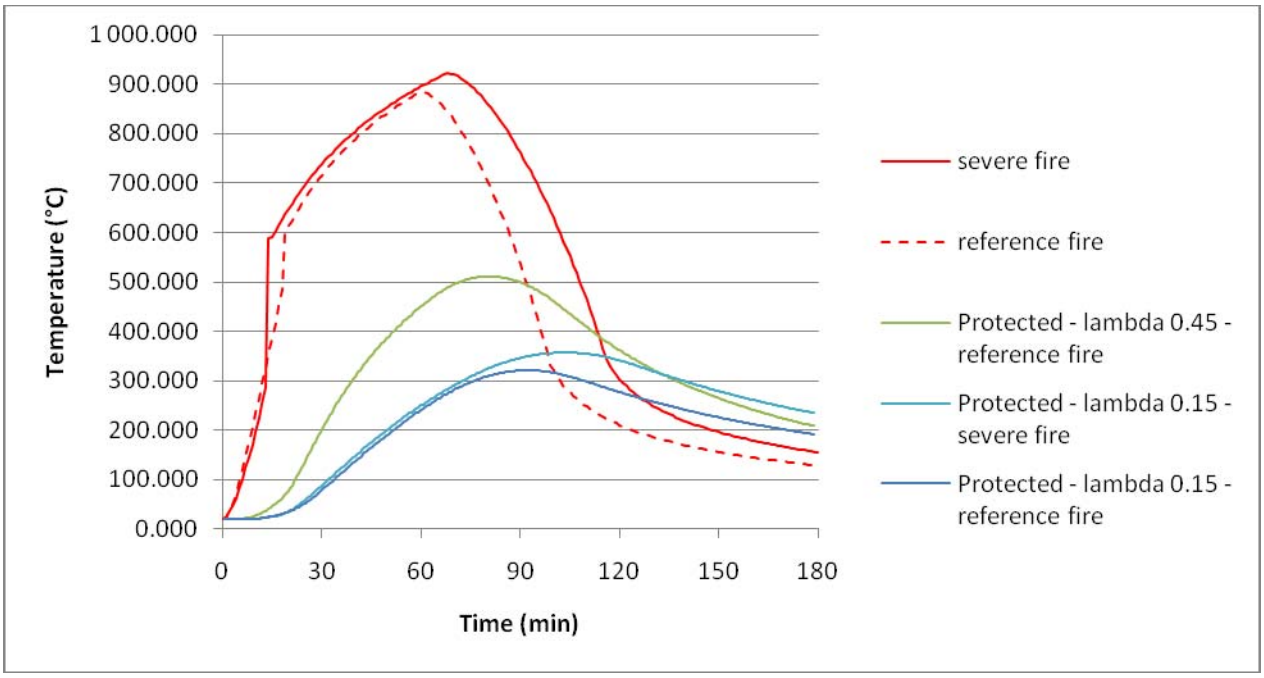

Figure 7–16: T in the bottom tee of the beam profile 3

As a conclusion, it can be observed that a multiplication of the thermal conductivity by a factor of 3 has much higher consequences than an increase of the fire load from 570 to 700 MJ/m².

7.3.3.1. Thermal analysis of the concrete slab

The overall height of the slab is 120 mm. In this case, the Eurocode EN1994-1-2 defines an effective thickness for the slab. This effective thickness represents the height of the slab to consider for the thermal response. The height to consider for mechanical calculation is the concrete height above the steel deck (=h_1+h_3). So the height (h_{eff}-(h_1+h_3)) is made in thermal concrete which is a material without mechanical resistance.

Here, the height of the structural concrete is 69.0 mm and the height of the thermal concrete (see EN 4.2) is 39.8 mm. So the effective height of the slab is 108.8 mm. In conclusion, the model for the thermal analysis is a 108.8 mm depth flat slab. Then for the structural analysis, only a thickness of 69.0 mm is considered.

For the structural analysis, there are two different slabs because the mesh is different in the central zone and in the extremities. But for the thermal analysis, the section is the same.

For the structural analysis, there is a gap of 120-108,8=11,2mm between the upper flange of the steel sections and the bottom surface of the slab.

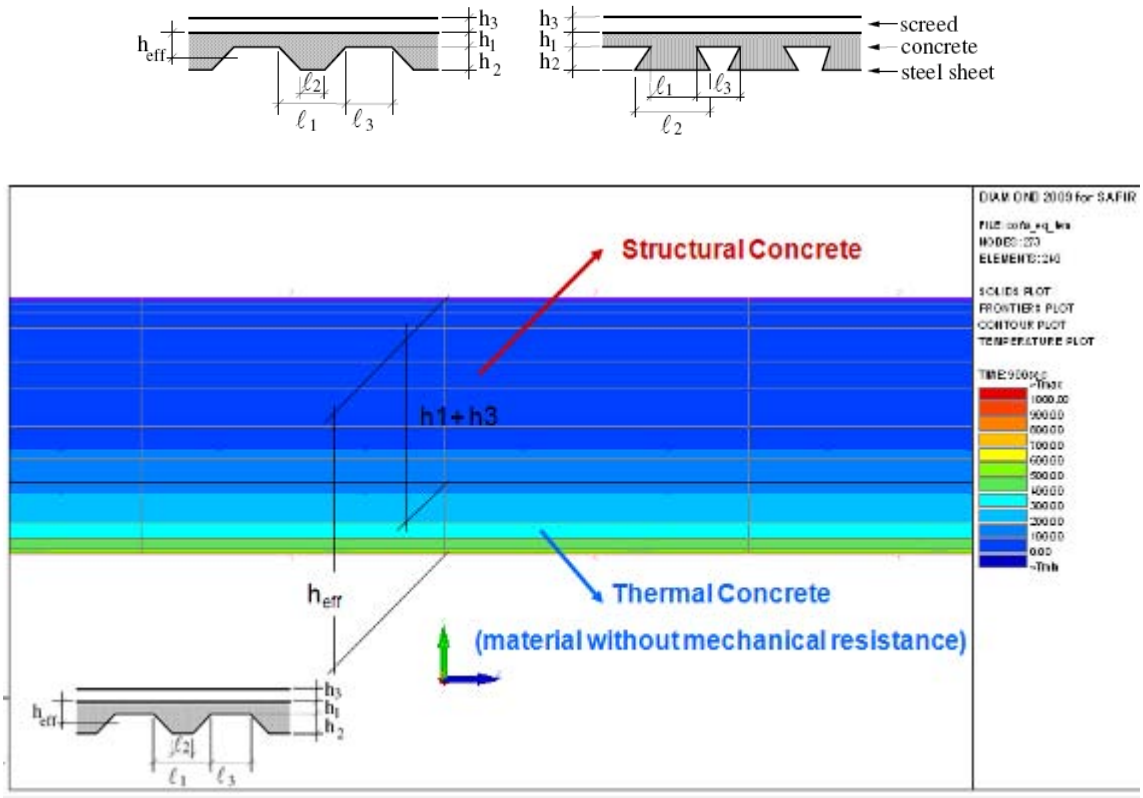

Figure 7–17 : Thermal model of the slab

Figure 7–17 gives the evolution of the temperature in the rebars.

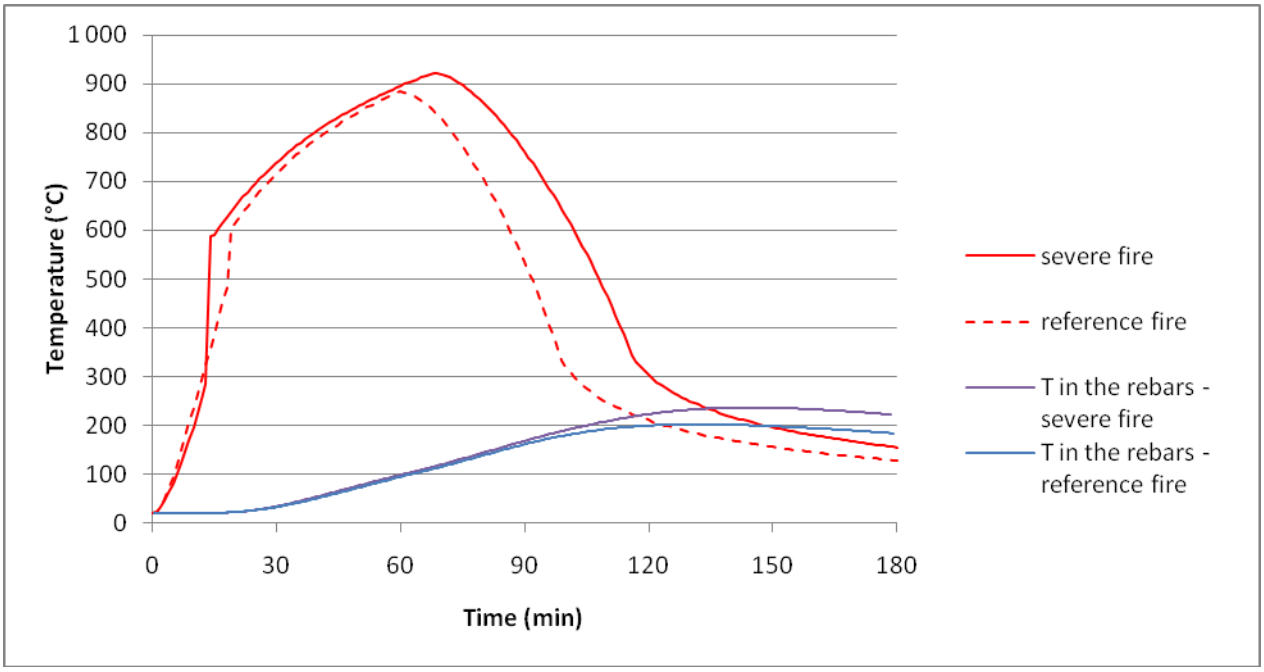

Figure 7–18 : T in the rebars

7.3.3.2. Torsional analysis of the steel profiles

At cold temperature, a torsional analysis of the steel profiles is performed which gives the following values of GJ:

- 0.526615e+5 for the secondary beams (1)
- 0.828150e+5 for the primary beams (2)
- 0.130206e+5 for the primary beams (3)

When performing an analysis in fire situation, the torsional stiffness of the beams must be reduced according to the reduction of the steel modulus with the temperature. Accordingly, the GJ must be reduced. Here, it was decided to multiply the values of GJ by the k_θ (reduction factor of E with the temperature) at 2 hours in a node in the bottom tee. Indeed, the temperatures in the steel vary both spatially and temporally so it is not easy to know by which factor the GJ should be reduced, but after 2 hours the temperature of the protected profiles is close to its maximum. For example for the reference case, the temperatures after 2 hours are 330°C for the unprotected profiles (central beam profiles (1)), 305°C for the protected profiles (1), 307°C for the protected profiles (2) and 280°C for the protected profiles (3). Consequently the k_θ is equal to 0.77 for the unprotected profiles, 0.79 for the protected profiles (1) and (2), and 0.82 for the protected profiles (3).

7.3.3.3. Structural analysis: the slab

For the structural analysis, the center-slab has a reinforcement mesh of 393mm²/m in both directions, at 5.5 mm below the central plane of the structural concrete. The side-slab has a reinforcement mesh of 786 mm²/m in both directions, at the same position. The node line of the beams is positioned 364.5 mm above mid-level of the profile for the beam profile (1), 385.5 mm for the beam profile (2) and 237.2 mm for the beam profile (3).

The node 766 is represented on Figure 7–19; it is the central node for which the deflections are given in the following part of the report.

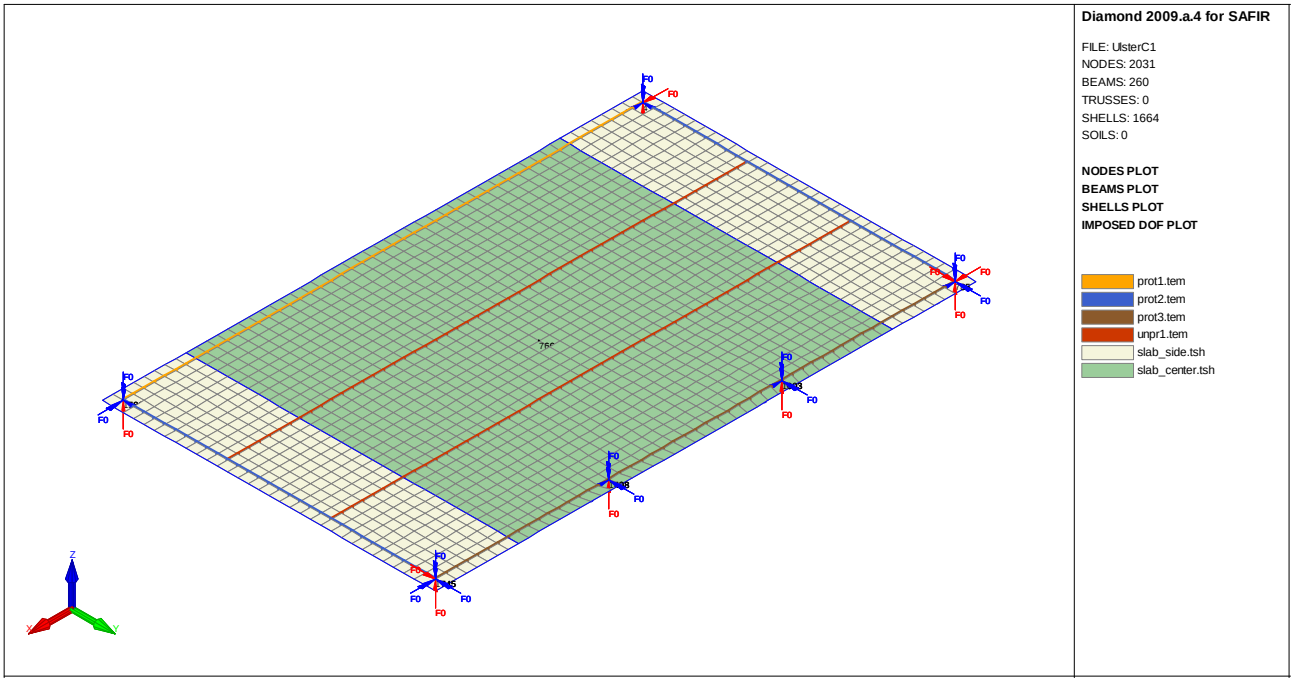

Figure 7–19 : Structural analysis model

The supports are as indicated on Figure 7–19. The steel profiles are all simply supported. To represent the connexion between the protected beam (1) and the protected beam (2) for example, three nodes are created with the same coordinates: one node belongs to the protected beam (1), one to the protected beam (2) and one to the slab. The following displacements of the node of the slab are restrained: vertical displacement, one displacement in the plan of the slab and the three rotations. Then, the two other nodes with the same coordinates (belonging to the beams) must have the same displacements (x,y,z) as the node of the slab and the same torsional rotation, but the other rotations are free.

The slab and the beams are axially unrestrained.

7.3.4. Results

7.3.4.1. Studied cases

The parametric study considers the following parameters as major parameters for the fire resistance of the structure:

- Conductivity of the protective material on the edge beams
- Strength of the steel rebars
- Severity of the fire

Moreover, another parameter is studied which is:

- Model of the cellular section of the secondary unprotected beams

The reference case is the one considering the values given as data.

7.3.4.2. Results

Preliminary study – loading at room temperature

The following graph gives the central deflection as a function of the uniformly distributed load, at room temperature. It can be observed that the structure is able to support a load about three times higher that the load of 6.08 kN/m² applied for the test. The deflection when a 6.08 kN/m² load is applied is about 66 mm that is 1/230 of the span. It is important to notice that the corrugated steel profiles are not considered in the model.

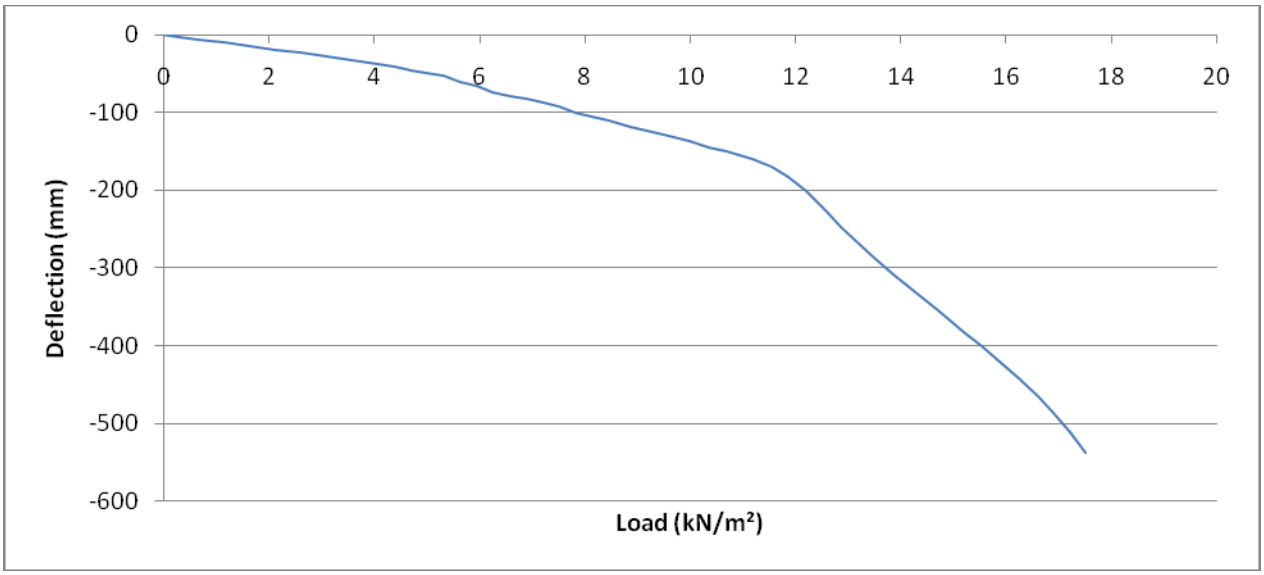

Figure 7–20 : Cold loading - mid-span deflection

The collapse mode at room temperature is shown on Figure 7–21. The structural behavior at room temperature is a flexional mode: the bending of the slab between the steel profiles (span of 3 m) can be observed on Figure 7–21. The collapse occurs when the bending moment acting on the slab exceeds the slab resistance for bending.

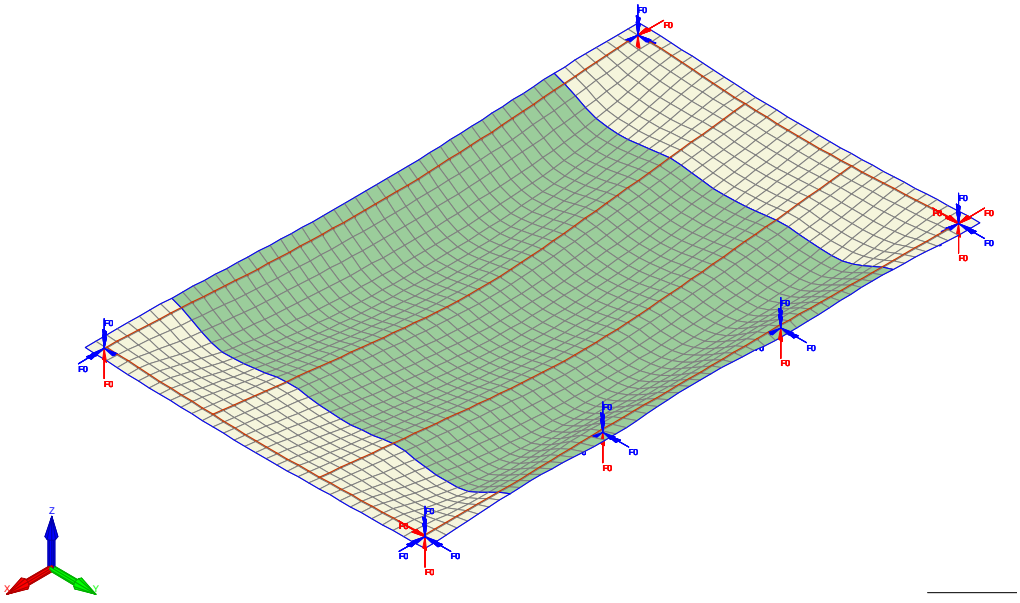

Figure 7–21 : Collapse mode at room temperature (displaced x2)

Reference case – influence of the model of the unprotected beams

The reference case gives the following results for the evolution of the mid-span deflection as a function of time (blue curve). The maximum deflection is reached after 75' and its value is 659 mm.

The red curve is obtained by modeling only the upper tee of the unprotected beams, what is explained by the fact that web post buckling will appear in these sections and will prevent the bottom tee from playing any structural function. In this case the deflection at room temperature has no physical signification since the real contribution of the secondary beam is largely underestimated. But in fire situation, the results are interesting. For example, it can be observed that the deflection does not decrease when the temperature decreases, because the steel profiles do not recover their stiffness. This model can be considered as a good assumption since the cellular beams, after the web post buckling, will probably not be able to recover their initial stiffness when the temperature decreases.

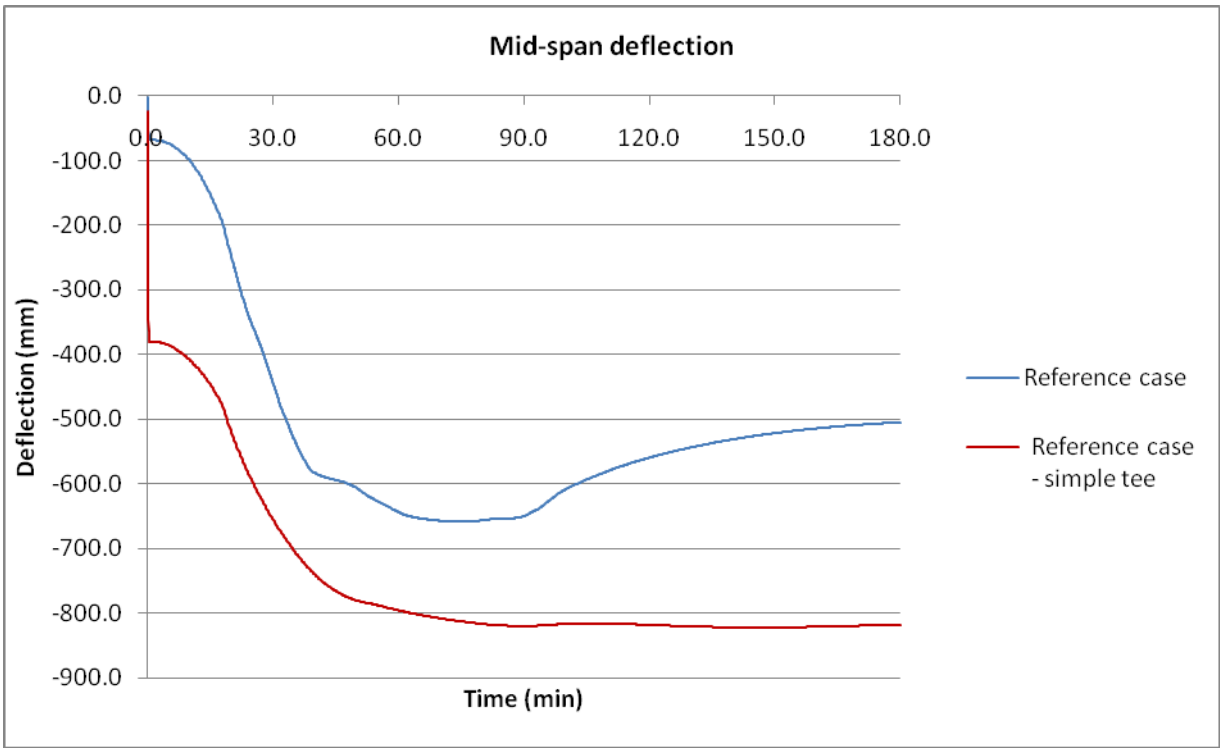

Figure 7–22 : Influence of the model of the unprotected beams

The analysis of the membrane forces in the slab for the reference case allows a better understanding of the behavior of the structure. First, during the loading at room temperature, the slab is in compression. It resists by bending between the secondary unprotected beams (Figure 7–23). Then, after approximately 20-25 minutes, the structural behavior changes and the structure begins to resist thanks to a membrane mode, because the secondary unprotected beams have lost their stiffness. The tension in the rebars equilibrates the external forces. When the temperature increases and the steel strength decreases, the deflection increases so that the tension in the rebars continues to equilibrate the external forces. The slab develops a compressive ring to equilibrate the tension in the central zone (Figure 7–24).

After approximately 90 minutes, the gas temperature has decreased so that the stiffness of the unprotected secondary beams stops to decrease and begins to increase. The structural response of the structure begins to return from membrane mode to flexional mode. After 2 hours, the analysis of the membrane forces in the slab shows that the slab is mostly in compression again (Figure 7–24 and Figure 7–25).

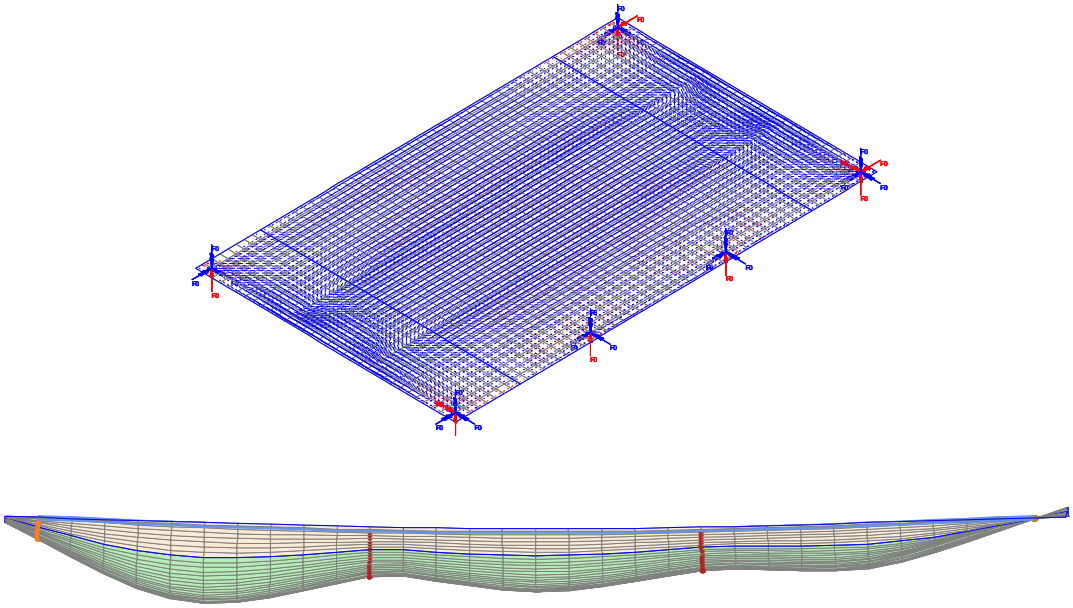

Figure 7–23 : Loading at room temperature: membrane forces and front view of the displacements (x10)

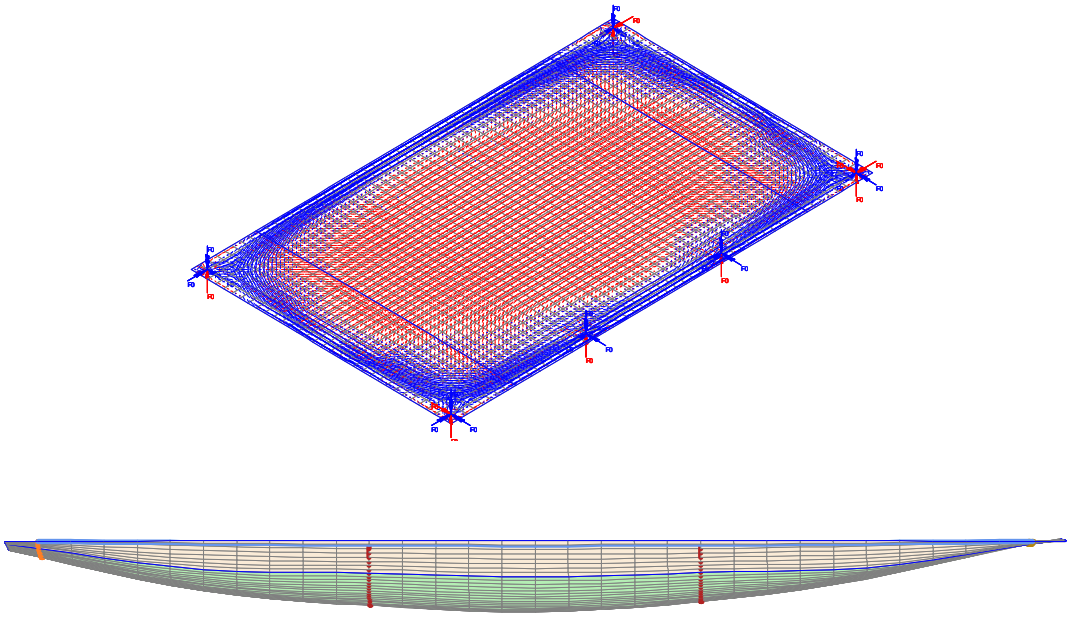

Figure 7–24 : After 1 hour for the reference case: membrane forces in the slab and front view of the displacements (x1)

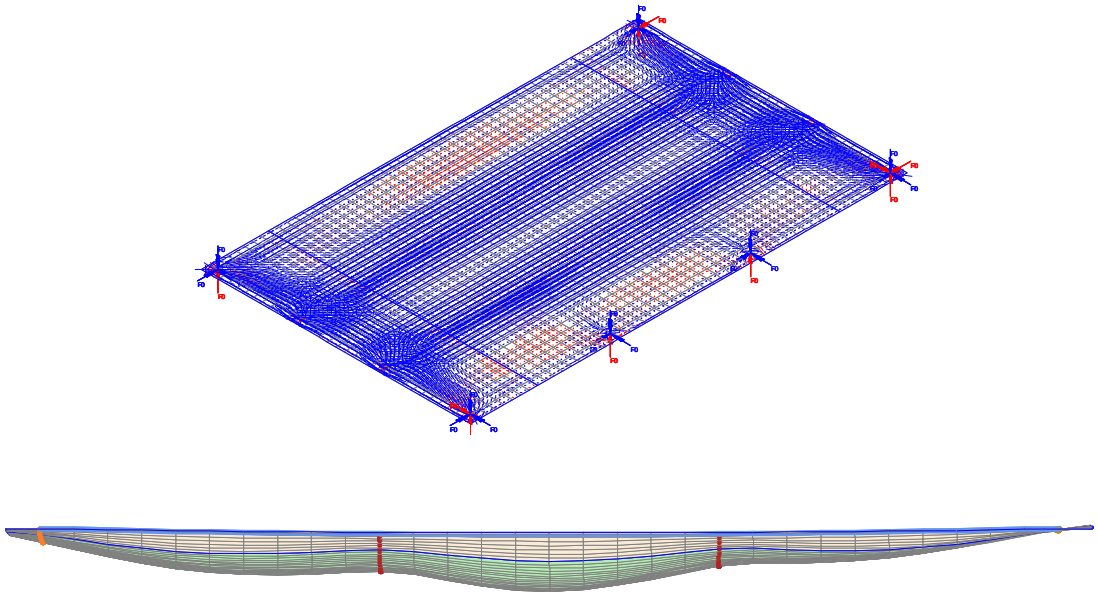

Figure 7–25 : After 2 hours for the reference case: membrane forces in the slab and front view of the displacements (x1)

If only the upper tee of the secondary unprotected profiles is modeled, the structural behavior under the loading at room temperature is a membrane behavior. Indeed, the secondary unprotected beams are not able to act as supports for the slab. Consequently, the span is too important for the slab to resist by bending. This explains why the deflection at room temperature is so important in the case of the analysis with only the upper tee of the unprotected profiles.

Influence of the conductivity of the protective material

This parameter has a big influence on the temperature of the protected beams. Moreover, the uncertainty on this kind of parameter is usually important. For these reason, it is essential to analyze the response of the structure when considering a very conservative value of the conductivity of the protective material. Here, a three times higher value has been considered, which leads to temperature around 540°C in the protected beams 1 and 2 and 650°C in the protected beam 3 (see Figure 7–13, Figure 7–15 and Figure 7–16).

The following relationship between the time and the deflection has been obtained (green curve). The maximum deflection is 72.8 cm after 77'. The red curve is the curve obtained with a simple tee model of the unprotected beams and the high values of conductivity.

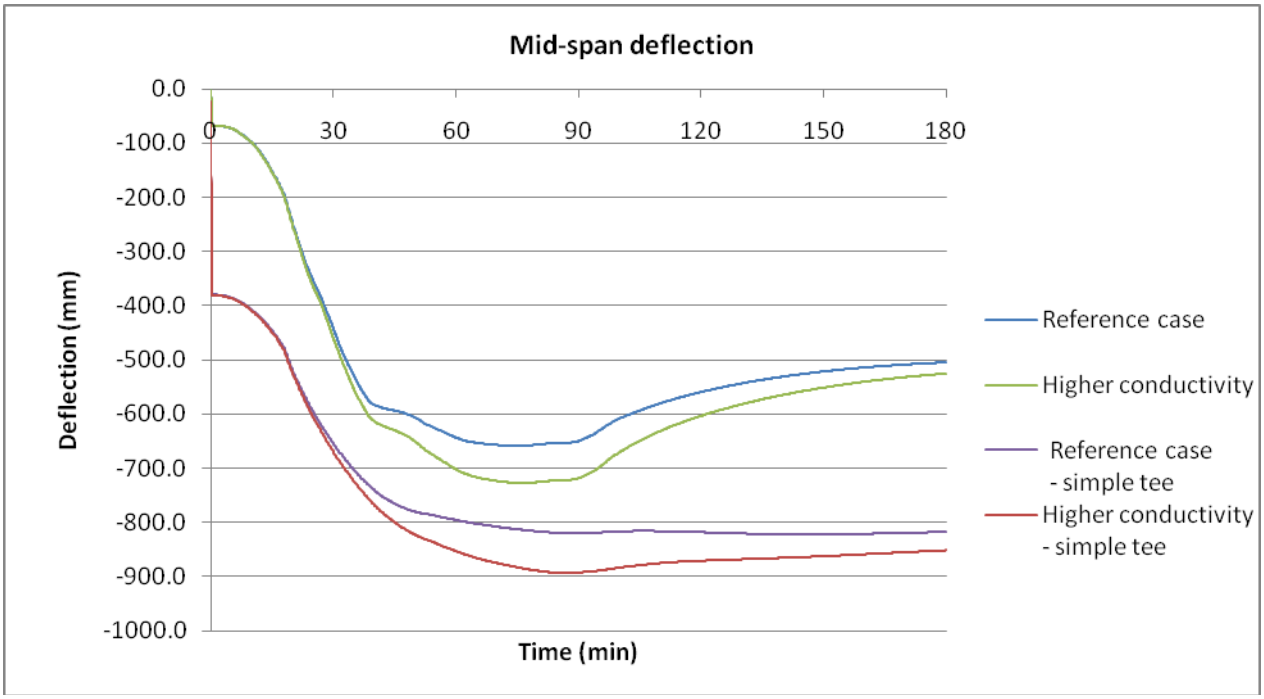

Figure 7–26 : Influence of the conductivity of the protective material

Influence of the rebars strength

Here, it is considered that the strength of the steel rebars is lower than expected: its value is reduced from 500 MPa to 350 MPa. This can represent the accidental situation where some rebars are missing or where the steel strength is lower than expected.

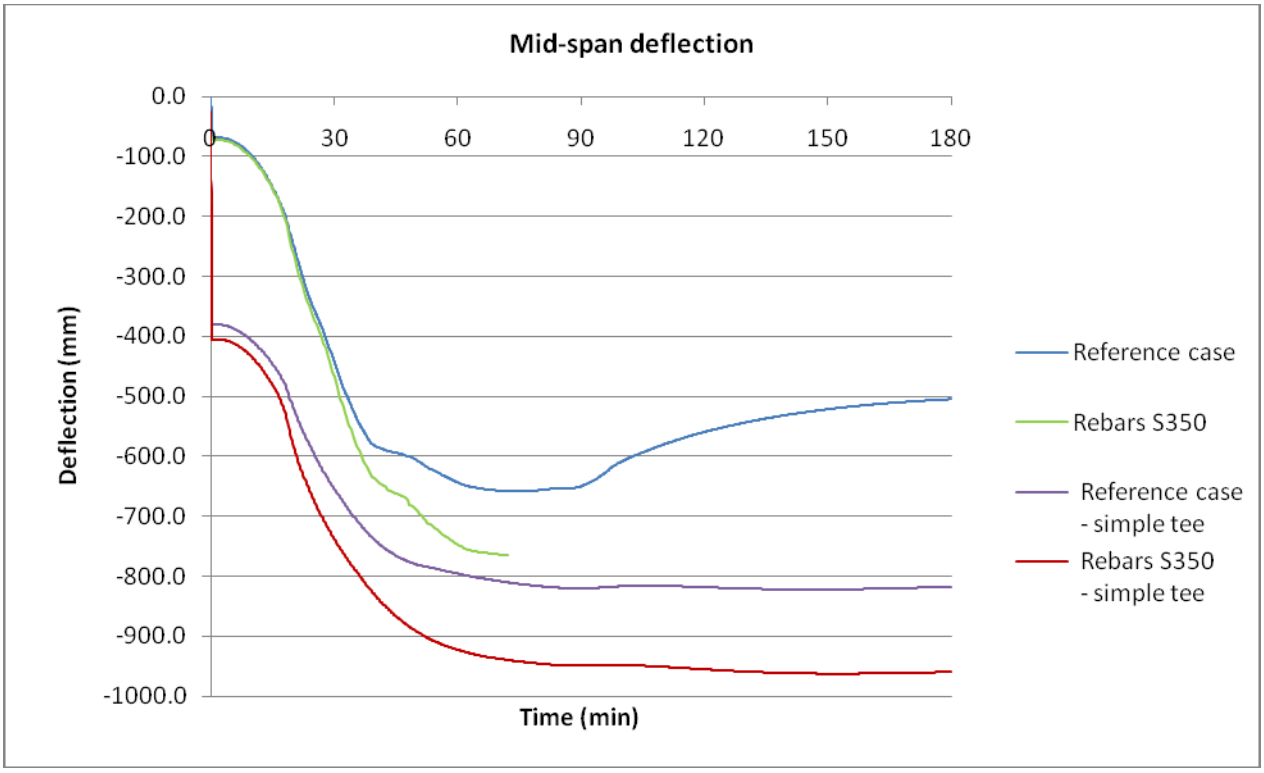

Figure 7–27 : Influence of the rebars strength

In this case, the numerical simulation considering simple tee profiles for the secondary beams shows that the mid-span deflection almost reaches 1 m. When considering double tee profiles, the numerical analysis cannot go beyond 70 minutes but the failure seems to be due to a numerical problem rather than a physical collapse. Because of the lower strength of steel rebars in the concrete slab, there might be some numerical problems in the concrete slab – steel beams interface, because of the difference in the thermal expansion. These problems probably do not appear when considering only simple tees for the secondary beams because the stiffness of the beams is then much lower.

Influence of the fire

Here, the analysis is performed with a more severe model of fire. The aim is to take into account a situation where the peak temperature would be higher and high temperatures would be maintained during a longer period (see Figure 7–14, Figure 7–15 and Figure 7–16).

The maximum deflection is reached after 155' and its value is 84.9 cm.

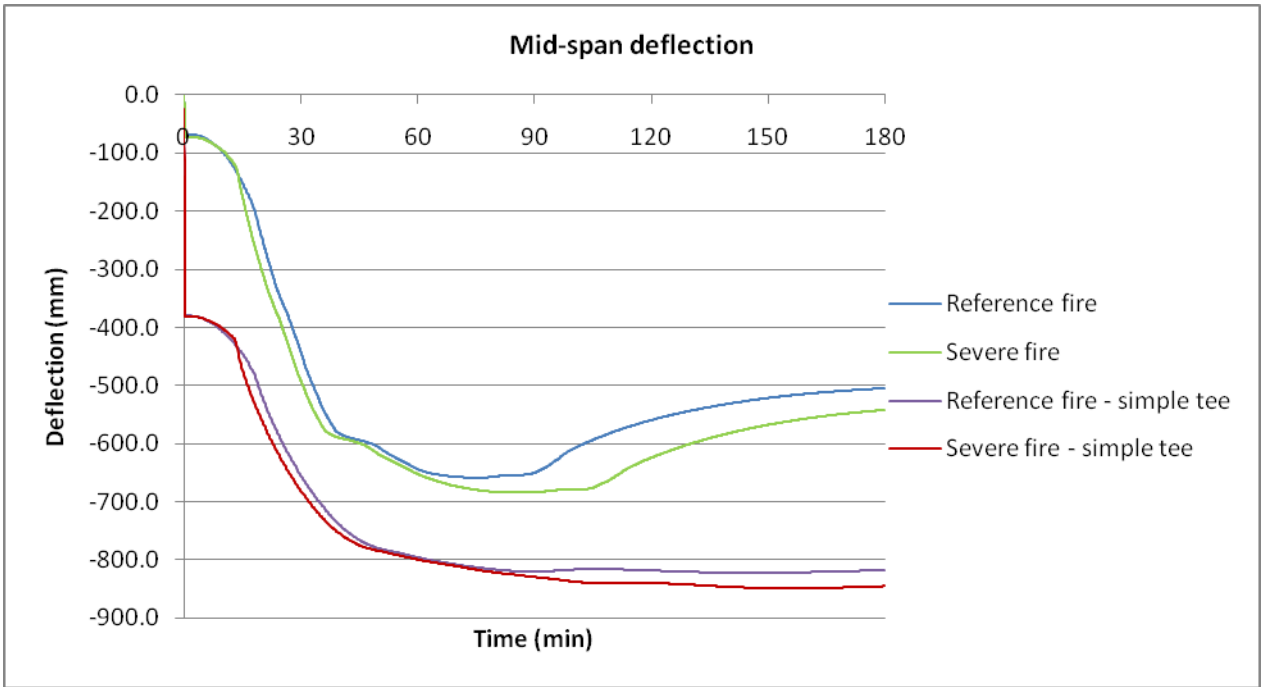

Figure 7–28 : Influence of the fire

High conductivity and S400 for rebars

Here, the analysis is performed for the extreme situation where the conductivity of the protective material is higher than expected and the steel strength for the rebars is lower than expected. The aim of this analysis is to confirm the fact that there is a security factor for the structure to resist during the test.

The maximum deflection is reached after 85' and its value is 96.0 cm.

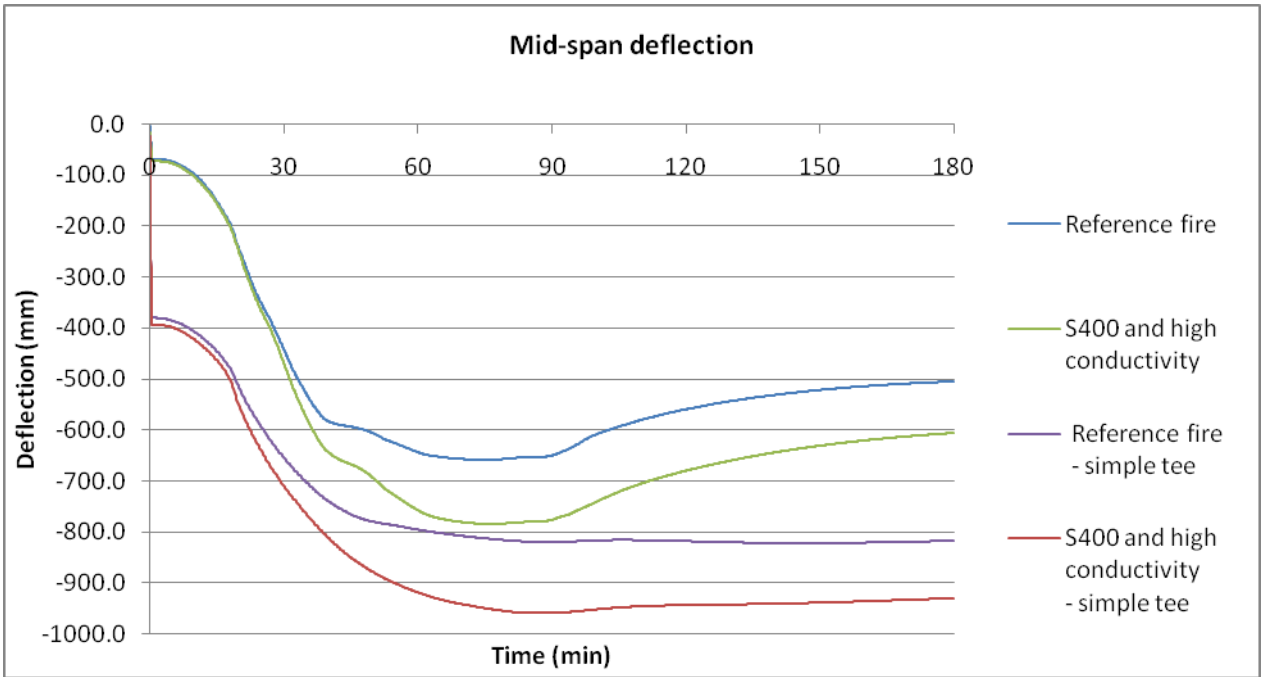

Figure 7–29 : High conductivity and S400 for rebars

7.3.5. Conclusion ULg SAFIR Model

The aim of this paragraph was to present the numerical simulations for the Ulster test that has take place in Ulster in February 2010. A parametric study was performed in order to take into account an uncertainty in some parameters values.

The results showed that the structure should be able to withstand the test without collapse. The deflections are important, reaching 0.96 m in an extreme case where the parameters values are chosen as particularly unfavorable. In the reference case modeling the test as accurately as possible, the maximum deflections reach 0.82 m if only the upper tee of the unprotected secondary beams is modeled.

The structural behavior during the fire is a membrane behavior, which explains the values of the deflections observed. The slab resists thanks to the tension in the rebars and the formation of a compressive ring. During the cooling, if the entire profile of the unprotected secondary beams is modeled, the behavior becomes a flexional behavior again when the beams get its stiffness back. So, in this case, the deflection decreases significantly. On the other hand, if only the upper tee of these profiles is modeled, the structure cannot get its stiffness back so that the deflection remains important at the end of the test. The behavior remains a membrane behavior because the secondary unprotected beams are not able to act as supports for the slab if only the upper tee of these profiles is modeled.

7.4. CTICM ANSYS Model

The model developed by CTICM is based on that used for FRACOF research project. The whole structure, i.e. the composite slab, the beams, the columns and the shear studs, are modelled. The mesh comprises 3 types of finite elements, with an average size of 500 mm (see Figure 7–30):

- Multilayered shell elements (SHELL91) for the reinforced concrete slab above the steel deck (see Figure 7–31);
- Beam elements (BEAM24) for the concrete ribs, the steel deck, the beams and the columns;
- Pipe elements (PIPE16) for the shear studs linking the beams to the composite slab.

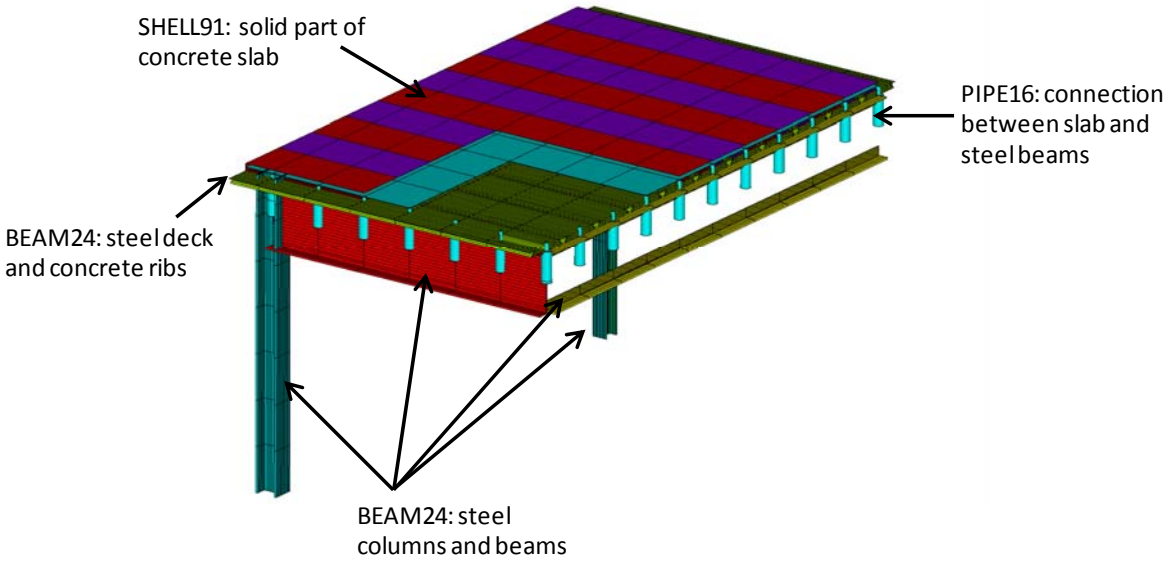

Figure 7–30 : Floor finite element model under ANSYS

Figure 7–31 : Composite slab mesh

As shown in Figure 7–30, the protected cell beams are modelled by considering their gross cross-section, i.e. by infilling all their openings. The unprotected cell beams are modelled by considering their net cross-section, i.e. with a double tee cross-section.

The results of the numerical simulations with ANSYS will be reported in WP8.

8. WP 7 : FULL-SCALE FIRE TESTS ON CELLULAR FLOORS

8.1. General Structural Details

8.1.1. Compartment construction

The choice of such compartment is more practical as it can be located near the central zone of any office building and can cover an area of 15m by 9 m with an internal floor to soffit 3.0m (see Figure 8–1). Figure 8–2 shows foundation and steel frame erection. The surrounding walls of the compartment were constructed using block works of 7 N/mm^2 except the façade where three openings were considered to be 1.5m by 3m (see Figure 8–2). The surrounding walls were not fixed to the composite floor at the top which allowed vertical movement of the floor and also to have a realistic catenaries action forces. Figure 8–5 to Figure 8–8 shows connection detail which used in joint of this steel work.

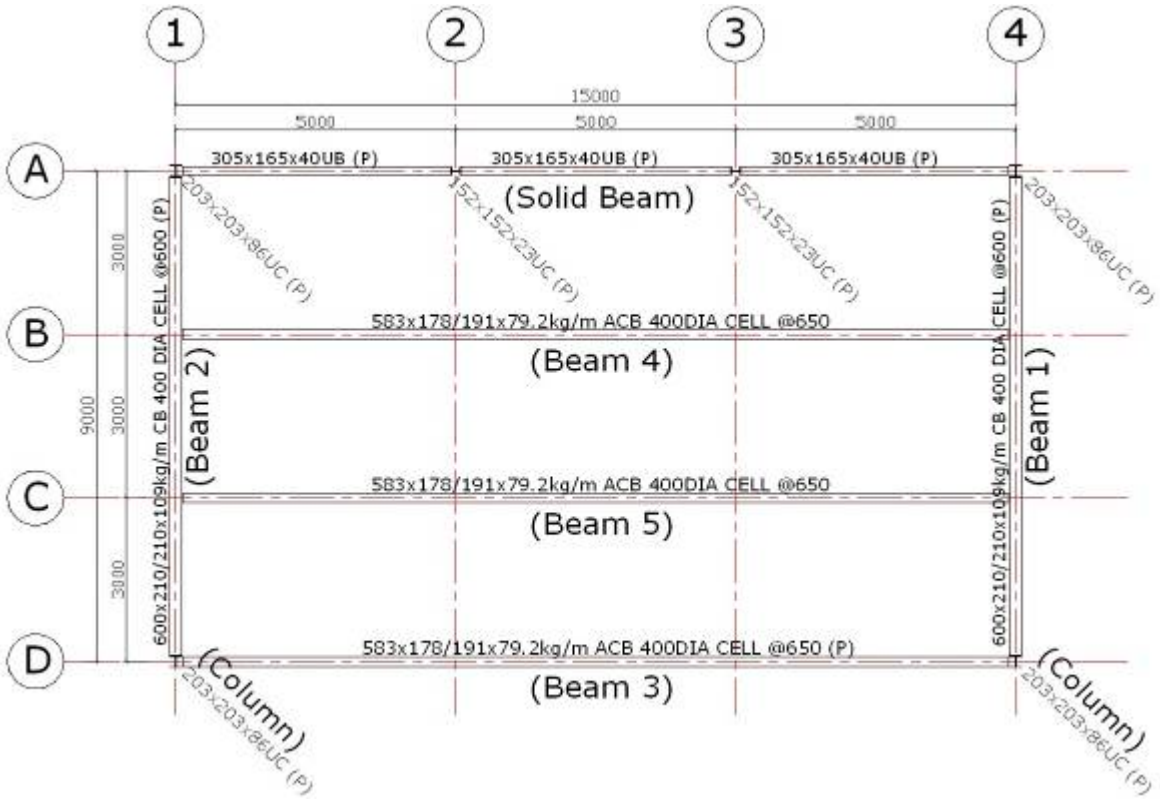

Figure 8–1 : Steel structural data information

Figure 8–2 : Foundation preparation

Figure 8–3 : Frame erection

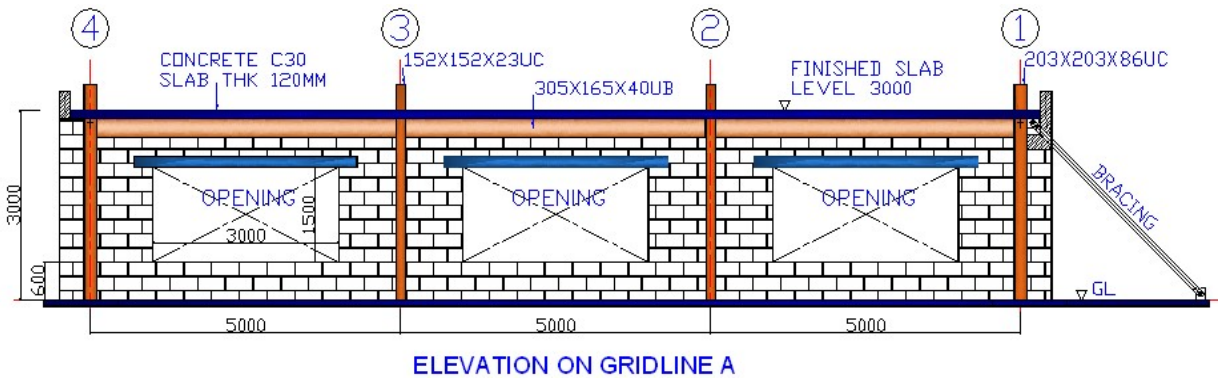

Figure 8–4 : Front elevation of compartment.

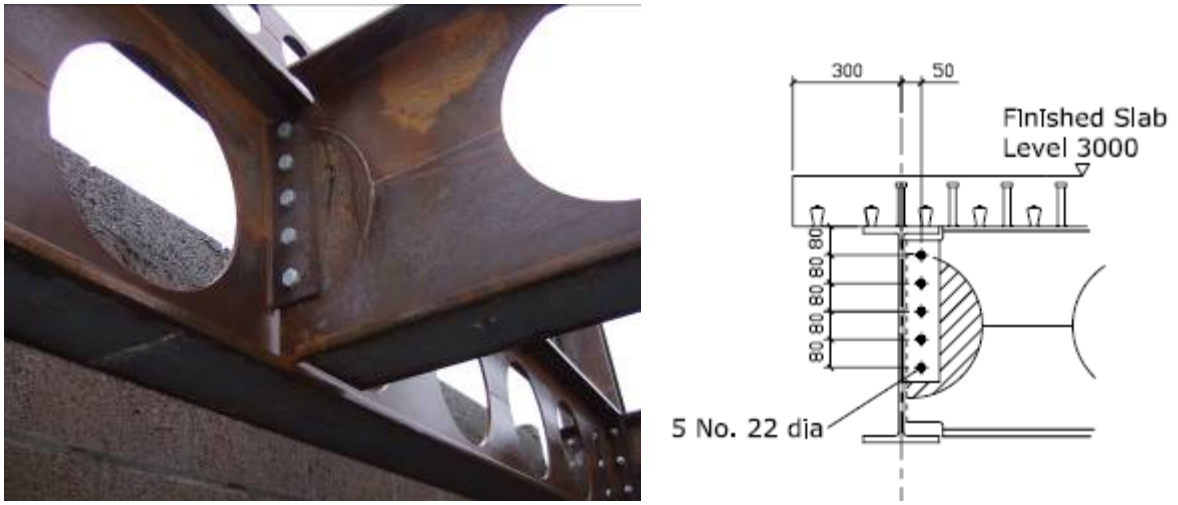

Figure 8–5 : Connection between Beam 2 and 4

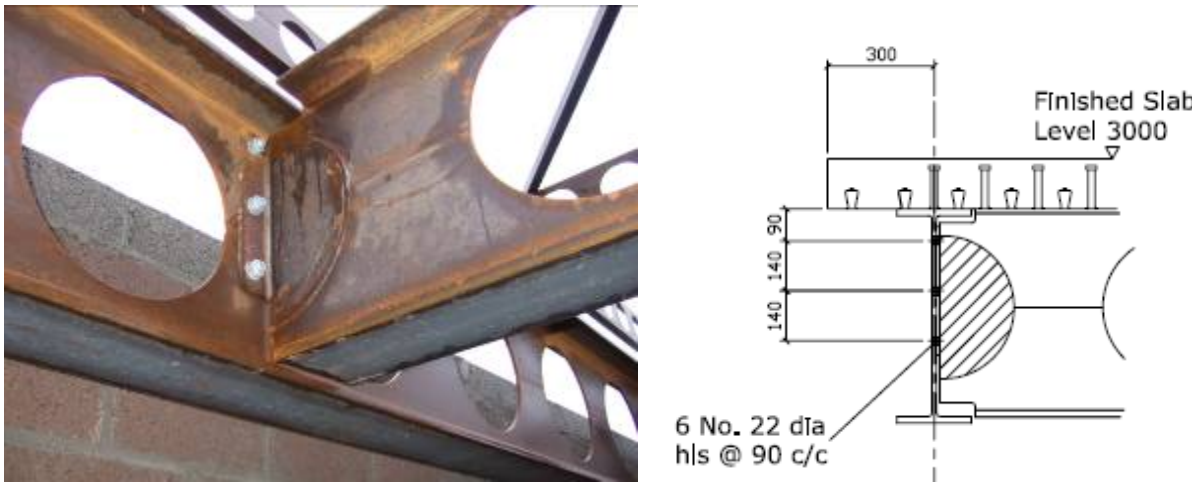

Figure 8–6 : Connection between Beam 2 and 5

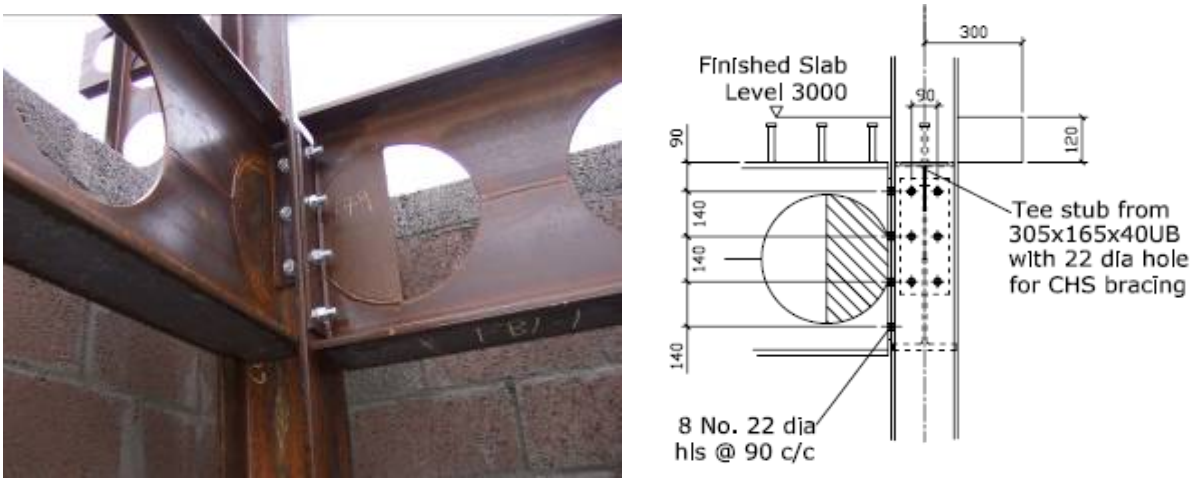

Figure 8–7 : Connection between Beam 2,3 and Column

Figure 8–8 : Connection between Beam 1, Column and solid beam

8.1.2. Floor slab

The concrete slabs were all nominally 120 mm thick and the slab reinforcement consisted of welded wire mesh reinforcement A393 (Figure 8–9) having yield strength of 500N/mm^2 and located at a vertical distance of 40 mm above the steel sheets. The minimum lap length used was a 400 mm. Full interaction between the slab and beam was ensured in all specimens by the use of a high density of shear connectors of 19mm diameter studs at height 95 mm. The shear studs have been equally distributed in one row with a distance of 200 mm over the beam length of the unprotected beams. A holorib sheets HR 51/150 with a thickness of 1 mm was used as sheeting. The measured yield stress from a tensile test was F_y = 327 N/mm^2.

Concrete compressive strength was determined at different stages of time: after 1 week, 28 days and during the testing day giving an average of 50N/mm^2 using a compressive strength calibrated machine at the University of Ulster. No additives or air entraining agent was used, with the mix design (for 1m^3) comprising: 320kg OPC, 918kg 10mm limestone, 691kg sharp sand, 380kg 6mm limestone, 30kg grey water and 142kg cold water. The slab was exposed in an external environment and, at the time of the test, the measured moisture content of the concrete slab was 6.4% by weight.

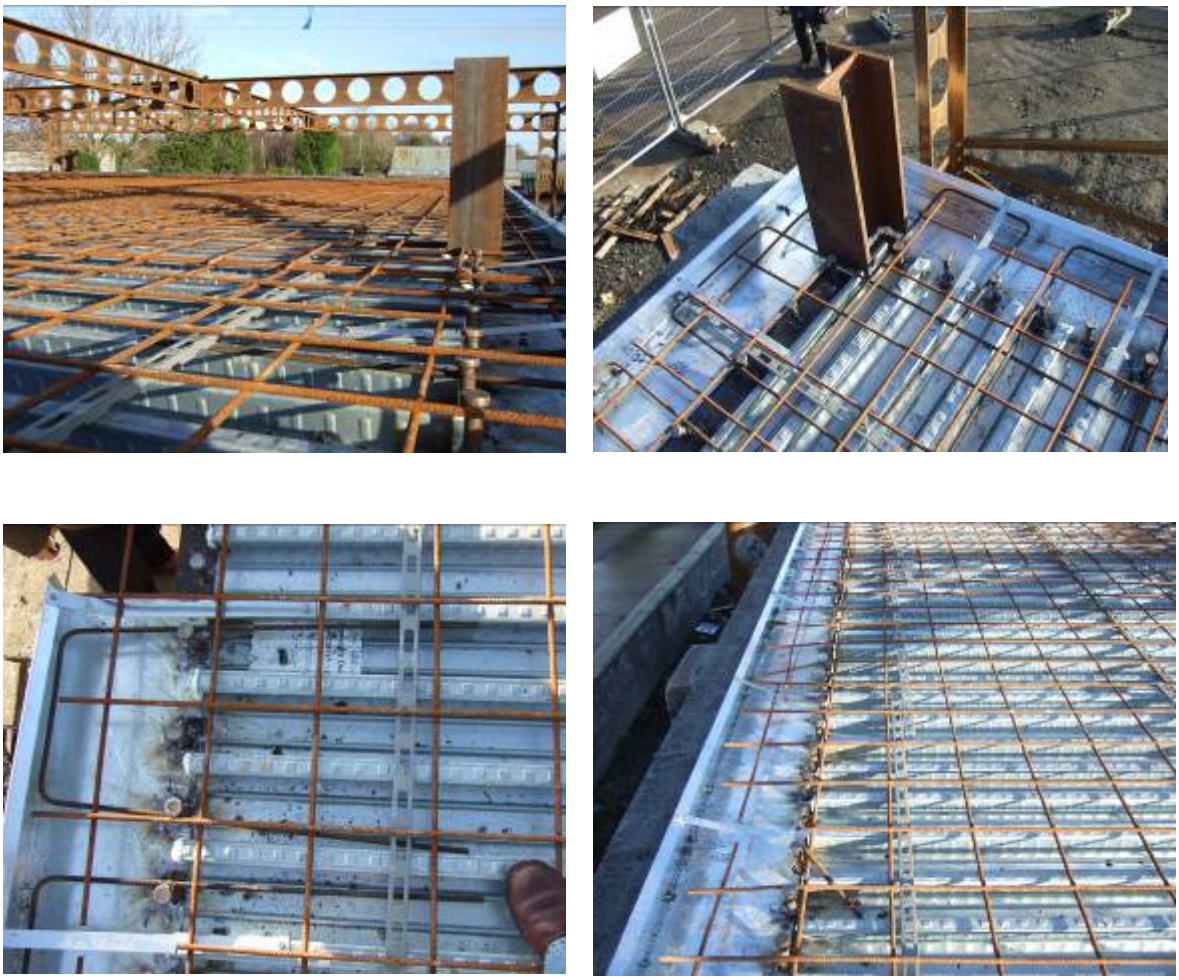

Figure 8–9 : Mesh reinforcement & steel decking before concrete casting

The requirements for U-bars is not a special requirement for fire design, but needed to ensure that the correct reinforcement details for room temperature design based on the following comments on SCI P300 and AD325. At all section the U-bars should be 10mm diameter and should be placed with 30mm cover to the edge of the slab. On the secondary beams were transverse reinforcement is not required the bars should be curtailed 40 bar diameters 400 mm from the inside toe of the top flange.

Where transverse reinforcement is required, the curtailment rules shown in AD325 should be followed. The bar in these cases should extend a distance equal to the greater of 40 bar diameters 400mm beyond the critical plane and 12 bars diameters more than the effective width, span/8 + 12d (1245mm). An illustration of slab reinforcements is shown in Figure 8–10. Figure 8–11 to Figure 8–13 shows concrete casting and curing on the slab.

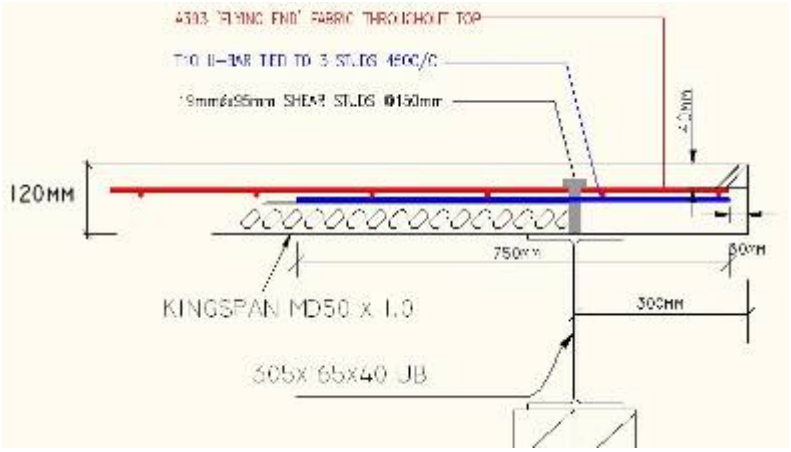

(a) Section Grid-A

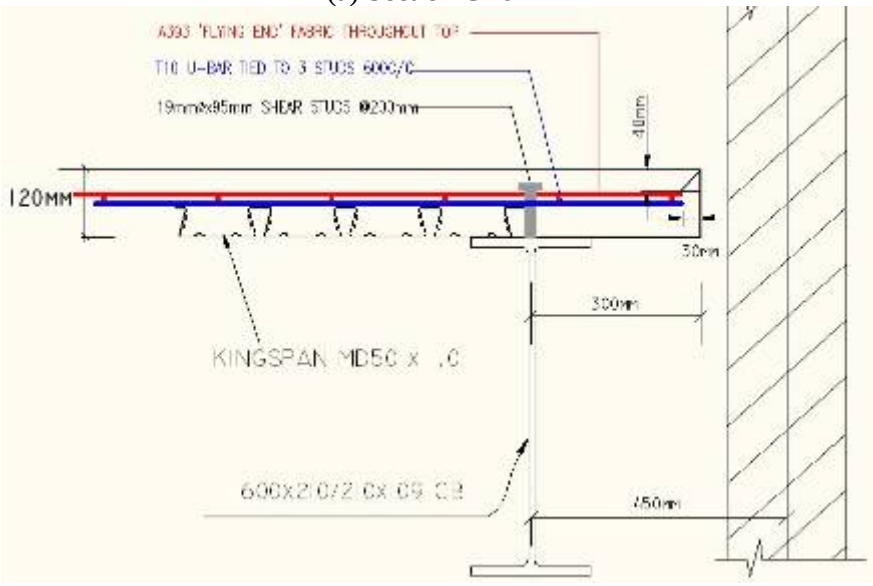

(b) Section Grid-1 and 4

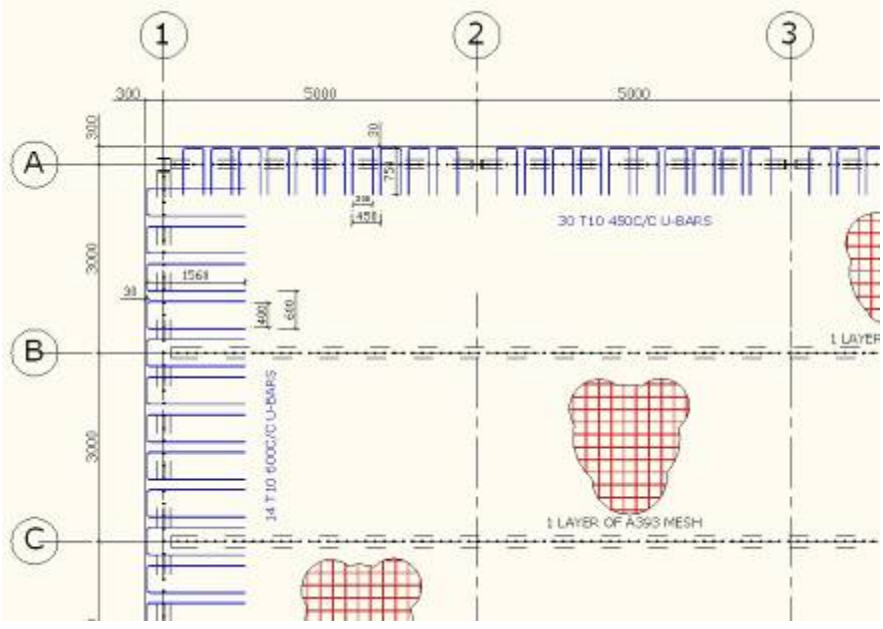

Figure 8–10 : Mesh reinforcement & steel decking before concrete casting

Figure 8–11 : Concrete casting

Figure 8–12 : Props supporting beams and slab edges during pouring concrete

Figure 8–13 : View of the compartment in December 2009

8.1.3. Fire protection

All the columns and solid beams on the opening side were protected for duration of two hours using fire boards of 20 mm thickness. The surrounding cellular beams were also protected using ceramic fibers (see Figure 8–14). The fire protection was fitted using an approved contractor. It was reported that the fire protection would achieve at least 120mins fire resistance in a standard fire test. All connections from secondary beams to main beams and from beams to columns are simple connections. Horizontal bracing was provided in 4 positions leaving the slab completely free of external horizontal restraint.

The only reason to choose the ceramic fiber was because the weather conditions can not satisfy the existing protection available in the market to be used due to high condensation, frost and wet environment. However, the ceramic fiber where tested in the laboratory of FireSERT at Ulster University to optimise the thickness and validate its application in comparison with other existing practical protection used in construction. The properties of this Module block are 150kg/m^3 in mass, 800J/kgK in specific heat and 0.142W/mK in conductivity. Figure 8–15 demonstrate that the fiber used satisfy the application in comparison with 20 mm spray cementitious protection. In addition to that the ceramic fiber was used in similar fire compartment tested previously by Bin Zhao.

Figure 8–14 : Board and fiber protection used inside the compartment

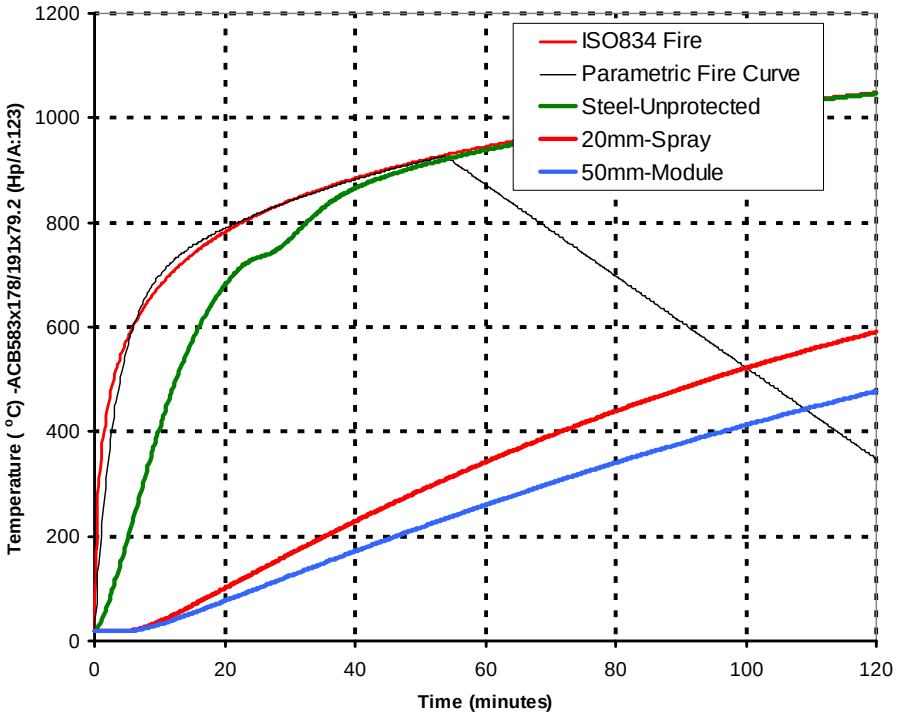

(a) ACB 583x178/191x79.2kg/m (H_p/A = 123 M^{-1})

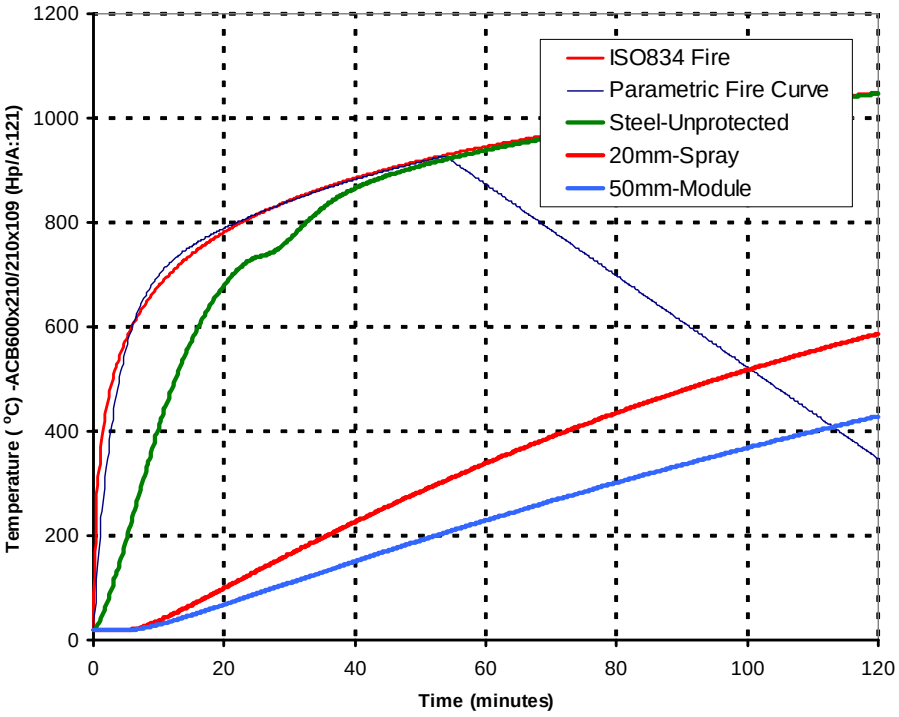

(b) CB 600x210/210x109kg/m (H_p/A = 121 M^{-1})

Figure 8–15 : Insulation comparison between fiber(50mm) and spray(20mm) material

8.1.4. Measuring instrumentation

Instrumentation was distributed in different compartment location to measure atmosphere temperatures, the temperature distributed through the decking, the temperature of the protected and unprotected cellular beams, and vertical and horizontal displacements (see Figure 8–16). A total of 350 thermocouples were used to monitor the temperature in the beams (see Figure 8–17 to Figure 8–23, protected and not protected), the temperature distribution through the slab and the atmosphere temperature within the compartment (see Figure 8–24and Figure 8–25).

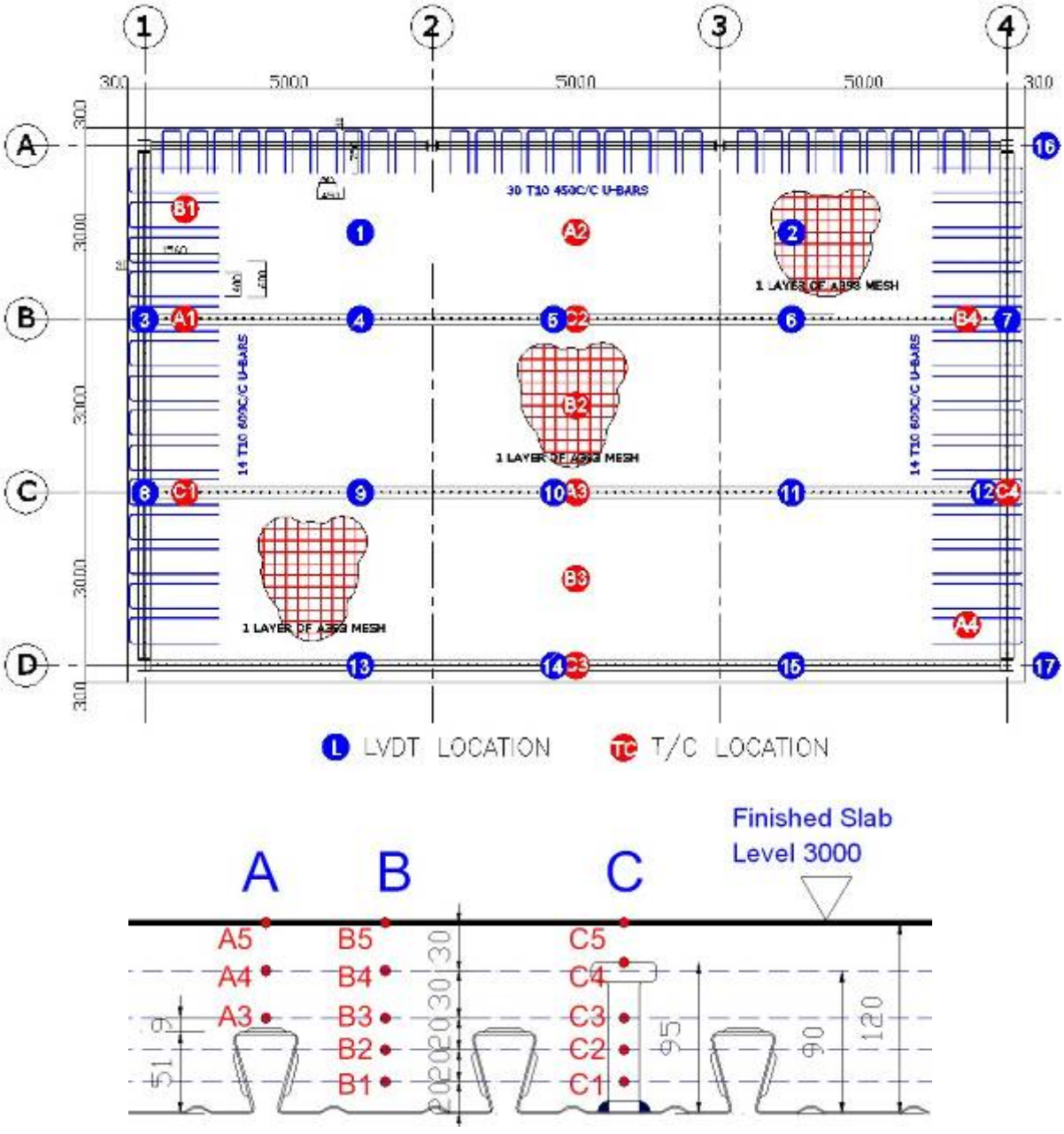

Figure 8–16 : LVDT and thermo couples locations to measure deflections and temperatures.

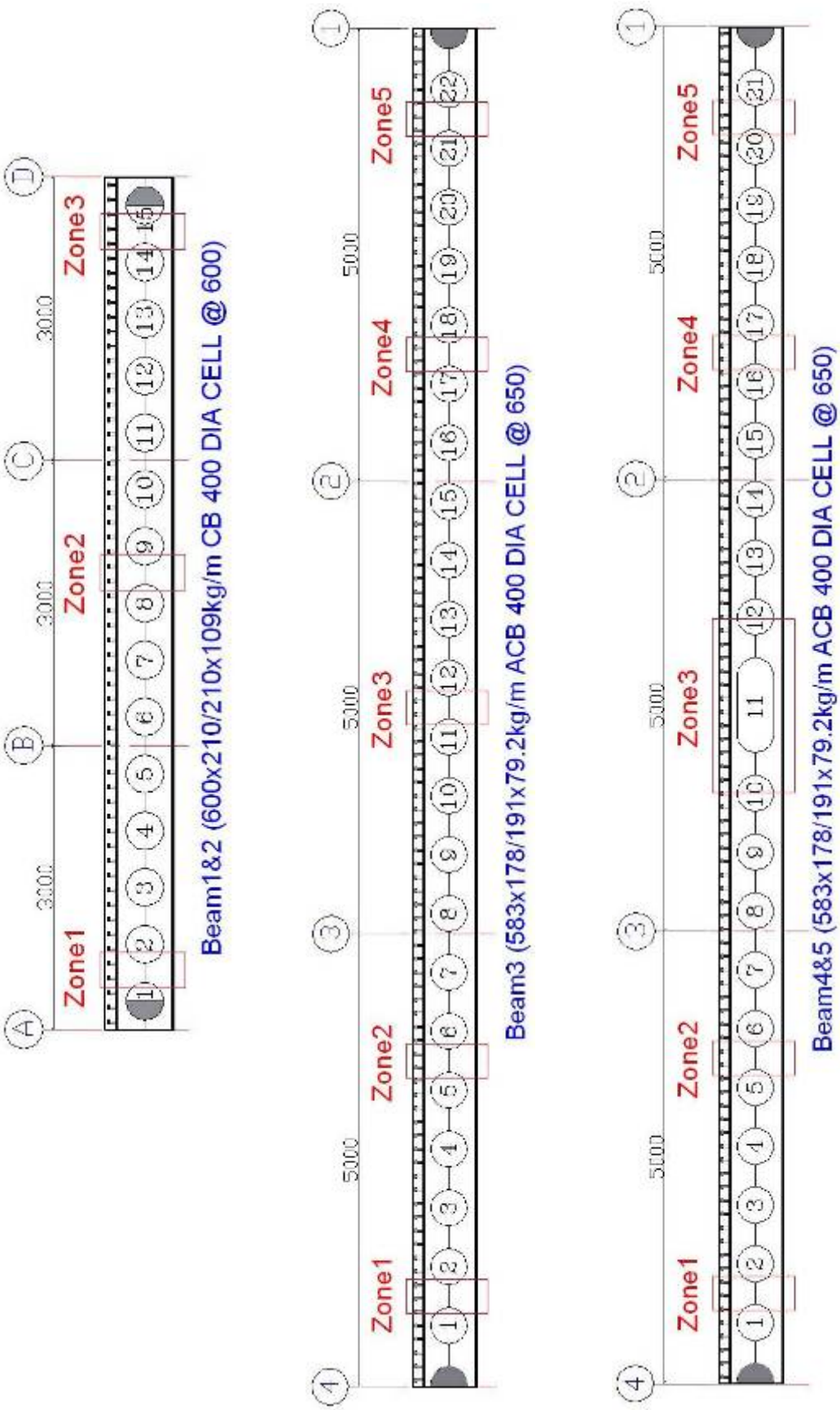

Figure 8–17 : Zoning for TC arrangement (Beam 1-5).

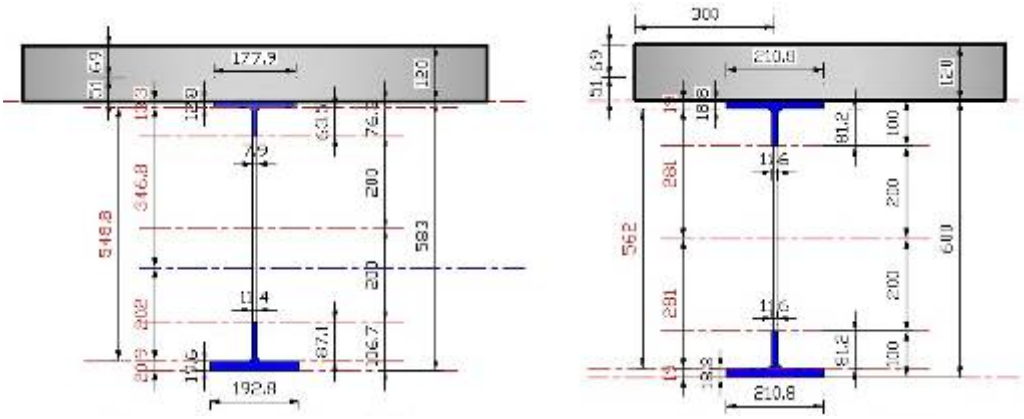

Beam 3,4 and 5 Beam 1 and 2

Figure 8–18 : Dimension of the CB section.

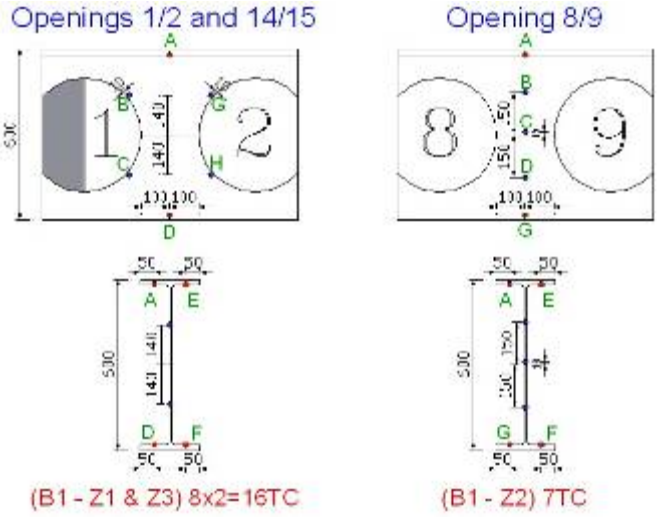

Figure 8–19 : TC location on Beam 1.

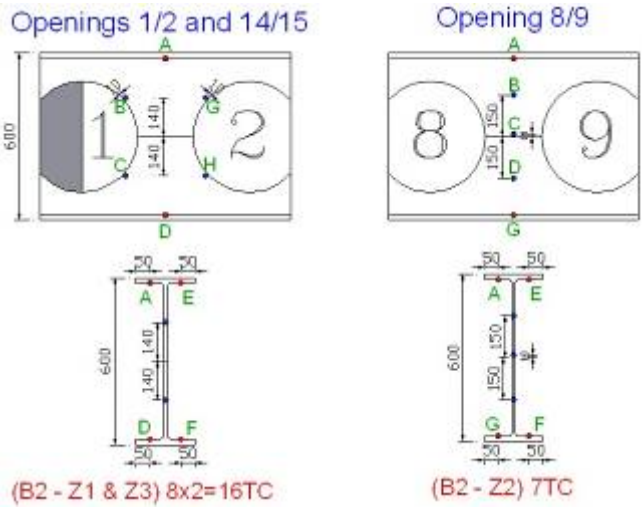

Figure 8–20 : TC location on Beam 2.

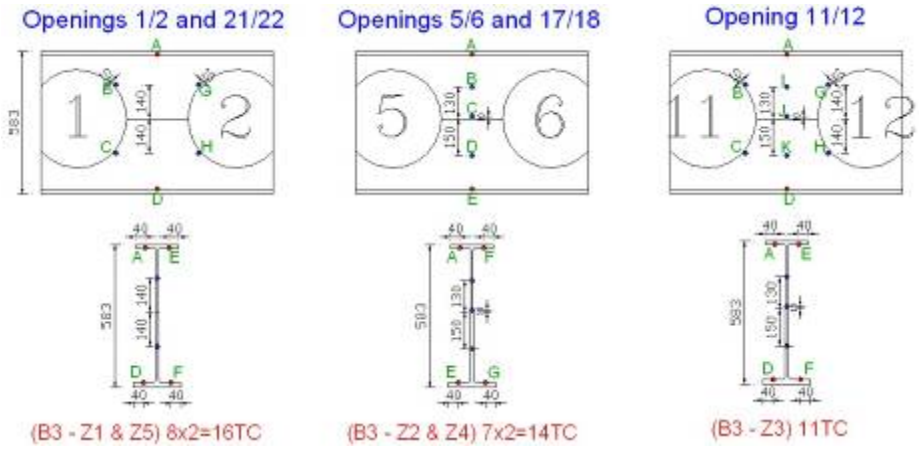

Figure 8–21 : TC location on Beam 3.

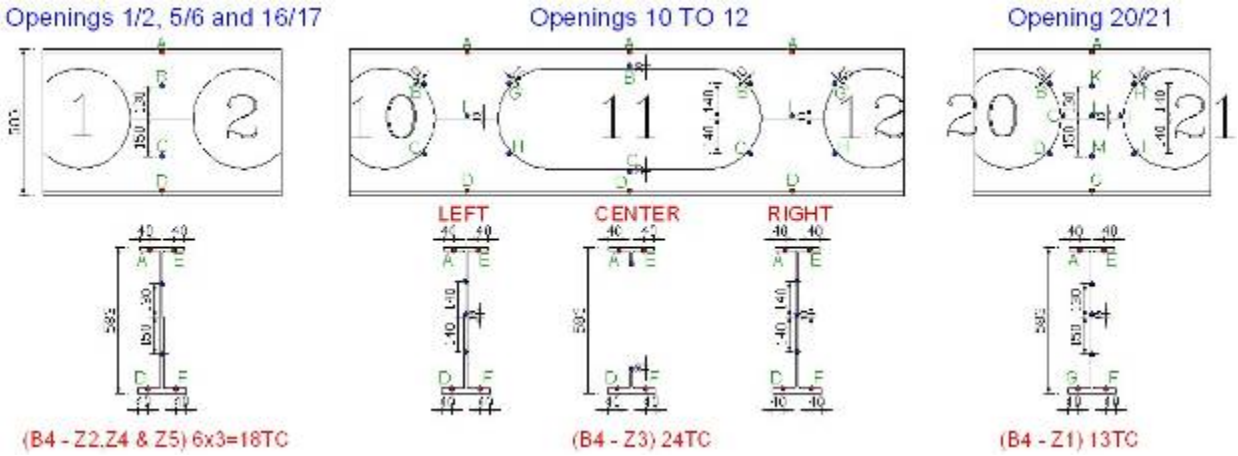

Figure 8–22 : TC location on Beam 4.

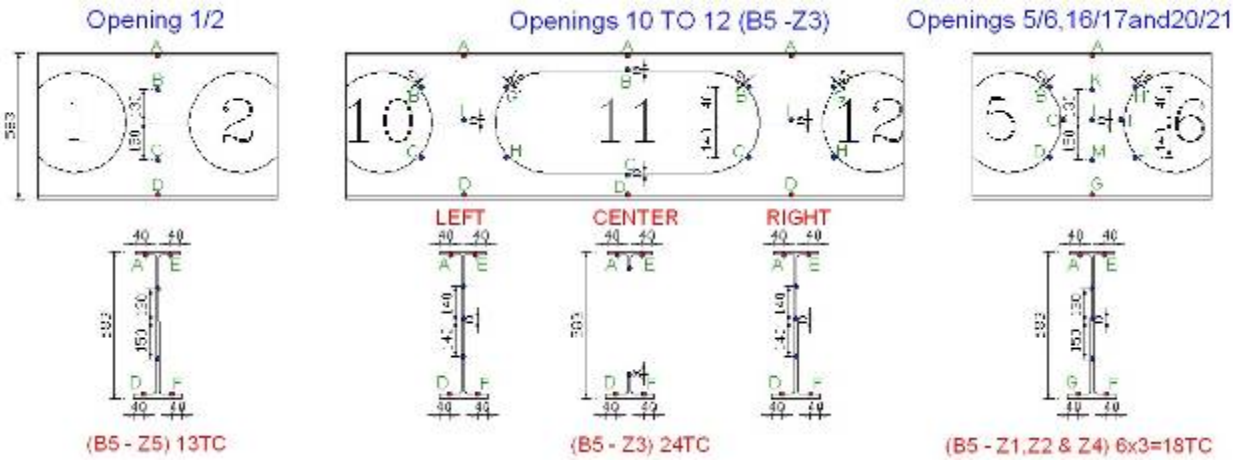

Figure 8–23 : TC location on Beam 5.

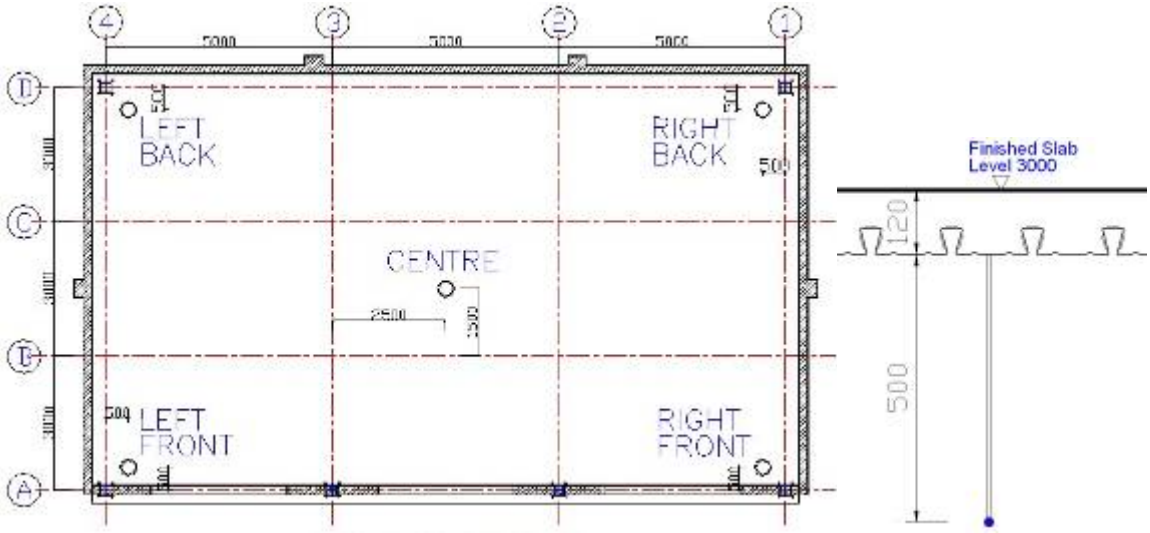

Figure 8–24 : TC locations for atmosphere temperature

Figure 8–25 : Positioning of Thermo couples

8.2. Fire Test

8.2.1. Design loads

The loads used within the structure are the same as those which are commonly used in the design of office buildings and are as outlined in Table 8-1.

The applied load of 3.25 KN/m^2 was achieved using 44 sandbags (each weighting 1t) evenly positioned over the floor plate, as shown in Figure 8–26 and Figure 8–27a. Taking the floor plate are 15m by 9m, this gives an applied load of 3.25 KN/m^2. The self weight of the slab of 120 mm thickness is about 2.90 KN/m^2, creating a total load of 6.15 KN/m^2.

Table 8-1 : Design Loads

Description	Characteristics KN/m^2	Fire Factor	Design Load KN/m^2
Partition	1.0	1.0	1.0
Services & Finishes	0.5	1.0	0.5
Live Load	3.5	0.5	1.75
		Total	3.25

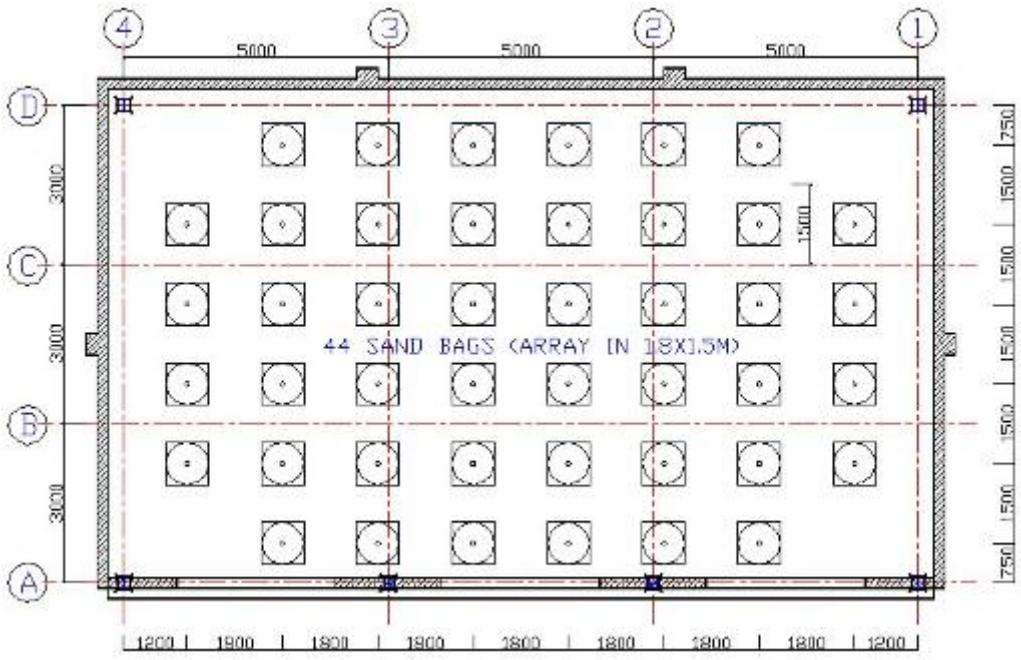

Figure 8–26 : Sand bags lay out on slab.

8.2.2. Fire load

The natural fire was designed using Annex A (Parametric temperature-time curves) of BS EN 1991-1-2. The fire load was achieved using 45 standard (1m x 1m x 0.5 m high) wooden cribs, comprising 50mm x 50 mm x 1000mm wooden battens, positioned evenly around the compartment (Figure 8–27b).The fire load was 40 kg of wood per square metre of floor area. The wood density provided is 510 kg/m^3 with calorific value of 17.5 MJ/kg for wood and the fire load density for the tested compartment was is 700 MJ/m^2.

Figure 8–27 : a) Vertical static load b) Wooden cribs used for the fire load

8.2.3. Ignition

As a general rule natural fires start up from a single ignition source to have a smooth and steady development (Figure 8–28). After 7 minutes of the first ignition middle compartment location two more ignitions sources were added in different places and the rest of cribs were left to ignite by its neighbour. Each crib was connected to its neighbour by mild steel channel section. Pourous fibre board was laid into channels, and approximately 30 min before ignition, some 20 litre of paraffin was poured into channel. In this way, the cribs were ignited simultaneously in a consistent manner to ensure rapid fire development.

Figure 8–28 : Setting up of ignition

8.3. Test Results

8.3.1. Temperature in the compartment

The ambient temperature prior to the test was 5°C. The maximum recorded atmosphere temperature in the centre of the compartment was 1051°C below 500 mm from the ceiling after 75 minutes. The duration of the pick temperature took 20 minutes before starting to go down to 200°C after 155 minutes. Figure 8–29 to Figure 8–33 show atmosphere time /temperature compared with the OZone model and the parametric fire curve. If we adjust a delay of five minutes ignition we may see that both curves are very close the fire temperature compartment. Figure 8–34 to Figure 8–37 show recorded temperatures at the each part of structure members.

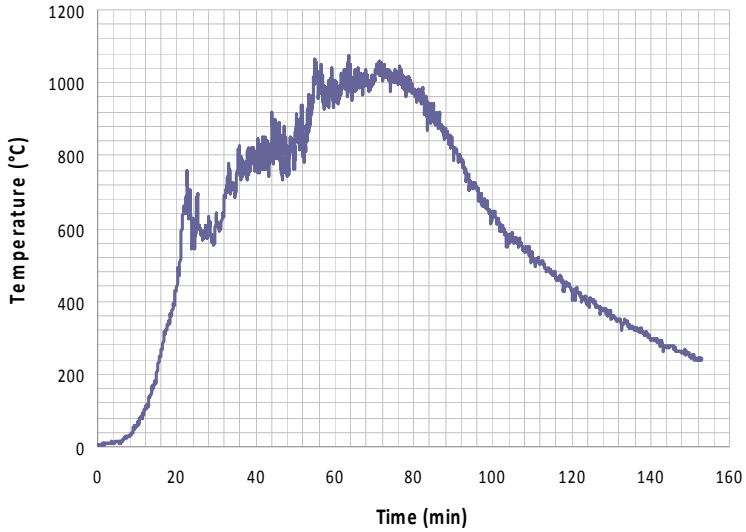

Figure 8–29 : Compartment temperature at center

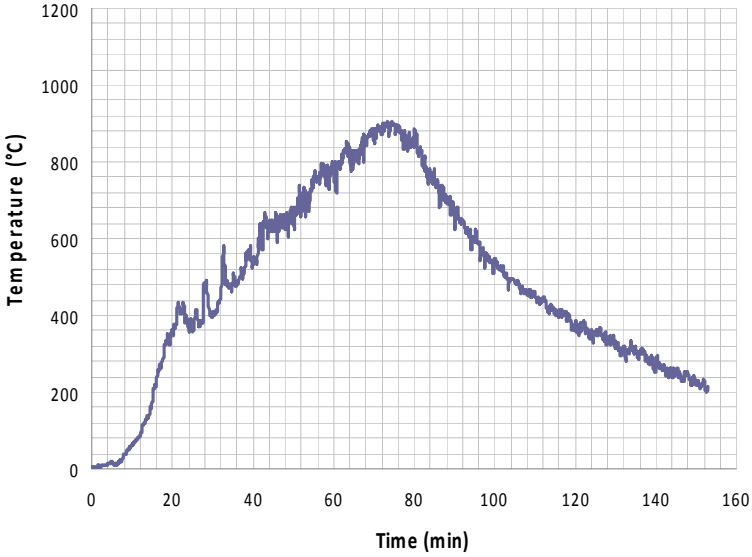

Figure 8–30 : Compartment temperature at left back corner

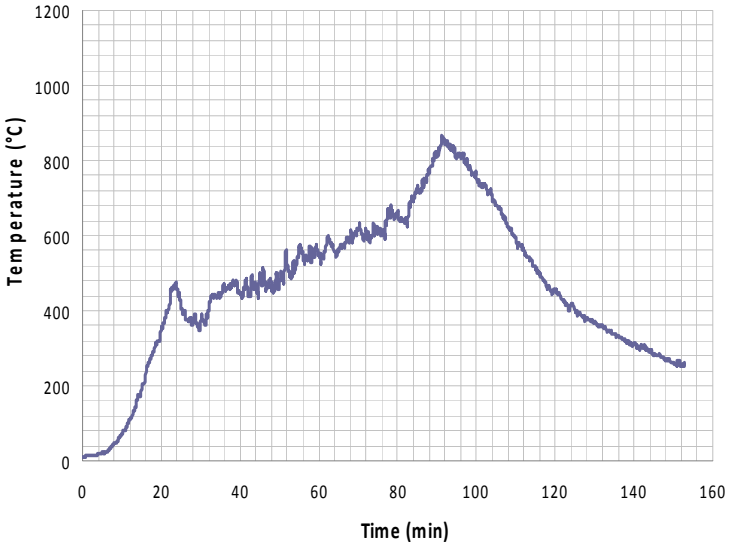

Figure 8–31 : Compartment temperature at right back corner

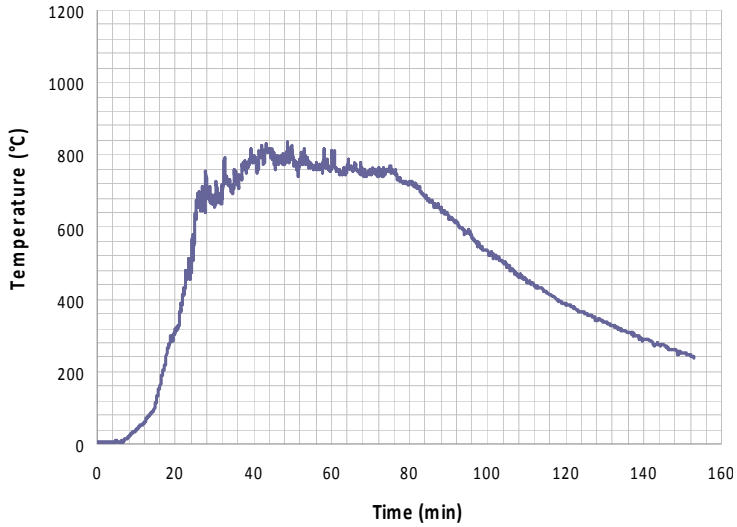

Figure 8–32 : Compartment temperature at left front corner

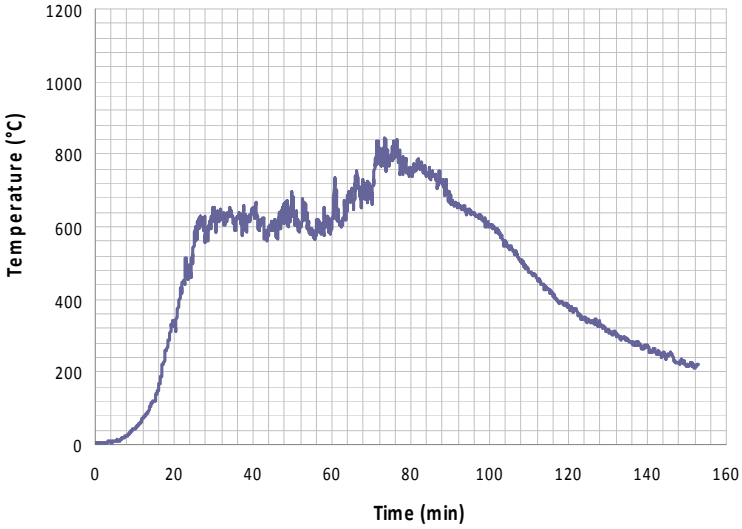

Figure 8–33 : Compartment temperature at right front corner

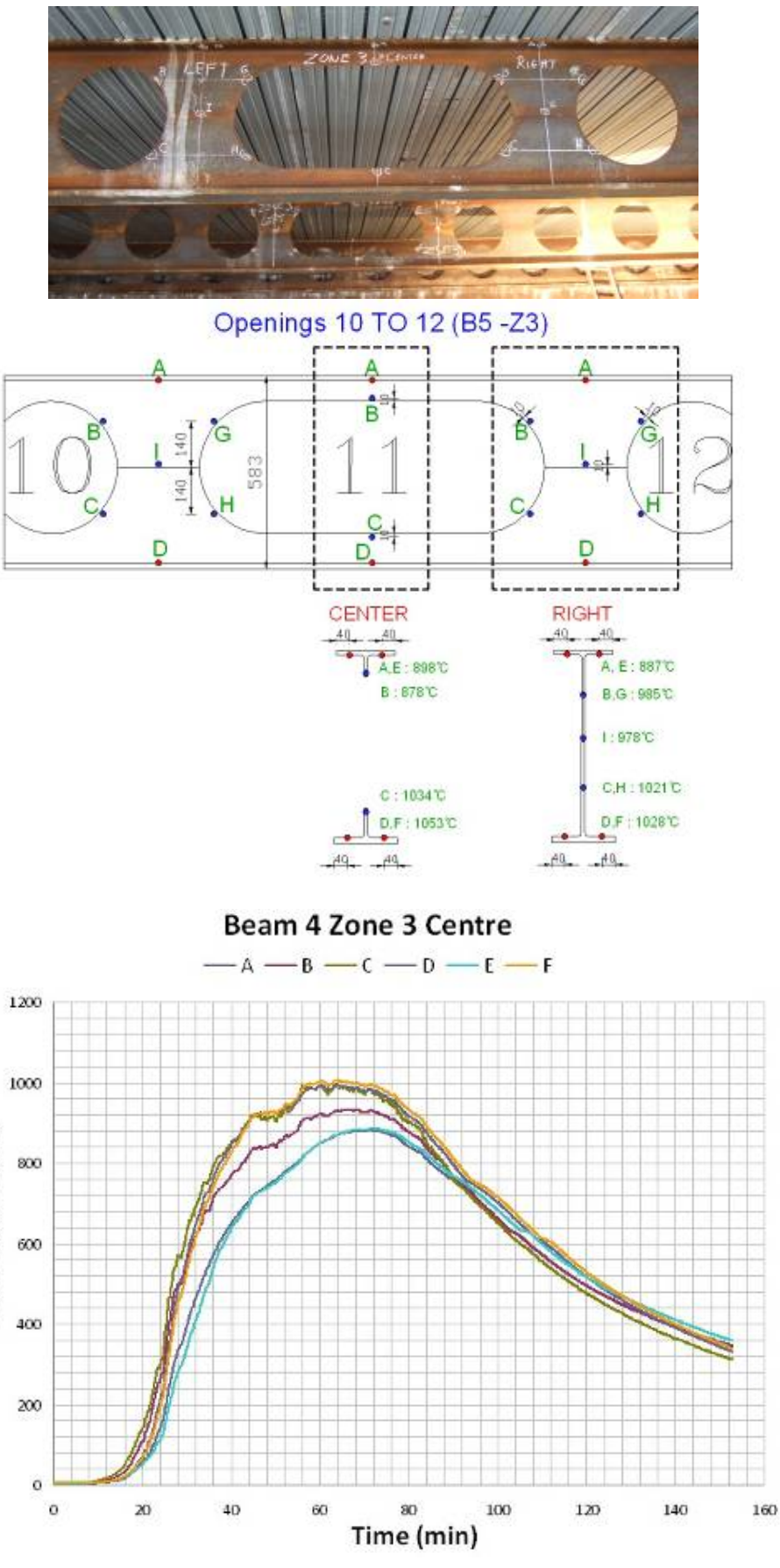

Figure 8–34 : Recorded temperatures at the central part of the unprotected members.

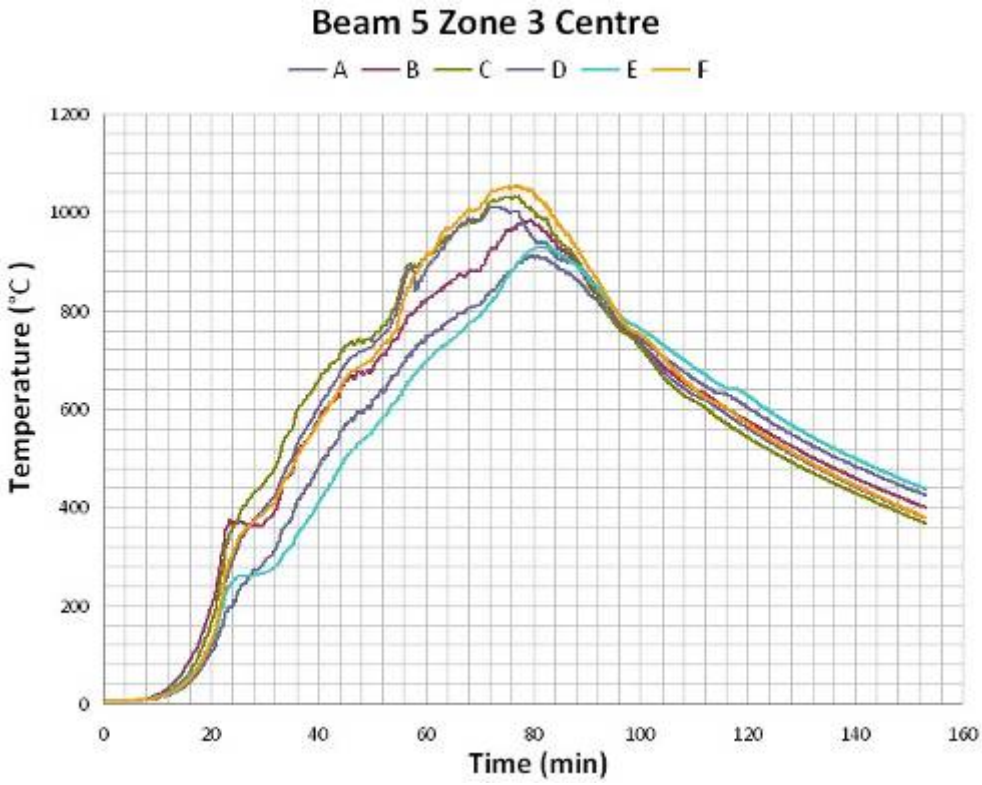

Figure 8–35 : Temperatures at the central part of the unprotected beams

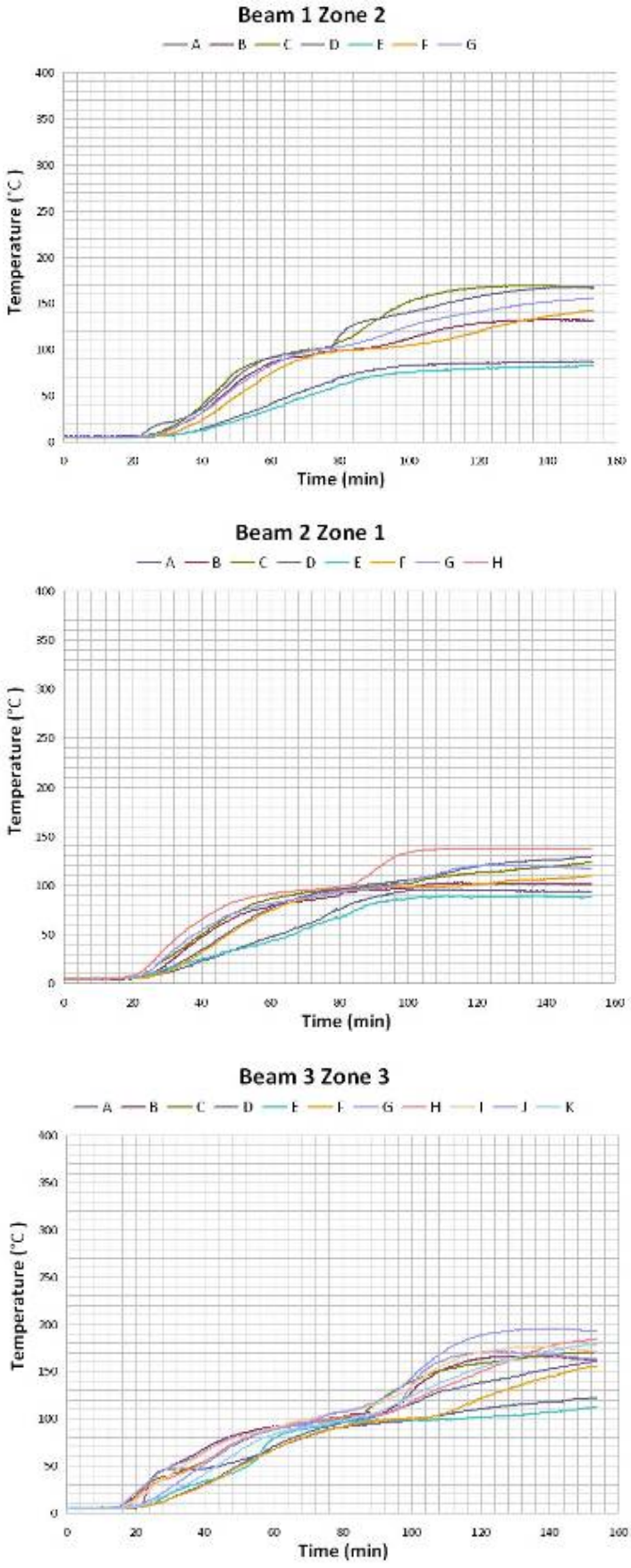

Figure 8–36 : Temperatures at the protected beams

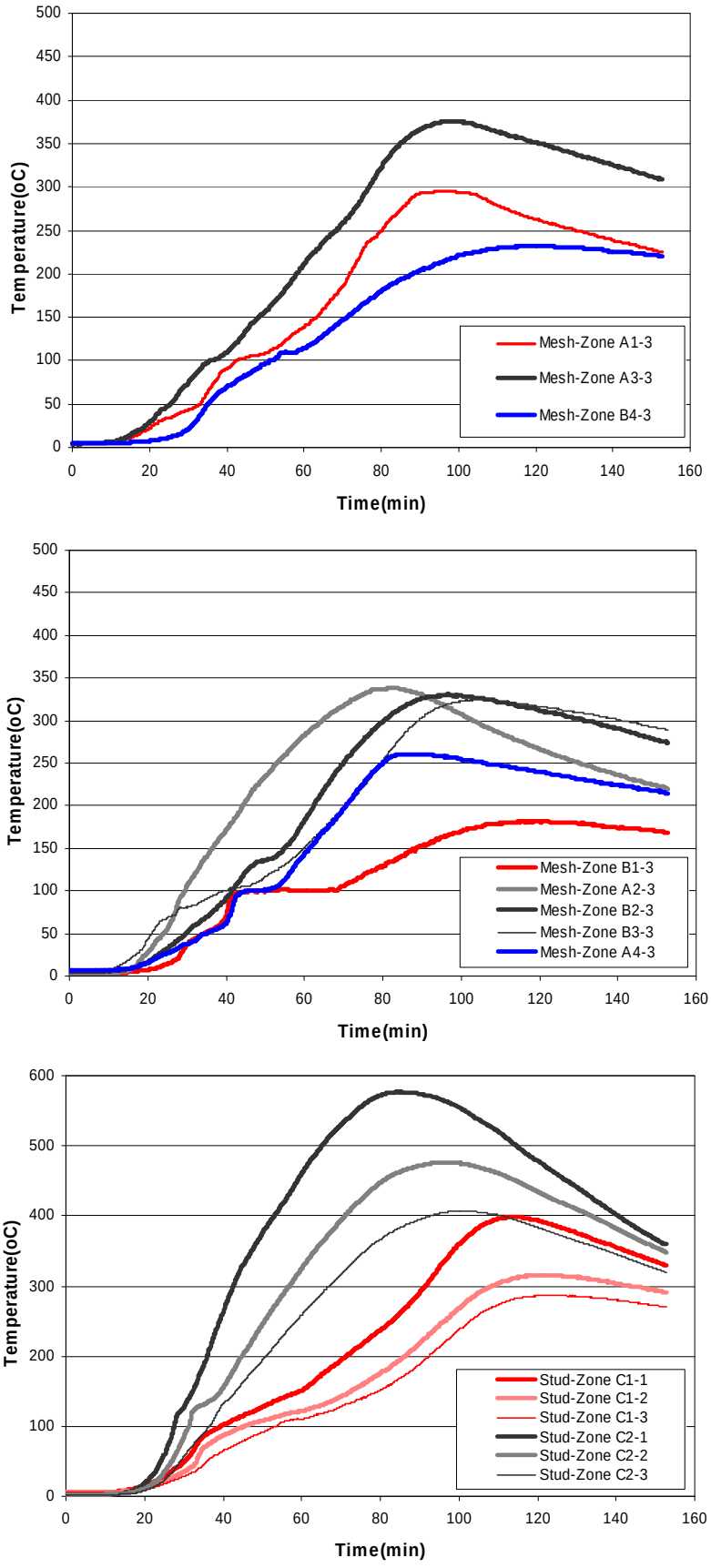

Figure 8–37 : Heat transfer at the slab decking

8.3.2. Beam/Slab Deflection

Under fire conditions, the deflection in the unprotected steel beam (Figure 8–38) is comprised of two parts: the thermal bowing deflection and the mechanical deflection. The thermal bowing deflection is due to non-uniform temperature distribution in the steel beam. The mechanical deflection is the increase in the beam deflection under constant load at decreasing stiffness due to reduced steel strength and stiffness at high temperatures at the web posts of the unprotected beams. It is expected that at low temperatures (less than 500°C), the beam deflection is controlled by thermal bowing.

Figure 8–38 : Deflection of Long cellular beams in real fire

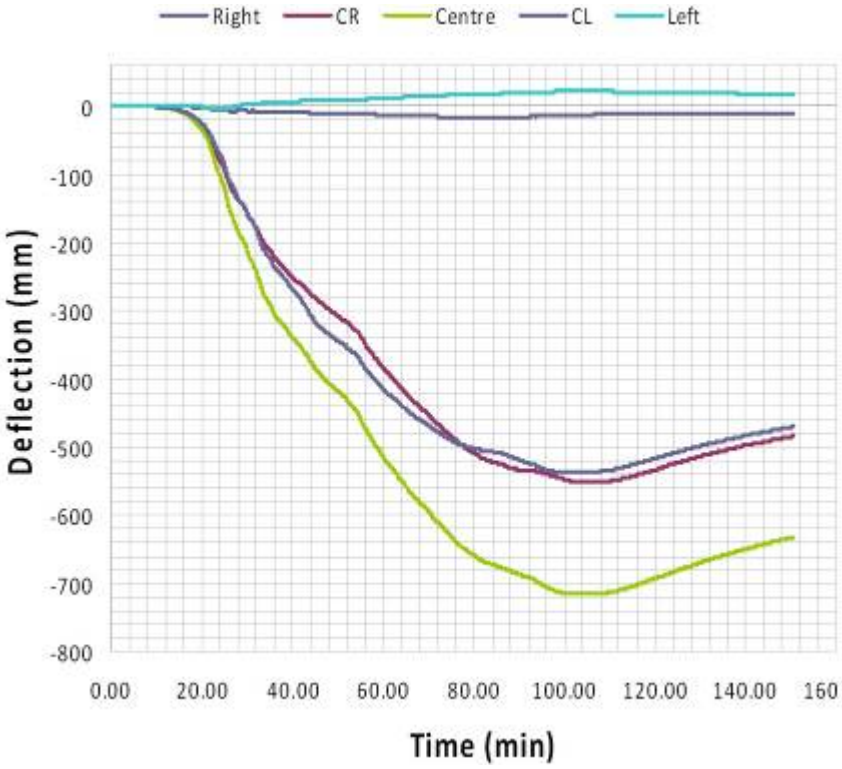

Figure 8–39 : Beam 4 deflection

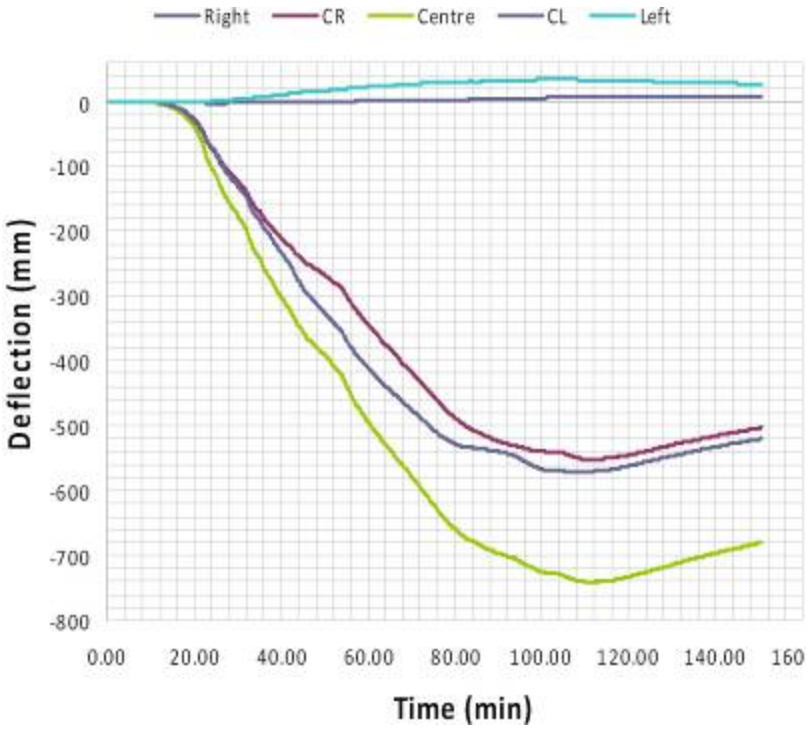

Figure 8–40 : Beam 5 deflection

At higher temperatures, mechanical deflection dominates and the beam deflection increases at a faster rate (Figure 8–39 and Figure 8–40) with a rise in the beam temperature at the web post (Figure 8–35). The maximum recorded steel temperature of 1053^{o}C occurred after 77 minutes on the bottom flange with elongated opening of the unprotected beam4/5 in the middle of the member. Figure 8–34 shows the temperatures distribution at the critical part of the unprotected central part of the cellular beams members. The cross sections temperatures are non-uniform despite the long duration of the fire which is not the case if it is tested in laboratory furnaces.

Figure 8–41 : Deflection of the slab/unprotected beam: post web buckling and lateral torsion effect.

With temperatures increasing on the unprotected steel section, the post web buckling occurs initially before the slab does prevent twisting of the steel section as a whole. At that stage, the tendency for the bottom flange to displace laterally causes bending of the steel web, and twisting at top flange level, which is resisted by bending of the slab as shown in Figure 8–41. The long cellular beam became as a cable with only top flange considered working at temperature reaching the 800^0C. The maximum recoded deflection value of beam deflection occurred in the centre of the slab after 130 minutes where it reached a value of 750mm. However, by the next morning the slab had recovered to a displacement of 160mm.

8.3.3. Membrane action in floor slabs

Recorded results show very high temperatures in the steel decking, reaching the maximum of about 900°C. The steel decking was also observed to have de-bonded from the concrete slab in most areas. Thus it may be assumed that the steel decking contributed very little to the slab strength at the maximum fire severity.

Large deflection occurs of around 750 mm on the composite slab and large cracks occur in the tension face as shown in Figure 8–42. The concrete slab was not horizontally restrained around its perimeter and subjected to large vertical displacements, membrane action developed with the reinforcement utilizing its full tensile capacity and supporting the load by acting a kind of net. This behaviour is commonly referred to as tensile membrane action. The slab supports the load by tensile membrane action occurring in the centre of the slab and compressive membrane action forming a supporting ring around the perimeter of the slab.

Figure 8–43 show internal beam's residual movement in half-span and connection after test. The unprotected cellular beams become as cables with only top flange considered from when the most weakest part(upper web) yield so that the vertical shear forces induced by web post caused a rotation of the lower tee. Web post buckling, which is commonly observed in isolated fire test, have occurred around first opening where the displacements are restricted closely by the stiff boundaries.

The 3-dimensional behaviour of the floor slab causes a slope which brings rotational angle of top flange in steel beam. This makes secondary moment at the section and vertical shear force lead to lateral buckling of CB which drives for lower tee to move out of original plane line. Protected steel members and connections appeared no serious damages(Figure 8–44) even though exposed steel members have experienced nearly failure during the fire.

Figure 8–42 : Crack distribution on the slab

Figure 8–43 : Internal beam near mid span and end connection after fire(Beam 4)

Figure 8–44 : Joint connection after fire

8.4. Conclusions

Full scale cellular beams were exposed to the natural compartment fire to investigate its fire performance. In the test, the temperature of the membrane action occurred to carry the applied load instead of bending mechanism due to large deflection, when the composite floors slab was subjected to fire. The fire test have demonstrated the inherent fire resistance of modern composite steel frame buildings while highlighting the importance of protecting key elements within the structure. Such a strategy based on high quality data will allow a more rational approach to the passive fire protection strategy for buildings without constraining innovation through prescriptive legislation.

The fire resistance of the unprotected secondary steel beams of a spans of 15m was fulfilled up to more than 90 minutes. The cellular beams failed due to web buckling at the restrains locations and combination of web buckling with lateral torsional buckling movement at the rest of the beams length.

The masonry wall forming the boundary of the compartment retained its integrity despite a significant thermal gradient across the wall and substantial lateral deformation. The fire resistance partitions performed adequately and prevented any appreciable heat rise outside the boundaries of the compartment.

9. WP8 : ADDITIONAL FIRE RESISTANCE THROUGH 3D MEMBRANE EFFECT - FINAL METHODS (2D AND 3D) FOR LONG SPAN BEAM MINIMISING THE FIRE PROTECTION THROUGH MEMBRANE EFFECT AND ADEQUATE CONNECTION DESIGN

9.1. Material properties

9.1.1. Steel

The steel mechanical behaviour follows the stress-strain relationships given in EN1994-1-2 [21], and a Von Mises yield criterion. As no experimental data have been provided, the steel nominal values are used in the simulation, i.e.

- structural steel strength: $f_{ay,20°C}$ = 355 N/mm^2;
- reinforcement steel strength: $f_{sy,20°C}$ = 500 N/mm^2.

During the fire test, the unprotected beams had moved towards each other, due to web-post buckling, even though the structure had not failed yet (see Figure 8–41). This may suggest that their lower tee did not play any part in the global behaviour of the floor from this web-post buckling. In consequence, two simulations are run:

1) In the first simulation, the steel stress-strain curves given in EN 1994-1-2 are used for both tees of the unprotected beams;
2) In the second simulation, curves from EN 1994-1-2 are used in the upper tee. In the lower tee, the steel reduction factors are reduced to 1/1000th of their actual values from 90 min to the end of the simulation, including cooling phase (see Figure 9–1). This irreversible loss of strength aims at checking whether it is reasonable to neglect the contribution of the unprotected lower tees to the global strength of the structure once they reach a given temperature, say 600 °C.

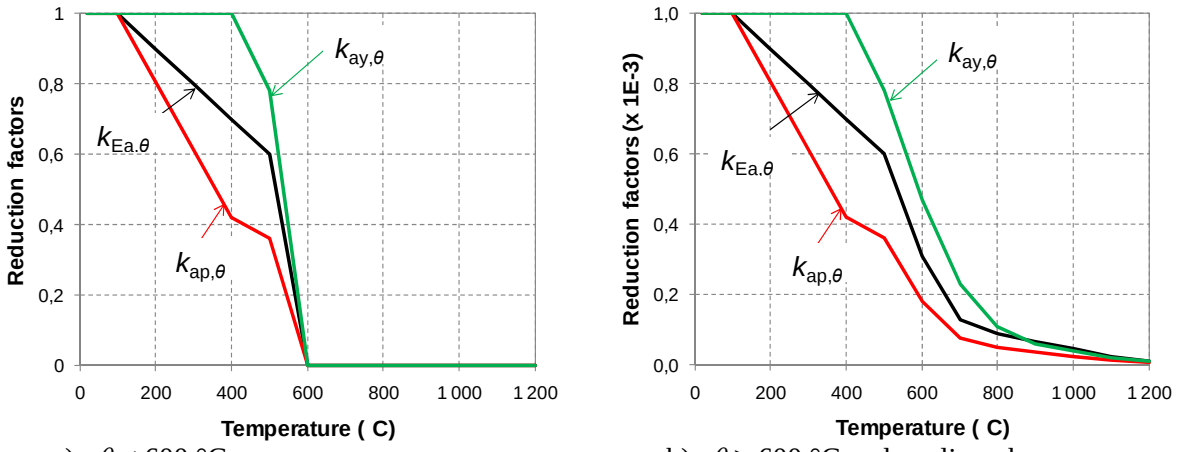

a) $\theta < 600$ °C b) $\theta \geq 600$ °C and cooling phase

Figure 9–1 : Reduction factors of structural steel in unprotected cell beam lower tee

9.1.2. Concrete

Tests on small concrete specimens give an average compressive strength equal to 55 N/m^2, and this value is kept in the test simulation..

9.2. CTICM ANSYS Model

9.2.1. Finite element mesh

The model developed by CTICM is based on that used for FRACOF research project. The whole structure, i.e. the composite slab, the beams, the columns and the shear studs, are modelled. The mesh comprises 3 types of finite elements, with an average size of 500 mm (see Figure 9–2):

- Multilayered shell elements (SHELL91) for the reinforced concrete slab above the steel deck (see Figure 9–3);
- Beam elements (BEAM24) for the concrete ribs, the steel deck, the beams and the columns;
- Pipe elements (PIPE16) for the shear studs linking the beams to the composite slab.

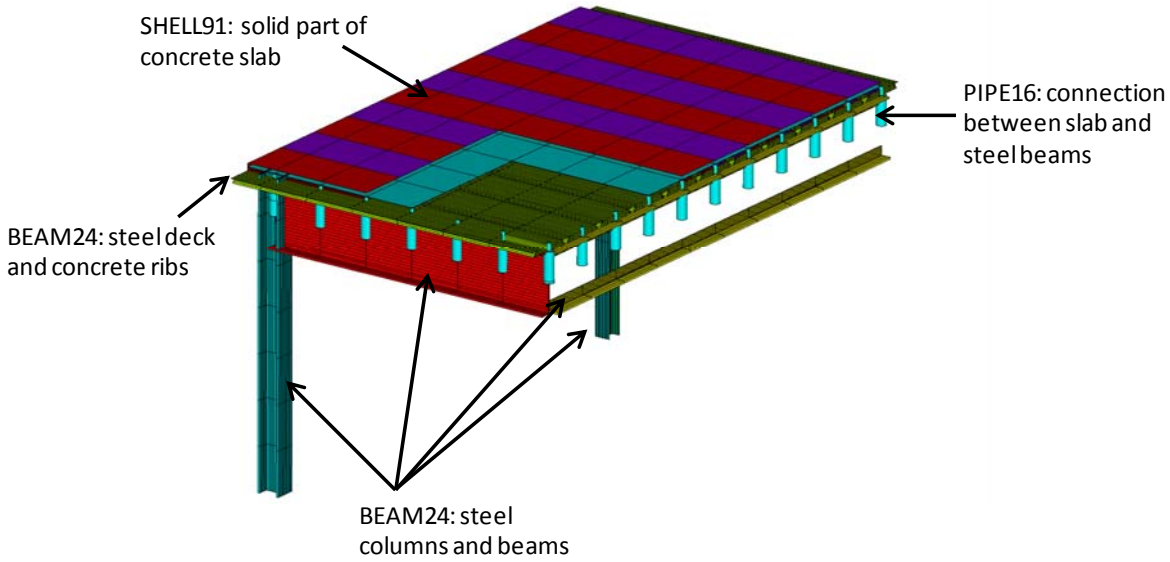

Figure 9–2 : Floor finite element model under ANSYS

Figure 9–3 : Composite slab mesh

As shown in Figure 9–2, the protected cell beams are modelled by considering their gross cross-section, i.e. by infilling all their openings. The unprotected cell beams are modelled by considering their net cross-section, i.e. with a double tee cross-section.

9.2.2. Boundary and load conditions

The boundary conditions applied to the structure are given in Figure 9–4, where:

- X is the horizontal axis parallel to the longer span of the slab;
- Y is the horizontal axis parallel to the shorter span of the slab;
- Z is the vertical axis normal to the slab plane;
- U relates to displacements;
- R relates to rotations.

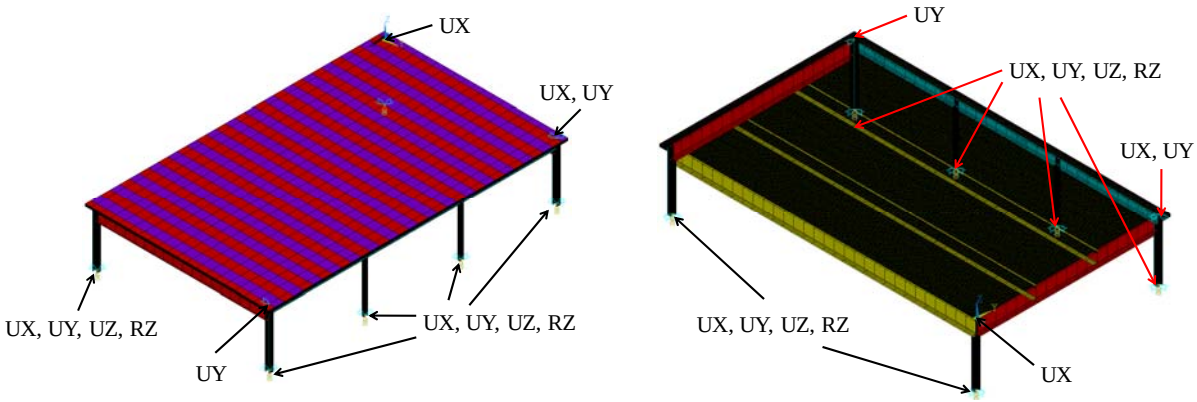

a) Top view b) Bottom view

Figure 9–4 : Boundary conditions

The mechanical load takes account of the 3.25 kN/m^2 fire factored load and the self-weight of the structure, and is applied on the top of the slab.

9.2.3. Temperature distribution

9.2.3.1. Slab

A 2D heat transfer analysis is conducted on the composite slab by dividing the compartment in 3 zones and assuming a fire exposure from beneath (see Figure 9–5). The gas temperature curve in each zone is given by an average fire curve from the test results (see Figure 9–6). Hence, the temperature distribution in a slab section depends on its location (see Figure 9–7 to Figure 9–9).

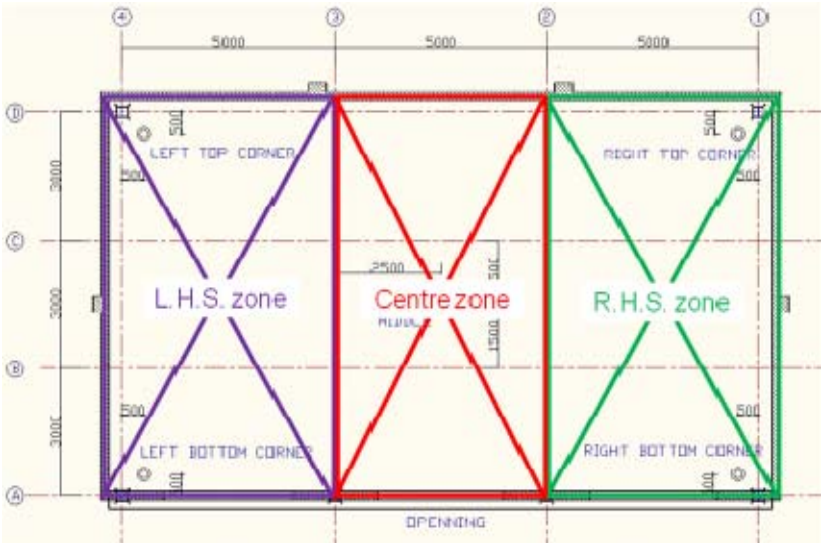

Figure 9–5 : Compartment division

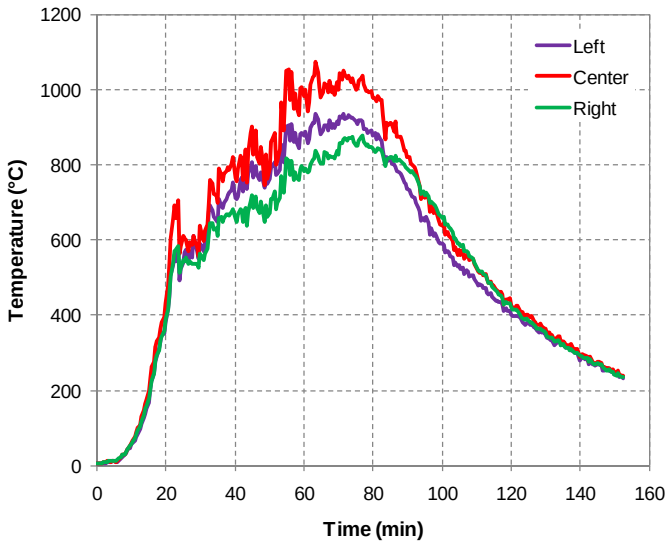

Figure 9–6 : Average fire curves in the compartment

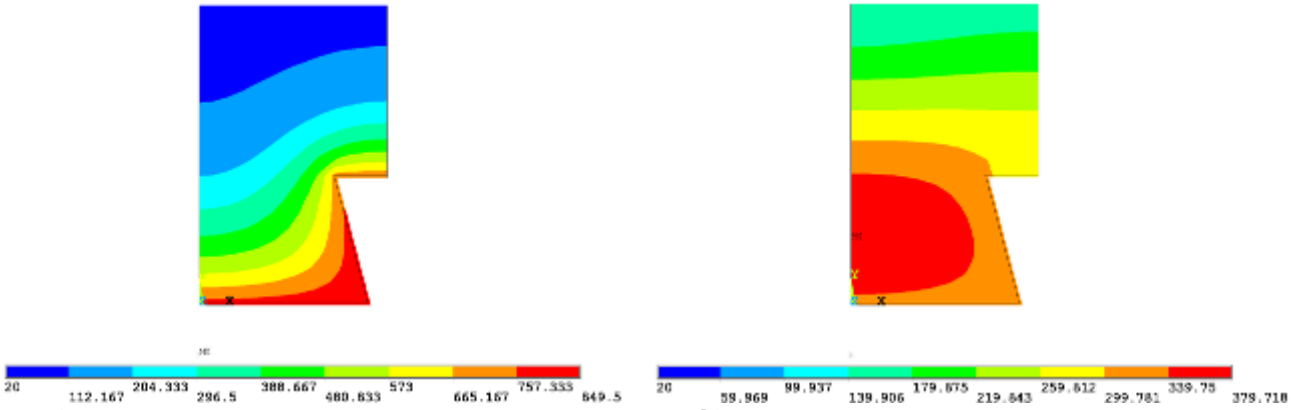

a) t = 75 min b) t = 150 min

Figure 9–7 : Temperature distribution in a R.H.S. slab cross-section (°C)

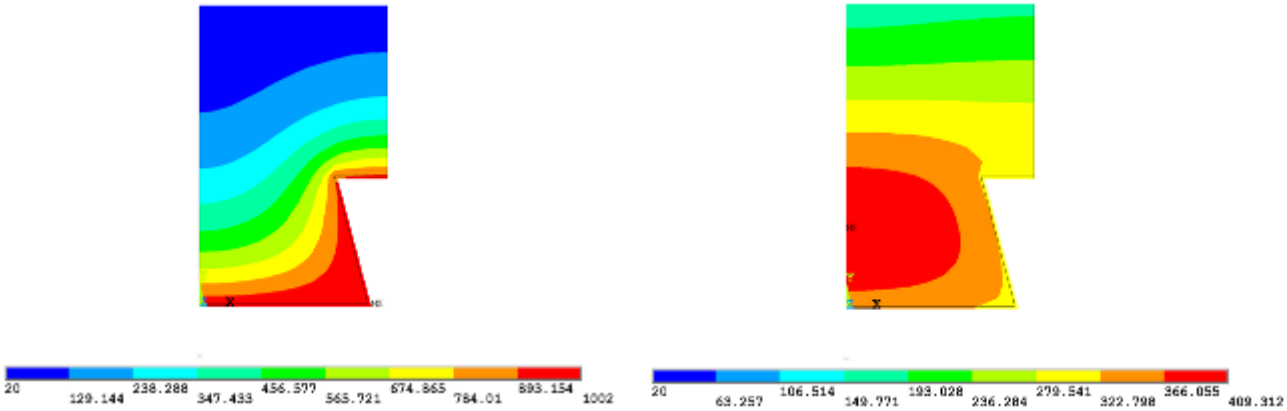

a) t = 75 min b) t = 150 min

Figure 9–8 : Temperature distribution in a central slab cross-section (°C)

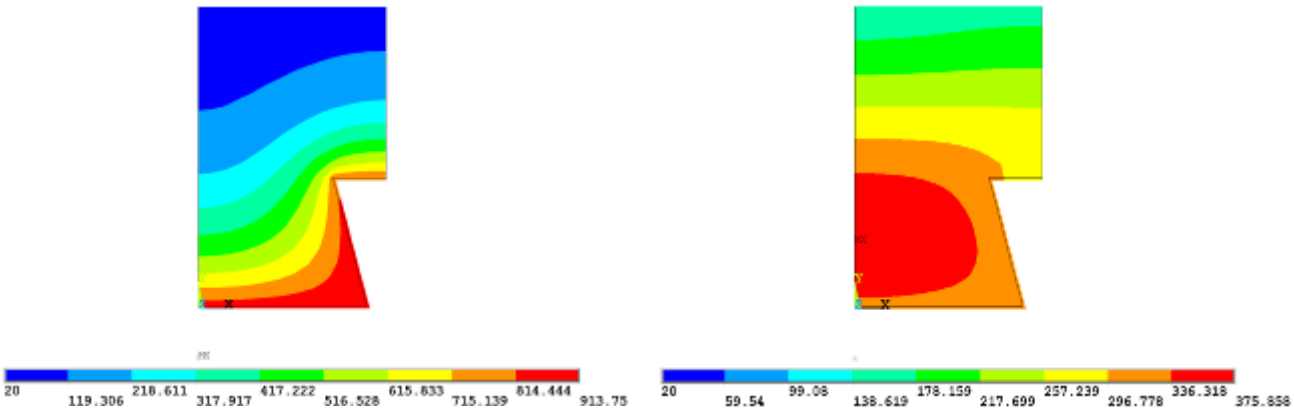

a) t = 75 min b) t = 150 min

Figure 9–9 : Temperature distribution in a L.H.S. slab cross-section (°C)

9.2.3.2. Steel beams

The average temperatures measured on the steel beams during the test are kept in the finite element simulations: no heat transfer calculation is run for the cell beams, whether they are protected or not.
No axial thermal gradient is considered for the protected beams: for each edge beam, all the cross sections are assumed to have the same temperature distribution. The cross section of the solid beams above the openings of the building is assumed to heat up at the same rate as Beam 2, which is the "coolest" one (see Figure 9–10).

The unprotected beams are divided in the same zones as in the tests, allowing simulating an axial thermal gradient (see Figure 9–11 to Figure 9–13).

One can notice that the upper flange is always the coolest part of a given steel beam, as it is connected to the bottom side of the slab. The temperatures of the web and the lower flange are very close. Moreover, the hottest part of the unprotected beams is located in their central zone, confirming that the gas temperature was hotter in this particular zone than on the right and left hand sides of the compartment.

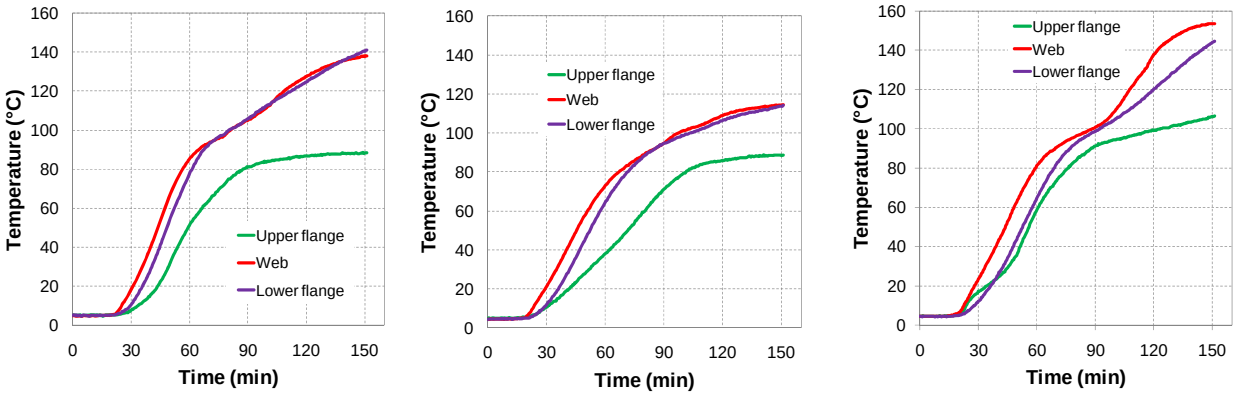

a) Beam 1 b) Beam 2 c) Beam 3

Figure 9–10 : Average temperatures of unprotected beams

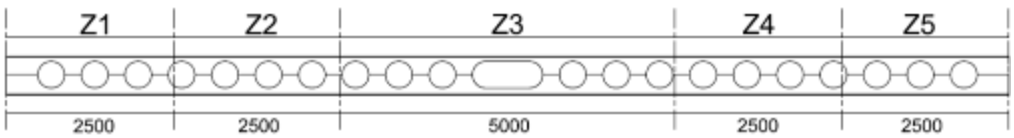

Figure 9–11 : Thermal zones of unprotected beams

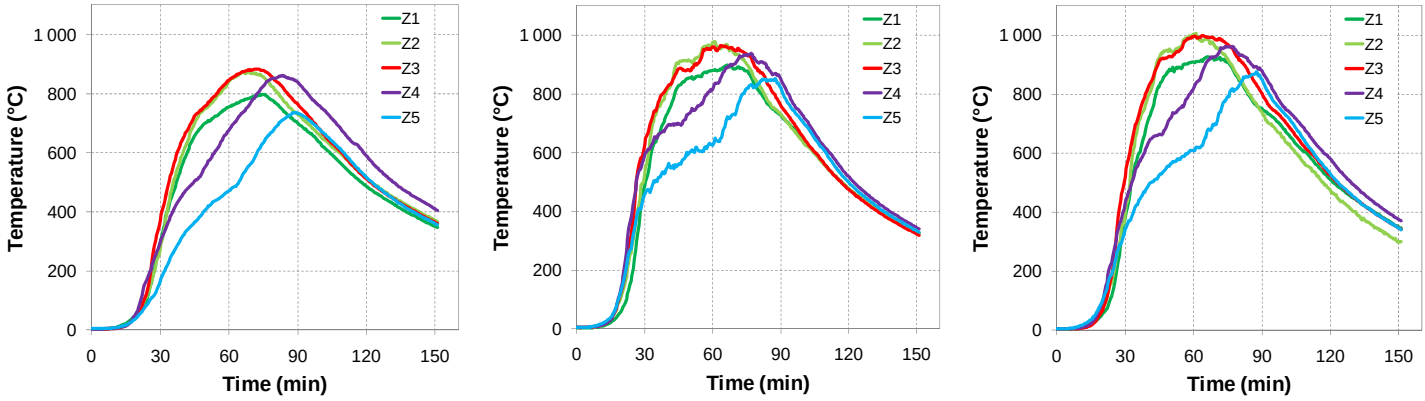

a) Upper flange b) Web c) Lower flange

Figure 9–12 : Average temperatures of Beam 4

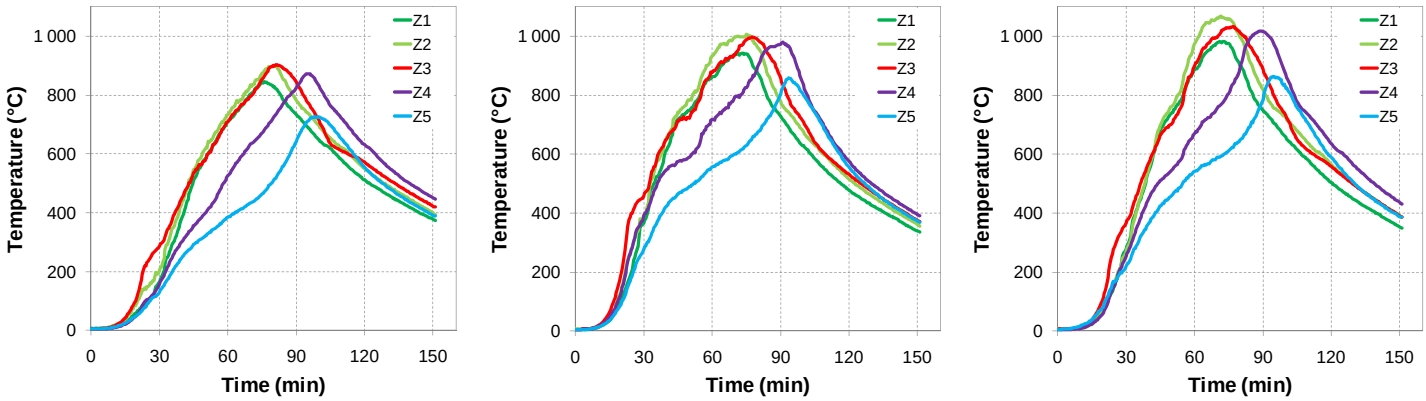

a) Upper flange b) Web c) Lower flange

Figure 9–13 : Average temperatures of Beam 5

9.2.3.3. Columns

As the columns are applied a fire protection that keeps them from heating up, a constant temperature of 20 °C is assumed on all the column sections for the whole test simulations.

9.2.4. Results

9.2.4.1. Temperature field

Slab

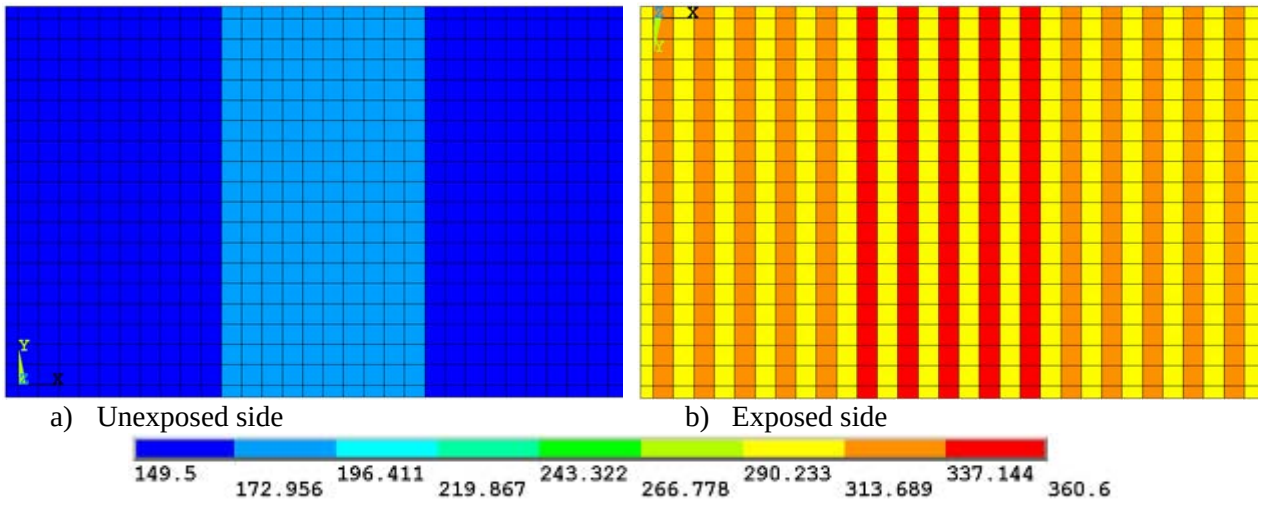

a) Unexposed side b) Exposed side

Figure 9–14 : Temperature field in the solid slab after 150 min (°C)

The temperature distribution after 150 min is given in Figure 9–14. The temperature field on the exposed side of the solid slab shows that the slab cools down more slowly than the gas once heated up, due to its thermal inertia (see Figure 9–6). Also, for each compartment zone, the hottest parts on the unexposed side correspond to the coolest ones on the exposed side. They are located just above the gaps of the composite slab, i.e. in its thinnest zones (see also Figure 9–7 to Figure 9–9).

Beams and columns

The temperature distribution in the structural steel elements is given in Figure 9–15. One can see that the protected elements cool down to less than 150 °C, while the unprotected beams remain rather hot, with temperatures higher than 400 °C. One can also notice that the hottest zone of Beam 4 is not located in its central part, according to the thermal behaviour given in Figure 9–12 (t = 150 min).

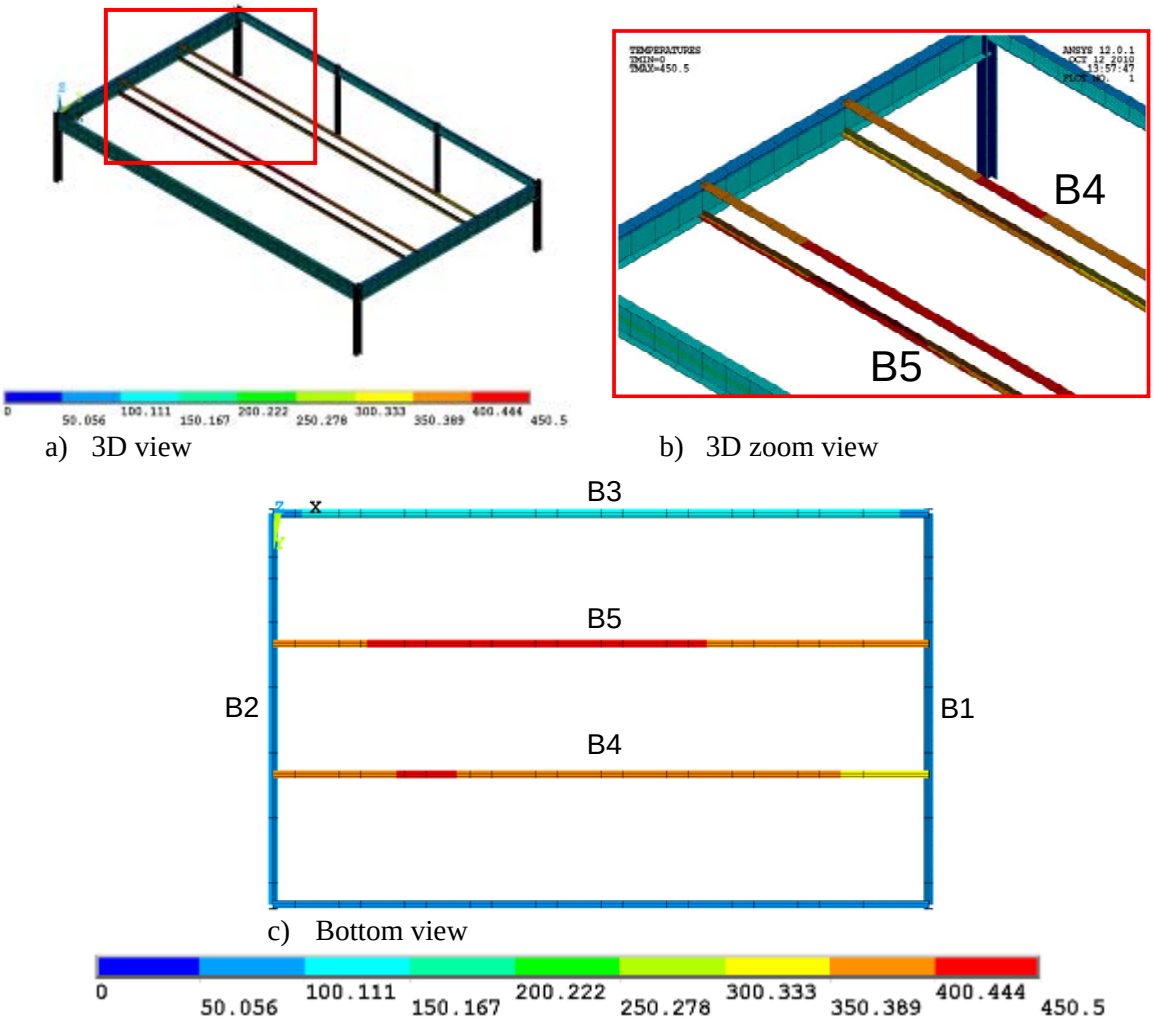

a) 3D view b) 3D zoom view

c) Bottom view

Figure 9–15 : Temperature field in the beams and columns after 150 min (°C)

9.2.4.2. Deformed shape and deflections

The vertical displacements at the end of the two simulations are given in Figure 9–16 and Figure 9–17.

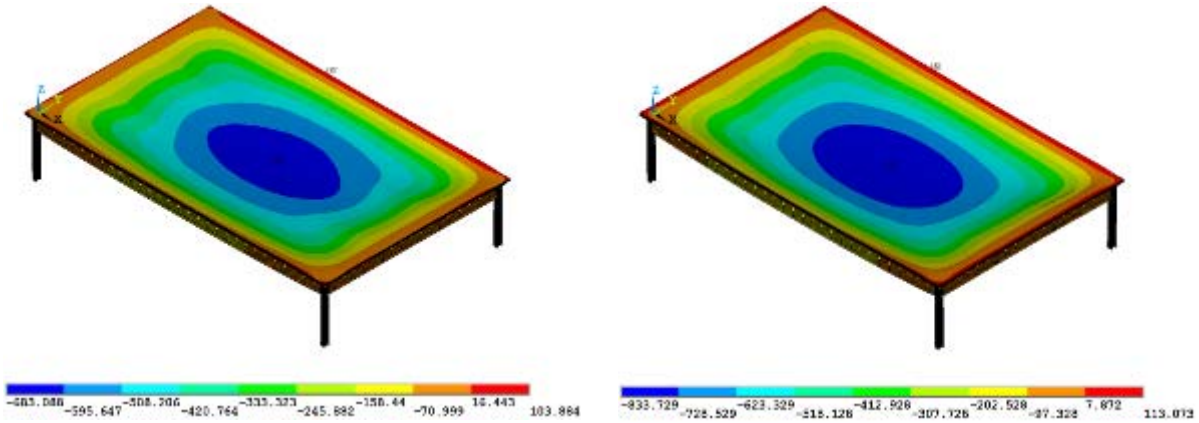

a) Model 1 b) Model 2

Figure 9–16 : Vertical displacements of the whole structure after 150 min (mm)

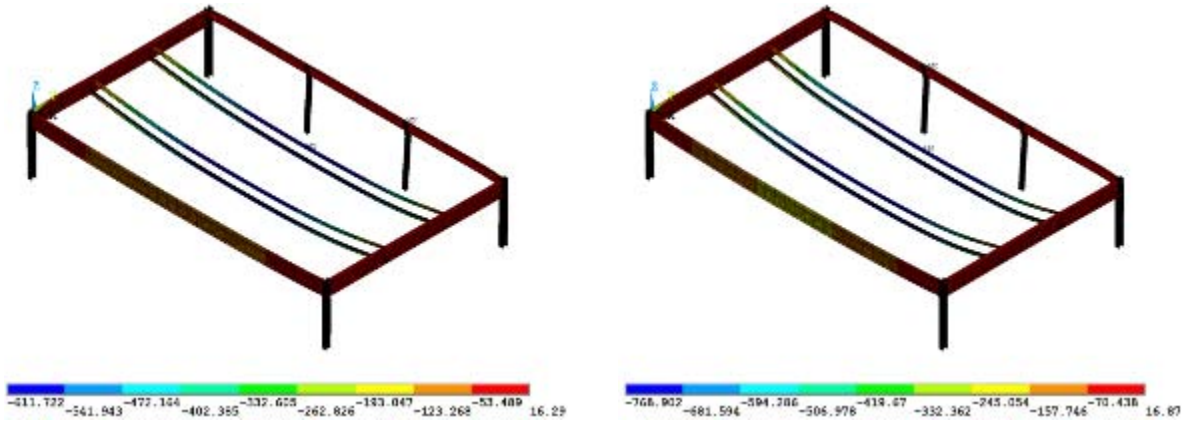

a) Model 1 b) Model 2

Figure 9–17 : Vertical displacements of beams and columns after 150 min (mm)

The maximum displacements are observed in the middle of the slab, while the minimum ones are observed on the edge beams. Indeed, these beams do not really move, which shows that the edge support is maintained for the entire fire duration. However, according to Figure 9–18 and Figure 9–19, one can see that, for the first 15 min, the primary beams bend a little down, while the edge cell beam bends up. Then, the latter starts bending down, while the former bend up, as if their mechanical load is reduced. The three protected cell beams recover their initial deformed shape at the same time, i.e. 23 min, when they start to heat up. Furthermore, Beam 3, which has a less stiff cross-section than the primary beams, undergoes much greater displacements than the latter.

At this particular time, the maximum temperature in the unprotected beams exceeds 200 °C, and the deflection of the floor is equal to 100 mm, for both test and simulation (see Figure 9–20). Then, the analysis deflection rate becomes greater than the experimental one, for all the secondary beams, protected or not, until the deflection reaches a peak very close to the test. Regardless of their location, all the beams start bending up at the same time, i.e. around 70 min.

At this moment, the deflection of Beam 4 and Beam 5 are rather close to the experimental peak values, especially when the lower tees are not neglected. On the other hand, an irreversible loss of strength causes greater deflections on the whole floor, which do not really decrease in the cooling phase.

Hence, in spite of a lag between the simulation and the test, the global behaviour of the structure can be achieved by the proposed finite element model (see also Figure 9–21). This lag is probably due to an overestimate of the lateral compartment temperatures, leading to unsafe results in terms of thermal behaviour of the slab.

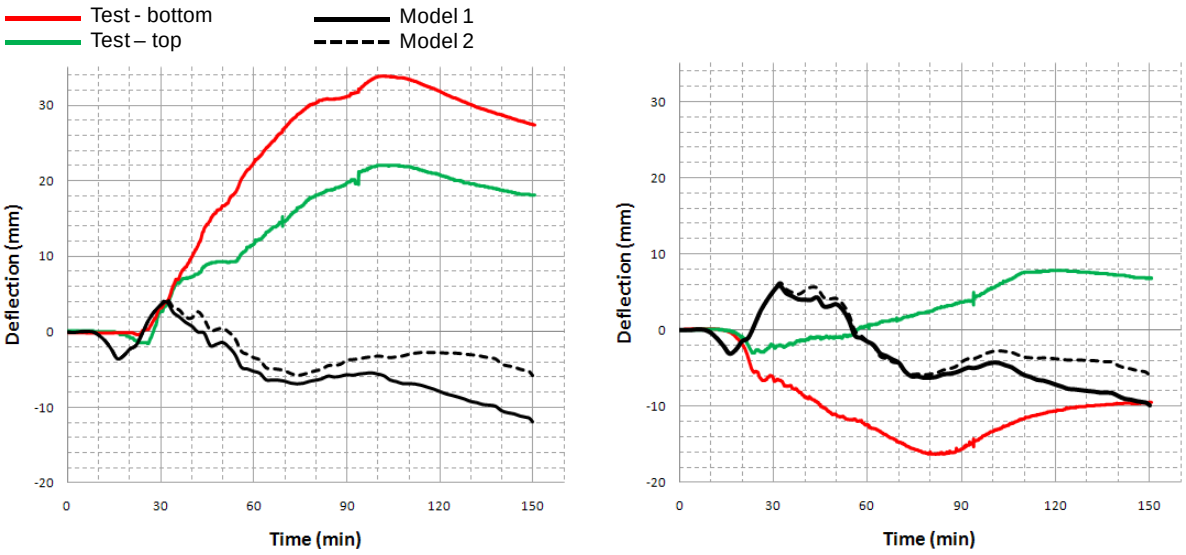

a) Beam 1 b) Beam 2

Figure 9–18 : Deflection of primary beams vs. Time

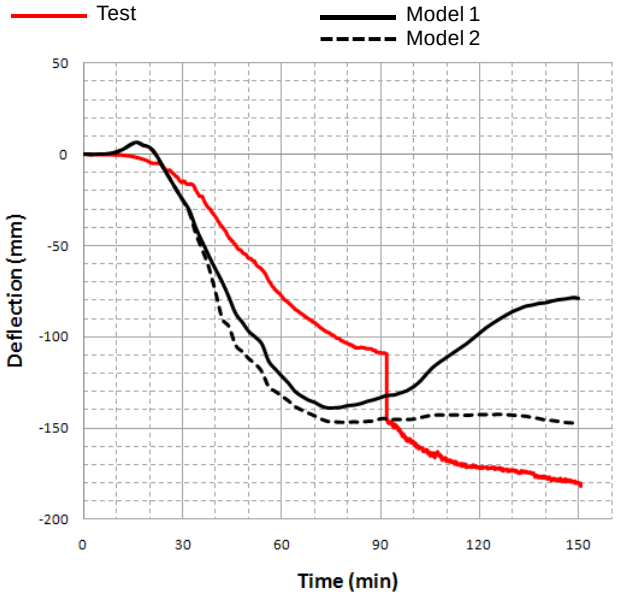

Figure 9–19 : Deflection of Beam 3 vs. Time

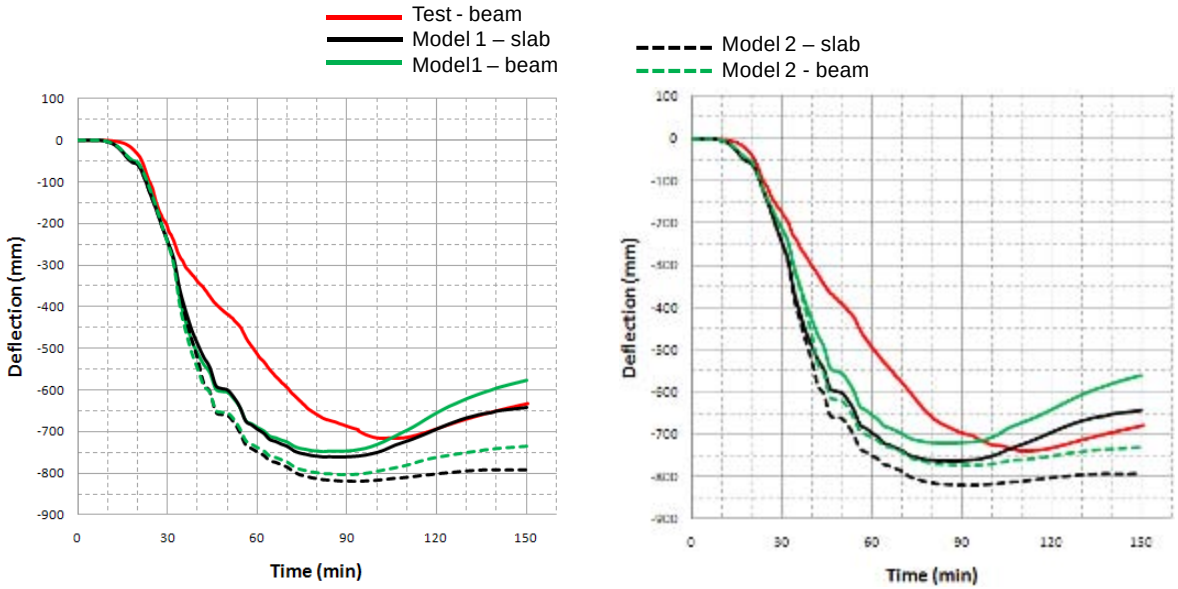

a) Beam 4 and slab b) Beam 5 and slab

Figure 9–20 : Deflection of the unprotected beams and the slab vs. Time

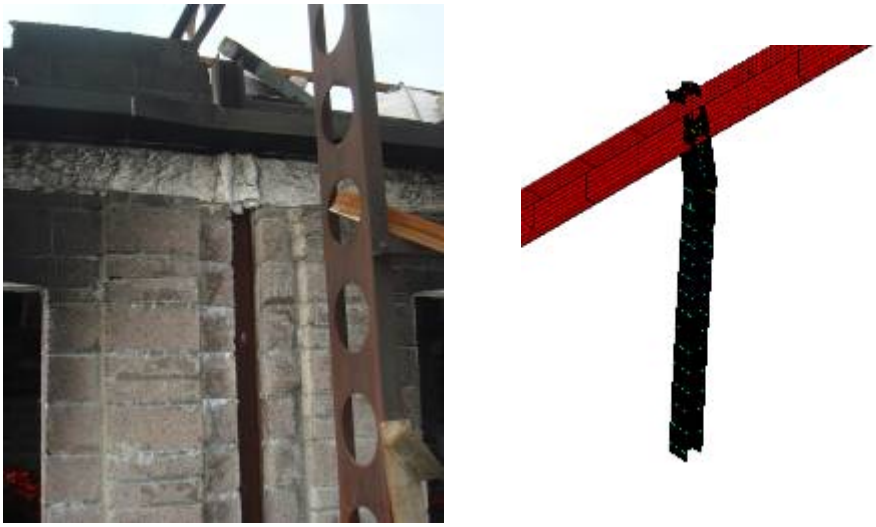

a) Test b) ANSYS simulation

Figure 9–21 : Deformed shape of one front column

9.2.5. Conclusion

The experimental results were used to calibrate a finite element model under ANSYS. The unprotected cell beams were modelled using a double T cross-section, and two cases were studied. In the first one, the steel of the whole cross-section followed the stress-strain relationships given in EN 1994-12, whereas the lower tees had an irreversible loss of mechanical strength from 600 °C in the second one. A good correlation between the test and the numerical simulation in terms of displacements and global behaviour was observed. Yet, considering an irreversible behaviour provided less safe results in terms of deflections.

9.3. ULg SAFIR - Ozone Model

9.3.1. Model of the fire

The fire was started from a single ignition source (Figure 9–22). After 5 minutes two additional ignitions sources were started in different places and the rest of cribs were left to ignite naturally. Each crib was connected to its neighbours by mild steel channel section with porous fibre board laid into the channels and, approximately 30 minutes before ignition, some 20 litres of paraffin was poured into channel.

Figure 9–22 : Ignition and fully engulfed fire

A blind prediction of the temperature development was made using the software OZone with the following hypotheses:

- The fire load density: 570 MJ/m²
- Combustion model: extended fire duration
- Fuel height: 0.5 m
- RHRf: 1250 kW/m²
- Combustion heat of fuel: 17.5 MJ/kg
- Fire growth: medium
- Combustion efficiency: 0.8

As the fire test was conducted with a fire load of 700MJ/m², a second calculation was performed with this fire load without changing other parameters. Figure 9–23 shows the comparison between the measured temperatures in the compartment and the OZone predictions. Considering a fire load of 570MJ/m², the maximum temperature reaches 884°C whereas with the fire load of 700MJ/m², it reaches 921°C. The calculated fire curve has been delayed by 5 minutes in order to fitting with real flash over.

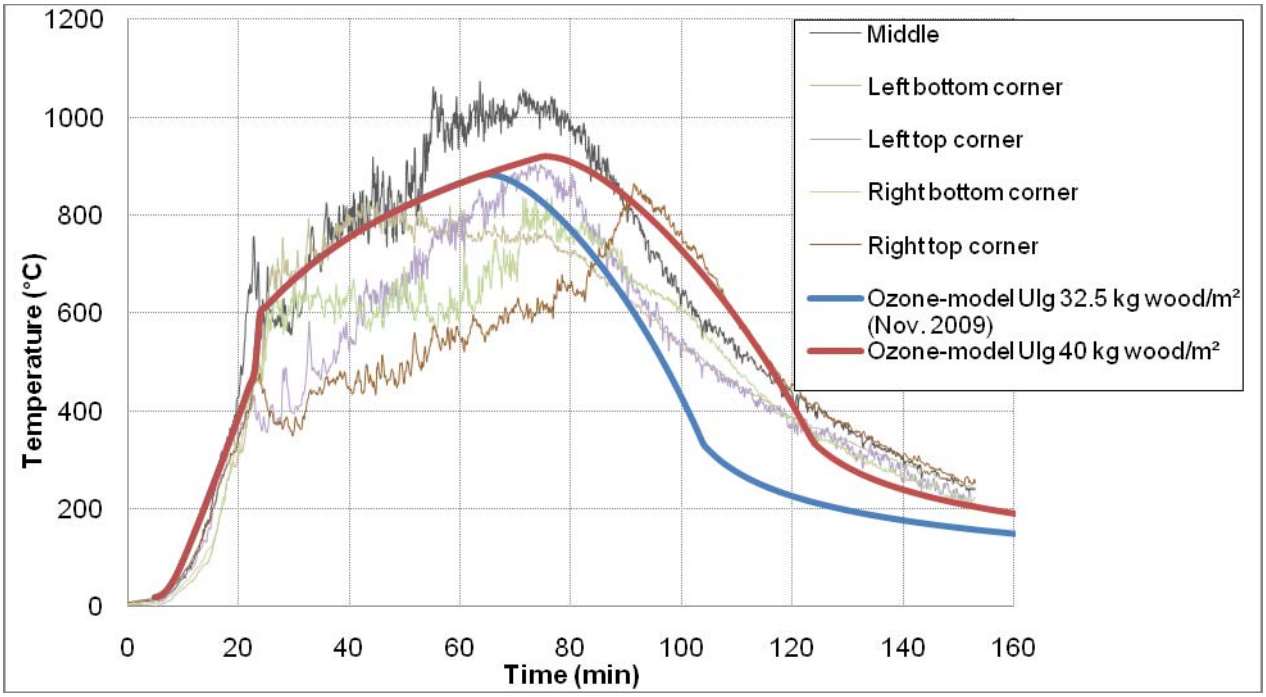

Figure 9–23 : Measured temperatures in the compartment VS Ozone prediction

9.3.2. Beam thermal analysis

9.3.2.1. Description of the numerical model

The software SAFIR has been used for the thermal analysis. Solid finite elements are used to model the steel profiles. The two central beams being unprotected, the shadow factor is calculated and its value is k_{shadow} = 0,716. The material used is steel according to EN1993-1-2 in which:

- convection coefficient on hot surfaces is 35.0 W/m²K for unprotected sections and 25. W/m²K for protected sections
- convection coefficient on cold surfaces : 4.0 W/m²K
- relative emissivity is 0.7 for unprotected sections and 0.5 for protected sections

The steel profiles are cellular beam profiles. As the section that is here analyzed thermally is then used as the section of a beam finite element in the subsequent structural analyses, a section passing through the center of a circular opening is considered. Indeed, the longitudinal stresses of a beam model cannot “enter” in the web posts that separate two openings.

The concrete slab is modeled in order to take into account its capacity of absorbing heat. The material used for the concrete slab is siliceous concrete according to EN1992-1-2 with a specific mass of 2400 kg/m³, a moisture content of 72 kg/m³, a convection coefficient on hot surfaces of 35 W/m²K, a convection coefficient on cold surfaces of 4 W/m²K, a relative emissivity of 0.8 and a parameter for thermal conductivity of 0.5. The concrete above the upper flange of the steel profile is only considered for thermal analysis. The thermal concrete has no mechanical resistance. The steel profiles and the bottom face of the slab are submitted to the calculated fire while the upper face of the slab is submitted to a frontier condition F20, i.e. that the upper face remains in contact with gas at 20°C during all the calculation.

The temperatures reached in the unprotected section are much higher than the critical temperature for such cellular beams. Indeed, when performing a structural analysis of such beams using shell elements, instabilities (mostly web post buckling or distortional buckling) can be observed for temperatures around 600°C. So, the structural model of the unprotected sections should take into account the fact that their behavior is affected by web post buckling. A simple way to take this

phenomenon into account, while keeping beam elements in the structural model, is to model only the upper tee of the section. Obviously, the deflection at room temperature will be much higher than the real one; but at high temperature, the behavior should be more accurate with this model. In the predictive model, the simulations have been performed twice for each parametric case: once with the whole section as shown and once with only the upper tee (Figure 9–24), to represent the section after web post buckling. After the test, the simulation was performed using a modified steel material for the bottom flange of the unprotected beams. This modified steel material has the same mechanical properties as the steel from EN1993-1-2 under 500°C and loses irreversibly its mechanical properties between 500°C and 600°C, to take into account the instability phenomenon.

Figure 9–24 : Double tee section (left) and upper tee section (right)

For the protected sections, the insulation material is modeled. Solid finite elements have been used for the insulation material, which was only considered for thermal analysis. The insulation material has no mechanical resistance. The protected steel sections are affected by the fire on one side and on the bottom flange, while the other side of the profile, in front of a wall, is supposed to be an adiabatic boundary (Figure 9–25). The temperatures in the protected sections remained below the critical temperature for these cellular beams so that the model with only the upper tee had not to be considered for the protected sections.

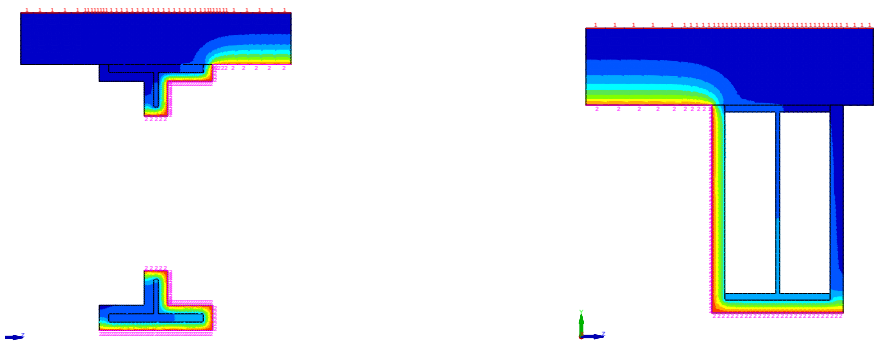

Figure 9–25 : Temperature distribution in the protected sections

The fire protection of cellular beams is a key parameter that is determinant for ensuring a good membrane effect of composite floor system in case of fire. Several thermal analyses have been performed before the test in order to take into account the uncertainty on the thermal properties of the fire protection.

9.3.2.2. Results

The predictive thermal analysis of the unprotected beams has been launched before the test using the predictive fire curve in Figure 9–23. After the test, the simulation was launched again using the measured temperatures in the middle of the compartment. The computed results are compared with measured data in Figure 9–26.

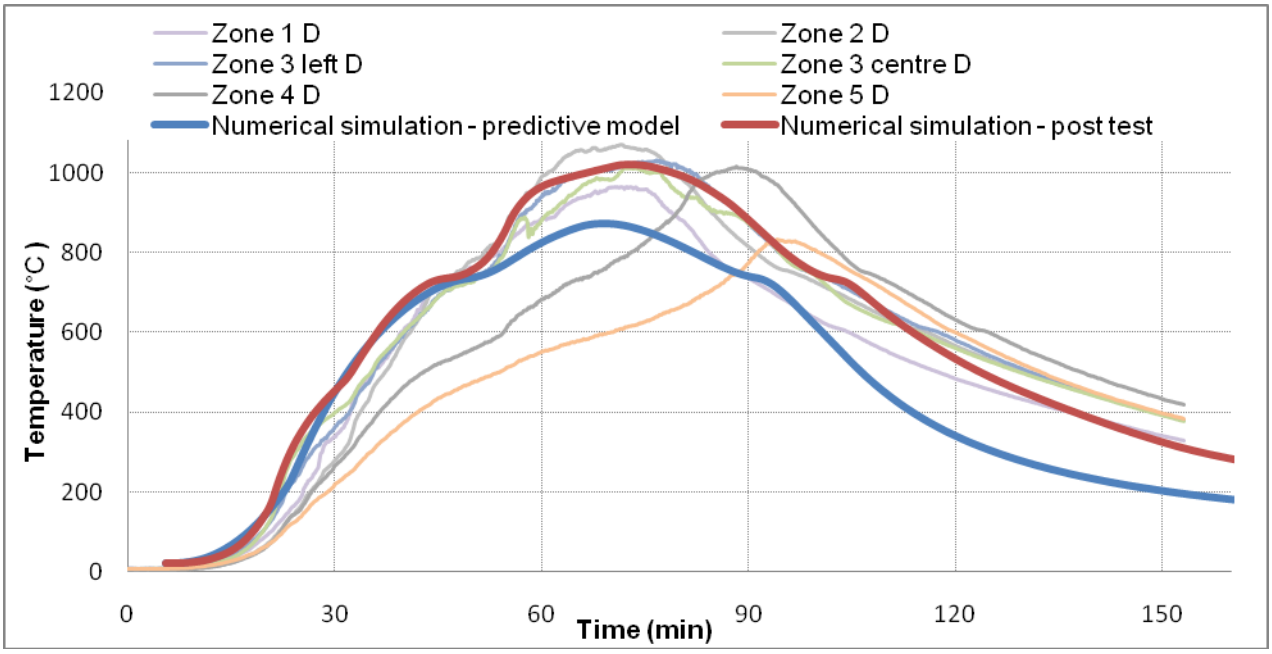

Figure 9–26 : Unprotected beam 5 – Thermal analysis

For thermal analysis of the protective edge beams, the simulation performed before the test considered conservative values for the thermal conductivity of the protective material because of the uncertainty on this parameter. Finally the protective material used during the test was more insulating than initially predicted. After the test, the thermal properties of the protective material were calibrated to fit with the measured temperatures on the protected sections. The results are given in Figure 9–27, compared with predictive numerical results and measured results.

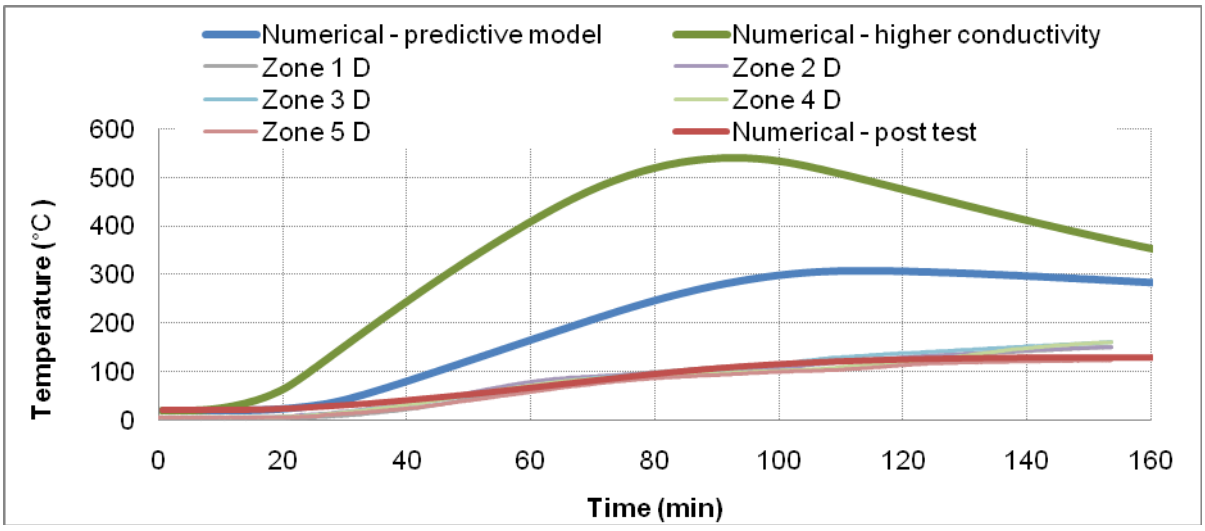

Figure 9–27 : Protected beam (beam 3 zone 4) – Comparison between computed and measured temperatures

9.3.3. Slab thermal analysis

9.3.3.1. Description of the numerical model

For thermal analysis, the effective thickness model for the slab as defined in Eurocode EN1994-1-2 has been used. This effective thickness represents the height of the slab to consider for the thermal response. The height to consider for mechanical calculation is the concrete height above the steel deck. Here, the height of the structural concrete is 69.0 mm and the height of the thermal concrete (see EN

4.2) is 41.6 mm (Figure 9–28). It was verified that the geometric properties of the composite slab are in the field of application of the formula. The thermal properties of concrete have been given previously. The slab is submitted to the fire on its lower face and to a frontier condition F20 on its upper face, i.e. its upper face remains in contact with a gas at 20°C. Due to this model of the slab with an effective thickness, for the structural analysis, there is a gap of 120-110=10mm between the upper flange of the steel sections and the bottom surface of the slab.

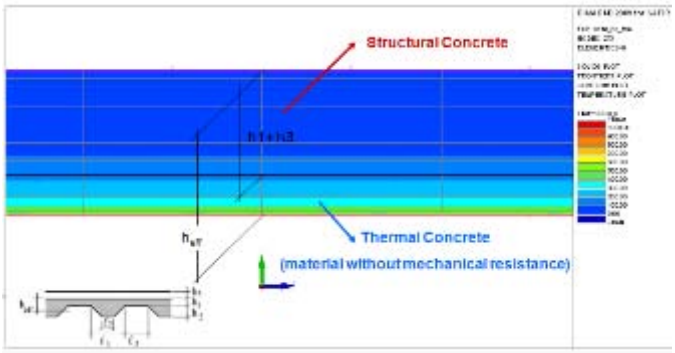

Figure 9–28 : Effective thickness calculation for the slab thermal analysis

9.3.3.2. Results

The temperatures in the slab were recorded at different locations and different height across the section (Figure 9–29). After the test, the numerical calculation was launched again considering the uniform thickness slab model and the measured fire. In Figure 9–30 and Figure 9–31, the computed temperatures are compared with the measured temperatures in the slab above the rib. For the two considered height above the rib (A3, A4), three measures are given corresponding to three plan location. A-4 corresponds to the steel rebars location. The computed temperatures matches well the measured temperatures.

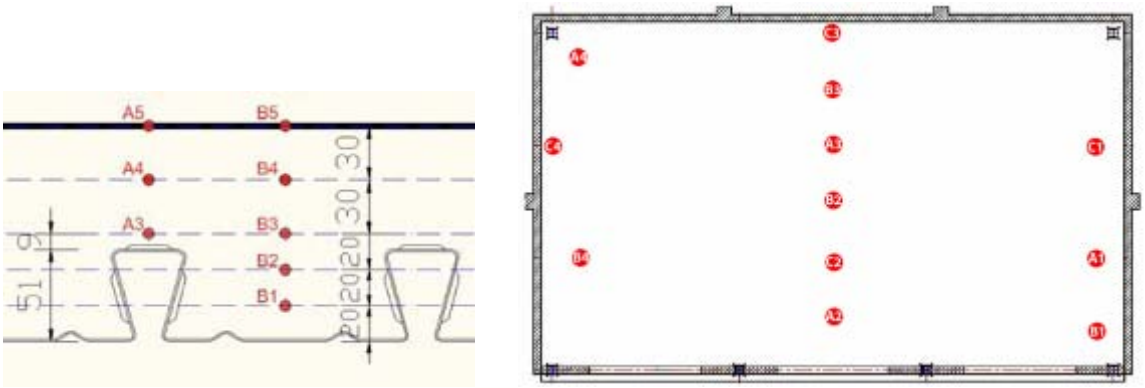

Figure 9–29 : Thermal couple locations at slab cross and thermal couples plan

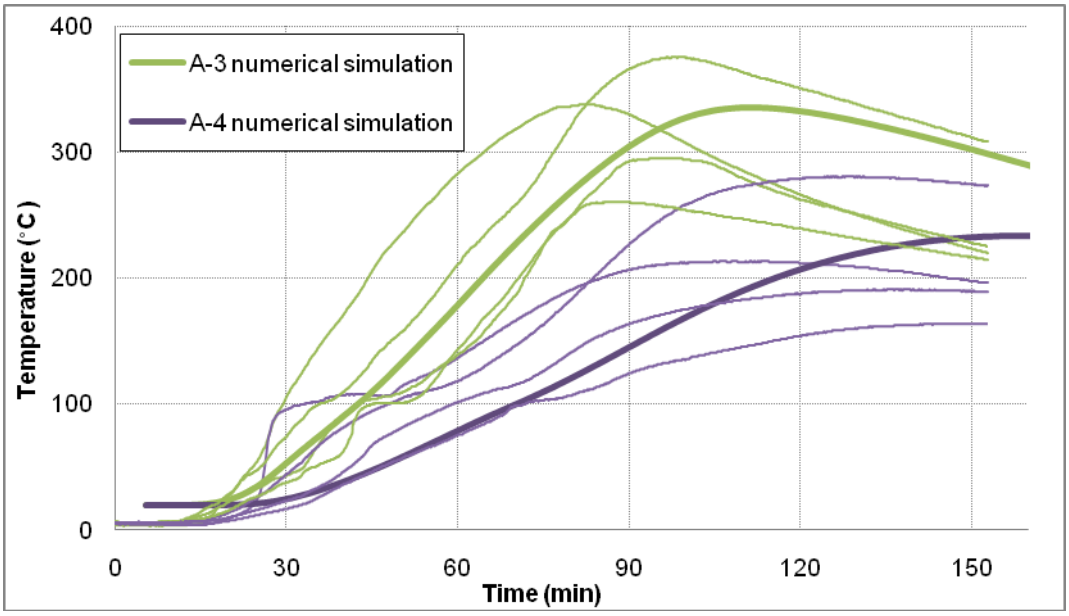

Figure 9–30 : Heat transfer in zones A1, A2 and A3 at height A-3, A-4 and A-5 through cross section. Comparison between measured and computed results.

In Figure 9–31, the computed temperatures are compared with the measured temperatures in the plain cross section (B). The temperatures at 20 mm above the lower face of the slab (B-1) are overestimated by the numerical simulation compared with the corresponding measured temperatures. However for the temperatures at 60 mm (B-3) and 90 mm (B-4) above the lower face of the slab, the numerical simulations show a good correlation with measured results. As B-4 corresponds to the steel rebars location, the temperatures in the steel rebars are well approximated by the numerical results with the uniform thickness method.

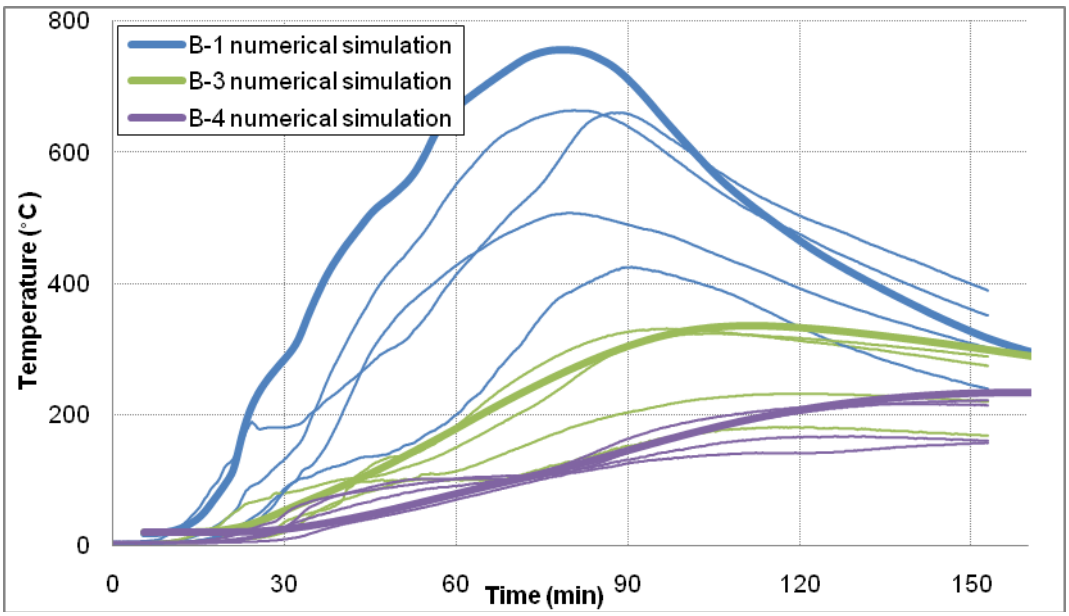

Figure 9–31 : Heat transfer in zones B1, B2, B3, B4 at height B-1, B-3, B-4 through cross section. Comparison between measured and computed results.

9.3.4. Structural analysis

9.3.4.1. Description of the numerical model

A finite element model was built in the SAFIR software. The structure is modelled using BEAM elements for the beams and SHELL elements for the slab. The edge beams are simply supported on the columns as indicated in Figure 9–32. The slab and the beams are axially unrestrained. The material used for the beams is steel according to EN1993-1-2 with yield strength of 355 MPa. The material used for the slab is siliceous concrete according to EN1992-1-2 with compressive strength of 55 MPa. The slab has a reinforcement mesh of 393 mm²/m in both directions.

The structural behaviour at room temperature is a flexional mode whereas during the fire, membrane action occurs (Figure 9–32). The membrane forces for room and elevated temperatures can be observed in Figure 9–33.

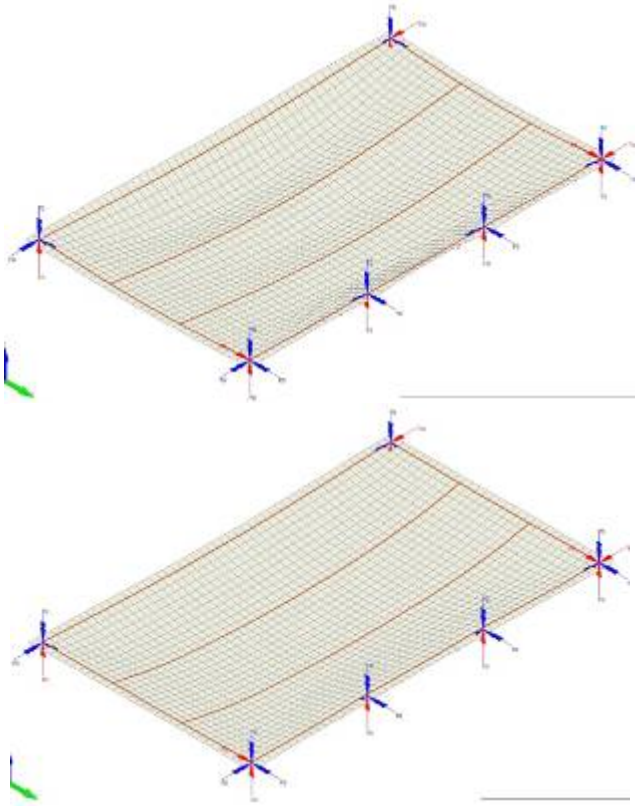

Figure 9–32 : Deformed shape at room temperature (bending mode amplified x15, left) and at elevated temperature (membrane mode x1, right)

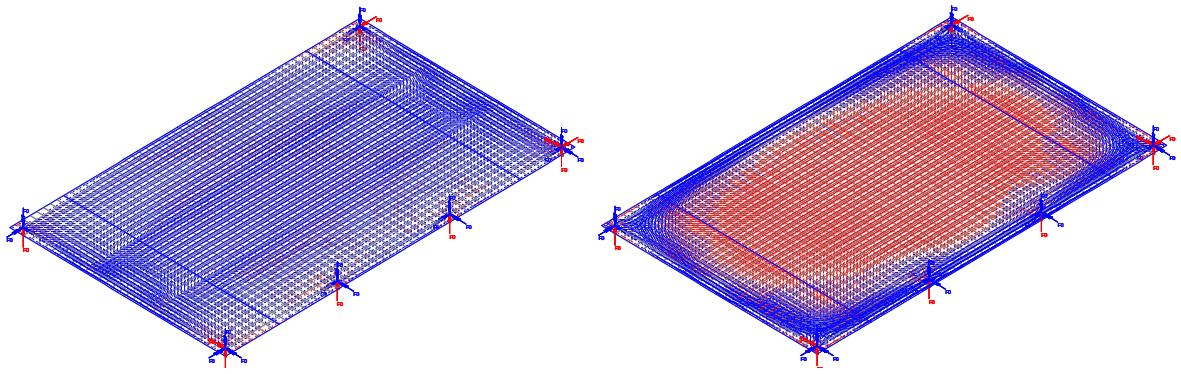

Figure 9–33 : Comparison between bending mode (left) and tensile membrane action (right): membrane forces within the slab

The model was made blind before the test in order to predict the behaviour of the structure. As BEAM finite Element does not allow taking into account the web post buckling instabilities, the simulation was run twice, once with cellular beams modelled as the double tee section and once as only the upper tee section (Figure 9–24). This leaded to two curves for the modelling of the structural behaviour. The lower curve in Figure 9–34 is obtained by modelling only the upper tee of the unprotected beams, what is justified by the fact that web post buckling will appear in these sections and will prevent the bottom tee from playing any structural function. In this case the deflection at room temperature has no physical signification since the real contribution of the secondary beam is largely underestimated. But in fire situation, the results are interesting. For example, it can be observed that the deflection does not decrease when the temperature decreases, because the steel profiles do not recover their stiffness. This model can be considered as a reasonable model for a simulation of such type of floor system in the fire situation since the cellular beams, after the web post buckling, will probably not be able to recover their initial stiffness when the temperature decreases.

After the test, a new numerical simulation was launched using a special material for the bottom flange of the unprotected beams. Indeed, the considered material has the same mechanical properties as the steel from EN1993-1-2 under 500°C but it loses irreversibly its material properties between 500°C and 600°C, to take into account in a simplified way the instability phenomenon. Considering this modified steel material allow for a modelling of the structural behaviour during the entire test with one single numerical calculation. The numerical calculation with the hybrid model was performed first using the same data as in the predictive model, in order to compare the hybrid model with the double tee and simple tee models. Then, the structural calculation was performed again using the hybrid model and the thermal results obtained after the test.

As it can be seen in Figure 9–34, the structural calculation obtained with the hybrid model using the same data as the predictive model gives exactly the same behaviour as the double tee predictive model during approximately 30 minutes. After 30 minutes, the temperature of the bottom flange of the unprotected profiles overreaches 500°C. Then, the bottom flange loses quickly all mechanical properties and the deflection becomes much higher than with the double tee model. However, the obtained deflection is still lower than with the simple tee model. The hybrid model with measured temperatures gives lower maximal deflection than the hybrid model with predicted temperature, which is mostly due to the fact that the protective material used for the edge beams was more insulating than initially predicted.

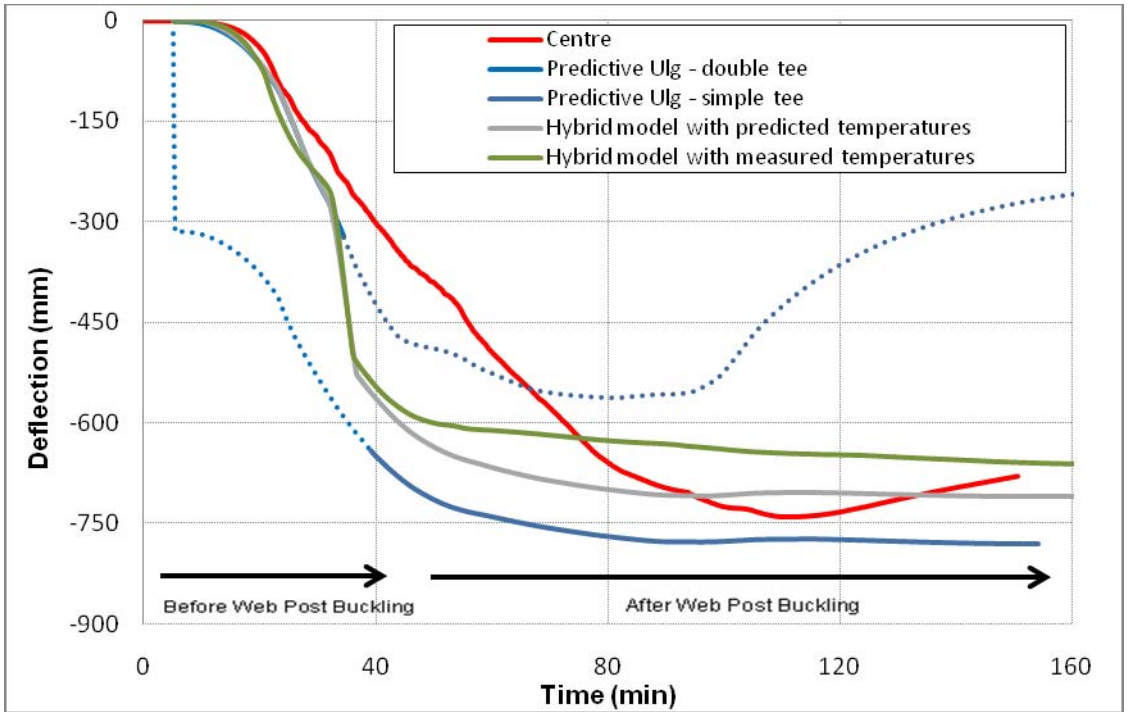

Figure 9–34 : Comparison between computed and measured results of the vertical deflection of central beam 5

Figure 9–34 shows a good correlation between the FEM model and the real behaviour of the test. Of course, some differences remain. The differences can be explained principally by two factors: the simplifications in the model and the considered values of the data, different from the measured values. Examples of simplifications are the modelling of the instability phenomenon of the unprotected beams and the modelling of the columns as perfect vertical supports. Differences in the data concern mostly the temperatures in the structural members. But the results already give some confidence that this model is capable of predicting the fire behaviour of such type of floor system with a satisfying level of accuracy. It would also be possible to model the steel cellular beams in detail with shell elements, but such model would be too large for practical applications.

9.3.5. Conclusion

This fire test provided a unique opportunity to study the behaviour of long cellular steel beams in a complete compartment office in building structure under realistic fire conditions. The objective of WP6 was to perform predictive numerical simulations of the test in order to define the appropriate structure to be used for the full scale fire test. The predictive results had shown that the structure would be able to withstand the test without collapse, reaching maximal deflections of the order of 70 cm. The test was very successful, fire was more intense and of longer duration that assumed in the initial studies yet the structure performed as predicted. As shown in the numerical simulations, it appeared clearly during the test that the fact to use cellular beams to support the composite slab does not jeopardise the tensile membrane action that develops in the slab in a fire situation.

The Ozone model provides a rather good estimation of the fire development, provided that the correct amount of fire load is introduced.

The thermal analysis performed with SAFIR gave good estimation of the temperature distribution in the steel profiles and in the slab. However, the results are strongly related to the estimation of the fire. For protected steel profiles, the thermal properties of the protective material are a key issue. For the slab analysis, the effective thickness method has been shown to give good results for the temperature distribution inside the section, especially near the steel rebars location.

The SAFIR structural model was capable of predicting with an acceptable level of accuracy the complex behaviour of cellular beams acting in membrane action. Using a modified steel material for the bottom flange of the unprotected cellular beams can be a simplified but efficient way for taking into account the instability phenomenon in such complex models where BEAM elements are preferable for the beams.

9.4. Design guide

The first part of the design guide will be devoted to the description of the simplified calculation method developed in WP4 to assess the resistance of cellular beams in fire conditions. This method has been implemented in the Software ACB^{+} [22] available for free on www.arcelormittal.com/sections.

The second part of the design guide will be devoted to the improvement of the Bailey's method to long span cellular beams.

Large-scale fire tests conducted in a number of countries and observations of actual building fires have shown that the fire performance of composite steel framed buildings is much better than is indicated by fire resistance tests on isolated elements. It is clear that there are large reserves of fire resistance in modern steel-framed buildings and that standard fire resistance tests on single unrestrained members do not provide a satisfactory indicator of the performance of such structures.

The document annexed presents guidance on the application of a simple design method, as implemented in FiCEB design spreadsheet, that has been developed as a result of observation and analysis of the BRE Cardington large-scale building fire test programme carried out during 1995 and 1996 and thanks to this project on floor slabs containing cellular beams. The recommendations are conservative and are limited to structures similar to those tested, i.e. non-sway steel-framed buildings with composite floors. The guidance gives designers access to whole building behaviour and allows them to determine which members can remain unprotected while maintaining levels of safety equivalent to traditional methods.

In recognition that many fire safety engineers are now considering natural fires, a natural fire model may be inputted or calculated using the parameteric fire method from EN1991-1-2. These options are included alongside the use of the standard fire model; all three are expressed as temperature-time curves.

10. CONCLUSION

The aim of this project was to develop uniform European design rules for protected and unprotected cellular beams (CB) constructed of rolled sections subjected to fire. The use of cellular beams (CB) will be increased by minimising and optimising the cost of fire protection and by allowing a wider use of unprotected CB. This will greatly benefit long span construction, and increase market share of steel.

These results will be achieved based on the development of a new design code of single CB submitted to fire as well as an extended methodology considering the whole floor structure and the beneficial effects of the adjacent members.

The reliability of the developed tools was based on large scale tests in order to provide a cost effective design methodology. A set of practical design recommendations was developed in order to satisfy all the requirements of fire safe engineering.

This project was divided into two different large parts. The first part was devoted to the development of a simplified calculation model for the assessment of the cellular beam made of hot rolled sections in case of fire and the second part was devoted to the general behaviour of the whole floor structure in membrane action taking into account the specificities of cellular beam.

Part 1: Simply supported cellular beam

A first task was to obtain and collate all available heating rate data on cellular type beams, including intumescently coated, passively protected and bare steel cellular sections. This database was used, in a first time, to calibrate Finite Element Model, and in a second step to define the furnace tests that were performed in the furnace.

A second task was the realisation of four furnace tests in Maisière les Metz, theses tests aimed to have a better understanding of the complex behaviour of the Composite cellular beam in case of fire including the local instabilities. The Figure 10–1 shows the shape of the cellular beams after the different fire tests.

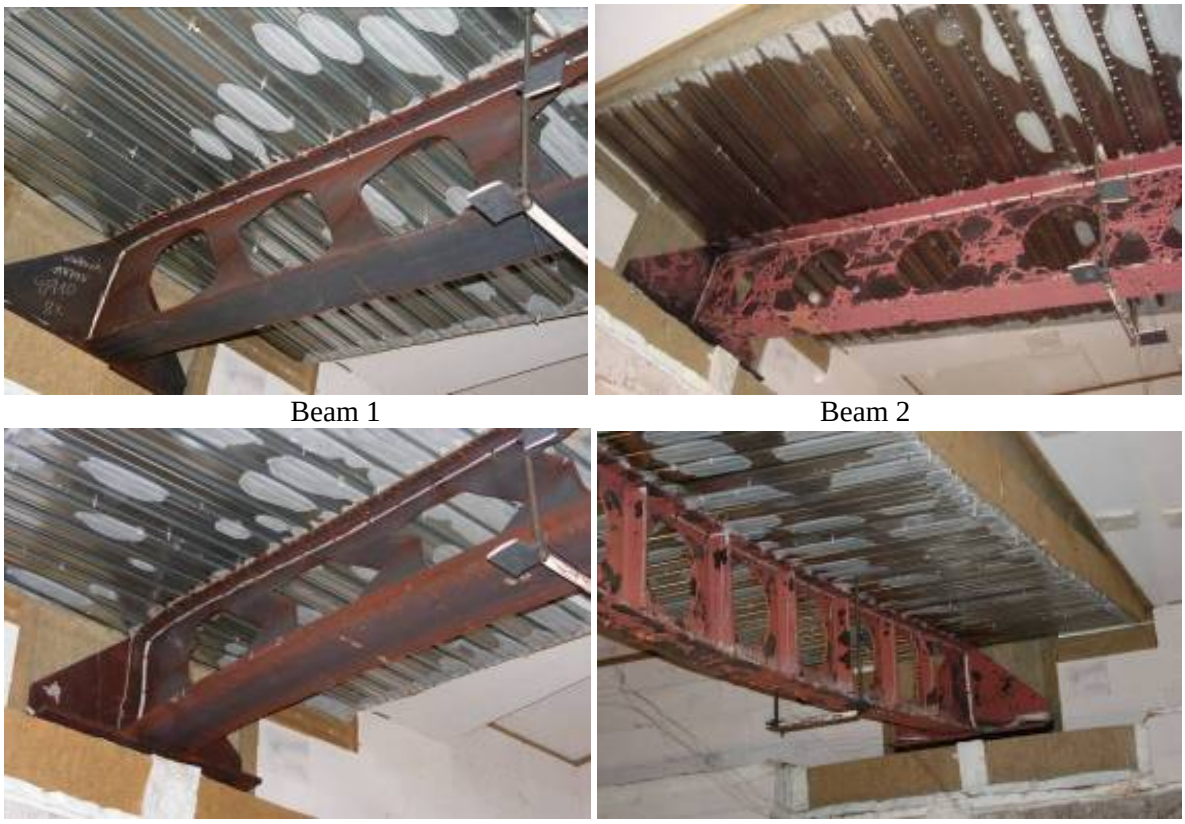

Beam 1 Beam 2

Beam 3 Beam 4

Figure 10–1 : Deformed beams in their RHS zone

The results of theses tests were used to calibrate Finite Elements Model in Software ANSYS, CAST3M and SAFIR.

A good agreement between the tests and both FEM models is observed, in terms of failure modes and critical temperatures (SAFIR and ANSYS). Thus, theses models can accurately predict the mechanical behaviour of a simply-supported composite cellular beam at elevated temperatures, and can be used for the parametric study which aims to check the relevance of the simplified design method.

The CAST 3M Model was able to reproduce with an acceptable level of accuracy the thermal behaviour of composite cellular beams.

Theses Software were used to perform a large parametrical study in order to compare two analytical models with the FEM results.

Eurocode based Model

The Eurocode based analytical model was again validated by this parametrical study and can be used for the prediction of the critical temperature of cellular beam in case of fire. This model takes into account the complex behaviour of cellular beams in fire conditions and is based on the Eurocodes principles taking into account the loss of material properties and stiffness required in the Eurocodes. This model was implemented in a design software called ACB+ and can be downloaded for free on www.arcelormittal.com/sections .

SCI Engineering Model

Comparison between the Cellbeam and FE models of the 15 case studies on cellular composite floors carried out by SCI showed that Cellbeam results were slightly non-conservative in some cases. In particular, cellbeam results were unconservative by a maximum of 12% (in UDL) and 10% (in critical temperature), for design of cellular beams at room and elevated temperatures. Unconservative results were not limited to only one failure mode.

Cellbeam results were also compared against the results of the FE analyses carried out on bare cellular steel section in the scope of the parametrical study, by other project partners. These comparisons show that Cellbeam results for bare steel sections tend to be generally slightly unconservative.

The Eurocode base Model was introduced in the design guide including a hand design example.

Part 2: General behaviour of the whole floor structure in membrane action

The first step devoted to the extension of the Bailey's method to long span Cellular beam. The Figure 10–2 explains the basis of the Model equilibrium and the complete method is described in the document and in the design guide. This method has been implemented in an Excel spreadsheet which simplifies a lot the use of the methodology by the practitioners.

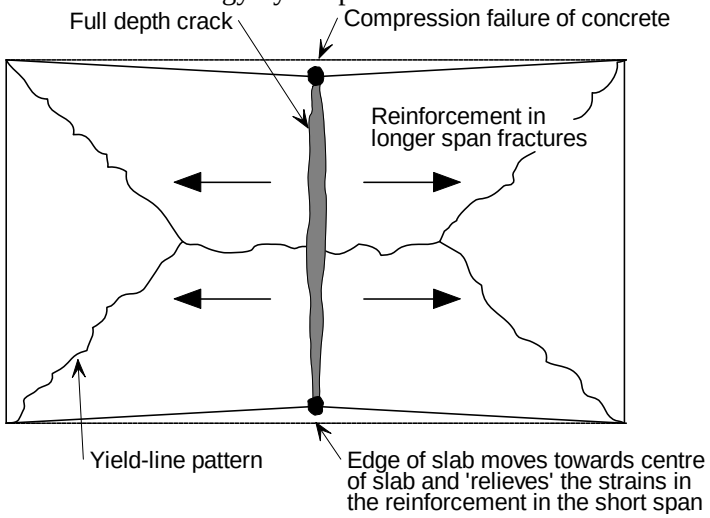

(a) Tensile failure of mesh reinforcement

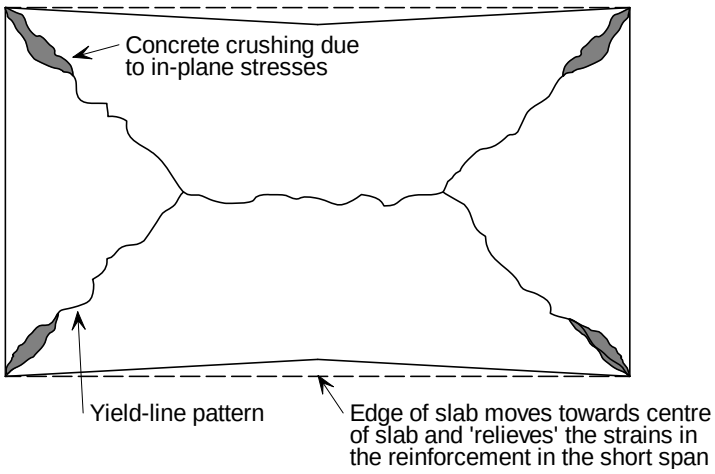

(b) compressive failure of concrete

Figure 10–2 : Assumed failure mode for composite floor

The next step was experimental test programme at Ulster. This task was the essential core of this project and has the aim to investigate the behaviour of the composite cellular beams under accurately simulated applied static loads in a realistic compartment fire (Figure 10–3).

Figure 10–3 : Compartment in fire test.

The two central secondary beams were unprotected. This test provided unique experimental data on the performance of the cellular beams acting in membrane action.

Complete tests results are available on a DVD (pictures, movies, data).

To design the building tested and after to perform a finial validation, FEM models were built in SAFIR and ANSYS. Theses models are able to reproduce with an acceptable level of accuracy the complex behaviour of cellular composite beams acting in membrane action.

The last part of the project was devoted to the redaction of a design guide. The first part of the design guide is devoted to the description of the simplified calculation method developed in the project to assess the resistance of cellular beams in fire conditions. This method has been implemented in the Software ACB^{+} [22] available for free on www.arcelormittal.com/sections.

The second part of the design guide is devoted to the improvement of the Bailey's method to long span cellular beams.

This project gave a unique opportunity to have a good understanding of the complex behaviour of Cellular Beam in case of fire. Not only for simply supported cellular beam but also for composite sections action in membrane action.

All the specificities of the cellular beams sections (local instabilities, increased bending resistance compared to mother section…) have been introduced in the different analytical models.

The design guide can be used as recommendation for designers and will be also presented to the CEN TC250/SC3 and SC4 for analyse and future incorporation in the next Eurocodes releases.

11. EXPLOITATION AND IMPACT OF THE RESEARCH RESULTS

This project provided a lot of useful experimental results and design models.

Different publications will be made in international Journals and in conferences by the different partners of the project.

Concerning the simply supported cellular beam, the developed analytical model is already used by the practitioners to assess properly the critical temperature of the cellular beams. Many projects were already built using this design method.

The Ulster fire test shows the perfect behaviour of the cellular beams action in membrane action. The size of the compartment used 9m x 15m reflects properly the actual architecture in steel and shows that the design method and the behaviour of cellular beam acting in membrane action are safe.

The dissemination of the results will be made first, through the different publications that the different partners will make. And in a second step, the FICEB+ consortium has introduced a dissemination proposal : “Membrane Action in fire design of Composite Slab with solid and cellular steel beams - Valorisation “ MACS^{+}.

The technical objective of this RFCS proposal is to disseminate methodology for design of partially protected composite slabs for fire conditions using both solid and cellular steel beams. Number of tests performed in various countries for natural and ISO fire enabled to gain good understanding of the behaviour of such structures. The project will be addressed to practicing engineers in various countries and it focuses on transferring knowledge about utilisation in the design of membrane action which is created in the reinforced slab during fire.

This project will be a really large project because it will involve 19 partners and 18 seminars will be organised in Europe in the mother tongue of each country.

12. LIST OF FIGURES

13. LIST OF TABLES

14. REFERENCES

[1] D. Bitar, T. Demarco, P.O. Martin, Steel and non composite cellular beams – Novel approach for design based on experimental studies and numerical investigations, brochure EUROSTEEL, june 2005

[2] A. Nadjai, O. Vassart, A. Faris, D. Talamona, A. Allam and M. Hawes Performance of cellular composite floor beams at elevated temperatures , SIF 2006

[3] "Fire Protection for Structural Steel in Buildings", Second Edition, ASFP/SCI/FTSG, (1992).

[4] Bailey C.G. Indicative Fire Tests to Investigate the Behaviour of Cellular Beams Protected with Intumescent Coatings. Fire Safety Journal. Fire Safety Journal. 39 2004 pp 689-709.

[5] "RT1006 Version 02: Fire Design of Cellular Beams with Slender Web Posts", SCI, Ascot, (2004).

[6] Newman G.M., Robinson J,T. and Bailey C.G., Fire Safe design: A New Approach to Multi-Storey Steel-Framed Buildings (Second Edition). SCI Publication P288. The Steel Construction Institute, Ascot. 2006.

[7] Large web Openings for service integration in composite floor, ECSC contract 7210-PR-315, 2004

[8] P.-O. Martin - Rapport de recherche CTICM "ACB Design optimisation – Flambement du Montant" – CTICM – Novembre 2003.

[9] Y. Galéa, P.-O. Martin - Rapport de recherche CTICM "ACB Design optimisation – Calcul des flèches" – CTICM – Décembre 2003.

[10] D. Bitar, P.-O. Martin, Y. Galéa, T. Demarco - Poutres cellulaires acier et mixtes - Partie 1 : proposition d'un modèle pour la résistance des montants. Revue Construction Métallique n°1-2006. CTICM.

[11] Bailey, C. G., Lennon, T. and Moore, D. B., The behaviour of full-scale steel framed buildings subjected to compartment fires, The Structural Engineer, Vol. 77, No. 8, April 1999. pp. 15-21.

[12] Wang Y.C. Tensile membrane action in slabs and its application to the Cardington fire tests. Fire, Static and Dynamic Tests of Building Structures. Proceedings of the Second Cardington Conference, England 12-14 March 1996. pp 55-67.

[13] Bailey C.G. and Moore D.B. The structural behaviour of steel frames with composite floor slabs subject to fire: Part 1: Theory. The Structural Engineer Vol. 78 No. 11 June 2000 pp. 19 – 27.

[14] Bailey C.G. Membrane action of unrestrained lightly reinforced concrete slabs at large displacements. Engineering Structures. 23 (2001) pp. 470-483.

[15] Wood R.H. Plastic and elastic design of slabs and plates, with particular reference to reinforced concrete floor slabs. Thames and Hudson, London. 1961

[16] Hayes B. Allowing for membrane action in the plastic analysis of rectangular reinforced concrete slabs. Magazine of Concrete Research Vol. 20 No. 65 Dec 1968. pp 205-212.

[17] Pr EN1994-1-2. Eurocode 4. Design of composite steel and concrete structures. Part 1.2. General rules. Structural fire design. Final Draft European Committee for Standardization, Brussels.

[18] Westok Limited, Input data – design summary, 2008

[19] Efectis, Rapport d'essais, 2009

[20] CEN, Eurocode 4 - Design of composite steel and concrete structures – Part 1.1: General rules and rules for buildings, 2005

[21] CEN, Eurocode 4 - Design of composite steel and concrete structures – Part 1.2: General rules - Structural fire design, 2005

[22] ACB+ Design software, ArcelorMittal, www.arcelormittal.com/sections

[23] O. Vassart, Analytical model for cellular beams made of hot rolled sections in case of fire, PhD Thesis, Université Blaise Pascal Clermont-Ferrand II, 2009

[24] 'Fire Safe Design: A new approach to multi-storey steel framed buildings' P288, The Steel Construction Institute, 2006.

[25] 'The behaviour of Multi-storey steel framed buildings in fire', A European joint research programme, British Steel Swinden Technology Centre, 1999

[26] Lennon, T., 'Cardington fire tests: instrumentation locations for large compartment fire test.', Building Research Establishment Report N100/98, June 1996.

[27] Lennon, T., 'Cardington fire tests: instrumentation locations for corner fire test.', Building Research Establishment Report N152/95, June 1996

[28] Wainman, W. and Kirby, B., Compendium of UK standard fire test data, No.1 - Unprotected structural steel, British Steel, Swinden Technology Centre, 1987

[29] Investigation of Broadgate Phase 8 Fire, SCI, Ascot, 1991.

[30] Thomas, I. R., Bennetts, I. D., Dayawansa, P., Proe, D. J. and Lewins, R. R., 'Fire Tests of the 140 William Street Office Building.', BHPR/ENG/R/92/043/SG2C, BHP Research, Melbourne Australia, 1992

[31] Proe, D. J. and Bennetts, I. D., 'Real Fire Tests in 380 Collins Street Office Enclosure.', BHPR/PPA/R/94/051/SG021A, BHP Research Melbourne Australia, 1994.

[32] Brand Verhalten Von Stahl und Stahlverbund Konstructionen (Fire behaviour of steel and composite construction), Verlag TUV Rheinland, 1986.

[33] Johansen, K.W., 'The Ultimate strength of Reinforced Concrete Slabs.', International Association for Bridge and Structural Engineering, Final Report, Third Congress, Liege, September 1948.

[34] Ockleston AJ. Load tests on a 3-storey reinforced concrete building in Johannesburg. Struct Eng 1955;33(10):304-22

[35] Bailey C.G. and Moore D.B., The structural behaviour of steel frames with composite floor slabs subjected to fire: Part 1: Theory

[36] Bailey C.G. and Moore D.B., The structural behaviour of steel frames with composite floor slabs subjected to fire: Part 2: Design

[37] Park, R, Ultimate strength of rectangular concrete slabs under short term uniform loading with edges restrained against lateral movement. Proceedings, Institution of Civil Engineers, 28, pp125-150.

[38] Wood R. H. Plastic and elastic design of slabs and plates, with particular reference to reinforced concrete floor slabs Thames and Husdon, London. 1961.

[39] Taylor R. A note on a possible basis for a new method of ultimate load design of reinforced concrete slabs. Magazine of concrete research VOL 17 NO. 53 Dec 1965 pp. 183-186

[40] Kemp. K.O. Yield of a square reinforced concrete slab on simple supports allowing for membrane forces. The structural Engineer Vol 45, No.7 July 1967 pp. 235-240.

[41] Sawczuk A. and Winniki L. Plastic behaviour of simply supported reinforced concrete plated are moderately large deflections. Int J. Solids Structures Vol 1 1965 pp. 97 to 111.

[42] Hayes B. Allowing for membrane action in the plastic analysis of rectangular reinforced concrete slabs Magazine of concrete research Vol. 20 No. 81 Dec 1968. pp 205-212.

[43] Bailey C. G., White D.S. and Moore D.B. The tensile membrane action of unrestrained composite slab under fire conditions, Engineering Structures, vol. 22, no12, pp. 1583-1595

[44] Bailey C. G. & Toh, W.S. 'Behaviour of concrete floor slabs at ambient and elevated temperature', Fire Safety Journal, 42, oo425-436, 2007.

[45] Hayes B. and Taylor R. Load-Testing RC slabs. The Consulting Engineer. Nov. 1969. pp 46-47

[46] Taylor R., Maher D.R.H. and Hayes B. Effect of arrangement of reinforcement on the behaviour of the reinforce concrete slabs. Magazine of concrete research Vol 18 No. 55. June 1966. pp 85-94

[47] Moy S.S.J. Load-deflection characteristics of rectangular reinforced concrete slabs. Magazine of concrete research Vol 24 No. 81 Dec. 1972. pp 209-218.

[48] Bailey, C.G., Efficient arrangement of Reinforcement for membrane behaviour of composite slabs in fire conditions, Journal of Constructional Steel Research, 59, 2003, pp931-949.

[49] Bailey C.G., Membrane action of lightly reinforced concrete slabs at large displacements, Engineering Structures, 23, 2001, pp470-483.

[50] Bailey, Colin G. and Toh, Wee Siang. Experimental behaviour of concrete floor slabs at ambient and elevated temperatures. SIF06

[51] O'Conner MA, Kirby BR, Martin DM. Behaviour of a multi-storey composite steel framed building in fire. Struct Eng 2003;81(2):27–36.

[52] Bailey CG, Lennon T, Moore DB. The behaviour of full-scale steel framed buildings subjected to compartment fires. Struct Eng 1999; 77(8):15–21.

[53] Bailey CG, Membrane action of slab/beam composite floor systems in fire. Engineering Structures 26 2004:1691-1703.

[54] Wang YC. Tensile membrane action in slabs and its application to the Cardington fire tests. Fire, static and dynamic tests of building structures. Proceeding of the second Cardington conference, England, 12-14 March1996: 55–67

[55] EN 1992-1-2, Eurocode 2, Design of concrete structures. Part 1.2: General rules. Structural fire design, CEN

[56] EN 1994-1-2, Eurocode 2, Design of composite steel and concrete structures. Part 1.2: General rules. Structural fire design, CEN

[57] EN 1994-1-1, Eurocode 4 Design of composite steel and concrete structures – Part 1-1: General rules and rules for buildings, CEN

[58] EN 1993-1-8, Eurocode 3 Design of steel structures – Part 1-8: Design of joints, CEN

[59] EN 1992-1-1, Eurocode 2 Design of Concrete Structures – Part 1-1: General rules and rules for buildings, CEN

[60] EN 1992-1-2 - Eurocode 2 "Design of Concrete Structures" – Part 1-2: Structural fire design, CEN.

[61] EN 1363-1 - Fire resistance tests – Part 1: General requirements, CEN.

ANNEXES

ANNEX 1

Full list of reports covering Cellular Beams in Fire

WP1 Fire Related Research Testing And Papers On Cellular Beams Made From Rolled Section

Reference Number	Source/Author/Group	Discription	Confidential
1	Prof. Colin Bailey Manchester University, Westok	Asymmetric bare steel heating rate tests, with and without holes	
2	Prof. Colin Bailey Manchester University, Westok	Symmetric bare steel heating rate tests, with and without holes	
3	Prof. Colin Bailey Manchester University, Westok	Intumescent heating rate tests on asymmetric beams with and without holes	Confidential
4	Prof. Colin Bailey Manchester University, Westok	Intumescent heating rate tests on symmetric beams with and without holes	Confidential
5	Prof. Ali Nadjai Ulster University, Westok	Loaded bare steel against slow heat furnace 575x140CUB39	
6	Prof. Ali Nadjai Ulster University, Westok	Loaded bare steel against slow heat furnace 630x140/152ACUB46	
7	Prof. Ali Nadjai Ulster University, Westok	Loaded bare steel against ISO furnace 575x140CUB39	
8	Prof. Ali Nadjai Ulster University, Westok	Loaded bare steel against ISO furnace 630x140/152ACUB46	
10	Prof. Ali Nadjai Ulster University, Westok	SIF paper on the above tests	
11	Prof. Ali Nadjai Ulster University, Westok	Intumescent heating rate tests on asymmetric beams with and without holes	Confidential
12	Prof. Ali Nadjai Ulster University, Westok	Intumescent heating rate tests on symmetric beams with and without holes	Confidential
13	CTICM Metz Arcelor	Passive fire spray on loaded cellular beams to ISO furnace heating	
14	Olivier Vassart Arcelor & Ulster University	FE work and paper on Ulster tests ref 5 to 8 above.	
15	Ameron (now PPG)	Intumescent heating rate tests comparing identical beams with and without holes in the webs	Confidential
16	Dr. Simon Jones, Nulifire.	Bare and intumescently coated heating rate tests on various products	Confidential
16	Dr. Simon Jones, Nulifire.	Loaded and unloaded cellular beams with intumescent to ASFP protocol	Confidential
18	Dr. Simon Jones, Nulifire.	2Hr Intumescents on narrow web post tests to ASFP protocol	Confidential
19	International Paints	Loaded and unloaded cellular beams with intumescent to ASFP protocol	Confidential
20	PPG	Loaded and unloaded cellular beams with intumescent to ASFP protocol	Confidential

WP1 Fire Related Research Testing And Papers On Cellular Beams Made From Rolled Section

Reference Number	Source/Author/Group	Discription	Confidential
21	CAFCO International (Now PROMAT) Westok	Passive fire spray unloaded heating rate comparisons between beams with and without holes	Confidential
22	CAFCO International (Now PROMAT) Westok	Passive fire spray unloaded heating rate comparisons between circular and rectangular openings with web posts of the same width	Confidential
23	Jotun-Henry Clarke	Loaded and unloaded cellular beams with intumescent to ASFP protocol	Confidential
24	PPG	Loaded and unloaded cellular beams with intumescent to ASFP protocol	Confidential

ANNEX 2

DVD with

- Large scale fire test reports and data (temperature, deflection,…)
- Design software
  - ACB^{+} v2.05
  - FiCEB_Spreadsheet_V01.xls

ANNEX 3

Design Guide

Contents

1. ANALYTICAL MODEL FOR THE CELLULAR BEAM MADE OF HOT ROLLED SECTIONS IN CASE OF FIRE

1.1. Objectives

The aim of this document is to describe the calculation methods developed to assess the resistance of simply supported cellular beams in fire conditions. This development has been made in the scope of the RFCS FiCEB^{+} [23] and in the scope of the PHD of O.Vassart [24].

This calculation procedure has been introduced in the ACB+ software available on www.arcelormittal.com/sections

1.2. Principles

The assessment of the fire resistance of a beam consists in calculation for each of the strength criteria, the critical temperature (for which this strength criterion is equal to 1) and the corresponding heating up time. This calculation is made for each of the loads combinations in fire situation.

Among the strength criteria, two types are distinguished:

- the " plastic resistance " criteria, for which the resistance depends only on the steel strength limit f_y
- the " resistance to instability " criteria, for which the resistance depends on the steel strength limit f_y and on the Young modulus E.

Table 1-1 : Criteria taken into account for the fire resistance calculation

Criteria in Plastic Resistance
Resistance of the gross sections (at the level of the web post and filled openings):
Γ_M (*): Bending resistance
Γ_V: Shear resistance
Γ_{MV}: Interaction MV
Resistance of the web posts :
Γ_{Vh}: Resistance to horizontal shear of a web post
Resistance of the net section (at the level of an opening) :
Γ_M (*): Bending resistance
Γ_N (*): Axial resistance
Γ_V: Shear resistance
Γ_{MN} (*): Interaction MN
Γ_{MV} (*): Interaction MV
Γ_{MNV} (*): Interaction MNV
(*): criteria for which a section classification is necessary.
Criteria resistance to instability
Resistance of the gross sections:
Γ_{Vbw}: Resistance to shear buckling
Resistance of the web posts :
Γ_b: Web post buckling resistance
Resistance of the beam :
Γ_{LT}: Resistance to lateral torsional buckling (Only for pure steel beam).

1.2.1. Fire resistance for the plastic criteria

1.2.1.1. Principles

The principles for the calculation of the fire resistance for the plastic criteria are the following:

1. The value of the strength criterion Γ for the time 0 of the fire is calculated taking into account the load combination chosen for the fire calculation. The calculation of the Γ is made in a similar way than in cold conditions by replacing the partial coefficient γ_{M0} with $\gamma_{M,fi}$ see [26].

   For the strength criteria dependent on the section classification, the classification differs from the one in cold conditions (cf. 3.1.2).

2. The critical temperature associated with the value Γ obtained in 1 is calculated from the steel strength reduction factor $k_{y,\theta}$ given in Table 1-3.

   If the value of Γ was obtained for a section of class 4, the critical temperature is calculated with the reduction factor $k_{p0,2,\theta}$, given in the following table (Table E1 of the EN 1993-1-2).

Table 1-2 : Steel strength reduction factor for a class 4 section

Steel Temperature θ (°C)	Reduction Factor $k_{p,0,2,\theta}$
20	1,000
100	1,000
200	0,890
300	0,780
400	0,650
500	0,530
600	0,300
700	0,130
800	0,070
900	0,050
1000	0,030
1100	0,020
1200	0,000

3. From the massivity factor associated with the considered section and from the critical temperature calculated in 2, the heating up time of the section is calculated in a incremental way.
4.

The following parameters are considered:

θ_{Ref}: "ambient" temperature of the beam; by default θ_{Ref} : = 20°C
Δt: increment of time ; by default Δt = 1 sec
k_{sh}: correction factor for the shadow effect (value of the factor for the rebuilt section) by default k_{sh} = 0.7
ρ_a: density of the steel; ρ_a = 7850 kg / m3

Assuming that the temperature of the section in time t_i is equal to θ_i, the temperature θ_{i+1} in time $t_{i+1} = t_i + \Delta t$ is calculated in the following way (formula (4.25) of EN 1993-1.2):

$$\theta_{i+1} = \theta_i + \Delta\theta$$
$$\Delta\theta = k_{sh} \frac{Am/V}{c_a \rho_a} h_{net} \Delta t$$

Hence c_a is the specific heat of the steel, calculated according to the temperature θ_i with the following formulae (according to 3.4.1.2 of EN 1993-1-2 - all the relations are expressed in J / kgK):

for $20°C \leq \theta_i < 600°C$:
$$c_a = 425 + 0.773\,\theta_i - 1.69\,10^{-3}\,\theta_i^2 + 2.22\,10^{-6}\,\theta_i^3$$
for $600°C \leq \theta_i < 735°C$:
$$c_a = 666 + \frac{13002}{738 - \theta_i}$$
for $735°C \leq \theta_i < 900°C$:
$$c_a = 545 + \frac{17820}{\theta_i - 731}$$
for $900°C \leq \theta_i \leq 1200°C$:

$c_a = 650$

h_{net} is the value of calculation of the heat flux, determined according to 3.1 of EN 1991-1-2 by the following relations:

$h_{net} = h_{net,c} + h_{net,r}$
$h_{net,c}$ is the convective part and $h_{net,r}$ is the radiative part.
$h_{net,c} = \alpha_c (\theta_{Gi} - \theta_i)$
$h_{net,c} = \Phi \varepsilon_m \varepsilon_f \sigma [(\theta_{Gi}+273)^4 - (\theta_i +273)^4]$

Where:

θ_{Gi} is the hot gas temperature for the time i, calculated from the normalised ISO Curve (Eq 3.4 of EN 1991-1-2), according to the following function:

$$\theta_{Gi} = 20 + 345 \log_{10}(8 t_i + 1) [°C]$$

α_c is the thermal transfer coefficient for convection. It's equal by default to 25 W/m^2K (value recommended in 3.2.1 (2) of EN 1991-1-2).
Φ is the shape factor. By default equal to 1.0.
ε_m is the steel surface emissivity, by default equal to 0.7.
ε_f is the fire emissivity, by default equal to 1.0.
σ is the Boltzmann constant (= $5.67\ 10^{-8}$ W/m^2K^4)

The critical heating up time is reached when $\theta_i = \theta_{Critique}$.

1.2.1.2. Classification of the sections

For a criterion in fire resistance involving the classification of the studied section, the class of the section is determined with the parameter ε_θ:

$$\varepsilon_\theta = 0.85\ \varepsilon = 0.85 \sqrt{\frac{235}{f_y}}$$

All the other parameters of the verification (in particular the reduced slenderness for the calculation of the participating widths) remain unchanged in respect to the cold calculation.

1.2.2. Fire resistance for the instability criteria

The principles of justification of the resistance in fire condition for the instability criteria are the following:

1. From the stresses formed by the fire load combination, the critical temperature is reached when the instability criterion is equal to 1. The calculation of the strength criterion according to the temperature is detailed in the following chapters. The partial safety factor $\gamma_{M,fi}$ is used.
2. From the massivity criterion described below and from the critical temperature calculated in 1, the heating up time is calculated in an incremental way according to the same method as in 2.1.

The considered massivity criterions are the following ones:

- Criterion of instability of the web post: massivity of a straight web post section can be estimated by the following value:
  $A_m / V = 2 / t_w$,
  where t_w, is the thickness of the considered web.
- Lateral torsional buckling criterion: massivity of a "T" section at the level of an opening for the compressed member giving the considered criterion Γ.

1.2.2.1. Instability of a web post

The criterion for resistance to buckling of an intermediate web post at elevated temperature is given by the following equation:

$$\Gamma(\theta_m) = \frac{\left|\sigma_{w,fi,Ed}\right|}{\kappa_\theta \, \sigma_{w,fi,Rd}(\theta_m)}$$

It is based on the calculation of the principal stress resistance in fire situation for the half post being studied $\sigma_{w,fi,Rd}$ and the principal compressive stress in fire situation in the half post being studied $\sigma_{w,fi,Ed}$ ($\sigma_{w,fi,Ed,up}$ for the upper half post and $\sigma_{w,fi,Ed,low}$ for the lower half post).

$\sigma_{w,fi,Ed}$ is calculated from the fire load combinations in the same way as in cold situation (see. 5.8 (5) [27]).

$\sigma_{w,fi,Rd}$, the principal stress resistance is calculated using the following formula based on EN1993-1-2 :

$$\sigma_{w,fi,Rd} = \frac{\chi_{fi} \cdot \xi \cdot k_{y,\theta} \cdot f_y}{\gamma_{M,fi}}$$

Where:

f_y is the steel strenght limit of the considered member

$\gamma_{M,fi}$ is the partial safety factor in fire condition

ξ is a shape factor for the critical section that has been calibrated using the Finite Element modelling (see 5.8 (9) [27])

χ_{fi} is a reduction factor for out-of-plane buckling of the web post adapted for fire situation following EN1993-1-2, and calculated using the following formulae :

$$\chi_{fi} = \frac{1}{\phi_\theta + \left(\phi_\theta^2 - \bar{\lambda}_\theta^2\right)^{0.5}} \quad \text{and} \quad \chi_{fi} \le 1.0$$

$$\phi_\theta = 0.5[1 + \alpha \, \bar{\lambda}_\theta + \bar{\lambda}_\theta^2]$$

$$\alpha = 0.65\sqrt{\frac{235}{f_y}}$$

The reduced non-dimensional slenderness $\bar{\lambda}_\theta$ of the web post being considered in case of fire is given by:

$$\bar{\lambda}_\theta = \bar{\lambda}\sqrt{\frac{k_{y,\theta}}{k_{E,\theta}}} = \sqrt{\frac{\xi f_{yw}}{\sigma_{w,fi,cr}}}\sqrt{\frac{k_{y,\theta}}{k_{E,\theta}}}$$

Where $k_{y,\theta}$ and $k_{E,\theta}$ are the reduction factors for steel strength limit and Young modulus, respectively, at elevated temperature.

$\bar{\lambda}$ is the non-dimensional slenderness in « cold » conditions (See 5.8 (10) [27])

The values of $k_{y,\theta}$ and $k_{E,\theta}$ are given in Table 1-3 (from table 3.1 of EN 1933-1-2) :

Table 1-3 : Reduction factor for the steel strenght limit and the Young Modulus

Steel temperature θ (°C)	Reduction factor $k_{y,\theta}$	Reduction factor $k_{E,\theta}$
20	1,000	1,000
100	1,000	1,000
200	1,000	0,900
300	1,000	0,800
400	1,000	0,700
500	0,780	0,600
600	0,470	0,310
700	0,230	0,130
800	0,110	0,090
900	0,060	0,0675
1000	0,040	0,0450
1100	0,020	0,0225
1200	0,000	0,000

For the intermediate values of temperature, a linear interpolation is used.

In the calculation of the critical stress, the reference Euler buckling load depends on the Young Modulus E but remains independent from the temperature.

The post-critical reserve of strength κ_θ is calculated from the following relation:

$\kappa_\theta = 1 + 0.625\ (\psi_\theta - 0.3)$ and $1 \leq \kappa_\theta \leq 1.25$

$\psi_\theta = k_{y,\theta}\ \psi$

Where ψ is the non-dimensional factor calculated in the same way as in cold situation (see 5.8 (13) [27]).

1.2.2.2. Resistance to shear buckling

It is suggested not to calculate the shear buckling in fire situation.

1.2.2.3. Lateral torsional buckling

In fire situation, the composite beams are not concerned by this criterion.
As for the cold calculation, the resistance criterion for the lateral torsional buckling of the beam in fire situation is calculated like the buckling of the compressed member. It can be written for a member at the temperature θ:

$$\Gamma_{LT}(\theta) = \frac{N_{m,fi,Ed}}{N_{b,fi,Rd}(\theta)}$$

Where:

$N_{m,fi,Ed}$ is the normal force in the member taking into account the fire load combination. This value is independent of the temperature θ.

$N_{b,fi,Ed}$ is the resisting force to buckling of the member.

This member is the "T" shape between two lateral supports. This value depend on the temperature θ :

$$N_{b,fi,Rd} = \chi_{fi}\, A_0\, k_{y,\theta}\, f_y / \gamma_{M,fi}$$

Where,

$k_{y,\theta}$ is the reduction factor for the steel strength given in the Table 1-3.

A_0 is the surface of the considered section at the level of the opening ("T" section) see relation given in 5.10.1 [27].

$\gamma_{M,fi}$ is the partial safety factor in fire situation

χ_{fi} is the reduction factor for lateral torsional buckling given by the following relationships:

$$\chi_{fi} = \frac{1}{\phi_\theta + (\phi_\theta^2 - \bar{\lambda}_\theta^2)^{0.5}}$$

$$\phi_\theta = 0.5\left[1 + \alpha\,\bar{\lambda}_\theta + \bar{\lambda}_\theta^2\right]$$

$$\alpha = 0.65\sqrt{\frac{235}{f_y}}$$

The reduced non-dimensional slenderness $\bar{\lambda}_\theta$ considered in case of fire is given by:

$$\bar{\lambda}_\theta = \bar{\lambda}\sqrt{\frac{k_{y,\theta}}{k_{E,\theta}}}$$

Where $k_{y,\theta}$ and $k_{E,\theta}$ are the reduction factors for steel strength limit and Young modulus, respectively, at elevated temperature given in Table 1-3.

$\bar{\lambda}$ is the non-dimensional slenderness in « cold » conditions calculated from 5.10.1 (4) [27]

Nota: the critical load N_{cr} used in the calculation of $\bar{\lambda}$ is independent of the temperature and is obtained from the relationship given in 5.10.1 (5) [27].

1.3. Example of application

1.3.1. Characteristics of the beam

Beam:	IPE400 non composite
Steel grade:	S355
Span:	20m
a_0:	500mm
w:	125mm
H_t:	633.8mm
Distance between beams:	3m
Permanet Load:	1kN/m^2
Snow Load:	0.5kN/m^2
Fire load Combinations:	1*G + 0*Q

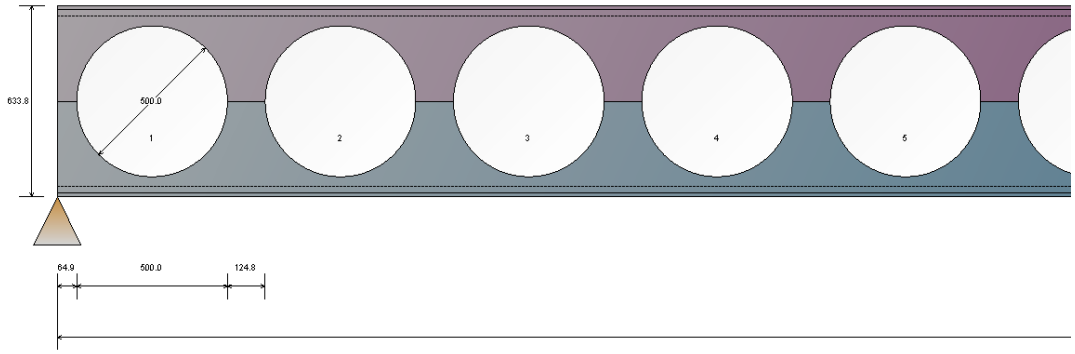

Figure 1–1 : Geometry of the beam

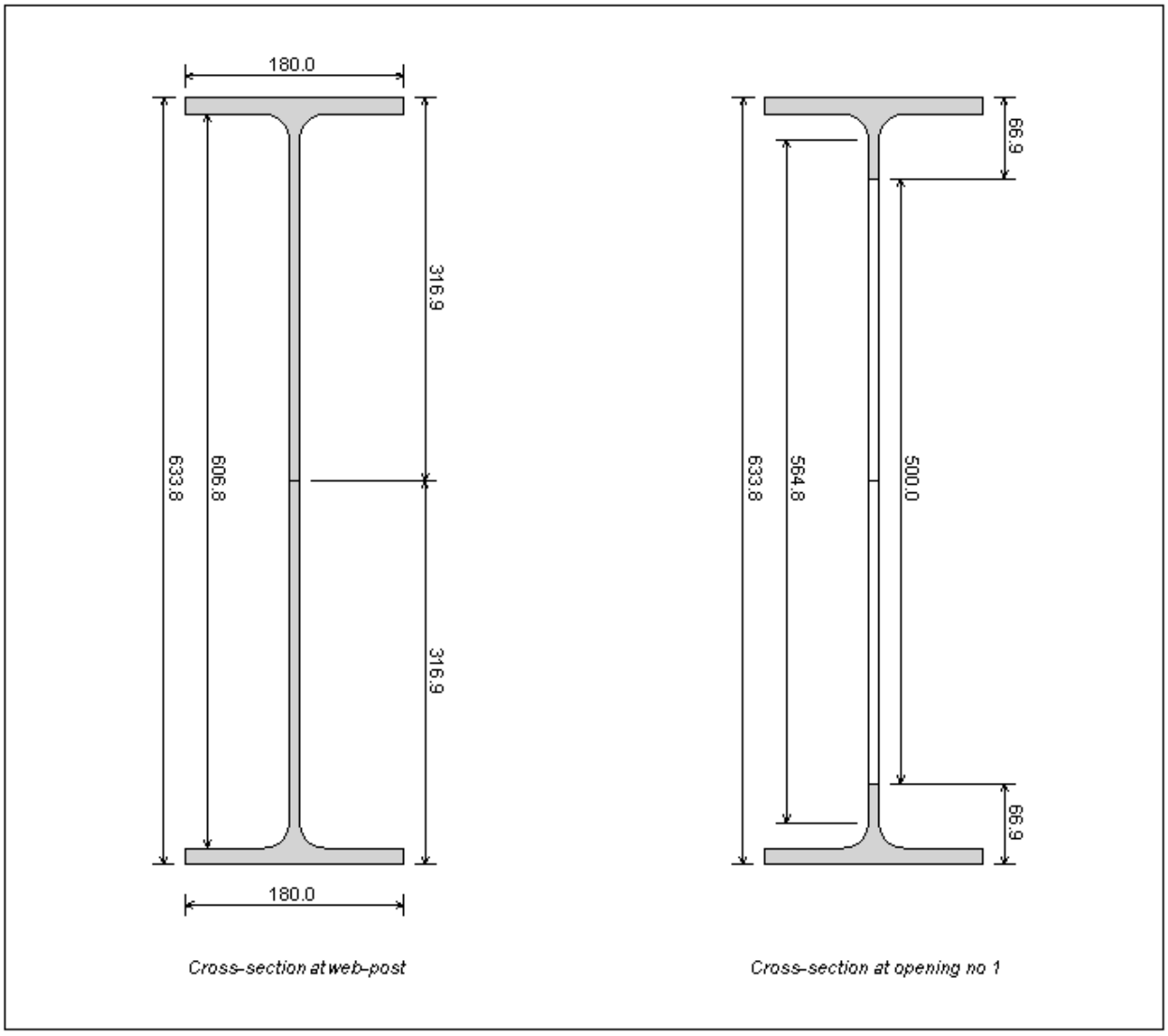

Figure 1–2 : Cross section of the beam

1.3.2. Resistance check

1.3.2.1. Net section at opening no 1 : Resistance to bending moment

Bending moment	M_{Ed} = 11.07 kNm	
Shear forces	$V_{Ed,l}$ = -34.85 kN	$V_{Ed,r}$ = -34.85 kN
Axial forces	$N_{Ed,l}$ = 0.0 kN	$N_{Ed,r}$ = 0.0 kN
Axial forces in chord	$N_{m,sup,l}$ = 18.17 kN	$N_{m,sup,r}$ = 18.17 kN
	$N_{m,inf,l}$ = -18.17 kN	$N_{m,inf,r}$ = -18.17 kN
Shear forces in chord	$V_{m,sup,l}$ = -17.42 kN	$V_{m,sup,r}$ = -17.42 kN
	$V_{m,inf,l}$ = -17.42 kN	$V_{m,inf,r}$ = -17.42 kN
Angle	ϕ = 24.0	
Partial factor	$\gamma_{M,fi}$ = 1.00	
Yield strengths	$f_{y,top}$ = 355 Mpa	$f_{y,bot}$ = 355 MPa

Top chord

Inclined Tee section	h_ϕ = 96.9 mm	
	A_ϕ = 3555 mm^2	$A_{v\phi}$ = 1269 mm^2
Projected forces	N_ϕ = 23.69 kN	V_ϕ = -13.28 kN
	M_ϕ = -2.266 kNm	
Class of the chord	Class 2	
Bending resistant moment at 20°C	$M_{c,Rd\phi}$ = 16.05 kNm	
Criterion	$\Gamma_{M,fi}$ = 0.141	

Bottom chord

Inclined Tee section	h_ϕ = 96.9 mm	
	A_ϕ = 3555 mm^2	A_v = 1269 mm^2
Projected forces	N_ϕ = -9.515 kN	V_ϕ = -18.56 kN
	M_ϕ = -2.400 kNm	
Class of the chord	Class 1	
Bending resistant moment	$M_{c,Rd\phi}$ = 16.05 kNm	
Criterion	$\Gamma_{M,fi}$ = 0.150	
Critical temperature Γ_M :	767°C	
Am/V Γ_M:	150.7 m^{-1}	

1.3.2.2. Net section at opening no 16 - Resistance to normal force

Bending moment	M_{Ed} = 179.7 kNm	
Shear forces	$V_{Ed,l}$ = -1.124 kN	$V_{Ed,r}$ = -1.124 kN
Axial forces	$N_{Ed,l}$ = 0.0 kN	$N_{Ed,r}$ = 0.0 kN
Axial forces in chord	$N_{m,sup,l}$ = 295.1 kN	$N_{m,sup,r}$ = 295.1 kN
	$N_{m,inf,l}$ = -295.1 kN	$N_{m,inf,r}$ = -295.1 kN
Shear forces in chord	$V_{m,sup,l}$ = -0.562 kN	$V_{m,sup,r}$ = -0.562 kN
	$V_{m,inf,l}$ = -0.562 kN	$V_{m,inf,r}$ = -0.562 kN
Angle	ϕ = 0.0	
Partial factor	$\gamma_{M,fi}$ = 1.00	
Yield strengths	$f_{y,top}$ = 355 Mpa	$f_{y,bot}$ = 355 MPa

Top chord

Inclined Tee section	h_ϕ = 66.9 mm	
	A_ϕ = 3078 mm^2	Avϕ = 990.0 mm^2
Projected forces	N_ϕ = 295.1 kN	Vϕ = -0.562 kN
	M_ϕ = 0.0 kNm	
Class of the chord	Class 2	
Normal resistant force at 20°C	$N_{c,Rd\phi}$ = 1093 kN	
Criterion	$\Gamma_{N,fi}$ = 0.270	

Bottom chord

Inclined Tee section	h_ϕ = 66.9 mm	
	A_ϕ = 3078 mm^2	$A_{v\phi}$ = 990.0 mm^2
Projected forces	N_ϕ = -295.1 kN	V_ϕ = -0.562 kN
	M_ϕ = 0.0 kNm	
Class of the chord	Class 1	
Normal resistant force at 20°C	$N_{c,Rd\phi}$ = 1093 kN	
Criterion	$\Gamma_{N,fi}$ = 0.270	
Critical temperature Γ_N :	683°C	
Am/V Γ_N:	154.5 m^{-1}	

1.3.2.3. Net section at opening no 15 - Resistance to shear force

Bending moment	M_{Ed} = 178.3 kNm	
Shear forces	$V_{Ed,l}$ = -3.372 kN	$V_{Ed,r}$ = -3.372 kN
Axial forces	$N_{Ed,l}$ = 0.0 kN	$N_{Ed,r}$ = 0.0 kN
Axial forces in chord	$N_{m,sup,l}$ = 292.8 kN	$N_{m,sup,r}$ = 292.8 kN
	$N_{m,inf,l}$ = -292.8 kN	$N_{m,inf,r}$ = -292.8 kN
Shear forces in chord	$V_{m,sup,l}$ = -1.686 kN	$V_{m,sup,r}$ = -1.686 kN
	$V_{m,inf,l}$ = -1.686 kN	$V_{m,inf,r}$ = -1.686 kN
Angle	ϕ= -39.0	
Partial factor	$\gamma_{M,fi}$ = 1.00	
Yield strengths	$f_{y,top}$ = 355 MPa	$f_{y,bot}$ = 355 MPa

Top chord

Inclined Tee section	h_ϕ = 158 mm	
	A_ϕ = 4523 mm^2	$A_{v\phi}$ = 1836 mm^2
Projected forces	N_ϕ = 226.5 kN	V_ϕ = -76.10 kN
	M_ϕ = 3.652 kNm	
Shear resistant force at 20°C	$V_{c,Rd\phi}$ = 376.3 kN	
Criterion	$\Gamma_{V,fi}$ = 0.202	

Bottom chord

Inclined Tee section	h_ϕ = 158 mm	
	A_ϕ = 4523 mm^2	$A_{v\phi}$ = 1836 mm^2
Projected forces	N_ϕ = -228.6 kN	V_ϕ = 73.48 kN
	M_ϕ = -2.851 kNm	
Shear resistant force at 20°C	$V_{c,Rd\phi}$ = 376.3 kN	
Criterion	$\Gamma_{V,fi}$ = 0.195	
Critical temperature Γ_V :	723°C	
Am/V Γ_V:	145.4 m^{-1}	

1.3.2.4. Net section at opening no 12 - Interaction M-N-V

Bending moment	M_{Ed} = 165.6 kNm	
Shear forces	$V_{Ed,l}$ = -10.12 kN	$V_{Ed,r}$ = -10.12 kN
Axial forces	$N_{Ed,l}$ = 0.0 kN	$N_{Ed,r}$ = 0.0 kN
Axial forces in chord	$N_{m,sup,l}$ = 272.0 kN	$N_{m,sup,r}$ = 272.0 kN
	$N_{m,inf,l}$ = -272.0 kN	$N_{m,inf,r}$ = -272.0 kN
Shear forces in chord	$V_{m,sup,l}$ = -5.059 kN	$V_{m,sup,r}$ = -5.059 kN
	$V_{m,inf,l}$ = -5.059 kN	$V_{m,inf,r}$ = -5.059 kN
Angle	ϕ = -21.0	
Partial factor	$\gamma_{M,fi}$ = 1.00	
Yield strengths	$f_{y,top}$ = 355 MPa	$f_{y,bot}$ = 355 MPa

Top chord

Inclined Tee section	h_ϕ = 89.4 mm	
	A_ϕ = 3437 mm^2	$A_{v\phi}$ = 1200.0 mm^2
Projected forces	N_ϕ = 255.8 kN	V_ϕ = -29.31 kN
	M_ϕ 0.163 kNm	
Shear resistant force at 20°C	$V_{c,Rd\phi}$ = 246.0 kN	$\Gamma_{V,fi}$ = 0.119
Reduction	ρ = 0.000	(No reduction)
Normal resistant force at 20°C	$N_{V,Rd}$ = 1220 kN	$\Gamma_{NV,fi}$ = 0.210
Bending resistant moment at 20°C	$M_{V,Rd}$ = 14.04 kNm	$\Gamma_{MV,fi}$ = 0.012
Interaction MNV	$\Gamma_{MNV,fi}$ = 0.221	

Bottom chord

Inclined Tee section	h_ϕ = 89.4 mm	
	A_ϕ = 3437 mm^2	$A_{v\phi}$ = 1200.0 mm^2
Projected forces	N_ϕ = -252.1 kN	V_ϕ = -29.31 kN
	M_ϕ = -1.335 kNm	
Shear resistant force at 20°C	$V_{c,Rd\phi}$ = 246 kN	$\Gamma_{V,fi}$ = 0.158
Reduction	ρ = 0.000	(No reduction)
Normal resistant force at 20°C	$N_{V,Rd}$ = 1220 kN	Γ_{NV} = 0.249
Bending resistant moment at 20°C	$M_{V,Rd}$ = 14.04 kNm	Γ_{MV} = 0.095
Interaction MNV	Γ_{MNV} = 0.302	

Critical temperature Γ_{MNV} :	670°C
Am/V Γ_{MNV}:	151.5 m^{-1}

1.3.2.5. Shear resistance of Web post no 31

Tee geometrical centres	d_G = 608.9 mm	
Bending moments	$M_{Ed,l}$ = 32.14 kNm	$M_{Ed,r}$ = 11.07 kNm

Axial forces in tees	$N_{m,Sup,l}$ = 52.79 kN	$N_{m,Inf,l}$ = -52.79 kN
	$N_{m,Sup,r}$ = 18.17 kN	$N_{m,Inf,r}$ = -18.17 kN
Horizontal shear force in post	V_{hm} = -34.62 kN	
Post width	w = 125.0 mm	
Resistant shear forces at 20°C	$V_{hRd,top}$ = 220.33 kN	$V_{hRd,bot}$ = 220.33 kN
Checkings	$\Gamma_{Vh,top}$ = 0.157	$\Gamma_{Vh,bot}$ = 0.157
Critical temperature Γ_{Vh} :	761°C	
Am/V Γ_{Vh}:	232.6 m^{-1}	

1.3.2.6. Stability of Web post no 31

Diameter	a_0 = 500.0 mm	
Cells spacing	e = 625.0 mm	α = e / a_0 = 1.25
Height of cross section	H_t = 633.8 mm	
Heights of chords	$h_{m,top}$ = 316.9 mm	$h_{m,bot}$ = 316.9 mm
Heights of tees	$h_{Te,top}$ = 66.9 mm	$h_{Te,bot}$ = 66.9 mm
Tees geometrical centres	$d_{G,top}$ = 304.4 mm	$d_{G,bot}$ = 304.4 mm
dG = dG,top + dG,bot	d_G = 608.9 mm	
Area of tees	$A_{0,top}$ = 3078.4 mm^2	$A_{0,bot}$ = 3078.4 mm^2
Shear area of tees	$A_{v0,top}$ = 990.0 mm^2	$A_{v0,bot}$ = 990.0 mm^2
Yield strengths	$f_{y,top}$ = 355 MPa	$f_{y,bot}$ = 355 MPa
Shear forces	$V_{Ed,l}$ = -32.60 kN	$V_{Ed,r}$ = -34.85 kN
Moments	$M_{Ed,l}$ = 32.14 kNm	$M_{Ed,r}$ = 11.07 kNm
Shear parameters	η = 0.292	k_{Av} = 0.500
Normal forces in chords	$N_{m,ltop}$ = 52.79 kN	$N_{m,lbot}$ = -52.79 kN
	$N_{m,rtop}$ = 18.17 kN	$N_{m,rbot}$ = -18.17 kN
Shear forces in chords	$V_{m,ltop}$ = -16.30 kN	$V_{m,lbot}$ = -16.30 kN
	$V_{m,rtop}$ = -17.42 kN	$V_{m,rbot}$ = -17.42 kN
Forces in the post	V_{hm} = -34.62 kN	M_{hm} = 0.00 kNm
Critical section	d_W = 97.3 mm	L_W = 164.4 mm
Moments in the critical section	$M_{cEd,top}$ = -3.37 kNm	$M_{cEd,bot}$ = -3.37 kNm
Principal stresses	$\sigma_{W,fi,top}$ = 102 MPa	$\sigma_{W,fi,bot}$ = 102 MPa
Critical forces	$V_{hCr,top}$ = 341.48 kN	$V_{hCr,bot}$ = 341.48 kN
	$N_{mCr,top}$ = 1533.08 kN	$N_{mCr,bot}$ = 1533.08 kN
Critical coefficients	$\beta_{Cr,top}$ = 9.628	$\beta_{Cr,bot}$ = 9.988
	$\alpha_{Cr,top}$ = 9.805	$\alpha_{Cr,bot}$ = 9.988
Critical stresses	$\sigma_{Cr,top}$ = 1004 MPa	$\sigma_{Cr,bot}$ = 1023 MPa
Reduced slendernesses at 20°C	λ_{top} = 0.729	λ_{bot} = 0.723
With	ξ = 1.505	
Reduction factors at 20°C	χ_{top} = 0.834	χ_{bot} = 0.837
Resistant stresses at 20°C	$\sigma_{WRd,top}$ = 445 MPa	$\sigma_{MPa\ WRd,bot}$ = 447MPa
Plastic moments of tees at 20°C	$M_{plRd,Te,top}$ = 8.92 kNm	$M_{plRd,Te,bot}$ = 8.92 kNm

Psi factor at 20°C	$\Psi_{top} = 0.820$	$\Psi_{bot} = 0.820$
Post-buckling factor	$\kappa_{top} = 1.250$	$\kappa_{bot} = 1.250$
Critical temperature	$\theta_{crit,top} = 646°C$	$\theta_{crit,bot} = 647°C$
$k_{y,\theta}$ at critical temperature	$k_{y,\theta,top} = 0.3596$	$k_{y,\theta,bot} = 0.3572$
$k_{E,\theta}$ at critical temperature	$k_{E,\theta,top} = 0.229$	$k_{E,\theta,bot} = 0.2272$
Reduced slendernesses at θ_{crit}	$\lambda\theta_{,top} = 0.92$	$\lambda\theta_{,bot} = 0.92$
Reduction factors at θ_{crit}	$\chi_{\theta,top} = 0.53$	$\chi_{\theta,bot} = 0.53$
Psi factor at θ_{crit}	$\Psi_{\theta,top} = 0.24$	$\Psi_{\theta,bot} = 0.24$

1.3.2.7. Bending resistance of gross sections

Section at web post no 16 (Section no 33)		
Internal moment and force	$M_{Ed} = 179.86$ kNm	$N_{Ed} = 0.00$ kN
Upper flange under compression:	Class 1	
Class of the web		
Steel	$f_{y,w} = 355$ MPa	$\varepsilon_w = 0.814$
Slenderness:	$c / t = 65.67$	
Plastic distribution factor	$\alpha = 0.50$	
Class of the web	2	
Check of the resistance (Class2)		
Steel	$f_{y,top} = 355$ MPa	$f_{y,bot} = 355$ MPa
Partial factor	$\gamma_{M,fi} = 1.00$	
Plastic resistant moment at 20°C		$M_{pl,Rd} = 856.24$ kNm
Criterion	$\Gamma_{Mg,fi} = 0.210$	
Critical temperature Γ_{Mg} :	717°C	
Am/V Γ_{Mg}:	185 m^{-1}	

1.3.2.8. Shear resistance of gross sections

Section at left end (Section no 1)		
Height of the cross-section	$h = 633.8$ mm	
Shear area	$A_{v,top} = 3140.0$ mm^2	$A_{v,bot} = 3140.0$ mm^2
Yield strengths	$f_{y,top} = 355$ MPa	$f_{y,bot} = 355$ MPa
Shear design force	$V_{Ed} = 35.97$ kN	
Shear resistance force at 20°C	$V_{plRd} = 1287.14$ kN	$\gamma_{M,fi} = 1.00$
Criterion	$\Gamma_{Vg} = 0.028$	
Critical temperature Γ_{Vg} :	1060°C	
Am/V Γ_{Vg}:	232.6 m^{-1}	

1.3.3. Summary of the results

1.3.3.1. Checking of net sections at openings

Parameter	Γ	Angle (°)	Am/V (m^{-1})	θ_{crit} (°C)
Γ_M	0.150	24.0	150.7	767
Γ_N	0.270	0.0	154.5	683
Γ_V	0.202	-39.0	145.4	723
Γ_{MN}	0.302	21.0	151.5	670
Γ_{MV}	0.150	24.0	150.7	767
Γ_{NV}	0.270	0.0	154.5	683
Γ_{MNV}	0.302	21.0	151.5	670

1.3.3.2. Post checking

Parameter	Γ	Am/V (m^{-1})	θ_{crit} (°C)
Γ_{Vh}	0.157	232.6	761
Γ_b	-	232.6	646

1.3.3.3. Gross section checking

Parameter	Γ	Am/V (m^{-1})	θ_{crit} (°C)
Γ_{Mg}	0.210	185	717
Γ_{Vg}	0.028	232.6	1060

2. BAILEY'S METHODS EXTENDED TO LONG SPAN CELLULAR BEAMS

Executive summary

Large-scale fire tests conducted in a number of countries and observations of actual building fires have shown that the fire performance of composite steel framed buildings is much better than is indicated by fire resistance tests on isolated elements. It is clear that there are large reserves of fire resistance in modern steel-framed buildings and that standard fire resistance tests on single unrestrained members do not provide a satisfactory indicator of the performance of such structures.

This publication presents guidance on the application of a simple design method, as implemented in FiCEB design spreadsheet, which has been developed as a result of observation and analysis of the BRE Cardington large-scale building fire test program carried out during 1995 and 1996 and more recent testing on floor slabs containing cellular beams. The recommendations are conservative and are limited to structures similar to those tested, i.e. non-sway steel-framed buildings with composite floors. The guidance gives designers access to whole building behaviour and allows them to determine which members can remain unprotected while maintaining levels of safety equivalent to traditional methods.

In recognition that many fire safety engineers are now considering natural fires, a natural fire model may be inputted or calculated using the parametric fire method from EN1991-1-2. These options are included alongside the use of the standard fire model; all three are expressed as temperature-time curves.

2.1. Introduction

The design recommendations in this publication are based on the performance of composite floor plates, observed during actual building fires and full-scale fire tests[1,2,3]. These conservative recommendations for fire design may be considered as equivalent to advanced methods in the Eurocodes.

Large-scale natural fire tests carried out in a number of countries have shown consistently that the inherent fire performance of composite floor plates with unprotected steel elements is much better than the results of standard tests with isolated elements would suggest. Evidence from real fires indicates that the amount of protection being applied to steel elements may be excessive in some cases. In particular, the Cardington fire tests presented an opportunity to examine the behaviour of a real structure in fire and to assess the fire resistance of unprotected composite structures under realistic conditions. Most test evidence is available for composite beams with plain webs but this project has included a test on a 15m by 9m floor plate with cellular composite beams and similar good behaviour was observed.

Where national building regulations permit performance-based design of buildings in fire, the design method provided by this guide may be applied to demonstrate the fire resistance of the structure without applied fire protection. In some countries acceptance of such demonstration may require special permission from the national building control authority.

The recommendations presented in this publication can be seen as extending the fire engineering approach in the area of structural performance and developing the concept of fire safe design. It is intended that designs carried out in accordance with these recommendations will achieve at least the level of safety required by national regulations while allowing some economies in construction costs.

In addition to fire resistance for the standard temperature-time curve, recommendations are presented for buildings designed to withstand a natural fire. Natural fires can be defined using the parametric

temperature-time curve given in EN1991-1-2 or be user define time temperature curves from other fire analysis software.

The recommendations apply to composite frames broadly similar to the eight-storey building tested at Cardington, as illustrated in Figure 2–1. This project has shown that the scope may also be extended to cellular beams fabricated from rolled sections.

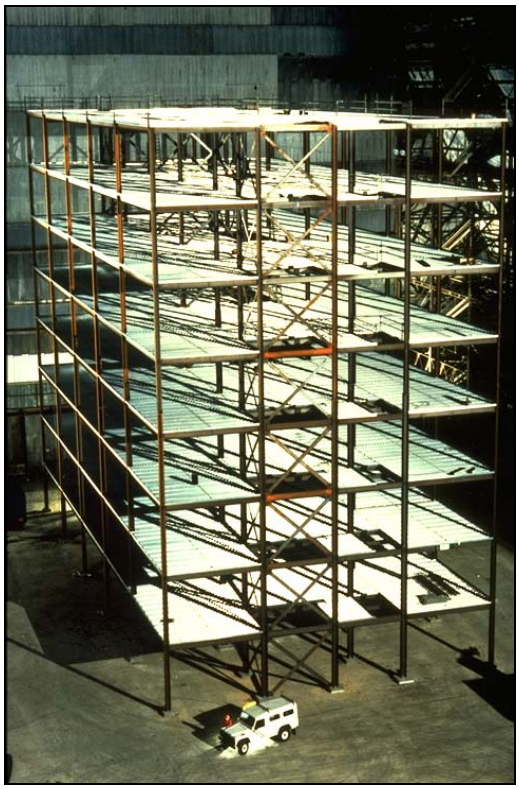

Figure 2–1 : Cardington test building prior to the concreting of the floors

2.2. Basis of design

This Section gives an overview of the design principles and assumptions underlying the development of the simple design method.

The design guidance has been developed from research based on the results from fire tests, ambient temperature tests and finite element analyses.

2.2.1. Fire safety

The design recommendations given in the simple design method have been prepared such that the following fundamental fire safety requirements are fulfilled:

- There should be no increased risk to life safety of occupants, fire fighters and others in the vicinity of the building, relative to current practice.
- On the floor exposed to fire, excessive deformation should not cause failure of compartmentation, in other words, the fire will be contained within its compartment of origin and should not spread horizontally or vertically.

2.2.2. Type of structure

The design guidance given in the simple design method applies only to steel-framed buildings with composite floor beams and slabs of the following general form:

- braced frames not sensitive to buckling in a sway mode,
- frames with connections designed using simple joint models,
- composite floor slabs comprising steel decking, a single layer of reinforcing mesh and normal or lightweight concrete, designed in accordance with EN1994-1-1 [7],
- floor beams designed to act compositely with the floor slab and designed to EN 1994-1-1.
- cellular beams fabricated from hot rolled steel sections

The guidance does **not** apply to:

- floors constructed using precast concrete slabs,
- internal floor beams that have been designed to act non-compositely (beams at the edge of the floor slab may be non-composite),
- beams with service openings (except cellular beams as defined above).

2.2.3. Simple joint models

The joint models adopted during the development of the guidance given in this publication assume that bending moments are not transferred through the joint. The joints are known as ‘simple’.

Beam-to-column joints that may be considered as ‘simple’ include joints with the following components:

- Flexible end plates (Figure 2–2)
- Fin plates (Figure 2–3)
- Web cleats (Figure 2–4)

Further information on the design of the components of ‘simple’ joints is given in Section 2.3.9.

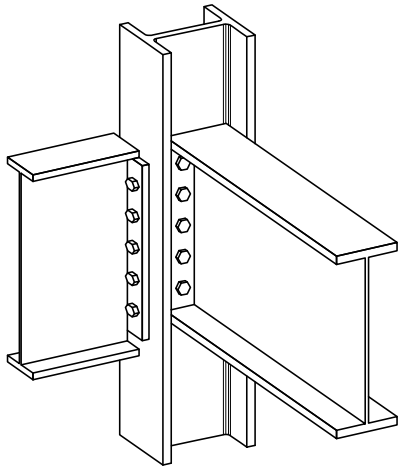

Figure 2–2 : Example of a joint with flexible end plate connections

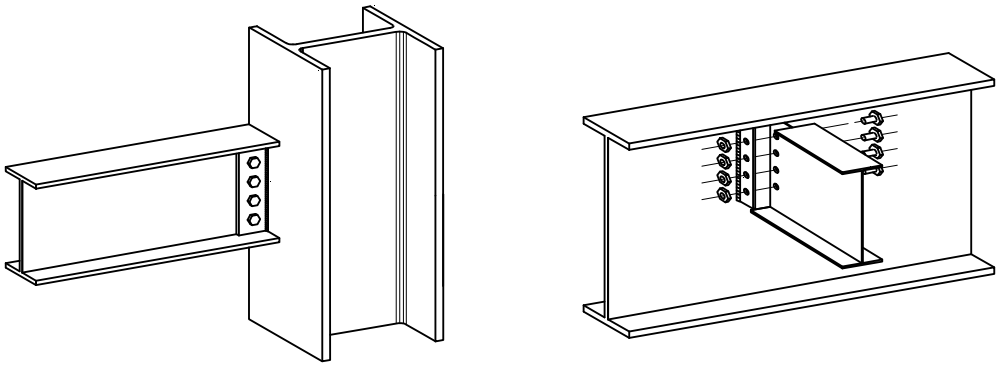

Figure 2–3 : Examples of joints with fin plate connections

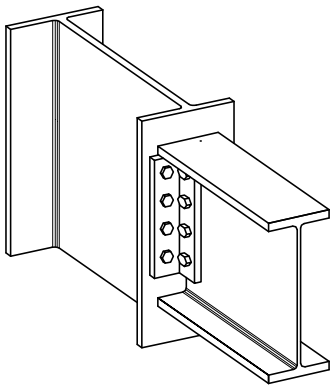

Figure 2–4 : Example of a joint with a web cleat connection

2.2.4. Floor slabs and beams

The design recommendations given in this guide are applicable to profiled steel decking up to 80 mm deep with depths of concrete above the steel decking from 60 to 90 mm. The resistance of the steel decking is ignored in the fire design method but the presence of the steel decking prevents spalling of the concrete on the underside of the floor slab. This type of floor construction is illustrated in Figure 2–5.

The design method can be used with either isotropic or orthotropic reinforcing mesh, that is, meshes with either the same or different areas in orthogonal directions. The steel grade for the mesh reinforcement should be specified in accordance with EN10080. As the design method requires ductile mesh reinforcement in order to accommodate large slab deflections Class B or Class C should be specified. The FiCEB design spreadsheet can only be used for welded mesh reinforcement and can not consider more than one layer of reinforcement. Reinforcement bars in the ribs of the composite slab are **not** required**.**

The software allows user defined sizes of welded mesh the user must input the area of the mesh in each direction. Common French and UK mesh sizes are given in the table below.

Table 2-1 : Fabric mesh as defined by BS 4483 [9]

Mesh Reference	Size of mesh (mm)	Weight (kg/m^2)	Longitudinal wires		Transverse wires	
			Size (mm)	Area (mm^2/m)	Size (mm)	Area (mm^2/m)
A142	200x200	2.22	6	142	6	142
A193	200x200	3.02	7	193	7	193
A252	200x200	3.95	8	252	8	252
A393	200x200	6.16	10	393	10	393
B196	100x200	3.05	5	196	7	193
B283	100x200	3.73	6	283	7	193
B385	100x200	4.53	7	385	7	193
B503	100x200	5.93	8	503	8	252

Table 2-2 : Fabric mesh commonly used in French market

Mesh Reference	Size of mesh (mm)	Weight (kg/m^2)	Longitudinal wires		Transverse wires	
			Size (mm)	Area (mm^2/m)	Size (mm)	Area (mm^2/m)
ST 20	150x300	2.487	6	189	7	128
ST 25	150x300	3.020	7	257	7	128
ST 30	100x300	3.226	6	283	7	128
ST 35	100x300	6.16	7	385	7	128
ST 50	100x300	3.05	8	503	8	168
ST 60	100x300	3.73	9	636	9	254
ST 15 C	200x200	2.22	6	142	6	142
ST 25 C	150x150	4.03	7	257	7	257
ST 40 C	100x100	6.04	7	385	7	385
ST 50 C	100x100	7.90	8	503	8	503
ST 60 C	100x100	9.98	9	636	9	636

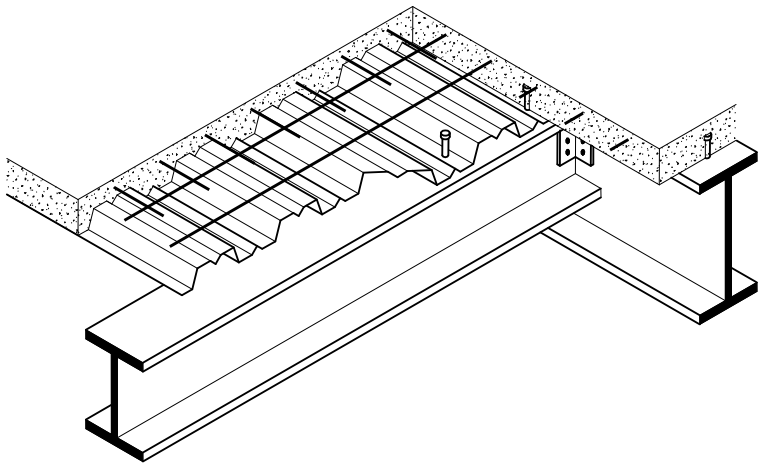

Figure 2–5 : Cut away view of a typical composite floor construction

It is important to define the beam sizes used in the construction of the cellular beams within the floor plate as this will influence the fire performance of the floor plate. The designer will need to have details of the serial size, steel grade and degree of shear connection available for the top and bottom tee of the internal cellular beams. The FiCEB spreadsheet allows the user to choose from a predefined list of serial sizes covering common British and European I and H sections.

2.2.5. Floor design zones

The design method requires the designer to split the floor plate into a number of floor design zones as shown in Figure 2–6. The beams on the perimeter of these floor design zones must be designed to achieve the fire resistance required for the floor plate and will therefore normally be fire protected.

A floor design zone should meet the following criteria:

- Each zone should be rectangular.
- Each zone should be bounded on all sides by beams.
- The beams within a zone should only span in one direction.
- Columns should not be located within a floor design zone; they may be located on the perimeter of the floor design zone.
- For fire resistance periods in excess of 60 minutes, or when using the parametric temperature-time curve, all columns should be restrained by at least one fire protected beam in each orthogonal direction.

All internal beams within the zone may be left unprotected, provided that the fire resistance of the floor design zone is shown to be adequate using the FiCEB spreadsheet. The size and spacing of these unprotected beams are not critical to the structural performance in fire conditions.

An example of a single floor design zone is given in Figure 2–6.

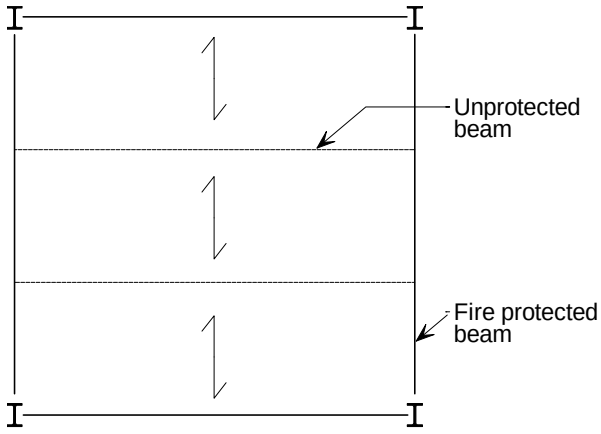

Figure 2–6 : Example of a floor design zone

2.2.6. Combination of actions

The combination of actions for accidental design situations given in 6.4.3.3 and Table A1.3 of EN 1990 [11] should be used for fire limit state verifications. With only unfavourable permanent actions and no prestressing actions present, the combination of actions to consider is:

$$\sum G_{\mathrm{k},j,\mathrm{sup}} + A_{\mathrm{d}} + (\psi_{1,1} \text{ or } \psi_{2,1})Q_{\mathrm{k},1} + \sum \psi_{2,i} Q_{\mathrm{k},i}$$

Where:

$G_{k,j,sup}$ Unfavourable permanent action
A_d Accidental action
$Q_{k,1}$ and $Q_{k,i}$ Accompanying variable actions, main and other respectively
$\psi_{1,1}$ Factor for the frequent value of the leading variable action
$\psi_{2,i}$ Factor for the quasi-permanent value of the *i*th variable action

The use of either $\psi_{1,1}$ or $\psi_{2,1}$ with $Q_{k,1}$ should be specified in the relevant National Annex. The National Annex for the country where the building is to be constructed should be consulted to determine which factor to use.

The values used for the ψ factors relate to the category of the variable action they are applied to. The Eurocode recommended values for the ψ factors for buildings are given in Table A1.1 of EN 1990; those values are confirmed or modified by the relevant National Annex. The ψ factor values for buildings in the UK and France are summarised in Table 2-3. For floors that allow loads to be laterally distributed, the following uniformly distributed loads are given for moveable partitions in 6.3.1.2(8) of EN 1991-1-1 [12]:

- Movable partitions with a self-weight ≤ 1,0 kN/m wall length: q_k = 0,5 kN/m^2
- Movable partitions with a self-weight ≤ 2,0 kN/m wall length: q_k = 0,8 kN/m^2
- Movable partitions with a self-weight ≤ 3,0 kN/m wall length: q_k = 1,2 kN/m^2.
- Moveable partitions with self-weights greater than 3.0 kN/m length should be allowed for by considering their location.

The Eurocode recommended values for variable imposed loads on floors are given in Table 6.2 of EN 1991-1-1; those values may also be modified by the relevant National Annex. Table 2-4 presents the Eurocode recommended values and the values given in the UK and French National Annexes for the imposed load on an office floor.

Table 2-3 : Values of ψ factors

Actions	Eurocode recommended values		UK National Annex values		French National Annex values	
	ψ_1	ψ_2	ψ_1	ψ_2	ψ_1	ψ_2
Domestic, office and traffic areas where: 30 kN < vehicle weight ≤ 160 kN	0.5	0.3	0.5	0.3	0.5	0.3
Storage areas	0.9	0.8	0.9	0.8	0.9	0.8
Other*	0.7	0.6	0.7	0.6	0.7	0.6

* Climatic actions are not included

Table 2-4 : Imposed load on an office floor

Category of loaded area	Eurocode recommended values		UK National Annex values		French National Annex values	
	q_k (kN/m^2)	Q_k (kN)	q_k (kN/m^2)	Q_k (kN)	q_k (kN/m^2)	Q_k (kN)
B – Office areas	3.0	4.5	2.5* or 3.0**	2.7	3.5 – 5.0	15.0

* Above ground floor level
**At or below ground floor level

2.2.7. Fire exposure

The recommendations given in the simple design method may be applied to buildings in which the structural elements are considered to be exposed to a standard temperature-time curve or parametric temperature-time curve, both as defined in EN 1991-1-2. Advanced model may also be used to define a temperature –time curve for a natural fire scenario. The resulting temperature-time time curve may be input to the 'User defined' worksheet on the FiCEB spreadsheet.

In all cases, the normal provisions of national regulations regarding means of escape should be followed.

2.2.8. Fire resistance

The Cardington fire tests were conducted using both real ('natural') fires and non standard gas fires. The tests did not follow the standard temperature-time curve that is used to define the fire resistance periods given in national regulations. Design temperatures in terms of the standard fire resistance temperature-time curve must therefore be calculated using thermal analysis.

The recommended periods of fire resistance for elements of construction in various types of building may be found in national regulations. The structural elements of most two-storey buildings require 30 minutes fire resistance and those in most buildings between three and five storeys require 60 minutes fire resistance.

The following recommendations may be applied to buildings in which the elements of structure are required to have up to 120 minutes fire resistance. Provided that they are followed, composite steel framed buildings will maintain their stability for this period of fire resistance, when any compartment is subject to the standard temperature-time curve [1].

All composite steel framed buildings with composite floors may be considered to achieve 15 minutes fire resistance without fire protection, and so no specific recommendations are given in this case.

2.2.8.1. Natural fire (parametric temperature-time curve)

The FiCEB software allows the effect of natural fire on the floor plate to be considered using the parametric temperature-time curve as defined in EN1991-1-2 Annex A [25]. It should be noted that this is an Informative Annex and its use may not be permitted in some European countries, such as France. Before final design is undertaken the designer should consult the relevant National Annex.

Using this parametric fire curve, the software defines the compartment temperature taking account of:

- The compartment size:
- Compartment length
- Compartment width
- Compartment height

The height and area of windows:

- Window height
- Window length
- Percentage open window

The amount of combustibles and their distribution in the compartment

- Fire Load
- Combustion factor
- The rate of burning
- The thermal properties of the compartment linings

The temperature of a parametric fire will often rise more quickly than the standard fire in the early stages but, as the combustibles are consumed, the temperature will decrease rapidly. The standard fire steadily increases in temperature indefinitely.

The standard temperature-time curve and a typical parametric temperature-time curve are shown in Figure 2–7.

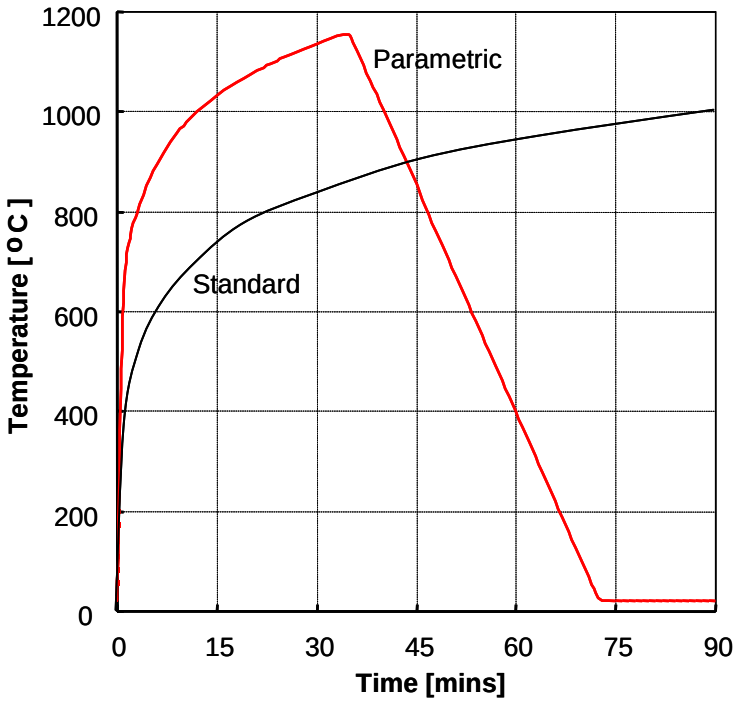

Figure 2–7 : Comparison of typical parametric and standard temperature-time curve

2.3. Recommendations for structural elements

2.3.1. Floor design zones

Each floor should be divided into design zones that meet the criteria given in Section 2.2.5.

The division of a floor into floor design zones is illustrated in Figure 2–8. Floor zones designated ‘A’ are within the scope of the design guide and their load bearing performance in fire conditions may be determined using the FiCEB spreadsheet. The zone designated ‘B’ is outside the scope of the software because it contains a column and the beams within the zone do not all span in the same direction.

A single floor zone is illustrated in Figure 2–9 showing the beam span designations used in the FiCEB software. Normal design assumes that floor loads are supported by secondary beams which are themselves supported on primary beams.

The fire design method assumes that at the fire limit state, the resistance of the unprotected internal beams reduces significantly, leaving the composite slab as a two way spanning element simply supported around its perimeter. In order to ensure that the slab can develop membrane action, the FiCEB spreadsheet computes the moment applied to each perimeter beam as a result of the actions on the floor design zone. To maintain the vertical support to the perimeter of the floor design zone in practice, the degree of utilisation and hence the critical temperature of these perimeter beams must be calculated using appropriate cellular beam design software. The fire protection for these beams should be designed on the basis of this critical temperature and the fire resistance period required for the floor plate in accordance with national regulations.

As noted in Section 2.2.4, a restriction on the use of the FiCEB spreadsheet is that for 60 minutes or more fire resistance, the zone boundaries should align with the column grid and the boundary beams should be fire protected. For 30 minutes fire resistance, this restriction does not apply and the zone boundaries do not have to align with the column grid. For example, in Figure 2–8, zones A2 and A3 have columns at only two of their corners and could only be considered as design zones for a floor that requires no more than 30 minutes fire resistance.

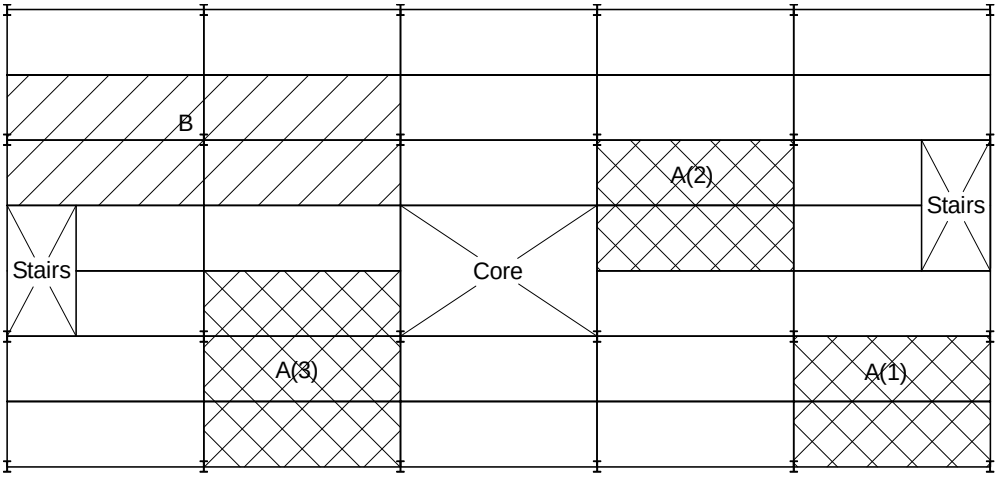

Key to figure

A: These zones may be designed using FiCEB
A(1) Any period of fire resistance
A(2) & A(3) only 30 minutes fire resistance

B: Outside the scope of FiCEB

Figure 2–8 : Possible floor design zones

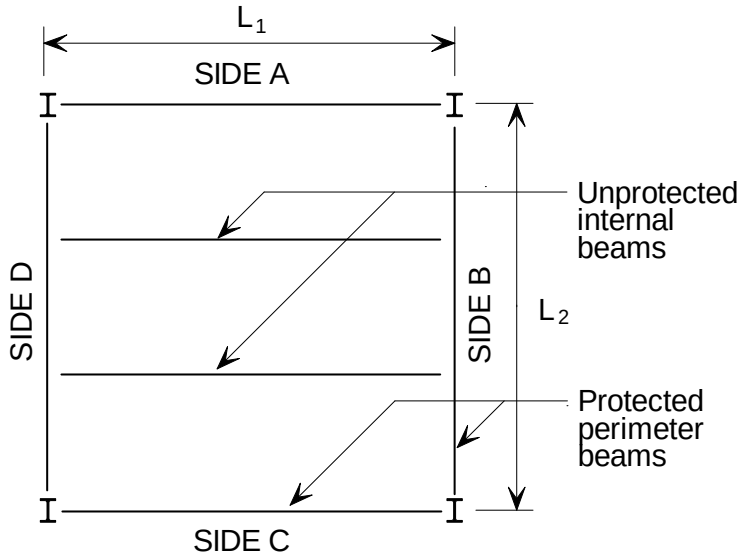

Figure 2–9 : Definition of span 1 (L1) and span 2 (L2) and the beam layout for a floor design zone in a building requiring fire resistance of 60 minutes or more.

2.3.2. Floor slab and beams

The FiCEB spreadsheet calculates the load bearing capacity of the floor slab and unprotected beams at the fire limit state. The simple design method, implemented in the software assumes that each floor design zone will have adequate support on its perimeter. This is achieved in practice by fire protecting the beams on the perimeter of each floor design zone. To ensure that adequate fire protection is provided, the software calculates the critical temperature for each perimeter beam based on the loading applied to the floor design zone.

2.3.3. Fire design of floor slab

Load bearing performance of the composite floor slab

When calculating the load bearing capacity of each floor design zone the resistance of the composite slab and the unprotected cellular beams are calculated separately. The slab is assumed to have no continuity along the perimeter of the floor design zone. The load that can be supported by the flexural behaviour of the composite slab within the floor design zone is calculated based on a lower bound mechanism assuming a yield line pattern as shown in Figure 2–10.

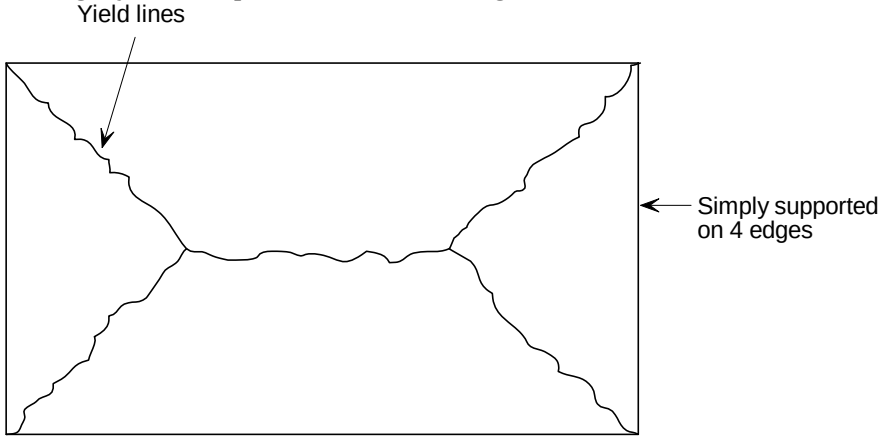

Figure 2–10 : Assumed yield line pattern used to calculate slab resistance

The value of the resistance calculated using the lower bound mechanism is enhanced by considering the beneficial effect of tensile membrane action at large displacements. This enhancement increases with increasing vertical deflection of the slab until failure occurs due to fracture of the reinforcement across the short slab span or compressive failure of the concrete in the corners of the slab, as shown by Figure 2–11. As the design method can not predict the point of failure, the value of deflection considered when calculating the enhancement is based on a conservative estimate of slab deflection that includes allowance for the thermal curvature of the slab and the strain in the reinforcement, as shown below.

$$w = \frac{\alpha(T_2 - T_1)l^2}{19.2h} + \sqrt{\left(\frac{0.5 f_y}{E_a}\right)\frac{3L^2}{8}}$$

The deflection allowed due to elongation of the reinforcement is also limited by the following expression.

$$w \le \frac{\alpha(T_2 - T_1)l^2}{19.2h} + \frac{l}{30}$$

Where

(T2 – T1)	is the temperature difference between the top and bottom surface of the slab
L	is the longer dimension of the floor design zone
l	is the shorter dimension of the floor design zone
fy	is the yield strength of the mesh reinforcement
E	is the modulus of elasticity of the steel
h	is the overall depth of the composite slab
α	is the coefficient of thermal expansion of concrete

All of the available test evidence shows that this value of deflection will be exceeded before load bearing failure of the slab occurs. This implies that the resistance predicted using the design method will be conservative compared to its actual performance.

The overall deflection of the slab is also limited by the following expression.

$$w \le \frac{L + l}{30}$$

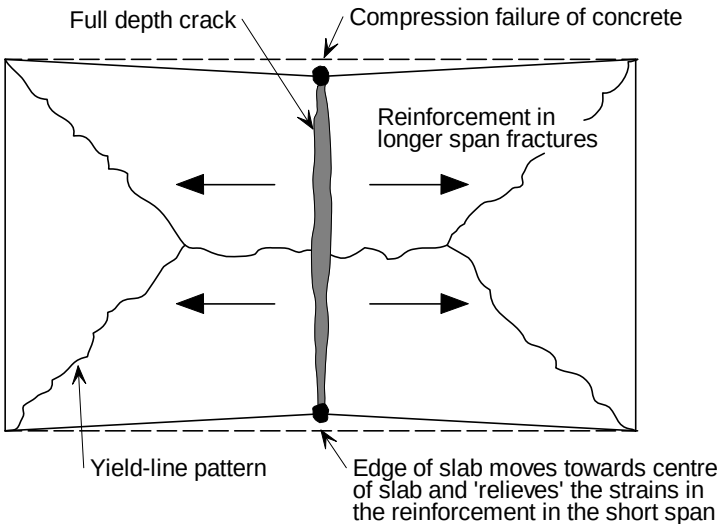

(a) Tensile failure of the reinforcement

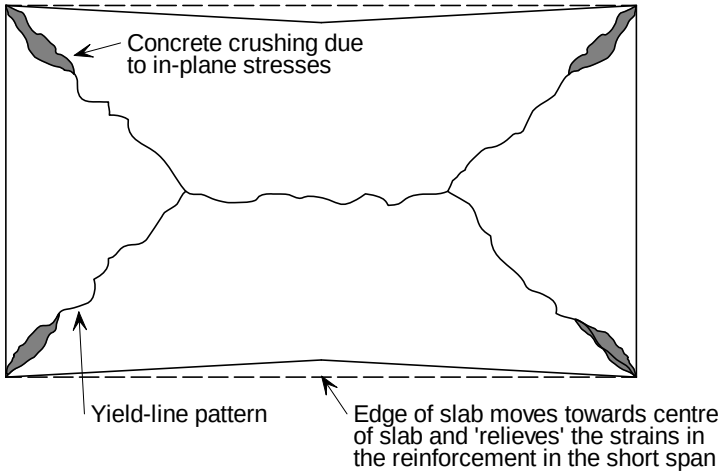

(b) Compressive failure of the concrete

Figure 2–11 : Failure mode due to fracture of the reinforcement

The residual bending resistance of the unprotected composite beams is then added to the enhanced slab resistance to give the total resistance of the complete system.

Integrity and insulation performance of the composite slab

The FiCEB spreadsheet does not explicitly check the insulation or integrity performance of the floor slab. The designer must therefore ensure that the slab thickness chosen is sufficient to provide the necessary insulation performance in accordance with the recommendations given in EN 1994-1-2.

To ensure that the composite slab maintains its integrity during the fire and that membrane action can develop, care must be taken to ensure that the reinforcing mesh is properly lapped. This is especially important in the region of unprotected beams and around columns. Further information on required lap lengths and placement of the reinforcing mesh is given in Section 2.3.5.

2.3.4. Fire design of beams on the perimeter of the floor design zone.

The beams along the perimeter of the floor design zone, labelled A to D in Figure 2–9, should achieve the fire resistance required for the floor plate, in order to provide the required vertical support to the perimeter of the floor design zone. This usually results in these beams being fire protected.

The FiCEB spreadsheet calculates the design effect of actions on these perimeter beams and reports this in the output. In order to determine the required fire protection of these beams the room temperature moment of resistance of the beam must be calculated, in order to calculate the degree of utilisation for each perimeter beam, which is calculated using the guidance given in EN 1993-1-2 §4.2.4, as shown below.

$$\mu_0 = \frac{E_{\text{fi,d}}}{R_{\text{fi,d,0}}}$$

Where

$E_{\text{fi,d}}$ is the design effect of actions on the beam in fire

$R_{\text{fi,d,0}}$ is the design resistance of the beam at time t = 0

Having calculated the degree of utilisation, the critical temperature of the bottom flange of the perimeter beams may be calculated using cellular beam design software. This critical temperature should be use when specifying the fire protection required by each of the perimeter beams on the floor design zone.

When specifying fire protection for the perimeter beams, the fire protection supplier must be given the section factor for the member to be protected and the period of fire resistance required and the critical temperature of the member. Most reputable fire protection manufacturers will have a multi temperature assessment for their product which will have been assessed in accordance with EN 13381-4[13] for non-reactive materials or EN 13381-8[14] for reactive materials (intumescents). Design tables for fire protection which relate section factor to protection thickness are based on a single value of assessment temperature. This assessment temperature should be less than or equal to the critical temperature of the member.

2.3.5. Reinforcement details

The yield strength and ductility of the reinforcing steel material should be specified in accordance with the requirements of EN 10080. The characteristic yield strength of reinforcement to EN 10080 will be between 400 MPa and 600 MPa, depending on the national market. In order that the reinforcement has sufficient ductility to allow the development of tensile membrane action, Class B or Class C should be specified.

In most countries, national standards for the specification of reinforcement may still exist as non-contradictory complimentary information (NCCI), as a common range of steel grades have not been agreed for EN 10080.

In composite slabs, the primary function of the mesh reinforcement is to control the cracking of the concrete. Therefore the mesh reinforcement tends to be located as close as possible to the surface of the concrete while maintaining the minimum depth of concrete cover required to provide adequate durability, in accordance with EN 1992-1-1[0]. In fire conditions, the position of the mesh will affect the mesh temperature and the lever arm when calculating the bending resistance. Typically, adequate fire performance is achieved with the mesh placed between 15 mm and 45 mm below the top surface of the concrete.

Section 2.3.6 gives general information regarding reinforcement details. Further guidance and information can be obtained from, EN 1994-1-1 [7] and EN 1994-1-2[6] or any national specifications such as those given in reference [20].

2.3.6. Detailing mesh reinforcement

Typically, sheets of mesh reinforcement are 4.8 m by 2.4 m and therefore must be lapped to achieve continuity of the reinforcement. Sufficient lap lengths must therefore be specified and adequate site control must be put in place to ensure that such details are implemented on site. Recommended lap lengths are given in section 8.7.5 of EN1992-1-1[19] or can be in accordance with Figure 2–8. The minimum lap length for mesh reinforcement should be 250 mm. Ideally, mesh should be specified with 'flying ends', as shown in Figure 2–12, to eliminate build up of bars at laps. It will often be economic to order 'ready fit fabric', to reduce wastage.

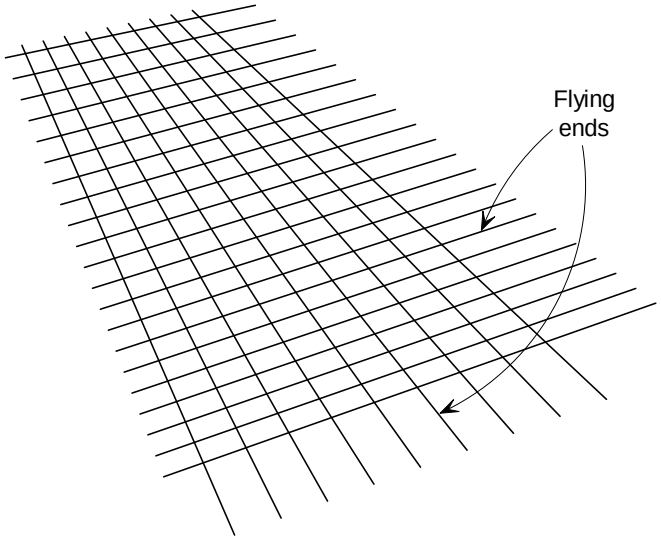

Figure 2–12 : Mesh with flying ends

Table 2-5 : Recommended tension laps and anchorage lengths for welded mesh

Reinforcement Type	Wire/Bar Type	Concrete Grade					
		LC 25/28	NC 25/30	LC 28/31	NC 28/35	LC 32/35	NC 32/40
Grade 500 Bar of diameter d	Ribbed	50d	40d	47d	38d	44d	35d
6 mm wires							
	Ribbed	300	250	300	250	275	250
7 mm wires							
	Ribbed	350	300	350	275	325	250
8 mm wires							
	Ribbed	400	325	400	325	350	300
10 mm wires							
	Ribbed	500	400	475	400	450	350

Notes:
These recommendations can be conservatively applied to design in accordance with EN 1992-1-1.
Where a lap occurs at the top of a section and the minimum cover is less than twice the size of the lapped reinforcement, the lap length should be increased by a factor of 1.4.
Ribbed Bars/Wires are defined in EN 10080
The minimum Lap/Anchorage length for bars and fabric should be 300 mm and 250 mm respectively.

2.3.6.1. Detailing requirements for the edge of a composite floor slab

The detailing of reinforcement at the edge of the composite floor slab will have a significant effect on the performance of the edge beams and the floor slab in fire conditions. The following guidance is based on the best practice recommendations for the design and construction of composite floor slabs to meet the requirements for room temperature design. The fire design method and guidance presented in this document assumes that the composite floor is constructed in accordance with these recommendations.

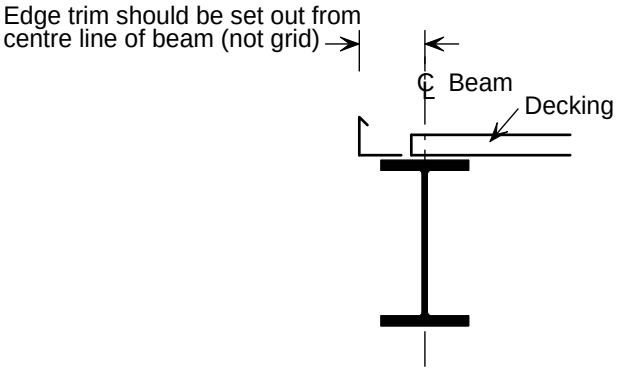

Figure 2–13 : Setting out of edge trim

The edge of the composite slab is usually formed using ‘edge trims’ made from strips of light gauge galvanized steel fixed to the beam in the same way as the decking, as shown in Figure 2–13. In cases where the edge beam is designed to act compositely with the concrete slab, U shaped reinforcing bars are required to prevent longitudinal splitting of the concrete slab. These reinforcement bars also ensure that the edge beam is adequately anchored to the slab when using this simple design method.

Some typical slab edge details covering the two deck orientations are given in Figure 2–14. Where the decking ribs run transversely over the edge beam and cantilevers out a short distance, the edge trim can be fastened in the manner suggested in Figure 2–14(a). The cantilever projection should be no more than 600 mm, depending on the depth of the slab and deck type used.

The more difficult case is where the decking ribs run parallel to the edge beam, and the finished slab is required to project a short distance, so making the longitudinal edge of the sheet unsupported Figure 2–14(b). When the slab projection is more than approximately 200 mm (depending on the specific details), the edge trim should span between stub beams attached to the edge beam, as shown in Figure 2–14(c). These stub beams are usually less than 3 m apart, and should be designed and specified by the structural designer as part of the steelwork package.’

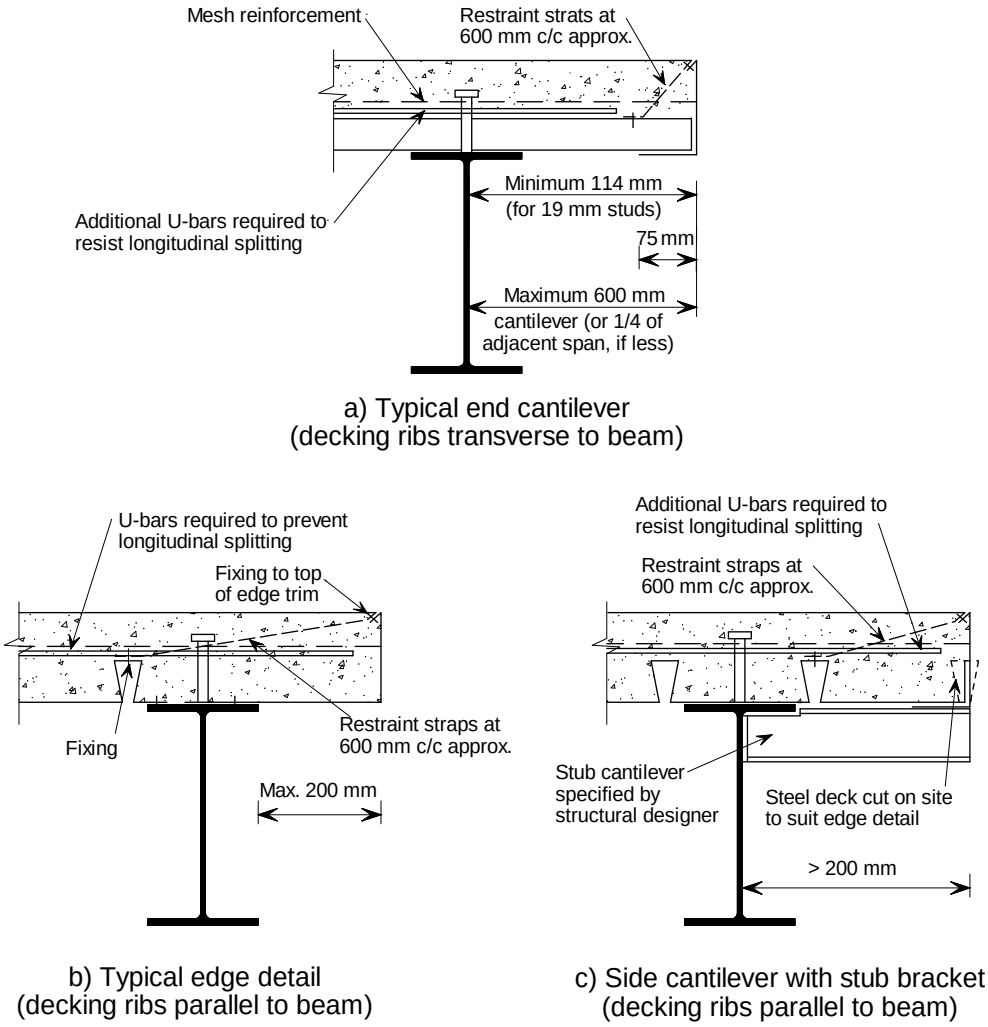

Figure 2–14 : Typical edge details

2.3.7. Design of non composite edge beams

It is common practice for beams at the edge of floor slabs to be designed as non composite beams. This is because the costs of meeting the requirements for transverse shear reinforcement are more than the costs of installing a slightly heavier non composite beam. For fire design, it is important that the floor slab is adequately anchored to the edge beams, as these beams will be at the edge of floor design zones. Although not usually required for room temperature design of non composite edge beams, this guide recommends that shear connectors are provided at not more than 300 mm centres and U shaped reinforcing bars positioned around the shear connectors, as described in Section 2.3.6.1.

Edge beams often serve the dual function of supporting both the floors and the cladding. It is important that the deformation of edge beams should not affect the stability of cladding as it might increase the danger to fire fighters and others in the vicinity. (This does not refer to the hazard from falling glass that results from thermal shock, which can only be addressed by use of special materials or sprinklers.) Excessive deformation of the façade could increase the hazard, particularly when a building is tall and clad in masonry, by causing bricks to be dislodged.

2.3.8. Columns

The design guidance in this document is devised to confine structural damage and fire spread to the fire compartment itself. In order to achieve this, columns (other than those in the top storey) should be designed for the required period of fire resistance or designed to withstand the selected natural (parametric) fire.

Any applied fire protection should extend over the full height of the column, including the connection zone (see Figure 2–15). This will ensure that no local squashing of the column occurs and that structural damage is confined to one floor.

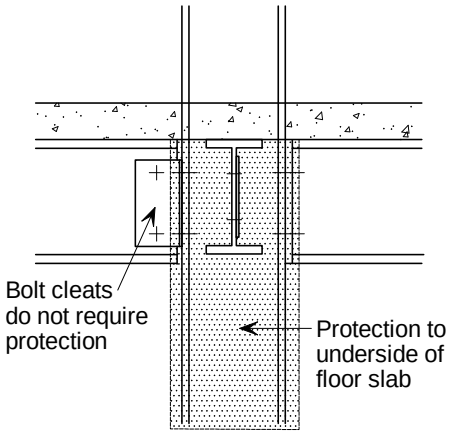

Figure 2–15 : Extent of fire protection to columns

In the Cardington fire tests, the protected columns performed well with no sign of collapse. However, subsequent finite element modelling has indicated the possibility that premature column failure could occur in some circumstances. A mode of behaviour has been identified [(0)] in which expansion of the floors induces moments in the columns. This can have the effect of reducing the temperature at which a column would fail.

It is recommended that, as a conservative measure, the protection to the columns at the edge of the floor plate in buildings of more than two storeys should be increased by basing its thickness on a critical temperature of 500°C, or 80ºC less than the critical temperature given in EN 1993-1-2, whichever is the lower.

For most board fire protection materials, this reduction in critical temperature will have no effect, as the minimum available thickness of board will suffice.

2.3.9. Joints

As stated in Section 2.2.3 the values given by the design method relate to ‘simple’ joints such as those with flexible end plates, fin plates and web cleats.

The steel frame building tested at Cardington contained flexible end plate and fin plate connections. Partial and full failures of some of the joints were observed during the cooling phase of the Cardington fire tests; however, no failure of the structure occurred as a result.

In the case where the plate was torn off the end of the beam, no collapse occurred because the floor slab transferred the shear to other load paths. This highlights the important role of the composite floor slab, which can be achieved with proper lapping of the reinforcement.

The resistances of the simple joints should be verified using the rules given in EN 1993-1-8[19].

2.3.9.1. Joint classification

Joint details should be such that they fulfil the assumptions made in the design model. Three joint classifications are given in EN 1993-1-8:

- Nominally pinned
  - Joints that transfer internal shear forces without transferring significant moments.
- Semi-rigid
  - Joints that do not satisfy the nominally pinned nor the rigid joint criteria.
- Rigid
  - Joints that provide full continuity.

EN 1993-1-8 §5.2 gives principles for the classification of joints based on their stiffness and strength; the rotation capacity (ductility) of the joint should also be considered.

As stated in Section 2.2.3 the values given by the simple design method have been prepared assuming the use of nominally pinned (simple) joints. To ensure that a joint does not transfer significant bending moments and so that it is a 'simple' joint it must have sufficient ductility to allow a degree of rotation. This can be achieved by detailing the joint such that it meets geometrical limits.

2.3.9.2. Fire protection

In cases where both structural elements to be connected are fire protected, the protection appropriate to each element should be applied to the parts of the plates or angles in contact with that element. If only one element requires fire protection, the plates or angles in contact with the unprotected elements may be left unprotected.

2.3.10. Overall building stability

In order to avoid sway collapse, the building should be braced by shear walls or other bracing systems. Masonry or reinforced concrete shear walls should be constructed with the appropriate fire resistance.

If bracing plays a major part in maintaining the overall stability of the building it should be protected to the appropriate standard.

In two-storey buildings, it may be possible to ensure overall stability without requiring fire resistance for all parts of the bracing system. In taller buildings, all parts of the bracing system should be appropriately fire protected.

One way in which fire resistance can be achieved without applied protection is to locate the bracing system in a protected shaft such as a stairwell, lift shaft or service core. It is important that the walls enclosing such shafts have adequate fire resistance to prevent the spread of any fire. Steel beams, columns and bracing totally contained within the shaft may be unprotected. Other steelwork supporting the walls of such shafts should have the appropriate fire resistance.

2.4. Compartmentation

National regulations require that compartment walls separating one fire compartment from another shall have stability, integrity and insulation for the required fire resistance period.

Stability is the ability of a wall not to collapse. For loadbearing walls, the loadbearing capacity must be maintained.

Integrity is the ability to resist the penetration of flames and hot gases.

Insulation is the ability to resist excessive transfer of heat from the side exposed to fire to the unexposed side.

2.4.1. Beams above fire resistant walls

When a beam is part of a fire resisting wall, the combined wall/beam separating element must have adequate insulation and integrity as well as stability. For optimum fire performance, compartment walls should, whenever possible, be located beneath and in line with beams.

Beams in the wall plane

The Cardington tests demonstrated that unprotected beams above and in the same plane as separating walls (see Figure 2–16), which are heated from one side only, do not deflect to a degree that would compromise compartment integrity, and normal movement allowances are sufficient. Insulation requirements must be fulfilled and protection for 30 or 60 minutes will be necessary; all voids and service penetrations must be fire stopped. Beams protected with intumescent coatings require additional insulation because the temperature on the non fire side is likely to exceed the limits required in the fire resistance testing standards[21,22].

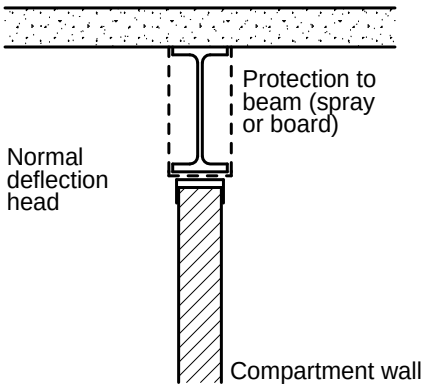

Figure 2–16 : Beams above and in line with walls

Beams through walls

The Cardington tests showed that floor stability can be maintained even when unprotected beams suffer large deflections. However, when walls are located off the column grid, large deflections of unprotected beams can compromise integrity by displacing or cracking the walls through which they pass. In such cases, the beams should either be protected or sufficient movement allowance provided. It is recommended that a deflection allowance of span/30 should be provided in walls crossing the middle half of an unprotected beam. For walls crossing the end quarters of the beam, this allowance may be reduced linearly to zero at end supports (see Figure 2–17). The compartment wall should extend to the underside of the floor.

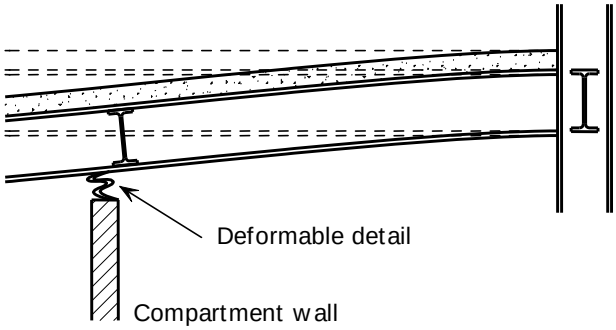

Figure 2–17 : Deformation of beams crossing walls

2.4.2. Stability

Walls that divide a storey into more than one fire compartment must be designed to accommodate expected structural movements without collapse (stability). Where beams span above and in the plane of the wall, movements, even of unprotected beams, may be small and the normal allowance for deflection should be adequate. If a wall is not located at a beam position, the floor deflection that the wall will be required to accommodate may be large. It is therefore recommended that fire compartment walls should be located at a beam positions whenever possible.

In some cases, the deflection allowance may be in the form of a sliding joint. In other cases, the potential deflection may be too large and some form of deformable blanket or curtain may be required, as illustrated in Figure 2–17.

National recommendations should be consulted for the structural deformations which should be considered when ensuring that compartmentation is maintained.

2.4.3. Integrity and insulation

Steel beams above fire compartment walls are part of the wall and are required to have the same separating characteristics as the wall. A steel beam without penetrations will have integrity. However, any service penetrations must be properly fire stopped and all voids above composite beams should also be fire stopped.

3. References

[1] BAILEY, C. G. and MOORE, D. B.
The structural behaviour of steel frames with composite floor slabs subject to fire, Part 1: Theory
The Structural Engineer, June 2000

[2] BAILEY, C. G. and MOORE, D. B.
The structural behaviour of steel frames with composite floor slabs subject to fire, Part 2: Design
The Structural Engineer, June 2000

[3] BAILEY, C. G
Membrane action of slab/beam composite floor systems in fire
Engineering Structures 26

[4] EN 1991-1-2:2002 Eurocode 1: Actions on structures – Part 1 2: General actions. Actions on structures exposed to fire
CEN

[5] EN 1993-1-2:2005 Eurocode 3. Design of steel structures. General rules. Structural fire design
CEN

[6] EN 1994-1-2:2005 Eurocode 4. Design of composite steel and concrete structures. Structural fire design
CEN

[7] EN 1994-1-1:2004 Eurocode 4: Design of composite steel and concrete structures – Part 1 1: General rules and rules for buildings
CEN

[8] EN 10080:2005 Steel for the reinforcement of concrete - Weldable reinforcing steel – General, CEN.

[9] BS 4483:2005 Steel fabric for the reinforcement of concrete. Specification. BSI

[10] BS 4449:1:2005 Steel for the reinforcement of concrete. Weldable reinforcing steel. Bar, coil and decoiled product. Specification
BSI

[11] EN 1990:2002 Eurocode – Basis of structural design
CEN

[12] EN 1991-1-1:2003 Eurocode 1: Actions on structures – Part 1-1: General actions – Densities, self-weight, imposed loads for buildings
CEN

[13] EN13381-4 Test methods for determining the contribution to the fire resistance of structural members. Applied passive protection to steel members, CEN, (To be published 2009)

[14] EN13381-8 Test methods for determining the contribution to the fire resistance of structural members. Applied reactive protection to steel members, CEN, (To be published 2009)

[15] EN 1992-1-1 Design of concrete structures – Part 1-1: General rules and rule for buildings
BSI

[16] COUCHMAN. G. H , HICKS, S. J and RACKHAM, J, W
Composite Slabs and Beams Using Steel Decking: Best Practice for Design & Construction (2nd edition)
SCI P300, The Steel Construction Institute, 2008

[17] BS 8110-1 Structural use of concrete. Code of practice for design and construction, BSI, London, 1997.

[18] BAILEY, C. G.
The influence of thermal expansion of beams on the structural behaviour of columns in steel framed buildings during a fire
Engineering Structures Vol. 22, July 2000, pp 755 768

[19] EN 1993-1-8:2005 Eurocode 3: Design of steel structures – Design of joints
BSI

[20] LAWSON, R. M.
Enhancement of fire resistance of beams by beam to column connections
The Steel Construction Institute, 1990

[21] EN 1363-1:1999 Fire resistance tests. General requirements
CEN

[22] EN 1365 Fire resistance tests for loadbearing elements.
EN 1365-1:1999 Walls
EN 1365-2:2000 Floors and roofs
EN 1365-3:2000 Beams
EN 1365-4:1999 Columns
CEN

[23] RFS2-CT-2007-00042 : FICEB^{+} - Fire resistance of long span cellular beam made of rolled profiles ; March 2011

[24] O. Vassart, Analytical model for cellular beams made of hot rolled sections in case of fire, PhD Thesis, Université Blaise Pascal Clermont-Ferrand II, 2009

[25] **NF EN 1991-1-2** : Eurocode 1 – Actions sur les structures – Partie 1-2 : Actions générales, actions sur les structures exposées au feu.

[26] **NF EN 1993-1-2** : Eurocode 3 – Calcul des structures en acier – Partie 1-2 : Règles générales, Calcul du comportement au feu.

[27] **MT ACB+** : ArcelorMittal Cellular Beams – Logiciel ACB+ - Descriptif Technique – CTICM Rapport 7.072-01

European Commission

EUR 25122 — Fire resistance of long span cellular beam made of rolled profiles (FICEB)

O. Vassart, M. Hawes, I. Simms, B. Zhao, J.-M. Franssen, A. Nadjai

Luxembourg: Publications Office of the European Union

2012 — 254 pp. — 21 × 29.7 cm

Research Fund for Coal and Steel series

ISBN 978-92-79-22428-7

doi:10.2777/38158

ISSN 1831-9424

HOW TO OBTAIN EU PUBLICATIONS

Free publications:

- via EU Bookshop (http://bookshop.europa.eu);
- at the European Union's representations or delegations. You can obtain their contact details on the Internet (http://ec.europa.eu) or by sending a fax to +352 2929-42758.

Priced publications:

- via EU Bookshop (http://bookshop.europa.eu).

Priced subscriptions (e.g. annual series of the *Official Journal of the European Union* and reports of cases before the Court of Justice of the European Union):

- via one of the sales agents of the Publications Office of the European Union (http://publications.europa.eu/others/agents/index_en.htm).

The aim of this project is to develop uniform European design rules for protected and unprotected cellular beams (CB) constructed of rolled sections subjected to fire. The use of cellular beams (CB) will be increased by minimising and optimising the cost of fire protection and by allowing a wider use of unprotected CB. This will greatly benefit long span construction, and increase the market share of steel.

These results will be achieved based on the development of a new design code of single CB subjected to fire as well as an extended methodology considering the whole floor structure and the beneficial effects of the adjacent members. The reliability of the developed tools will be based on large-scale tests in order to provide a cost-effective design methodology. A set of practical design recommendations will be developed in order to satisfy all the requirements of fire-safe engineering.

KI-NA-25122-EN-N

Publications Office

ISBN 978-92-79-11328-4